Long lived PET tracers for tracking labelled cells

Charoenphun, Putthiporn

Awarding institution:
King's College London

Long lived PET tracers for tracking labelled cells

A thesis submitted to King's College London

for the degree of

Doctor of Philosophy in Imaging Sciences and Radiation Biology

Putthiporn Charoenphun

Division of Imaging Sciences and Biomedical Engineering

King's College London

2014

Abstract

Cell tracking is important because the information it provides is required to inform cell based treatment development. Additionally, it has a diagnostic purpose for detecting infection/inflammation diseases with labelled cells, a technique that has become part of routine clinical practice. Currently only gamma emitting radiotracers for single photon emission computed tomography (SPECT) are available to label cells for routine service. PET (positron emission tomography) exhibits better resolution than SPECT and its use in cell tracking would improve image quality, detectability and quantification for smaller lesions.

The studies presented in this thesis report on development of cell labelling techniques with positron emitting radionuclides. The production and characterisation of complexes of copper-64 with dithiocarbamate (DTC) analogues and bis(thiosemicarbazones) (BTSCs) are described. Their labelling efficacies and stabilities were investigated. Although efficient and rapid extraction of ^{64}Cu (DEDTC)$_2$ and ^{64}Cu-GTSM were observed, a high percentage of the radiotracer leakage from the labelled cells was still problematic. Efflux kinetics were similar for all the complexes used suggesting that the efflux mechanism was the same in all cases. In an alternative approach, a novel lipophilic complex of the long lived PET isotope, zirconium-89, was synthesised and characterised. [^{89}Zr]-Zr(oxinate)$_4$ showed good retention in the labelled cells 24 hr after labelling as well as moderate uptake in many types of cells including human leucocytes and mouse multiple myeloma (MM) cells (eGFP-5T33). *In vivo* imaging and *ex vivo* tissues counting was used to compare cell tracking with [^{89}Zr]-Zr(oxinate)$_4$ and [^{111}In]-In(oxinate)$_3$ labelled MM cells. The main organs of the homing radiolabelled cells were similar in MM model. However, mice injected [^{111}In]-In(oxinate)$_3$ labelled cells showed higher accumulation of activity in the kidneys than

those of [^{89}Zr]-Zr(oxinate)$_4$ that might indicate the greater release and metabolism of the ^{111}In radiotracer released from the labelled cells. The localisation of [^{89}Zr]-Zr(oxinate)$_4$ in labelled MM cells was confirmed by sorting of homing organ (liver, spleen, bone marrow) homogenates based on green fluorescence protein (GFP) expression up to 7 days post inoculation, which showed that radioactivity remained predominantly in GFP-positive cells confirming that radionuclide loss from the labelled cells was minimal and that the cells remained alive at 7 days post injection. In addition we demonstrated that mice inoculated [^{89}Zr]-Zr(oxinate)$_4$ labelled cells can be tracked by PET imaging for 14 days after inoculation.

It was concluded that while Cu-64 radiolabelling of cells was ineffective because the majority of radioactivity was lost from cells by 24 hr, the novel complex [^{89}Zr]-Zr(oxinate)$_4$ can be successfully synthesised with acceptable quality and very promising long lived PET tracer for tracking labelled cells for up to weeks.

Acknowledgements

I would like to express my deepest gratitude to my supervisor, Prof. Phil Blower for giving me the huge opportunity to study PhD under his supervision. I would never have been able to be KCL's PhD student and to finish my programme without Phil's kindness, help, support, constant encouragement, inspiration and patience. I am grateful to my second supervisor, Dr. Greg Mullen, for his guidance and support. I owe special thanks to Dr. Jim Ballinger, for all the great advices for my PhD work and also for my work in Thailand. Thanks to Dr. Lefteris Livieratos for his encouragement to start and keep writing up my thesis. I am grateful to my post graduated co-ordinator, Prof. Steve Keevil, for his kindly consideration of my complicated progression over the years.

I owe a special thousand thanks to Dr. Levente Meszaros. Words cannot express how grateful I am to him (who seems to be like my third supervisor) for his massive help, support, encouragement, cheering up and patience. You will be the special man for me forever. I would also like to thanks my friend (like my brother), Mr. (soon to be Dr) Krisanat, for all his help in the lab and in my life. My greatest appreciation goes to Dr. Michelle, Dr. Ehsan, Dr. Florian, Dr. Maggie, Dr. Maite, Dr. Karen, Dr. Rafa, Dr. Kavitha, Dr. Dave and Dr. Kazumi for their helping, encouraging and valuable comments. Also big thanks go to David Thakor for the entire great lab organisation and also for his great patience with my mad habits. Thank you to Barry and Steve for helping me in our lab and also in preclinical lab.

I also want to thank all my friends in our group, Dr. Julia Blower, Alex Koers, Dr. Alex O'neill, Dr. Seckou, Dr. Jennifer, Dr. Fiona, Zaitul, Faiz, Julia Torres, Dr. Saima, Dr. Erica and people in our group for all the fun and a very pleasant experiences to work with all of you, these will be the some of my great memories. I

should certainly mention my very close brother, Dr. Sittiruk, for all of his great support and stood by me that he has always given me.

Many thanks to my friends in London, Dr.Pirada, Dr.Kankamol, Dr. Duantida, Dr. Saijai and Dr. Arcom for supporting and encouraging me to write my thesis. A massive thank you goes to Sujinna (Lookpla) for being a lovely housemate.

I would also like to thank my external examiners, Dr. Bev Ellis and Dr. Dan Lloyd, who provided valuable suggestions, corrections and constructive feedback as well as I would like to thank Dr. Graeme Hogarth for being my internal examiner.

The very generous studentship from Faculty of Medicine, Ramathibodi Hospital, Mahidol University is also acknowledged. I should mention all of my friends and my colleagues in Thailand for all their supports during my PhD programme.

Finally, I would like to thank my mom, my aunts, my uncles and especially for my brilliant sister, Pat, for their support, trust, believing in me and for all their love, throughout my life. I would like to dedicate this thesis and all my work to them.

Contents

List of Figures

Chapter 1

Chapter 2

Chapter 3

Chapter 4

List of Tables

Chapter 3

Chapter 4

Abbreviations

ATSM	diacetyl bis(N^4 –methylthiosemicarbazone)
BSA	bovine serum albumin
BSU	biological services unit
BTSC	bis(thiosemicarbazone)
BZDTC	N-benzyl dithiocarbamate
CCD	charged coupled device
CDCs	cardiac-derived stem cells
CPC	circulation progenitor cells
CPM	count per minute
CT	computed tomography
DC	dendritic cells
DEDTC	diethyldithiocarbamate
DMDTC	dimethyldithiocarbamate
DMSO	dimethylsulfoxide
DPDTC	dipropyldithiocarbamate
D_2R	dopamine subtype 2 receptor
DTPA	diethylenetriamine-pentaacetic acid

EBV	Epstein - Barr virus
eGFP	enhanced green fluorescent protein
ES	embryonic stem cells
^{18}F–FESP	^{18}F fluoroethylspiperone
FLI	fluorescent imaging
GBM	glioblastoma multiforme
GTS	glyoxal-bis(N^4-thiosemicarbazone)
GTSM	glyoxal-bis(N^4-methylthiosemicarbazone)
HBSS	Hanks' balanced salt solution
HEPES	4-(2-hydroxyethyl)-1-piperazineethanesulfonic acid
HMPAO	hexamethylpropyleneamine oxime
hNET	human norepinephrine transporter
HPCs	hematopoictic progenitor cells
HPLC	high performance liquid chromatography
HSV1-tk	herpes simplex virus type 1 thymidine kinase
^{131}I-FIAU	^{131}I-2-fluoro-2-deoxy-5-iodo-1-D-arabinofuranosyluracil
IFN	interferon
^{111}In-Merc	^{111}In-2-mercaptopyridine-N-oxide
ITLC	instant thin layer chromatography

i.v.	intravenous
MI	myocardial infarction
MM	multiple myeloma
MPO	2-mercaptopyridine-N-oxide
mrfp	monomeric red fluorescence
MRI	magnetic resonance imaging
MSC	mesenchymal stem cell
MV	measles virus
NIR	near infrared
NIS	sodium iodine symporter
OI	optical imaging
OVA	ovalbumin
PBS	phosphate buffered saline
PEI	polyethylenimine
PEG	polyethylene glycol
PET/CT	positron emission tomography/computed tomography
PIL	personal investigator licence
PPL	personal project licence
PTS	pyruvaldehyde bis(N^4–thiosemicarbazone)

PTSM	pyruvaldehyde bis(N^4–methylthiosemicarbazone)
RCP	radiochemical purity
Rf	retention factor
RPM	revolutions per minute
SN	supernatant
SPECT	single photon emission computed tomography
SPIO	superparamagnetic iron oxide particles
$SSTr_2$	somatostatin receptor subtype 2
TFA	trifluoroacetic acid
TILs	tumour-infiltrating lymphocytes
Ttk	truncated thymidine kinase
UV	ultraviolet
WBCs	white blood cells

Chapter 1: Introduction

Nowadays, cell labelling plays an important role in many imaging applications such as in infection and inflammation diseases (1) as well as the study of cell functions for better understanding and improving diagnostic and treatment of diseases (2). Extension of the advance knowledge of molecular biology in the medical field leads to the era of cell-based therapies such as stem cell therapy (3) and cancer immunotherapy (4). The cell labelling approach would therefore provide more important information about the *in vivo* fate, biodistribution and survival of cells in these applications. Properties of ligands and tracers chosen for labelling and tracking the labelled cells should be related to the applications. For instance, tracers for tracking stem cells requires a longer period of following than tracking of labelled cells for investigation of infection or inflammation foci. Then, the detectability period and stability of tracers after labelling the cells become the important criterion for finding suitable ligands or approaches.

For the last few decades, tracking of radiolabelled cells has been clinically approved as a routine service in nuclear medicine since the pioneering work on autologous blood cell labelling was launched in the 1970s (1, 5). Images of radiolabelled isolated white blood cells have been routinely used to detect infection/inflammation foci in a range of diseases. The basic principle for labelling is non-specific labelling using lipophilic and metastable complexes of ^{111}In (with oxine (6, 7), tropolone (8, 9) and occasionally other bidentate chelators (6, 10-12), and later technetium-99m,(2, 13, 14) for gamma camera imaging. Tracers used in studies of cell tracking more generally both in research and the clinic are summarised as follows.

1.1 Single photon emission computed tomography (SPECT) imaging

In gamma scintigraphy and SPECT imaging, radiotracers that emit gamma photons are injected into the body. The emitted photon in the body produces images based on cellular function and physiology rather than morphological information. Combination of SPECT (or PET, as described later) with the other modalities, such as Computed Tomography (CT), generates more detailed anatomical information. This combination of modalities has been accepted to produce the highest sensitivity among other techniques and is widely used in clinical practice. The spatial resolution in nuclear scintigraphy is limited. Since the spatial resolution of commercial micro SPECT and PET scanners are recently improved (15, 16), these techniques are becoming more valuable to investigate a wide range of diseases in animal models including monitoring cell tracking (16). It is presupposed that this labelling approach does not cause significant impairment of the biological function of labelled cells (17) and that alteration to cells' proliferation and function can be minimised by careful control of radiation dose (18). Although the biological effects of radiolabelling on cells needs much more investigation to fully understand the information provided by radionuclide cell tracking, SPECT isotopes have been widely employed to study cell trafficking, and planar imaging with gamma emitters has been used for more than thirty years for imaging the migration of white blood cells to detect infection and inflammation in the clinic. Cells can be labelled by direct labelling technique with radiotracers. The gamma radionuclides have been commonly used are ^{111}In and ^{99m}Tc as described below.

1.1.1 Indium-111 (^{111}In), a gamma emitting isotope, emits photons around 171 and 245 keV with physical half life of 67 hours. As mentioned above, several ^{111}In

complexes have been investigated for labelling cells. The following ^{111}In complexes have been used either in clinical practice or research.

1.1.1.1 ^{111}In-oxine (oxyquinoline) (structure of 8-hydroxyquinoline (oxine) shown in Figure 1.1) was approved as a clinical radiopharmaceutical used for imaging inflammation and infection (5) in routine Nuclear Medicine services and became a gold standard for intraabdominal infection detection (19).

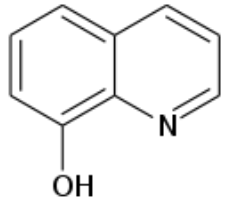

Figure 1.1: Structure of 8-hydroxyquinoline (oxine)

^{111}In-oxine which has neutral and lipophilic properties directly labels white blood cells by passive diffusion into the cells. The lipophilic complex is then dissociated and then ^{111}In strongly binds to intracellular macromolecules. The radionuclides remaining within the cells allow the gamma camera to detect labelled cells (20). However, ^{111}In prefers to form complex with transferrin in plasma with greater stability than oxine resulting in reduced efficiency to label leukocytes (21) in plasma. Therefore in the ^{111}In-oxine labelling procedure it is necessary to remove plasma before the labelling processes. Moreover, ^{111}In-oxine labels not only leukocytes but also erythrocytes in the same manner. Thus, for in *ex vivo* labelling of leukocytes with this tracer it is necessary to remove red blood cells and plasma before the labelling process. Disadvantages of this technique are that it requires well trained personnel and is time consuming (22). Because this isotope binds to intracellular macromolecules, free ^{111}In remains trapped in the reticuloendothelial system when labelled granulocytes undergo apoptosis or necrosis after finishing their functions (23).

The method has been used to investigate various applications of cells such as cell-based therapies. Techniques to label progenitor cells, stem cells, dendritic cells (DC) and tumour-infiltrating lymphocytes (TILs) with ^{111}In-oxine have been investigated (24, 25). However from *in vitro* studies, this tracer was shown to be released from the labelled hematopoietic progenitor cells (HPCs) to the extent of more than 30 % and 60 % after 24 and 48 hours, respectively (26). Comparison of *in vivo* biodistribution in rats with and without myocardial infarction 1 hr after injection of ^{111}In-oxine labelled HPCs, showed high uptake in lung which cleared by 24 hr in both groups. After 96 hr different uptake between infarcted and non-infarcted animals was visualised suggesting migration and function of ^{111}In-oxine labelled HPCs to the infarcted area.

1.1.1.2 ^{111}In-tropolone (tropolone structure shown in Figure 1.2) is another radioindium complex used to label cells. ^{111}In-tropolone can label cells in the presence of plasma (27).

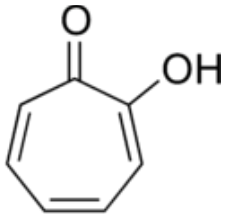

Figure 1.2: Structure of tropolone

This property offers benefit to label specific cell types such as platelets which need to be maintained under physiological conditions during the labelling procedure to decrease adverse effect on the radiolabelled cells. Reports from researchers using ^{111}In-tropolone (9, 27) suggest that the labelling efficiency to label blood components is comparable with that of ^{111}In-oxine.

1.1.1.3 Other chelators have been used to make ^{111}In complexes for assessment as radiotracers for labelling cells in plasma rather than in saline or buffer to overcome the limitations of the ^{111}In-oxine labelling procedure. In 1985, Thakur and colleagues

reported the use of ^{111}In-2-mercaptopyridine-N-oxide (^{111}In-Merc) to label leukocytes and platelets in presence of plasma (11, 28). The labelling efficiencies of ^{111}In-Merc with either leukocytes or platelets compared favourably to those of ^{111}In-oxine and ^{111}In-tropolone complexes. The success of platelet labelling was illustrated by minimisation of platelet aggregations and the high percentage of labelled platelets that could be recovered from dogs. Another advantage of this ^{111}In complex was that it enabled efficient labelling of blood components with either one or two steps using ^{111}In-Merc solution or in the form of lyophilised kit of Merc, respectively (11). In 1999, Ellis *et al*. reported studies of the heterocyclic bidentate ligands, 6-alkoxymethyl-3-hydroxy-4H-pyranones (3-hydroxy-6-propoxymethyl-4H-pyran-4-one and 6-butoxymethyl-3-hydroxy-4H-pyran-4-one), chelated with ^{111}In to assess cell uptake with leukocytes, erythrocytes, platelets (12). The function of the labelled cells was compared to those labelled with ^{111}In-tropolone, including the effect of plasma concentrations (12). Radiolabelling yields of both ^{111}In pyranone complexes with red blood cells was decreased by increasing of plasma concentrations. Efficient radiolabelling, however, was achieved when plasma concentration between 10% and 20% was presented. Although the cell labelling efficiency and intracellular stability of the radiolabel in the cells among ^{111}In complexes were similar, the perturbation of metalloenzymes was observed more in the ^{111}In-tropolone labelled cells than in the ^{111}In-3-hydroxy-6-propoxymethyl-4H-pyran-4-one labelled cells. Those results suggested the potential of ^{111}In pyranones complexes as radiotracers to label cells especially in the presence of a small amount of plasma.

1.1.2 Technetium-99m (^{99m}Tc) is the gamma emitting radionuclide most commonly used in diagnostic nuclear medicine due to generator availability and radiation energy suitable for detection with gamma camera. There are ^{99m}Tc complexes

which are either routinely used in the clinical practice or have been investigated for labelling of cells.

1.1.2.1 ^{99m}Tc hexamethylpropylene amine oxime (exametazime) (^{99m}Tc-HMPAO (Figure 1.3)), a neutral and lipophilic complex, has been used for imaging leukocytes since the 1980s in the same period as ^{111}In-oxine (29).

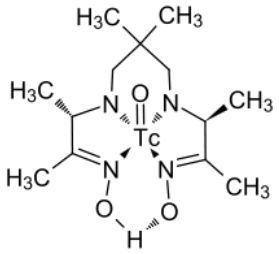

Figure 1.3: Structure of ^{99m}Tc-HMPAO

The ^{99m}Tc-HMPAO labelling procedure is similar to the ^{111}In-oxine labelling technique but it can be performed in plasma. The ^{99m}Tc-HMPAO becomes changed to a hydrophilic form after passing the cell membrane and moving to intact organelles. ^{99m}Tc-HMPAO showed preferential labelling of granulocytes over mononuclear cells (lymphocytes), and labelling yield was decreased when increasing the proportion of lymphocytes (30). Unlike ^{111}In-oxine, ^{99m}Tc-HMPAO does not bind to macromolecules in the cells, so higher amount of free ^{99m}Tc might be washed out. *In vitro* study showed 17 % dissociation of ^{99m}Tc-HMPAO from cell within one hour after cell labelling and an increased rate of efflux was found in biological conditions (23). Because of normal biodistribution of ^{99m}Tc-HMPAO-leukocytes in liver, spleen, bone marrow, kidneys and gastrointestinal tract, suboptimal detection of lesions in those areas occurs. However, labelling leukocytes with technetium-99m is cheaper and more available than indium-111. Moreover, its photon emission is more suitable for gamma camera to produce better resolution (31) with lower radiation exposure. This might be advantageous especially in paediatric patients. Comparisons of ^{99m}Tc-HMPAO and

^{111}In-oxine labelling to different cell types have been performed. ^{99m}Tc-HMPAO showed lower labelling efficiency (about 2-fold) and shorter retention time than ^{111}In-oxine (32). Migration of dendritic cells (DC) labelled with ^{99m}Tc-HMPAO *in vivo* was evaluated. The result indicated that ^{99m}Tc-HMPAO was not promising to study DC tracking because of low labelling efficiency and low stability in this cell type (33).

1.1.2.2 ^{99m}Tc tin fluoride colloid (^{99m}Tc–SnF_2 colloid) has been used to label white blood cells for scintigraphy of infection and inflammation in routine nuclear medicine especially in Australia (34). From *in vitro* studies, ^{99m}Tc–SnF_2 colloid preferentialy labelled erythrocytes (approximately 75%) over neutrophils (14%) and lymphocytes (12%) in whole blood. Additionally, most of radiotracer (75%) binds internally to neutrophils by phagocytosis mechanism whereas reversible and lower affinity binding to cells surface of other cell types was observed (35). Since biodistribution of whole blood containing ^{99m}Tc–SnF_2 colloid labelled leukocytes showed high accumulation in liver and spleen, those organs might take up the ^{99m}Tc–SnF_2 colloid released from the red cells *in vivo* (36). Limited detectability of lesions within or adjacent to those areas is a pitfall of this technique. Also the range of cell types that can be labelled is limited: it is only useful for phagocytic cells. However, technetium tin fluoride colloid is beneficial for imaging lesions in bowel (37).

1.1.2.3 ^{99m}Tc complexes with dithiocarbamates have been used to label cells. Dithiocarbamate (Figure 1.4) derivatives are known as chelators for variety of metals and are able to form lipophilic complex with radionuclides (38).

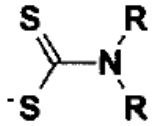

Figure 1.4: Structure of dithiocarbamates

Sampson and Solanki showed high efficiency of ^{99m}Tc diethyldithiocarbamate ($^{99m}TcN(DDC)_2$) to label white blood cells in crude leukocytes, with preferential labelling of granulocytes (39). In addition, after incubation with cell free plasma up to 4 hours, 77 % of tracer remained in the cells while no differences in cell viability between labelled cells and control were observed. Bis(N-ethoxy-N-ethyldithiocarbamate)nitride technetium-99m ($^{99m}TcN(NOET)_2$) (a lipophilic complex developed for myocardial perfusion imaging) showed high efficiency (more than 80%) to labelled pure granulocytes with no cytotoxicity. The localisation results from microautoradiography indicated that this tracer labelled nuclei rather than cytoplasm (40). A similar result was shown in ^{188}Re-$N(NOET)_2$ (40). Another study showed that increasing lipophilicity of dithiocarbamate derivatives ($CH_3(CH_2)_{n-2}CS_2MgBr$) by changing their aliphatic linear side chains leads to increased labelling efficiency with the whole blood as well as specific to label leukocytes (n =10 gave the highest labelling yield around 62%) (41).

1.2 Magnetic resonance imaging (MRI)

There have been large numbers of reports of methods for magnetic labelling of cells for tracking by magnetic resonance imaging (42, 43). In MRI a magnetic field is used to manipulate hydrogen nuclei (proton) in water in the tissues or organs to produce contrast. Differences in biochemical structures or proton density in tissues generate contrast in images which can be detected with MR imaging. MRI is commonly used in clinical practice because it is a non-invasive technique and generates high spatial resolution images that simultaneously give both physiological and anatomical information (44). Moreover, it is widely utilised for imaging labelled cells both in preclinical (45) and clinical studies (46). Basically, cells need to be labelled with magnetic resonance (MR) contrast agents such as gadolinium (Gd) based

compounds, superparamagnetic iron oxide particles (SPIO) or ultrasmall superparamagnetic iron oxide particles (USPIO).

1.2.1 Gadolinium (Gd) complexes have been widely used in clinical practice to detect tumours (47) and for labelling cells for experimental studies (48). Terreno *et al.*(49) demonstrated two approaches to incorporate Gd-based contrast agent (Gd-HPDO3A) into rat hepatocarcinoma cells. Electroporation and simple incubation showed differences in subcellular localisation of Gd, with Gd in the cytoplasm when delivered by electroporation but in endosomes when labelled by via simple incubation (49). However, the passive labelling required high concentration of Gd chelates and long incubation time (50). Electroporation techniques might stress labelled cells and cause a significant decrease in their viability and survival. In addition, the ability of cells to differentiate might be inhibited (51). Therefore, this method may be not suitable for clinical practice. A Gd chelate, Gadolinium-fullerenol, was developed and showed improvement of signal intensity in mesenchymal stem cells (MSC) however cell proliferation was diminished (52).

1.2.2 Superparamagnetic iron oxide nanoparticles (SPIO) consist of an iron oxide (magnetite) core and a hydrophilic coating (53). They have high relaxivities. There are many methods to prepare SPIOs resulting in variations in properties such as core size, shape and outer coating (e.g. dextran-coated). Those differences affect the ability to label cells (54), pharmacokinetics, biodistribution and intracellular uptake (55). Cells take up dextran-coated SPIOs via endocytosis mechanisms (e.g. phagocytosis, pinocytosis). Labelling studies were performed in non-phagocytic cells such as lymphocytes (56, 57) and in phagocytic cells such as neutrophils, macrophages and monocytes (58, 59) by incubating SPIOs with the cells. In addition, mesenchymal stem cells can be labelled with SPIO. Although this labelling technique has little or no

effected on cell properties, high concentration of labelled cells and long incubation times are required (60). Therefore, transfection reagents (61) or mechanical approaches such as electroporation (62) have been utilised to introduce contrast agents into the cells to improve labelling efficacy. In order to increase specificity to targeted cells, modifications of dextran coated SPIOs by covalently conjugating with polyclonal immunoglobulin G (63) or monoclonal antibody fragment (64) were developed.

Recently, there have been developments of magnetic resonance reporter genes for indirect labelling cells. Transduced cells expressing the iron storage protein ferritin can be visualised in MRI (65, 66). In addition, genes encoding the synthesis of iron oxide nanoparticles (like synthetic SPIO) from magnetotactic bacteria were used to transfect cells which could then be detected with MRI (67).

Ultrasmall superparamagnetic iron oxide particles (USPIO) around 10-40 nm in size, have strong relaxivity. USPIO were taken up by phagocytosis in macrophages in the reticuloendothelial system in the same manner as SPIO. There has been research to demonstrate accumulation of USPIO taken up cells in lymph nodes (68). The labelling efficiency of USPIO with non-phagocytic cells can be improved by attaching monoclonal antibodies to USPIO, resulting in increased labelling efficiency through receptor-mediated endocytosis (69). However, this technique could alter long term biological functions of cells so further investigation will be required.

Although MRI modality seems to be a promising technique to study cell migration, various limitations still remain. Sensitivity of this imaging technique is required to improve because currently MRI cannot detect low target density with small amounts of labelled cells. Signal in the labelled cells can be diluted along with cell division and the contrast agents can be transferred to neighbouring cells or tissues

especially following death of the labelled cells. Moreover, this modality is limited for implantable device patients.

1.3 Optical imaging (OI)

Optical imaging is another approach which has been widely used to label cells for tracking especially in preclinical research. For optical imaging, contrast agents used to label the cells generate visible light for detection by the specific devices. Two types of contrast are characterised according to how they produce the light: bioluminescence and fluorescence.

1.3.1 Bioluminescence used to label cells produces light from chemical reaction of substrates catalysed by enzymes converting chemical energy to light (3) which is detected by a charged coupled device (CCD) (70). This technique usually needs a genetic engineering approach to introduce a bioluminescence gene such as luciferase (*luc* gene) into target cells before transferring into the host (71). Consequently, transfected cells encode an enzyme to react with administered specific substrate (e.g. luciferin) to emit photons. In general, luminescence background level is very low in most animals resulting in rather high signal to noise ratio (72). However, the problems for this technique are the limited detection of signals in deep tissues (73) (because of light attenuation and scatter by tissues) and that the encoded enzymes and high administered amount of substrates have high potential to induce human immunogenicity (74). Therefore, this approach is limited to small animals for preclinical purposes.

1.3.2 Fluorescent imaging (FLI), fluorescent dyes or proteins which are incorporated into the cells are excited by external light to higher energy states before emitting longer wavelength photons (75). In the case of fluorescent proteins (such as

green fluorescent protein (GFP)), fluorescent genes are introduced to target cells genetically in the same manner as bioluminescence strategy. The expressed fluorescent proteins are excited and the emitted photons are detected. Alternatively, fluorescent dyes or probes are directly labelled to the cells. In case of dyes (e.g. DiD and DiO) which have lipophilic properties, they can intercalate in cell membrane of the targeted cells (76). However, the fluorescent signals can be decreased through cell proliferation and signals from labelled dead cells may be taken up by host phagocytic cells (77). Excitation light non-specifically activates endogenous molecules (e.g. collagen) in the tissues resulting in high background of autofluorescence (78). In addition, the limitation on imaging in deep tissues due to attenuation of both incident and emitted light is still a problem. Development of near infrared (NIR) fluorophores has helped solve these problem and detectable depth is enhanced to around 7-14 centimetres (79). Nonetheless, quantitative imaging from these depths is still difficult to address in clinical contexts.

Quantum dots (QD) are inorganic fluorophores that contain colloidal semiconductor cores usually coated with chemicals. The special properties of QD are that their emission is in the near infrared region, which reduces autofluorescence, and their photonic stability and brightness allows long observation in tissues, e.g. for over a week (80). The investigation of their potential toxicities still requires further research.

In the endogenous labelling techniques for both BLI and FLI, the targeted cells essentially require genetic engineering to express bioluminescent or fluorescent proteins. In case of exogenous label, probes or dyes can diffuse into cells or adhere to cell membranes (including unknown mechanisms) after simple incubation.

1.4 Positron emission tomography (PET) imaging

Since the advent of radionuclide cell tracking in the 1980's, advances in other areas of biomedicine have created new applications for *in vivo* cell tracking in humans. Understanding of the distinct role of different leukocyte types, and the development of methods for separating and isolating them, has led to new possibilities to exploit imaging to track individual immune cell types (81) (e.g. eosinophils (2, 82), neutrophils(2, 13, 82), T-lymphocytes (4) and dendritic cells (83) in cancer, atherosclerosis, stroke, transplant medicine, asthma and allergy. Developments in regenerative medicine and cell based therapies have created roles for tracking in cell-based therapies such as stem cells and chimeric antigen receptor-expressing T-lymphocytes (84, 85). Conventional cell labelling methods have been applied in some of these areas preclinically and in humans (2) but for clinical use some of these new applications will require detection of small lesions and small numbers of cells beyond the sensitivity of gamma camera imaging with ^{111}In (e.g. coronary artery disease, neurovascular inflammation and thrombus). This has led to widespread interest in developing positron-emitting radiolabels for cells to exploit the enhanced sensitivity, quantification and resolution of clinical PET compared to clinical scintigraphy and SPECT. Therefore positron-emitting radiotracers have been sought to label cells and are described below.

1.4.1 Fluorine-18 (^{18}F) is a short half life PET isotope (110 min). It is most often used clinically in form of ^{18}F-fluorodeoxyglucose (^{18}F-FDG). ^{18}F-FDG is a glucose analogue which can be taken up and incorporated into glucose metabolising cells (mostly in tumour cells) in a similar way to glucose. Since ^{18}F-FDG cannot be metabolised by enzymes after hexokinase in the glycolytic pathway, it is trapped after initial phosphorylation and the clearance is slow, thus resulting in accumulation of ^{18}F-

FDG inside the cells which can be detected by PET scanners (86). ^{18}F-FDG has been applied in diagnosis of many types of malignant cells including the staging of tumours. However, ^{18}F-FDG is not specific for tumour cells. Several studies indicated that infected and inflammatory cells also take up this tracer (87). Rudd *et al*. (87) reported that ^{18}F-FDG was accumulated in carotid plaques 3 hr after injection of radiotracer.

Since ^{18}F-FDG showed the possibility to detect inflammatory cells *in vivo*, several attempts to label autologous leukocytes with this tracer have been made but glucose in the incubation medium was found to influence the labelling efficiency and stability (88). In the labelling protocol from Forstrom *et al*., the highest labelling efficiency was approximately 78% when heparin was used as anticoagulant and ^{18}F-FDG was directly incubated with leukocyte pellets at 37^{o}C for 20 min (89). Viability of labelled cells was not affected after incubation with the tracer for 60 min. Loss of radiolabel was slightly increased from 13% at 1 hr to 26% at 4 hr of incubation. However, labelling efficiency of ^{18}F-FDG to leukocytes was not consistent (90-92) and lower than that of ^{111}In-oxine (90, 92). Prince and colleagues reported that the efflux rate of ^{18}F-FDG from labelled dendritic cells post labelling was more than 20% per hour (93). ^{18}F-FDG was used to label and image autologous human bone marrow cells in acute myocardial infarction (94). The labelled ^{18}F-FDG bone marrow cells (BMCs) and CD34 positive cells showed 92 to 96 % cell viability. Infarcted myocardium was also detected after intracoronary infusion by this tracer (94). Thus, this technique can possibly be applied to follow homing and distribution of BMCs in acute myocardial infarction treatment.

With the same number of lymphocytes, ^{18}F-FDG labelling of autologous T lymphocytes showed the same labelling efficiency as ^{111}In-oxine (around 64% and 68%) and was better than ^{99m}Tc-HMPAO (31%). Although those tracers did not affect

cell viability, ^{18}F-FDG and ^{111}In-oxine not only decreased T lymphocyte cytotoxic properties towards targeted cells (measured using the standard ^{51}Cr released assay) but also decreased cell proliferation (32). Circulating progenitor cells (CPC) from human and pig were labelled with ^{18}F-FDG to study tracking of CPC in acute myocardial infarction (MI) (95). The maximum labelling efficiency was around 90 % after incubation at 37^{o}C for 30 min. However, tracer was significantly dissociated from the cells to the extent of approximately 23% to 28% within 2 hr. The labelled cells in pig MI models were successfully delivered to myocardium infarction (95) and imaged with PET/CT. The attempt to use glucose transport inhibitor, phloretin (which previously showed efficiency to inhibit release of glucose in red blood cells), was only efficient to inhibit wash out of ^{18}F-FDG *in vitro* but not *in vivo* with C17.2 neural stem cells (C17.2 NSCs) in a tumour inflammation model (96).

Labelling efficiency and labelling stability are major disadvantages of ^{18}F-FDG labelled cells as well as short physical half life of ^{18}F (110 min) that is a significant limitation to following cells migration.

1.4.2 Gallium-68 (^{68}Ga) is a short lived positron emitting isotope (half life 68 min) which can be produced from either a ^{68}Ge/^{68}Ga generator or a cyclotron and now commercial generators are widely available. Since 1977, a lipophilic complex of gallium-68, ^{68}Ga-oxine, was reported for labelling erythrocytes and platelets (97). High labelling efficiency in RBCs was observed whereas inconsistent labelling yield with platelets was obtained. However, *in vivo* imaging of ^{68}Ga-oxine labelled red blood cells and platelets in dogs was successful, detecting the high blood pool organs (heart, liver and spleen) and showing accumulation in the endothelial injury of the carotid artery, respectively.

Other lipophilic complexes of ^{68}Ga such as those with tropolone and 2-mercaptopyridine-N-oxide (MPO) were investigated for the potential to label platelets (98, 99). Yano *et al*. studied the labelling of rabbit, dog and human platelets with ^{68}Ga-oxine, ^{68}Ga-tropolone and ^{68}Ga-MPO (98). The results showed that labelling yield of ^{68}Ga-MPO was most reproducible and labelling yield was dependent on the amount of the platelets. ^{68}Ga-MPO labelled platelets were used to image aorta injury in rabbit. The results of both PET imaging and tissue biodistribution of damaged aorta in rabbits injected with ^{68}Ga-MPO labelled platelets showed great accumulation of the activity in the lesions comparing to normal controls. ^{68}Ga-MPO labelled platelets showed good viability and *in vivo* labelling stability but were suboptimal to detect pulmonary embolus lesions in the patients (99) because ^{68}Ga-MPO labelled platelets remained in the blood circulation for hours after injection leading to low target to background ratio in the early period of study and later imaging was restricted dramatically by rapid decay of ^{68}Ga-MPO labelled platelets over the delay study.

Although ^{68}Ga complexes can be used to label cells, the major limitation is its short half life (68 min) that is not suitable for sequential studies.

1.4.3 Copper radioisotopes have been used for labelling cells. Copper (Cu) has various available radioisotopes including ^{60}Cu, ^{61}Cu, ^{62}Cu, ^{64}Cu and ^{67}Cu. Most are positron emitters which can be produced from either a cyclotron (^{60}Cu, ^{61}Cu, ^{64}Cu) or generator (^{62}Cu). Some copper radionuclides emit beta particles (^{64}Cu, ^{67}Cu), which are useful for therapeutic purposes. Copper isotopes have been reported to be promising for labelling peptides (100) and cells (92, 101-104). Among these copper isotopes, ^{64}Cu showed striking characteristics for studying cell migration. Physical decay modes of ^{64}Cu consist of electron capture (41%), positron (19%) which is suitable for PET imaging, and beta (40%) particles (105). In addition, its intermediate

half life, 12.7 hr, is appropriate for optimising labelling procedure as well as interval imaging for cell migration study over days. Cell labelling with copper-64 can be achieved using lipophilic tracers, such as complexes of bis(thiosemicarbazone) ligands (PTSM (106)), tropolonate (92) and PEG conjugates (104).

Bis-thiosemicarbazones (BTSCs) (such as diacetyl-bis(N^4-methylthiosemicarbazone) (ATSM) and pyruvaldehyde bis(N^4-methylthiosemicarbazone) (PTSM)) (Figure 1.5) form neutral lipophilic complexes with copper(II).

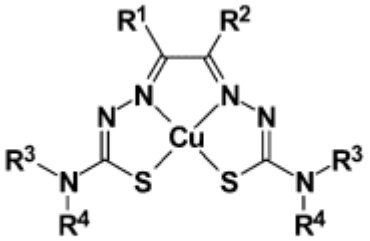

	R^1	R^2	R^3	R^4
GTS	H	H	H	H
GTSM	H	H	CH_3	H
PTS	CH_3	H	H	H
PTSM	CH_3	H	CH_3	H
$PTSM_2$	CH_3	H	CH_3	CH_3
PTSE	CH_3	H	C_2H_5	H
PTSP	CH_3	H	C_6H_5	H
ATS	CH_3	CH_3	H	H
ATSM	CH_3	CH_3	CH_3	H

Figure 1.5: Structure of bis(thiosemicarbazones (BTSCs) ligands complex with copper (107)

They have been utilised as bifunctional chelators (BFCs) (108) but the labelling yields were not consistent. In addition, high nonspecific binding to proteins and poor stabilities of these complexes were reported. Although complexes of bis-

thiosemicarbazones are not promising for BFC purposes, complex instability is an advantage for cell uptake. ^{64}Cu-ATSM has been investigated and available as a tracer for detecting hypoxic cells or tissues (109, 110) and has also been evaluated *in vitro* and *in vivo* as a therapeutic radiopharmaceutical (111). By imaging hypoxia it can potentially predict cancer patients' survival rate (112) in response to radiotherapy. However, the potential to label cells with ^{64}Cu-ATSM is limited owing to its redox potential allowed tracer efficient trapping only by cells in hypoxic conditions.

Another bis-thiosemicarbazone derivative, PTSM, forms a complex with copper that has less selectivity for hypoxia. PTSM is a lipophilic carrier molecule for carrying radiocopper to passively diffuse across cell membranes according to concentration gradients and its lipophilic property. The mechanism of Cu-PTSM labelling of cells has never been clearly proved. However, it is hypothesised that this copper complex passes into cells and becomes reduced to Cu(I) which is released from the complexes before copper trapping by intracellular molecules (101, 105) (Figure 1.6). Therefore, several studies have utilised Cu PTSM for labelling cells.

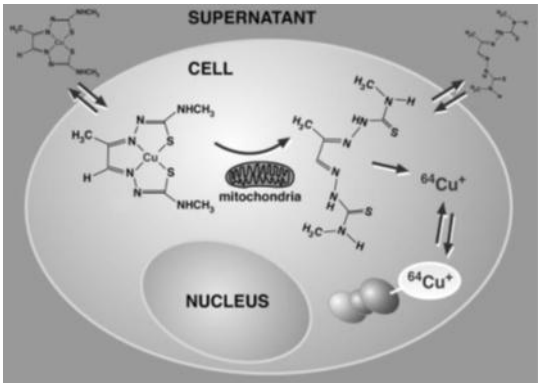

Figure 1.6: Diagram of Cu-PTSM uptake and retention by cell (101)

To study cell migration in mice, labelling of ^{64}Cu-PTSM and ^{18}F-FDG with glioma (C6) cells was compared (101). The labelling efficiency of ^{64}Cu-PTSM was moderately high, around 70%-80%, (in the presence of 5% FBS) after incubation for 5 hr with 5 μCi of ^{64}Cu-PTSM. The tracer influx into cells increased with incubation period. However, both tracers showed rapid efflux from labelled cells, to the extent of more than 15% and 35% of ^{64}Cu-PTSM and 15% and 45% of ^{18}F-FDG by 0.5 and 2 hr after labelling, respectively. Only approximately 22% of ^{64}Cu-PTSM was retained within the cells after incubation for 24 hr. Trypan blue and MTT assays indicated no alteration of cell viability and proliferation. *In vivo* imaging with C6 cells labelled with ^{64}Cu-PTSM in mouse models demonstrated that lungs were the initial distribution organs followed by migration into liver. In contrast, the free tracer was taken up directly in liver, which is known to be the main metabolising organ for copper. Thus, for the early time point (up to around 3 hr post injection) it was assumed that detectable radiocopper was mostly associated with the cells not free ^{64}Cu or ^{64}Cu-PTSM released from the cells. Although the *in vivo* imaging could be performed up to 2 days after injection (around 18 hr) due to relatively long half life of ^{64}Cu, tracking of radiolabelled cells over this period required the assumption that detected radioactivity in the liver is due to radiocopper labelled C6 cells or free ^{64}Cu-PTSM, which could not be proved, because the accumulation activity in the liver of mice injected ^{64}Cu-PTSM labelled C6 cells and ^{64}Cu-PTSM alone were in the same range. ^{64}Cu-PTSM-labelled lymphocytes have also been imaged in mouse models. The results showed firstly uptake in the lungs before homing to the spleen. Altogether, ^{64}Cu-PTSM showed potential to be a tracer for study cell tracking either *in vitro* or *in vivo* in the short term. The leakage issue, however, requires further attention and improvement before tracking over several hours or days could be relied upon.

Imaging of rhesus monkey mesenchymal stem cells (rhMSCs) and CD34 positive cells labelled with ^{64}Cu-PTSM was performed by Huang and co-workers (102). From the results of ^{64}Cu-PTSM radiolabelling cells, rhMSCs showed higher retention of radiocopper than $CD34^+$ cells. These phenomena possibly relate to either size (rhMSCs are bigger than $CD34^+$) or reduction potential differences between those cells. Studies of dose dependent effects of ^{64}Cu-PTSM labelled rhMSCs cells at the concentration of 40 μCi/ml showed that growth rate and some differentiation properties of rhMSCs (such as osteogenic, chondrogenic differentiation) were altered with increasing of ^{64}Cu-PTSM concentration. However, an optimum concentration of ^{64}Cu-PTSM was found at which it was able to label cells without any adverse effects and different responses to radiation depended on cell types. This leads to the conclusion that ^{64}Cu-PTSM can be used for cell migration studies but optimised doses have to be verified for each cell type.

For a recent study reported by Griessinger *et al*., ^{64}Cu-PTSM was used to label mouse Th1 cells (mouse ovalbumin (OVA) T-cells receptor transgenic interferon (IFN)-γ-producing CD4+T (Th1) cells). Tracking the homing of ^{64}Cu-PTSM labelled Th1 cells in OVA immunised and non-immunised mice challenged with OVA to induce airway hypersensitivity to OVA were evaluated (106). Although the *in vivo* imaging results showed that OVA-Th1 cells labelled with ^{64}Cu-PTSM could be tracked to the lymph node (pulmonary lymph nodes) in immunised mice challenged with OVA for up to 48 hr after injection labelled cells, the retention of the radiotracer in the labelled cells was less than 50% by 5 hr after labelling, and only 14% remained in the cells after 24 hr.

Copper complexes with different BTSC derivatives were compared to exploit selectivity of copper complexes in hypoxic cells (107, 109). The experiments compared

the uptake of the tracers in either mouse mammary tumour cells or Chinese hamster ovary cells with different oxygen levels. Among them, ^{64}Cu-GTS and ^{64}Cu-GTSM exhibited non-hypoxia-targeted uptake by the cells (i.e. efficient uptake both at low oxygen concentration and at normal oxygen concentration). Copper complexes of PTSM and PTS on the other hand showed marginally higher uptake in hypoxic cells than in normoxic cells, while several complexes of ligands related to ATSM showed high selectivity for hypoxia. Based on these structure-activity relationships, copper complexes of GTS and GTSM might be proposed to be the most suitable tracers for labelling cells because they are extremely efficiently taken up in cells independently of hypoxia.

Tropolone (water-soluble metal chelator used for ^{111}In-labelling as discussed above) has been used to complex with copper-64 for labelling human leukocytes, compared to ^{111}In-oxine and ^{18}F-FDG in the study of Bhargava *et al*. (92). The results showed significant instability of ^{64}Cu-tropolone association with the labelled cells. The labelling efficiency was in the same range as ^{111}In-oxine and greater than that of ^{18}F-FDG. However, the efflux of ^{64}Cu from the labelled cells was significant even in the first few hours after labelling and higher than 75% was eluted from the cells by 24 hr. The authors improved retention of ^{64}Cu-tropolone in the labelled cells by co-incubating a second chelator, a membrane-permeable divalent calcium chelator (quin-MF/AM [2-(2-amino-4-methyl-5-fluorophenozy) methyl-8-aminoquinoline-N, N, N', N'-tetra-acetic acid]), with ^{64}Cu-tropolone and the cells. After quin-MF/AM passes through the membrane, intracellular esterases enzymes convert the quin-MF/AM to a negatively charged (hydrolysed) form with high affinity for Cu^{2+} leading to rapid binding between the chelator and the free copper released from ^{64}Cu-tropolone (Cu-quin/MF) resulting in stable ^{64}Cu complex remaining trapped inside the cells. With this procedure, the retention of the radioactivity at 24 hr post labelling of ^{64}Cu labelled white blood cells

was significantly increased to around 80%, which can be compared with ^{111}In-WBC at the same time point. In comparison to viability of cells radiolabelled with the other radionuclides, ^{64}Cu-WBC showed highest viability 24 hr post labelling. The improvement of ^{64}Cu-tropolone retention in the cells was an innovative and promising approach, however, the modified procedure might not be suitable for the clinical setting.

An alternative approach has been to synthesis a copper-64 complex of polyethylenimine (PEI)-polyethylene glycol (PEG) (104). PEI it is widely used as a transfection agent so it was thought that the copper complex with this compound might efficiently deliver the radiocopper into cells. PEG was incorporated into the copper complex in order to decrease toxicity of PEI. Uptake and efflux in U87MG cells (human glioblastoma cells) were compared among ^{64}Cu-PTSM, ^{64}Cu-PEI and ^{64}Cu-PEI-PEG. ^{64}Cu-PTSM showed both greatest taken up into the cells and also highest percentage of retention (36%) in the labelled cells at 27 hr after labelling. Nevertheless the authors suggested that ^{64}Cu-PEI and ^{64}Cu-PEI-PEG can be used for cell tracking and tumour imaging. However, these radiocopper complexes were unable to overcome the problem of low retention of the tracers in the labelled cells.

Altogether, various copper complexes have been subjected to investigations and often offer excellent cell labelling yield but the efflux problem consistently remains. This might be caused by innate mechanism to control copper level in the cells, and is a severe limiting factor in the application of ^{64}Cu for cell tracking.

1.5 Indirect cell labelling

Genetic engineering of reporter genes is performed under regulation of their promoters within either plasmid vectors or viral vectors (113) prior to introduction into

the targeted cells. Stable transfected cells are selected to prevent loss of reporter gene expression upon cell division. Then, probes (SPECT or PET isotopes) that specifically interact with proteins encoded by the reporter genes are used to image with SPECT or PET. Currently used reporter genes encode for three types of proteins including surface receptors, enzymes that react with radiotracer probes, or transporter proteins.

1.5.1 Receptor gene, dopamine subtype 2 receptor (D_2R) is one of interesting reporter gene used to study cells in brain with PET probes such as ^{11}C-raclopride (114) and ^{18}F-fluoroethylspiperone (^{18}F–FESP) (115). However, D_2R is highly expressed in brain generating high background leading to difficulty in discriminating between normal and reporter protein expression. Thus, mutation of this receptor gene has been developed to overcome this problem (115).

Somatostatin receptor subtype 2 ($SSTr_2$) is another potential reporter gene (116). Transduced cells produced $SSTr_2$ which can bind to somatostatin analogs with high affinity. ^{111}In-octreotide (approved for use in clinical practice) is used as a specific probe for imaging or labelling these reporter gene-expressing cells (116).

However, the disadvantages of this technique still remain for examples, the encoding receptor protein must function as proper membrane protein and highly numbers of expressed receptors are needed.

1.5.2 Reporter gene, an example of a reporter gene encoding an enzyme is herpes simplex virus type 1 thymidine kinase (HSV1-tk) and its mutant form, HSV1-sr39tk. These have been widely used as reporter genes to monitor cell tracking *in vivo*. ^{131}I-2-fluoro-2-deoxy-5-iodo-1-D-arabinofuranosyluracil (^{131}I-FIAU) was used to study tracking of T-lymphocytes that had been transduced with HSV1-tk (85). No alteration of cytotoxicity property of those cells was shown in the study. Tracking of Epstein -

Barr virus (EBV) specific T cells by ^{131}I-FIAU both *ex vivo* and *in vivo* in mice has been investigated (117). Sequential imaging was performed at 1 hr, 1 day and 4 days after infusion of *ex vivo* labelled cells. The transduced cells accumulated ^{131}I-FIAU and showed no loss of their function to eliminate specific tumour. However, resolution of imaging with I-131 is suboptimum because its emitted gamma energy is unsuitable with SPECT detector.

Recently, imaging of reporter gene-modified CD8+ cytotoxic T cells (CTLs containing IL-13 and HSV1-tk used for treating glioblastoma multiforme (GBM)) was successfully performed in patients (118). Three days after administration of modified cells, ^{18}F-FHBG was used as a probe showing the localisation of engineered CTLs both in the tumour (in brain) and related organs. Furthermore, from a study by Su *et al*., not only can transduced cells be detected and imaged but it was also possible to estimate the number of cells by correlation between PET signal intensity and cell number (119).

1.5.3 Genes encoding membrane transporter proteins have been investigated, including the human norepinephrine transporter (hNET) and sodium iodide symporter (NIS). NIS has been used as either a reporter gene or a therapeutic gene (120). It is a membrane glycoprotein that actively transports two sodium ions with one iodide ion across the cell membrane. Usually, NIS is highly expressed in thyroid cells and to a lesser extent in other organs including salivary gland and stomach. Not only I^- but also other anions such as TcO_4^-, ReO_4^-, NO_3^-, Br^- and ClO_4^- can be cotransported with sodium ion (121) so cells transfected with NIS can be probed with a number of isotopes. However, because the organification processes that normally trap iodine in thyroid are absent in transfected cells, the probes are readily washed out.

Recently, imaging of measles virus engineered to express NIS (MV-NIS) and MV-Edm (not containing NIS) in myeloma xenografts mice was performed with

radioiodide (122). On days 3 and 9 after viral administration, only MV-NIS showed uptake of the radiotracers. The higher concentration of radioiodide in the tumour in day 9 might be due to proliferation of engineered virus causing an increase in NIS expression.

Tracking of rat cardiac-derived stem cells (rCDCs) transfected with human NIS (hNIS) in heart was performed post transplantation for 10 days by using I-124 as a probe (123). Although adverse effects on cell viability and proliferation were not observed, low contrast ratio was evident. This may be from non-ideal imaging characteristics of I-124, which emits positron from only 26% of decays. Thus, other PET isotopes which have better properties of imaging should be further considered. For example, ^{18}F-tetrafluoroborate (BF_4^-) may be transported via NIS similarly to other anions (124). Its tetrahedral geometry with an anionic volume similar to iodide ion and pertechnetate suggest the possibility to use it as a probe for NIS (125).

Recently, combinations of two or three reporter genes have been developed. Cao and co-worker utilised stable transfection of three reporter genes (monomeric red fluorescence (mrfp), firefly luciferase (fluc) and truncated thymidine kinase (ttk)) in murine embryonic stem cells (ES) to image ES transplantation in the myocardium (126). Significant differences in cell viability and proliferation between transfected cells and control cells were not observed by CyQuant cell proliferation assay and trypan blue exclusion assay for 4 weeks. Additionally, differentiation of transduced ES cells to cardiomyocytes showed the same rates as control cells in the *in vitro* studies. The bioluminescence and PET imaging demonstrated an increase in their signals during week 1 to 4, indicating that transduced ES cells survive and proliferate *in vivo*.

An advantage of reporter gene labelling is that reporter proteins expressed by stable transfected cells are not diluted over cell divisions or cell proliferations.

Radiotracer probes are able to repeat detection of cell tracking over time. Furthermore, detected signals are only generated from viable transduced cells. However, there are disadvantages of reporter genes for example reporter genes cause immunogenic responses or other toxicities. Reporter gene silencing and perturbation of transduced cell behaviour may occur. In addition, transfection stability needs to be improved to obtain stable transfected cells.

Conclusion

In conclusion, long lived PET radiotracers which offer efficient intracellular uptake and remain stably associated with the labelled cells over a sustained period of time would be desirable. New direct labelling tracers have been sought in order to implement into clinical routine services to use PET to improve quality of the diagnostic use of radiolabelled cells or for the advanced applications of cell labelling and cell trafficking, but satisfactory agents are not yet available. This thesis assesses two radiolabelling approaches to address this problem, using ^{64}Cu and ^{89}Zr.

Chapter 2: Synthesis and *in vitro* studies of lipophilic complexes of ^{64}Cu

2.1 Introduction

Various applications of cells labelling, such as following autologous radiolabelling blood components, stem cells and immune cells), require the half life of the radiotracers for labelling cells to be long enough to allow tracking labelled cells for period of times. Detecting particularly small lesions or tracking low numbers of radiolabelled cells poses particular challenges for cell labelling. Comparing positron emission radiotracers to those of single photon emission for tracking labelled cells, PET scanning is expected to provide better resolution and quantification of the amount of radiolabelled cells *in vivo*. The intermediate long lived PET radionuclide, ^{64}Cu is now increasingly produced in a number of cyclotron centres may provide a solution to the half life and positron emission requirement. It emits suitable low-energy positrons for PET detector with the physical half life of 12.7 hr. Therefore ^{64}Cu is an attractive PET radioisotope for *in vivo* tracking of labelled cells. Related copper information in the aspects of its chemistry, metabolism, production and chelators for copper was summarised as follows.

2.1.1 Chemistry of Copper

Copper in aqueous solution usually exists in one of three oxidation states (I, II and III) of which Cu(I) and Cu(II) are more usual. Cu(I) can form complexes with thioethers, phosphines, nitriles, isonitriles, nitriles, cyanide, iodide and thiolates (105). Some ligands (thiolates, phosphines and iodide) also act as reducing agents to reduce Cu(II) (e.g. in copper chloride) to Cu(I). Cu(II) on the other hand shows a preference to react with amines, imines and H_2O. These groups have less polarisation and bind less

covalently compared to those groups that bind to Cu(I) (105). Cu(II) forms various type of complexes such as square planar and octahedral. The preference for oxidation states depends on the ligand types. Bifunctional chelators (e.g. macrocycles, aromatic macrocycles) play an important role in stabilising Cu(II) in copper radiopharmaceuticals. The highest oxidation state of copper, Cu(III), needs strong π-donating ligands, typically deprotonated amide groups.

2.1.2 Metabolism of Copper

Most plasma copper binds to proteins such as albumin, ceruloplasmin, transcuprein and metalloenzymes, and to amino acids especially histidine. Copper(II) is found to associate with transport proteins (albumin and transcuprein) and then transfer to liver cells via small amino acid (histidine) complexes resulting in rapid copper clearance from blood. Liver synthesises ceruloplasmin and metallothionein from taken up copper. Thus, copper exists in blood circulation in form of ceruloplasmin (127). Although copper is cleared rapidly from blood, the retention time of radiocopper in circulation can be increased in the presence of bifunctional chelators.

2.1.3 Copper production

Radiocopper can be produced from a reactor (^{64}Cu, ^{66}Cu, ^{67}Cu), cyclotron (^{60}Cu, ^{61}Cu, ^{62}Cu, ^{64}Cu) or a generator (^{62}Cu). In reactor production, both direct (known as thermal neutron reaction (^{63}Cu (n, γ)) and fast neutron reaction (^{64}Zn(n, p)) generate copper-64 with varying specific activity. McCarthy et al. reported a method to produce copper-64 using enriched ^{64}Ni plated as a target from a small biomedical cyclotron (128). Ion exchange chromatography was used to separate the copper-64 product from the nickel target. This method showed high specific activity and purity of

copper-64. Moreover, the nickel target can be reused and the recovery yield of ^{64}Ni was around 90 %.

2.1.4 Chelators for Copper

In order to bind or incorporate copper to cells or interesting tissues, appropriate chelator ligands are required either to ensure kinetic stability of complexes (when radiolabelling proteins for example) or to exploit molecular properties of copper-chelates complexes such as redox. Targeting biomolecules such as proteins and antibodies requires bifunctional chelators (BFCs) to stabilize complexes with radiocopper *in vivo* (129).

The functions of BFCs (Figure 2.1) are coordination with metal ions and covalent binding to the targeting molecules. Various types of BFCs for copper radionuclides have been investigated.

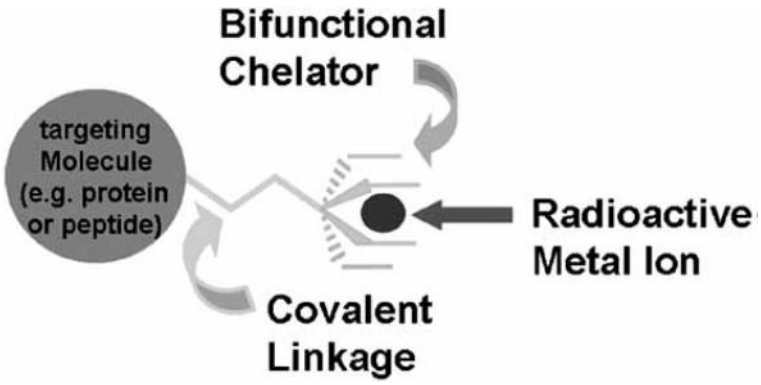

Figure 2.1: Diagram of bifunctional chelator function

Acyclic polyamine carboxylate ligands and their derivatives including DTPA and EDTA have been evaluated. Studies of serum stabilities of radiocopper complexes were performed and the results indicated a rapid dissociation of copper. Only 35% and

18% of the original copper complexes which remained intact in human serum after three days (130).

Development of macrocyclic polyaminocarboxylates (TETA, DOTA and NOTA) overcame the problem of instability in serum. BFCs in this group can enhance stability of copper complexes and are widely used to conjugate with biomolecules (e.g. antibodies, peptides) (131). Alternatively, cyclic polyamines (e.g. cyclam) rapidly form complexes with copper and show kinetic inertness in physiologic conditions. Other ligands have been studied such as N_2O_2 Schiff-base derivatives (for brain imaging), and diphosphine complexes (105).

Bis (thiosemicarbazones) (BTSCs) such as ATSM, PTSM and GTSM were described previously in Chapter 1, section 1.4.3. In brief, owing to instability of copper BTSCs complexes, BTSCs are unsuitable for bifunction chelator purpose. On the other hand the labile property of those lipophilic copper complexes is an advantage for delivering radiocopper into the cells because the complexes are reduced inside cells leading to release of copper which becomes bound to intracellular molecules (101). The selectivity of these copper complexes taken up by the cells is dependent on their redox potential. As summarised previously, the results of the uptake of copper BTSCs complexes indicated that GTSM was efficiently extracted into cells. Then, Cu-GTSM complex might be suitable as a tracer for labelling cells.

Sampson and Solanki studied lipophilic Tc-99m complexes of dithiocarbamate (widely used as metals chelator) for labelling leukocytes (39). Not only was excellent uptake of the radiotracer in white blood cells observed, but also stability in the labelled cells was higher than 75% after labelling for 4 hr. So, dithicarbamate ligands may also be suitable for investigation as lipophilic radiocopper chelators for the cell tracking purposes.

2.2 Aims

The aims in this section were to synthesise a range of lipophilic ^{64}Cu complexes with bis(thiosemicarbazone) and dithiocarbamate ligands, designed to enter cells by virtue of their lipophilicity and dissociate bioreductively inside cells. Characterisation of the radiotracer and optimisation of the amount of ligand for synthesis the radiocomplex was carried out.

In addition, the studies aimed to evaluate the copper complexes as cell labelling agents. Experiments were conducted to determine the rate and efficiency of cell labelling with ^{64}Cu BTSC and ^{64}Cu DTC complexes, and to determine the rate of efflux of radioactivity from cells labelled with these tracers and hence evaluate their potential as radiotracers for cell tracking over hours and days. Comparison of labelling efficiencies and cellular retention in various types of cells among tracers was performed in order to seek out the tracers best suited for labelling cells.

2.3 Methods

2.3.1 Radiolabelling of ^{64}Cu complexes

In order to synthesis ^{64}Cu BTSC complexes and ^{64}Cu DTC complexes, ^{64}Cu-PTSM and ^{64}Cu $(DEDTC)_2$ were chosen as the representative for each group of ligand. ^{64}Cu-PTSM complex was synthesised as follows. ^{64}Cu was kindly provided by Dr. Karen Shaw and was produced at the PET Centre, St Thomas' Hospital, London (132)**.** ^{64}Cu was produced from enriched ^{64}Ni bombarded with 11 MeV protons. ^{64}Cu was dissolved from the ^{64}Ni target with 9 M HCl and then purified using a column packed with AG1-8X anion exchange resin (Bio-Rad, UK). ^{64}Cu was eluted from the column with HCl. So, ^{64}Cu was provided in the form of $^{64}CuCl_2$ (typically the fractions

contained 1 M HCl). PTSM was kindly provided by Prof. Philip Blower, Department of Imaging Sciences and Biomedical Engineering, King's College London, London (133). PTSM was dissolved in dimethyl sulfoxide (DMSO) at a concentration of 1 mg/ml. Ten μl of PTSM solution was added to $^{64}CuCl_2$ (activity between 50 MBq to 80 MBq) and deionised water was used to make a final volume to around 1 ml before gentle shaking to mix the reaction solution. The mixture was incubated at the room temperature for 15 min. A SEP-PAK® C18 Classic cartridge (Waters, UK) was used to purify ^{64}Cu-PTSM. The cartridge had been previously equilibrated with 3 ml of absolute ethanol followed by 3 ml of deionised water. The solution was then filtered through the pre-equilibrated C18 cartridge. Five ml of water was washed through the column to remove free ^{64}Cu before ^{64}Cu-PTSM was eluted with 0.5 ml of absolute ethanol. The activity of ^{64}Cu-PTSM was measured using radioisotope dose calibrator (CRC-25R Capintec, USA).

Apart from PTSM, other BTSC ligands; PTS, GTS and GTSM kindly provided from Prof. Philip Blower were chosen to synthesise radiocopper complexes. The labelling procedure and determination of labelling purity followed those of ^{64}Cu PTSM.

For labelling of ^{64}Cu diethyl dithiocarbamate ($^{64}Cu(DEDTC)_2$), $^{64}CuCl_2$ was buffered with 2 equivalent volumes of 3 M sodium acetate to reach pH of 6.5 – 7.0. The amount of DEDTC was optimised to achieve acceptable radiolabelling efficiency with the lowest amount of ligand. A solution of sodium diethyldithiocarbamate trihydrate ($(C_2H_5)_2NCS_2Na.3H_2O$) (Sigma, UK) was prepared at concentrations of 1, 0.1, 0.01, 0.001 mg/ml in 0.9% normal saline. Twenty μl of the solution for each concentration was added (corresponding to 20 μg, 2 μg, 0.2 μg and 0.02 μg of DEDTC) and gently stirred with the ^{64}Cu acetate for 20 min at room temperature. The

^{64}Cu (DEDTC)$_2$ was purified by SEP-PAK® C18 column with the same procedure for ^{64}Cu-PTSM as described above.

Other ^{64}Cu DTC complexes e.g. dimethyldithiocarbamate (DMDTC) and dipropyldithiocarbamate (DPDTC) were synthesised in order to evaluate their potential for cell labelling. The optimised amount of DEDTC and synthesis procedure for ^{64}Cu (DEDTC)$_2$ were applied to synthesise the other ^{64}Cu DTC complexes (^{64}Cu (DMDTC)$_2$ and ^{64}Cu (DPDTC)$_2$).

2.3.2 Thin layer chromatography (TLC) and high performance liquid chromatography (HPLC) of copper diethydithiocarbamate

In order to verify the R_f and elution time^{64}Cu (DEDTC)$_2$ in HPLC and TLC systems, cold copper diethyldithiocarbamate (Cu (DEDTC)$_2$) was produced from the reaction between cupric sulphate ($CuSO_4.5H_2O$) (Sigma, USA) and sodium diethyldithiocarbamate trihydrate with a molar ratio 1:2, respectively. A solution of 125.5 mM sodium diethyldithiocarbamate trihydrate and 63 mM cupric sulphate was freshly prepared. The copper solution was added dropwise to the stirred sodium diethyldithiocarbamate solution. The solution was continuously stirred for 1 hr. Crystals of the product Cu (DEDTC)$_2$ were filtered, washed with water then dried in a 50^{o}C oven for 5 hr. Then 1 mg of Cu (DEDTC)$_2$ (black precipitate) was dissolved in 5 ml methanol. One microlitre of this solution was spotted on silica gel 60 F_{254} strips (1 cm x 10 cm), (TLC-SG), (Merck, Germany) as a stationary phase, ethanol was used as a mobile phase. The R_f of the copper complex in this system was determined. Meanwhile, copper sulphate ($CuSO_4$) solution was used as a standard for R_f of free copper in the same TLC system.

Additionally, sodium diethyldithiocarbamate, cold and hot Cu $(DEDTC)_2$ (^{64}Cu $(DEDTC)_2$) and ^{64}Cu acetate were analysed by reverse phase HPLC (RP-HPLC) using a C18 column (Agilent Eclipse XDB-C18, USA). The mobile phase was prepared as a gradient consisting of water with 0.1% trifluoroacetic acid (TFA) as a solvent A and acetonitrile containing 0.1% TFA as solvent B with a flow rate of 1 ml/min. The gradient was as follows: solvent A: solvent B as 90:10 % at start to 5:95 % over 15 min, hold for 15 min and then reverse to 90:10 % (A:B) over 5 min. The UV detection wavelength was set at 220 nm in series with radio-detector.

2.3.3 Determination of radiolabelling efficiency and radiochemical purity

Various amount of DEDTC (as mentioned in section 2.3.1) were used to synthesise ^{64}Cu $(DEDTC)_2$ and then radiolabelling efficiency was examined by radio-TLC using TLC-SG as the stationary phase and absolute ethanol as the mobile phase prior to purifying with SEP-PAK® C18 column. Radiochemical purities of the purified radiocopper complexes were also assessed by radio-TLC, using the same TLC system.

One microlitre of the synthesised solution and ^{64}Cu acetate was applied onto a TLC strip (1 cm x 10 cm) at 0.5 cm from the edge and the strip was placed in ethanol (lower than 0.5 cm in depth). The mobile phase was allowed to run to reach 9.50 cm of the strip. It was removed and dried in air. The radio-chromatogram of the TLC strip was then used to determine radiolabelling efficiency or radiochemical purity using a TLC scanner (LabLogic, UK) fitted with a $\beta^{-/+}$ detector (B-FC-3600) using Laura (v. 4.0.3.75) software (LabLogic, UK). The radiochemical purities of the radiocopper complexes were greater than 95% in all the subsequent experiments. In addition, to evaluate shelf life of ^{64}Cu $(DEDTC)_2$, quality control of this tracer was performed 24 hr after preparation.

2.3.4 Cell culture

Mouse macrophage cell line J774, human colorectal cancer cell line HCT 116, and murine multiple myeloma cell line eGFP-5T33 were chosen for the *in vitro* studies in this section. J774 cells were kindly provided by Dr. Helen Collins, Department of Infectious Diseases, King's College London and eGFP-5T33 cells were provided by Dr Yolanda Calle (University of Roehampton (former lecturer at King's College London; further information about this cell line is provided in chapter 4)) and HCT 116 cell line was purchased from European Collection of Cell Cultures (ECACC). J774 and HCT 116 cells were cultured as adhesion cells. J774 was grown in high glucose (4.5 g/L), Dulbecco's Modified Eagle's Medium (DMEM) supplemented with 2 mM L-glutamine, penicillin/streptomycin (5 ml/500 ml of 5000 UI/ ml pen /5000 μg/ml strep.), 1 mM sodium pyruvate, 10 mM HEPES and 10 % foetal bovine serum by volume, under humidified atmosphere at 37^{o}C with 5% CO_2. HCT 116 cells were cultured in McCoy's 5a supplemented with 2 mM L-glutamine, penicillin/streptomycin (5 ml/500 ml of 5000 UI/ ml pen./5000 μg/ml strep.) and 10 % foetal bovine serum. eGFP-5T33 cells were grown in suspension culture in RPMI 1640 supplemented with 10% foetal bovine serum, L-glutamine and penicillin/streptomycin. Cells were semi-continuously cultured in humidified 37^{o}C with 5% CO_2. Cells were subcultured by transferring cell suspensions to new 50 ml Falcon tubes followed by centrifugation at 2000 RPM for 5 min. The supernatant was discarded and the cell pellet was resuspended in fresh culture medium and transferred to new culture flask. In order to prepare cells for particular experiments, cell pellets were washed with PBS twice before counting cell numbers for preparing cell concentrations required for each study.

Radiolabelling of J774 and HCT 116 cells was investigated in 24 well plates. One day before the experiments, J774 and HCT 116 cells were harvested and seeded in

24 well plates with a density of 5 x 10^5 cells and 3 x 10^5 cells per well in 0.5 ml medium, respectively.

Radiolabelling of J774 and eGFP-5T33 cells was also studied in the glass tubes. On the experiment day, J774 cells were harvested by scraping and resuspended in the serum free medium. Washed eGFP-5T33 cells were prepared in serum free medium. Cells were counted and then 1 x 10^6 cells of either type in 450 μl serum free medium were dispensed into the glass tubes.

2.3.5 Radiolabelling the complexes of ^{64}Cu bis(thiosemicarbazones) (BTSCs) and ^{64}Cu dithiocarbamate (DTC) analogues for *in vitro* studies

BTSC ligands, PTS, PTSM, GTS and GTSM were provided by Prof. Philip Blower (133) and dipropyldithiocarbamate (DPDTC) was synthesised and provided by Dr. David Berry while dimethyldithiocarbamate (DMDTC) and diethyldithiocarbamate (DEDTC) were purchased from Sigma, USA.

All of BTSC ligands and DTC analogues were labelled with ^{64}Cu and evaluated for intracellular accumulation and retention. The labelling and quality control methods were described in section 2.3.1. In brief, $^{64}CuCl_2$ or ^{64}Cu acetate was used to synthesise the complexes with BTSCs and DTCs, respectively. Ten microlitres of 1 mg/ml BTSCs in DMSO were added to $^{64}CuCl_2$ and the product was purified with SEP-PAK® C18 column. The ^{64}Cu BTSC complexes were eluted with absolute ethanol. Meanwhile 20 μl of 1 mg/ml of DTCs in 0.9% saline were added to ^{64}Cu acetate and resulting complexes were purified with pre-equilibrated SEP-PAK® C18 cartridge (with ethanol). The purified ^{64}Cu complexes were eluted from the cartridge using absolute ethanol. Radiochemical purity (RCP) of the ^{64}Cu complexes was examined

with the TLC system previously described. RCP of the radiocopper complexes used in the following experiments was always greater than 95%.

2.3.6 *In vitro* cell uptake of ^{64}Cu complexes

This study aimed to determine the intracellular uptake of radiocopper complexes. Two different procedures were evaluated to determine the uptake as described below.

2.3.6.1 Reaction in 24 well plates with J774 cells and HCT 116 cells

The cell cultures in 24 well plates prepared as described in the previous section were used for radiotracer uptake study. Protocols for cell uptake were as follows. The cultured medium was removed from the wells and cells were washed twice with warmed Hanks' balanced salt solution (HBSS) (with calcium and magnesium). The exact radioactivity of tracers in ethanol (^{64}Cu-PTSM and ^{64}Cu $(DEDTC)_2$) was measured in a dose calibrator and each sample was diluted in warmed HBSS to a final concentration of 0.2 MBq per ml (containing ethanol less than 1% after dilution). The radiotracer (0.1 MBq, 500 µl) was added to each well and incubated at 37^{o}C with 5% CO_2. The uptake was evaluated after incubation for 1, 5, 10, 20, 40, 60 and 120 min (each experiment was done in triplicate). At each time point, the supernatant was removed from a well and the adherent cells were washed twice with 0.5 ml cold HBSS. Both supernatant and washing buffer were collected. Subsequently, cells were disrupted and collected by incubation with 500 µl of 1 M sodium hydroxide (NaOH) solution for 10 min. These cell lysates and supernatants from each well were measured by gamma counter (1282 Compugamma, LKB Wallac, Australia) as counts per minute (CPM). Following counting activity, the protein content of lysed cells (Pr) was assayed by using BCA protein assay kit. The cellular uptake was calculated as follows:

The cellular uptake/μg protein = ((CPM_{cell} / (CPM_{cell} + CPM_{sup})*100)/Pr).

Where CPM_{cell} = the count rate in the cells

CPM_{sup} = the count rate in the corresponding supernatant

Pr = the protein content of lysed cells (microgram)

2.3.6.2 Reaction in glass test tubes with J774 cells and eGFP-5T33 cells

In this section, intracellular uptake of the ^{64}Cu complexes was investigated in the tubes using the procedure described as follows.

The stock solutions of ^{64}Cu BTSCs and ^{64}Cu DTCs complexes in ethanol were prepared by diluting the radiocopper complexes to a concentration of 2 MBq/ml (0.1 MBq per 50 μl) with serum free medium. Then 50 μl of the stock solution was added to the test tube containing 1 x 10^6 cells in 450 μl (serum free medium) in triplicate for each time point. The reactions were incubated at the room temperature. The intracellular accumulations by the cells were determined after adding the radiocopper tracers for 1, 15, 30, 45 and 60 min. The ^{64}Cu (BTSC) complexes of PTS, PTSM, and GTSM (^{64}Cu-PTS, ^{64}Cu-PTSM and ^{64}Cu-GTSM, respectively) and ^{64}Cu (DTC) complexes of DMDTC and DEDTC (^{64}Cu $(DMDTC)_2$ and ^{64}Cu $(DPDTC)_2$, respectively) were investigated in J774 cells and eGFP-5T33 cells whereas ^{64}Cu-GTS and ^{64}Cu $(DPDTC)_2$ were also investigated in J774 cells. At the chosen time point, the reaction tube was centrifuged at 2500 RPM for 5 min and then 450 μl of the supernatant was pipetted into a new tube. The count rate of the cell pellets and their corresponding supernatants were counted in gamma counter. The actual count rate in the cells was corrected for the count rate of the residual 50 μl of supernatant. The

percentage of radiotracer uptake in the cells was calculated as shown in the equation as follows:

$$\% \text{ uptake in the cells} = (CPM_{act\ cell} * 100) / (CPM_{cell} + CPM_{sup})$$

$$CPM_{act\ cell} = CPM_{cell} - ((CPM_{sup} * 50)/450)$$

where $CPM_{act\ cell}$ = actual count rate of the cell pellet corrected with the count rate of 50 μl residual of supernatant

CPM_{cell} = count rate of the cell pellet

CPM_{sup} = count rate of the supernatant

2.3.7 Measurement amount of protein by BCA assay

Since the cells subjected for the uptake experiments were previously seeded into 24 well plate for 1 day before the study, growth and replication causes the number of cells to increase to a degree that varies among samples. Therefore the amount of protein in the taken up cells was measured after radiolabelling in order to normalise the results of accumulation of the radiotracers in the cells prior to comparing the uptake among samples. For this purpose we used a commercial bicinchoninic acid (BCA) protein assay to measure the protein content in the cells. The BCA assay is a colorimetric technique based on the Biuret reaction. Cu^{2+} is reduced to Cu^{+} and then reacts with BCA solution resulting in a purple complex the colour of which is proportional to the amount of protein in the sample. The optical density of this complex can be measured at 562 nm. The amount of protein in the sample is determined by comparing with protein standards. Following the uptake experiments in the plates, solutions of cells lysates were subjected to assay with a Novagen® BCA protein assay kit (Merck, Germany) following the manufacturer's standard procedure.

A range of protein standards was prepared by dilution in PBS from a stock solution of 2 mg/ml bovine serum albumin (BSA). Aliquots of 25 μl of the protein standards and samples were loaded into a 96 well plate in triplicate. 200 μl of BCA solution was then added to each well. Absorbance was measured at 562 nm, after incubation for 30 min at 37^{o}C, using a multiwell plate reader. Averages of triplicate samples and standards were calculated and the concentration of each sample was determined by comparison to a BSA standard curve.

2.3.8 Plasticware and tube testing

^{64}Cu-PTSM and ^{64}Cu (DEDTC)$_2$ were investigated for binding of radiotracers to the plastic 24 well plate. The tracer solutions (0.5 ml of 0.2 MBq/ml in HBSS) were incubated in the plates without cells. At the chosen time point, tracer solutions were removed and 500 μl of HBSS was used to wash each well twice. Both removed tracer and washing solutions were pooled together. In case of ^{64}Cu (DEDTC)$_2$, 0.5 ml of 1M NaOH was added and incubated for 10 min. NaOH solution was removed and collected separately. All samples were quantified by gamma counter to determine the percentage of tracer attached to the plate.

Since the cellular uptake of the radiotracers with some cell lines was carried out in glass tubes, we also determined the degree of binding between tracers and these test tubes. Cell free media were prepared in the reaction tubes then the radiocopper tracers were diluted and added to the tubes in the same manner as for the cell uptake experiments. The mixture was incubated and removed from the tubes at the chosen time points then collecting into a new tube. 0.5 ml PBS was used to wash the tube twice and the washing buffers were added into the collected supernatant tube. The activities in the tubes and the supernatant fractions were counted by gamma counter. The percentages of radiotracers bound to the tubes were calculated.

2.3.9 Efflux of radiotracers

From the uptake studies evaluated in multiwell plates, to study the efflux of ^{64}Cu-PTSM from various cell lines, the experiments were carried out in the same manner as cell uptake experiment. Cells in each well were incubated with 0.1 MBq tracer in 0.5 ml of HBSS for 30 min to allow cells to take up the tracer. Radioactive solution was removed before washing the cells with HBSS twice. New tracer-free media were added and incubated at 37^{o}C with 5% CO_2 for 0.5, 1, 2, 3, 4, 6, 20 and 24 hr. The efflux media of each sample were collected together with their washing buffer (0.5 ml HBSS, 2 times) in different time points. Cells were lysed and harvested in 0.5 ml of 1 M NaOH. The count rate of the activity in cells (CPM_{cell}) and in efflux media (CPM_{eff}) at each time point was determined by gamma counter. The percentage of radioactivity retention at each time point was calculated as follows:

Percentage of radioactivity retention in the cell = $(CPM_{cell} / (CPM_{cell} + CPM_{eff}))*100$

where CPM_{cell} = counts per minute of the cells

CPM_{eff} = counts per minute of the correspondent efflux media

Efflux studies in cells labelled in test tubes rather than multiwell plates were carried out as follows. On the day of experiment, 1 x 10^6 J774 cells in depleted serum medium were dispensing into the reaction tube and for the uptake, 0.1 MBq of the ^{64}Cu BTSC complexes (PTS, PTSM, GTS and GTSM) and DTC complexes (DMDTC, DEDTC and DPDTC) were added and serum free medium was added to reach a final volume of 500 μl then incubation the reaction mixture at room temperature for 30 min. The supernatants were removed and the residual radiotracers were eliminated by washing with 500 μl PBS twice before fresh culture media were added to the tubes. The percentage of the remaining activity in the cells was examined at 1 hr, 2 hr, 3 hr, 4

hr and 20 hr after the washing. The retained activities in the cells and the effluxed activities in the supernatants were counted using gamma counter. In addition, retention of ^{64}Cu-PTS, ^{64}Cu-PTSM, ^{64}Cu-GTSM and ^{64}Cu $(DEDTC)_2$ were also determined in eGFP-5T33 cells at 1 hr, 2 hr, 3 hr and 4 hr post the uptake.

2.4 Results

2.4.1 Radiolabelling and quality control of ^{64}Cu-PTSM

^{64}Cu-PTSM was synthesised and purified with SEP-PAK® C18 column prior to determining the radiochemical purity. The quality control performed with silica gel TLC constantly showed with R_f around 0.7 (Figure 2.2).

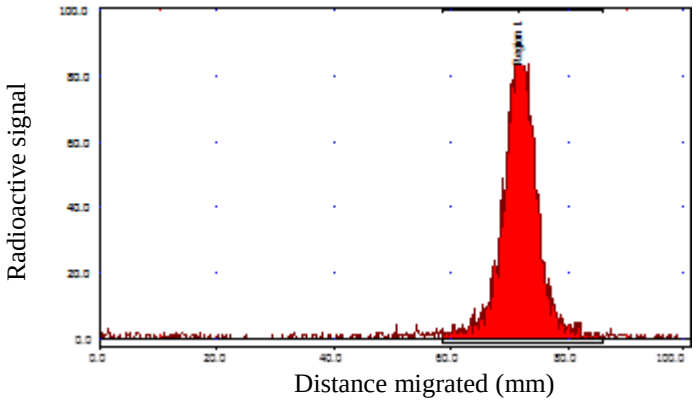

Figure 2.2: Radiochromatogram of purified ^{64}Cu-PTSM with silica gel TLC plate

2.4.2 Radiolabelling and quality control of ^{64}Cu $(DEDTC)_2$

Chromatograms of cold Cu $(DEDTC)_2$ performed with TLC-SG showed the R_f of copper complex at around 0.6, whereas free copper was observed at the origin.

The labelling efficiency of ^{64}Cu $(DEDTC)_2$ was 100 % (R_f around 0.6); no free copper was detected at the origin when using 20 μg of DEDTC as shown in Figure 2.3. This complex remains stable up to 24 hr after preparation (Figure 2.4).

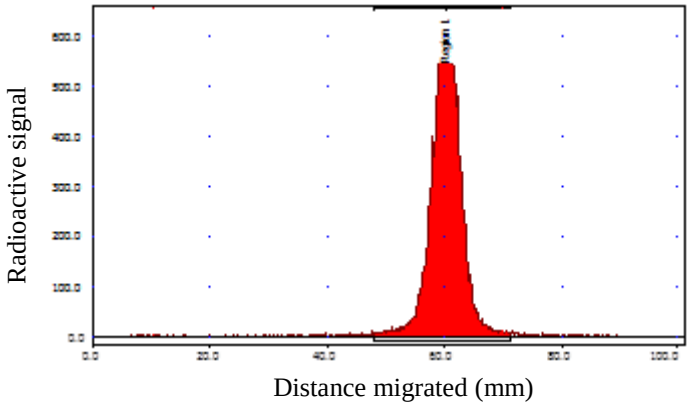

Figure 2.3: Labelling efficiency of ^{64}Cu $(DEDTC)_2$ (before purification, using DEDTC 20 μg) with silica gel TLC plate.

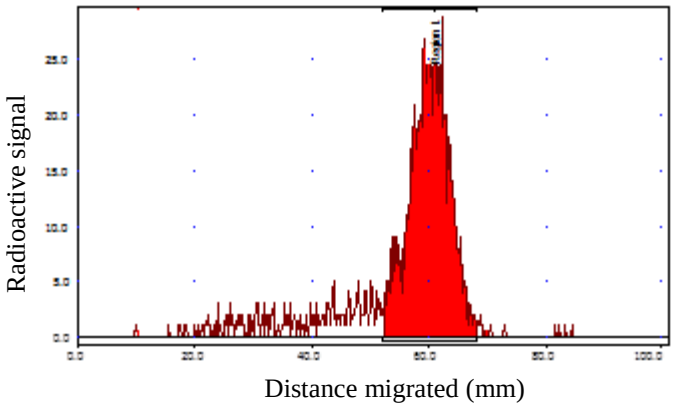

Figure 2.4: Radiochromatogram of ^{64}Cu $(DEDTC)_2$ 24 hr after synthesis.

Apart from pilot concentration (20 μg of ^{64}Cu $(DEDTC)_2$, the radiochemical testing results of ^{64}Cu $(DEDTC)_2$ synthesised from 2 μg, 0.2 μg and 0.02 μg of DEDTC were illustrated in Figure 2.5 and 2.6. These results indicated that impurity of complex was detected when using 2 μg DEDTC (Figure 2.5), and only free ^{64}Cu was detected when concentration of DEDTC was 0.2 μg /ml or below (Figure 2.6).

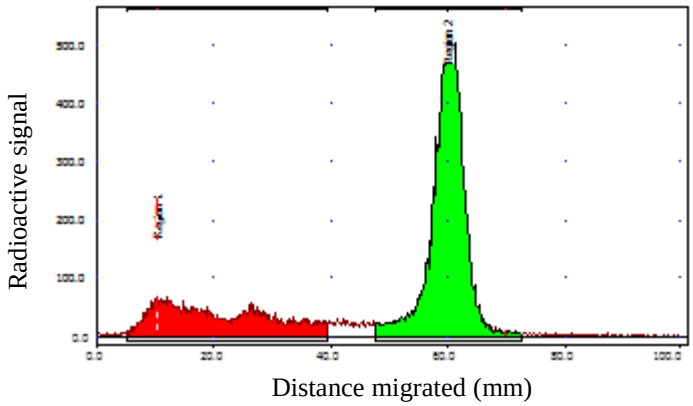

Figure 2.5: Radiochromatogram of ^{64}Cu $(DEDTC)_2$ using 2 μg of DEDTC.

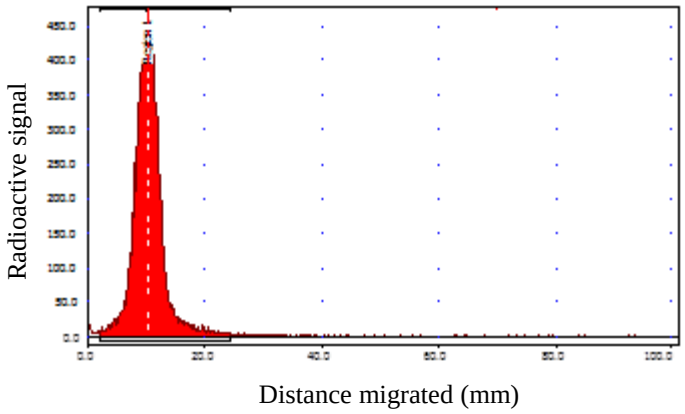

(A)

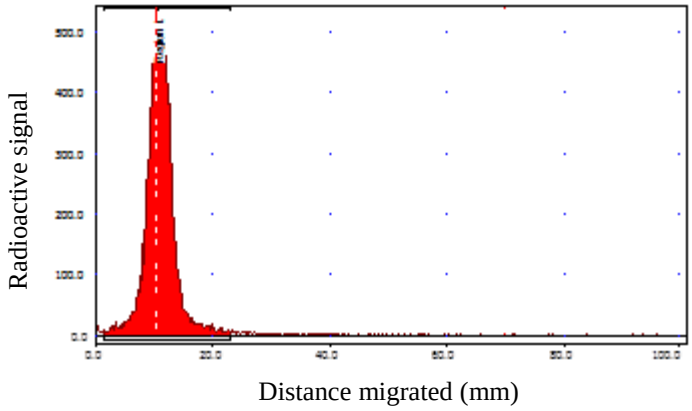

(B)

Figure 2.6: Radiochromatogram after incubation of ^{64}Cu with 0.2 µg (A) and 0.02 µg (B) of DEDTC. No labelled complex is detected under these conditions.

2.4.3 HPLC of Cu (DEDTC)$_2$

The HPLC results of sodium diethyldithiocarbamate and cold Cu (DEDTC)$_2$ using UV detector at wavelength 220 nm showed the main peaks at around 11 and 15.5 min, respectively, as shown in Figure 2.7. ^{64}Cu (DEDTC)$_2$ was evaluated both in the gamma detector and the UV detector. The peak of ^{64}Cu (DEDTC)$_2$ showed only one peak around 16 min by gamma detector while no correlated peak in UV detector was

observed as shown in Figure 2.8. For ^{64}Cu acetate, the gamma peak occurred at 2 min similar to peak monitored by UV detector as shown in Figure 2.9.

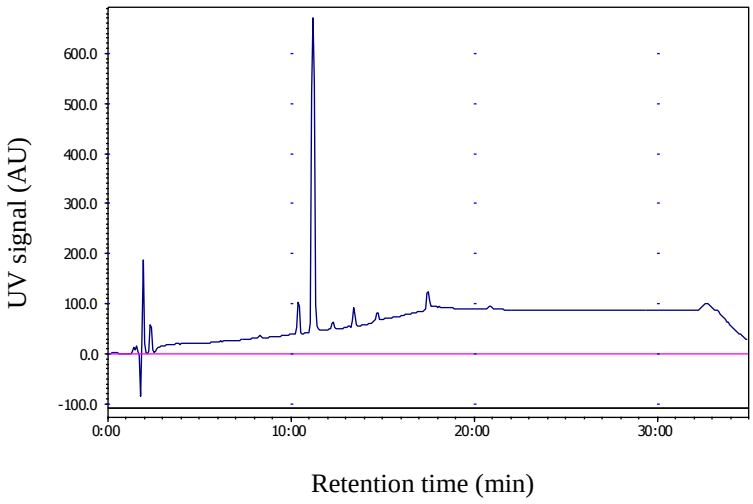

(A)

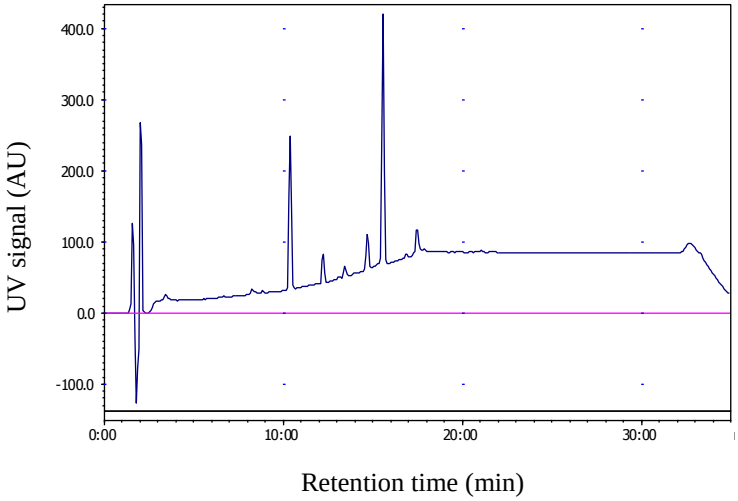

(B)

Figure 2.7: HPLC of sodium DEDTC (A) and cold Cu $(DEDTC)_2$ (B) with UV detector at 220 nm, show peak at 11 and 15.5 min, respectively.

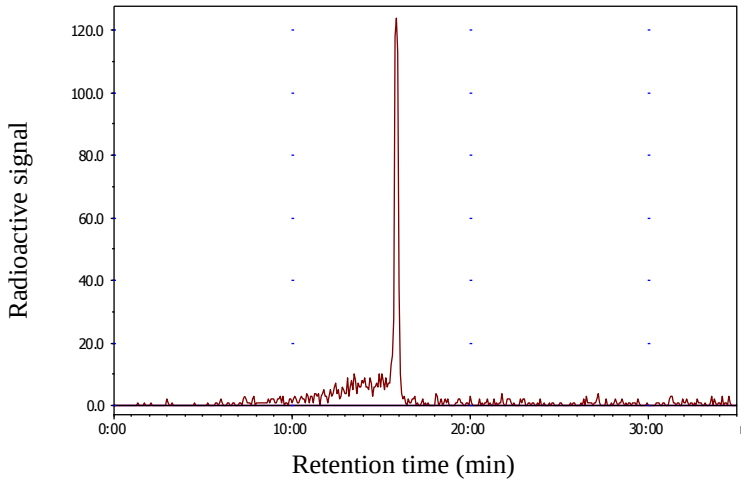

(A)

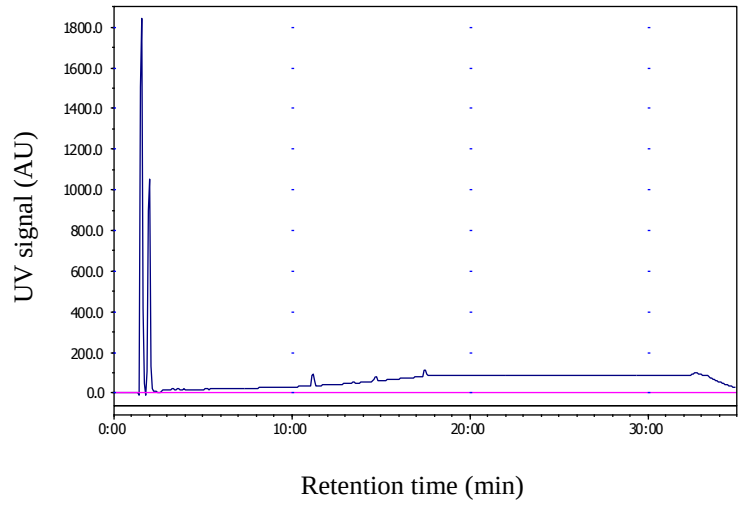

(B)

Figure 2.8: HPLC of $^{64}Cu(DEDTC)_2$ monitored by gamma detector (A) and UV detector at 220 nm (B). In A, single activity peak of ^{64}Cu was detected at nearly 16 min which correlated to peak in UV detector of cold $Cu(DEDTC)_2$.

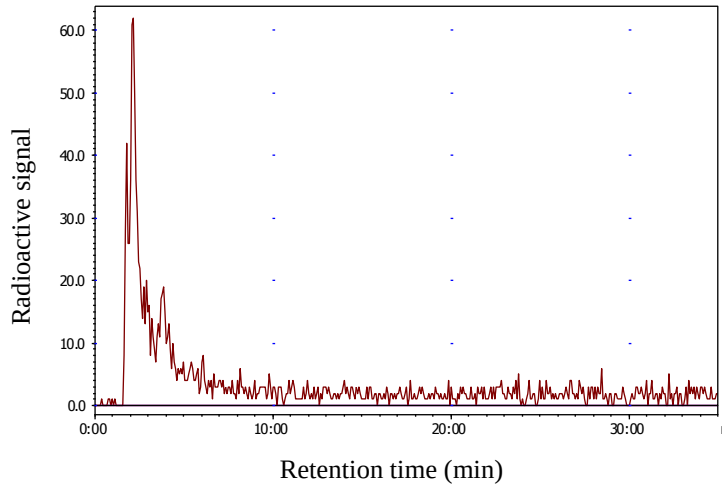

(A)

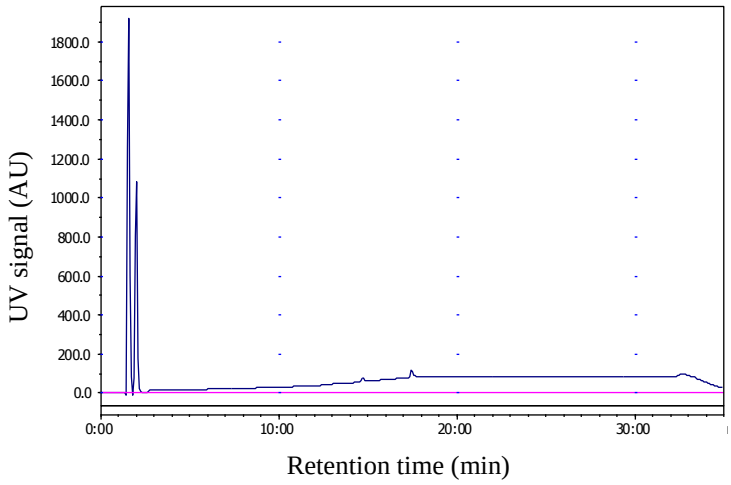

(B)

Figure 2.9: HPLC of ^{64}Cu acetate monitored by gamma detector (A) and UV detector at 220 nm (B). ^{64}Cu acetate was detected by gamma detector at 2 minutes.

2.4.4 Cell uptake of radiopharmaceuticals

In this section, cell labelling experiments conducted in 24 well plates are reported separately from those conducted in glass tubes. Radiopharmaceutical uptake studies in 24 well plates were performed using J774 and HCT116 cell lines for three tracers, $^{64}CuCl_2$, ^{64}Cu PTSM and $^{64}Cu(DEDTC)_2$. Uptake of each tracer in cells was

compared with and without normalisation against protein content shown in Figure 2.10, 2.11 and 2.12.

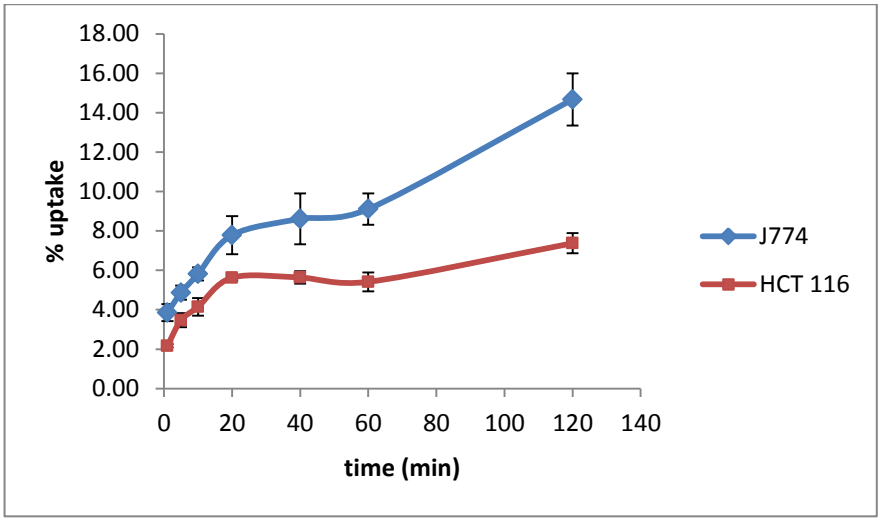

(A)

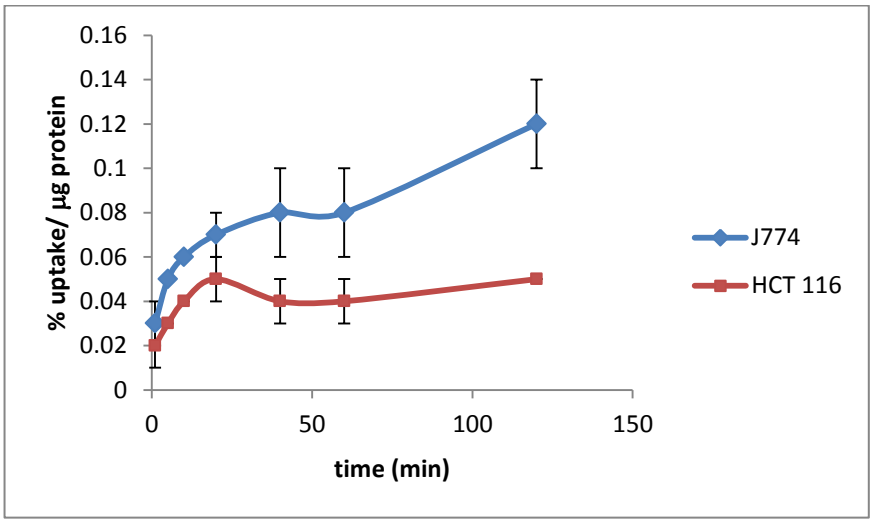

(B)

Figure 2.10: The percentage uptake of $^{64}CuCl_2$ into J774 cells and HCT 116 cells without (A) and with normalisation against microgram of protein (B), respectively. (n=3, mean ± SD)

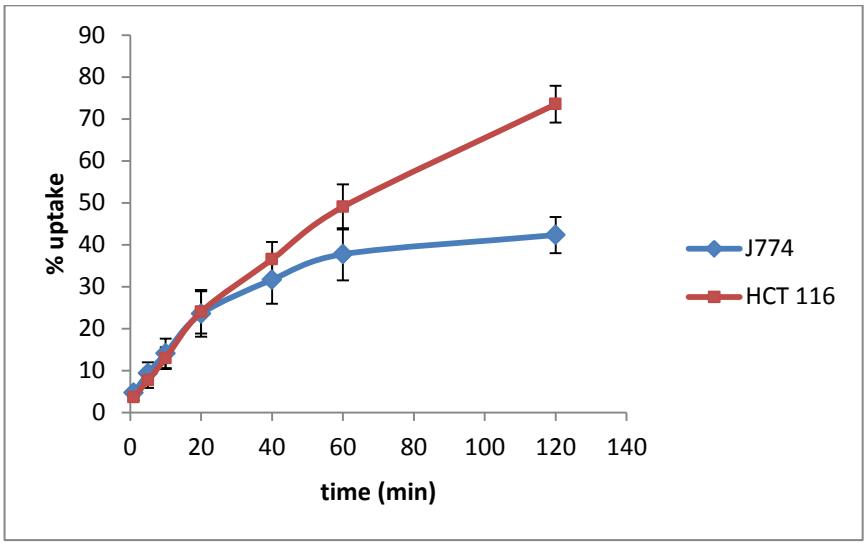

(A)

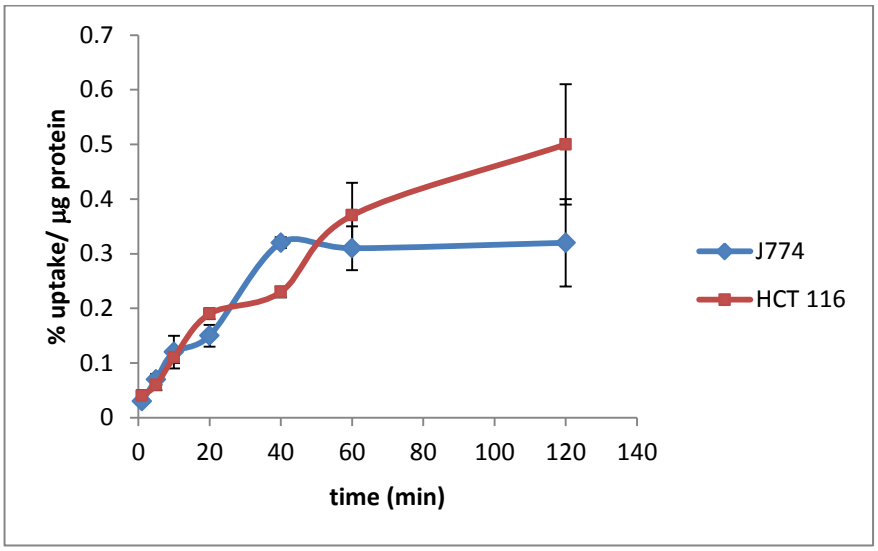

(B)

Figure 2.11: The percentage uptake of ^{64}Cu PTSM into J774 cells and HCT 116 cells without (A) and with normalised with microgram of protein (B), respectively. The data values are mean ±SD from 4 and 3 experiments in J774 and HCT 116, respectively.

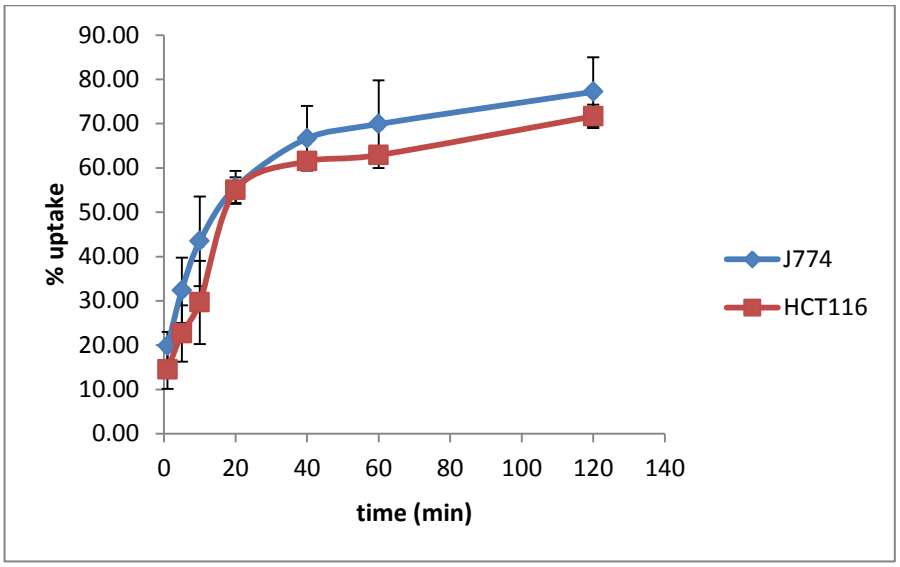

(A)

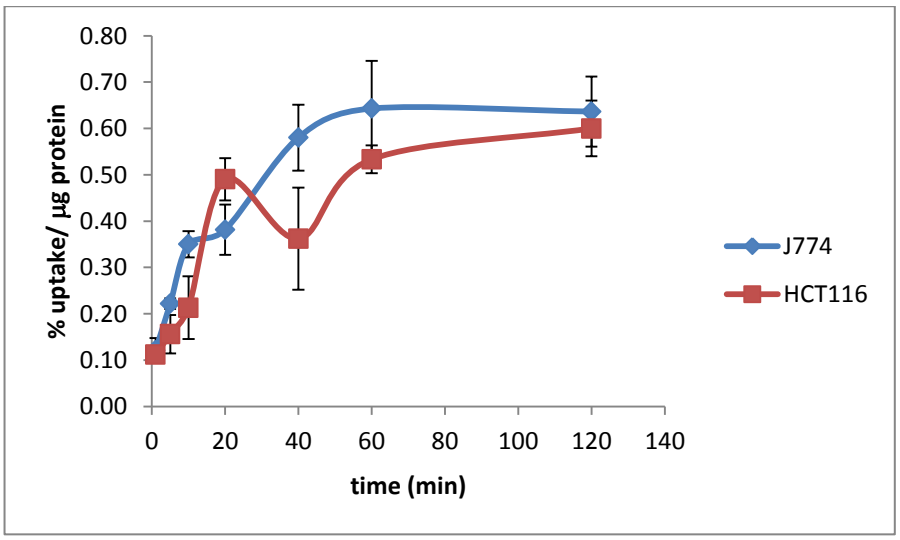

(B)

Figure 2.12: The percentage uptake of $^{64}Cu(DEDTC)_2$ into J774 cells and HCT 116 cells without (A) and with normalising against microgram of protein (B), respectively. The data values are mean ± SD from 3 experiments.

Cell labelling experiments in glass tubes were performed with a wider range of ^{64}Cu (BTSC) and ^{64}Cu $(DTC)_2$ complexes in J774 suspension cells and in eGFP-5T33 myeloma cells. Results are presented in Figures 2.13 - 2.16, respectively.

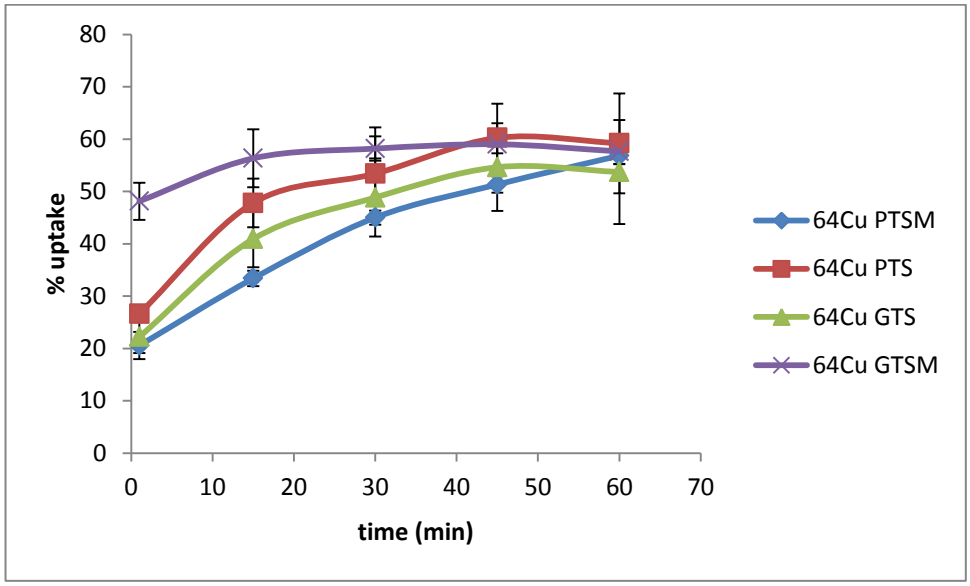

Figure 2.13: The percentage uptake of the ^{64}Cu (BTSC)s into J774 cells. The data values were mean ± SD from 3 experiments.

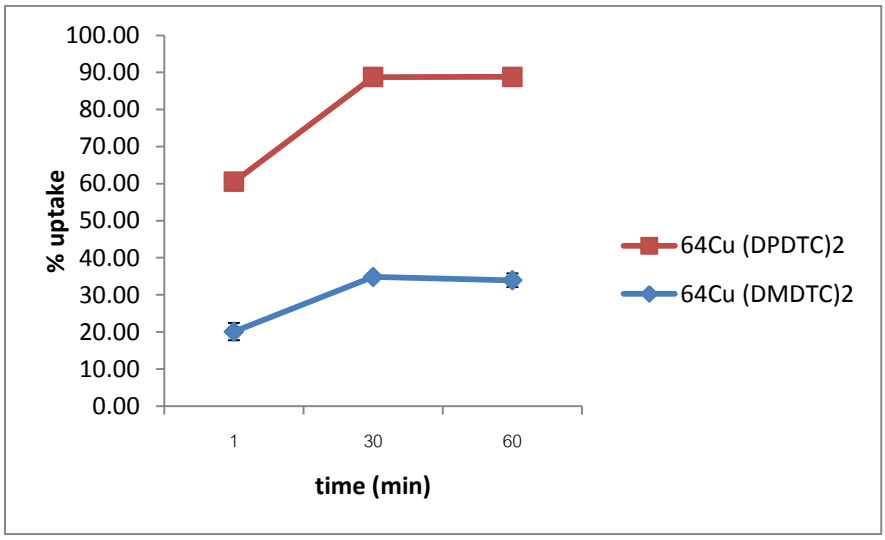

(A)

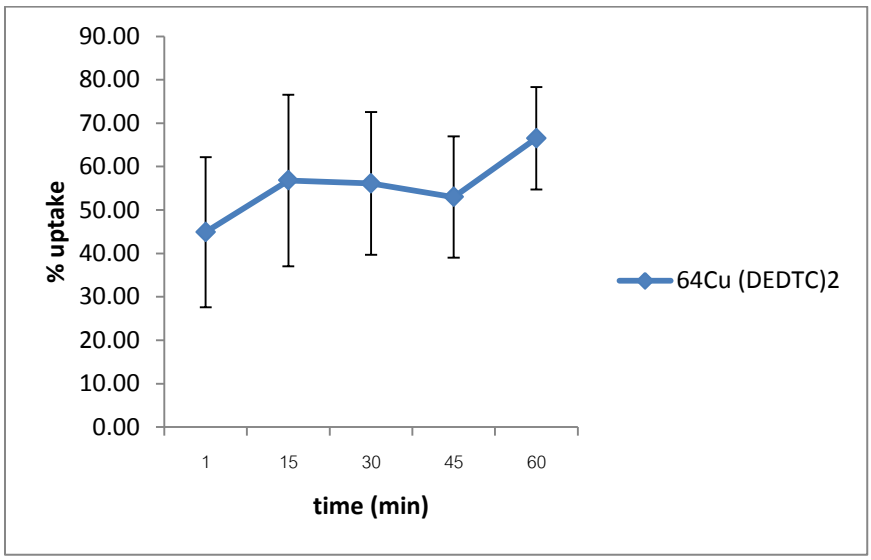

(B)

Figure 2.14: The percentage uptake of the complexes of $^{64}Cu(DTC)_2$ complexes into J774 cells, (A) $^{64}Cu(DMDTC)_2$ and $^{64}Cu(DMDTC)_2$ (B) $^{64}Cu(DEDTC)_2$. The data values were mean ± SD from 3 experiments.

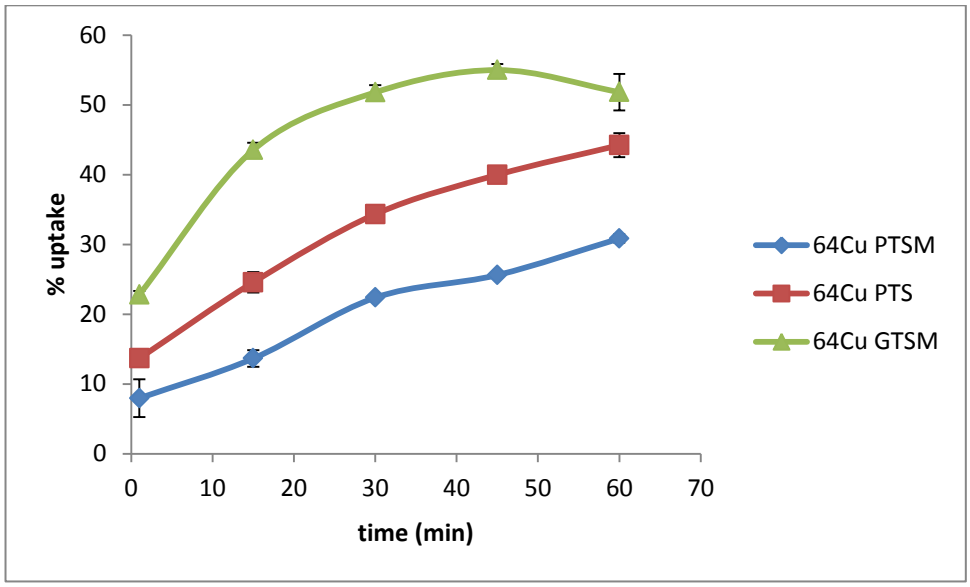

Figure 2.15: The percentage uptake of the complexes of ^{64}Cu (BTSC) complexes into eGFP-5T33 cells. The data values were mean ± SD of triplicate samples from 1 experiment.

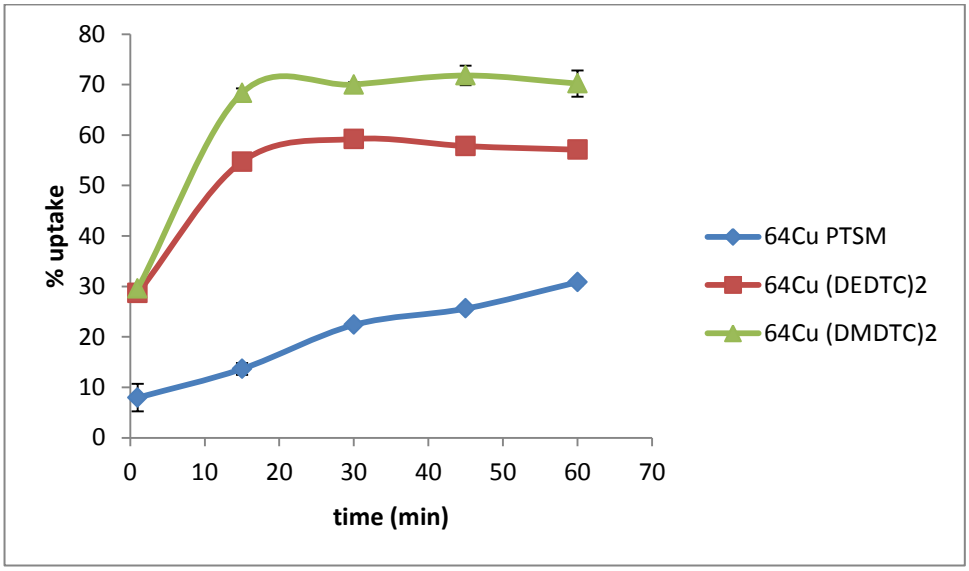

Figure 2.16: The percentage uptake of the ^{64}Cu $(DTC)_2$ complexes into eGFP-5T33 cells. The data values are mean ± SD of triplicate samples from 1 experiment. The percentage uptake of ^{64}Cu-PTSM was shown for comparison with those of ^{64}Cu $(DTC)_2$ complexes.

2.4.5 Plasticware testing

The degree of tracer attached to culture plates and glass tubes was investigated in order to ensure that measured activity from the cell lysates represented activity that had been taken up by the cells ant not merely bound to the plastic or glass. Tracers were added into cell free culture plate and were removed from plate at 20, 40, 60 and 120 min for ^{64}Cu-PTSM and at 20, 60 and 120 min for ^{64}Cu (DEDTC)$_2$. The result showed negligibly activity of ^{64}Cu-PTSM bound to the plate over period of the experiments. ^{64}Cu (DEDTC)$_2$ were significantly attached to cultured plate as shown in Figure 2.17. To determine whether this tracer can be recovered from plate with NaOH, radioactivity in the removed NaOH was measured and percentage of removal was calculated (also in Figure 2.17). Evaluation of adsorbable activity among the radiotracers to the glass tubes was illustrated in the graph (Figure 2.18).

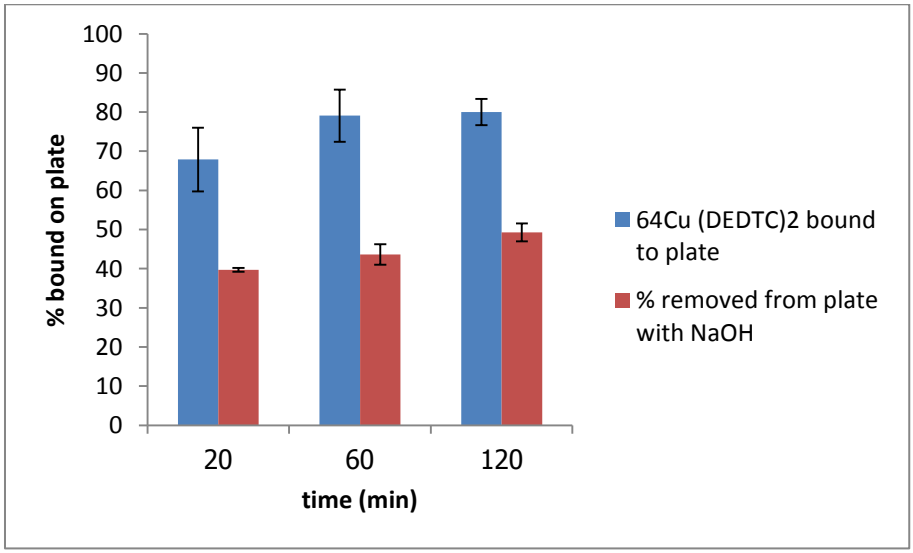

Figure 2.17: The percentage of ^{64}Cu (DEDTC)$_2$ bound to plastic plate, at 20, 60 and 120 min and removed with NaOH with the same time point based on total activity.

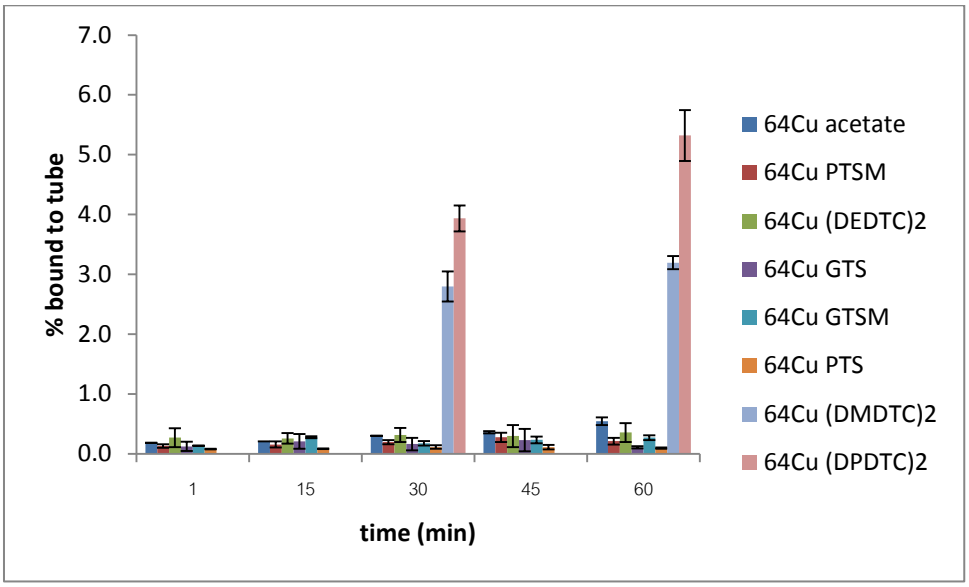

Figure 2.18: The percentage of ^{64}Cu complexes of BTSCs and DTCs bound to test tube, at 1, 15, 30, 45 and 60 min.

2.4.6 Efflux experiment

To study the efflux rate from cells after ^{64}Cu-PTSM labelling, the radioactive activity leakage in the normal culture medium from each cell line was measured and the percentage of tracer retention inside the cells at the particular time point was calculated. ^{64}Cu-PTSM was rapidly washed out from the cell lines: within 2 hr only half of activity remained in the J774 cells. After 24 hr, approximately 60% of the tracer had leaked from J774 cells. For HCT 116 cells, around 40% was eluted in the tracer-free medium post incubation for 6 hr while approximately 50% of activity remained in the cells 24 hr after labelling as shown in Figure 2.19. The activity effluxed from J774 and HCT 116 cells after labelling with ^{64}Cu $(DEDTC)_2$ at 24 hr was approximately 70% and 30%, respectively (Figure 2.20).

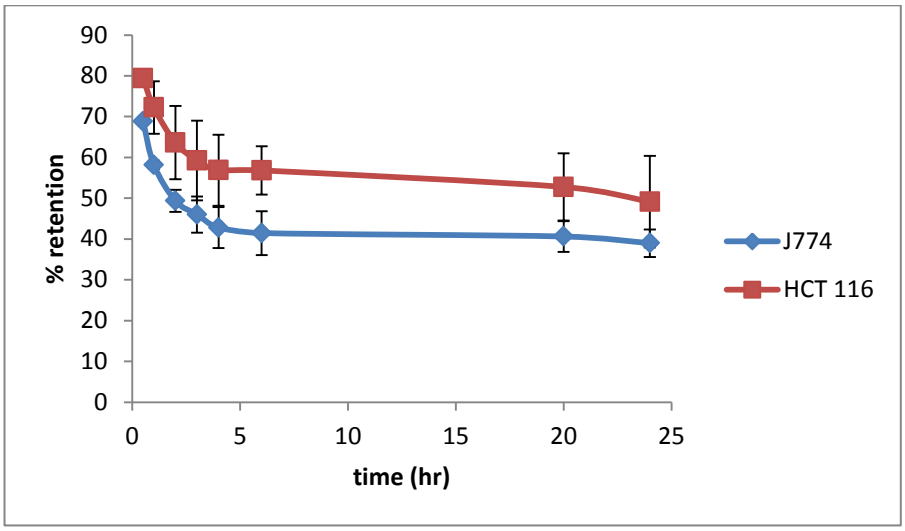

Figure 2.19: Percentage retention of ^{64}Cu-PTSM within J774 cells and HCT 116 cells during 24 hr, after labelling for 0.5 hr and washing (mean ± SD from 3 experiments)

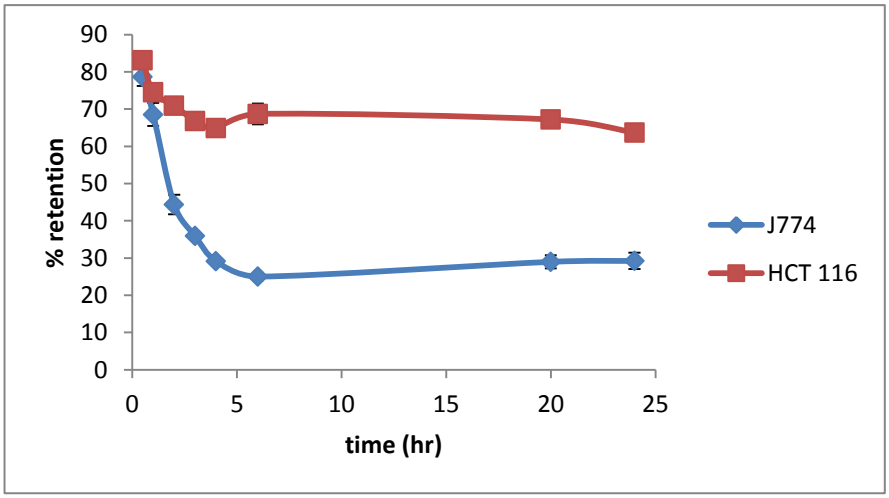

Figure 2.20: Percentage retention of ^{64}Cu (DEDTC)$_2$ within J774 cells and HCT 116 cells during 24 hr cells, after labelling for 0.5 hr (mean ± SD from 3 experiments).

The efflux rates of the ^{64}Cu (BTSC) complexes and ^{64}Cu $(DTC)_2$ complexes employed in J774 cells are shown in Figures 2.21 and 2.22. The retained activity of all ^{64}Cu (BTSC) complexes in J774 cells was lower than 30% at 20 hr after incubation cells in the tracer free medium (Figure 2.21). Approximately 40% of ^{64}Cu $(DTC)_2$ complexes was retained within the cells at 4 hr, decreasing to 16% and 28% at 20 hr post labelling (Figure 2.22).

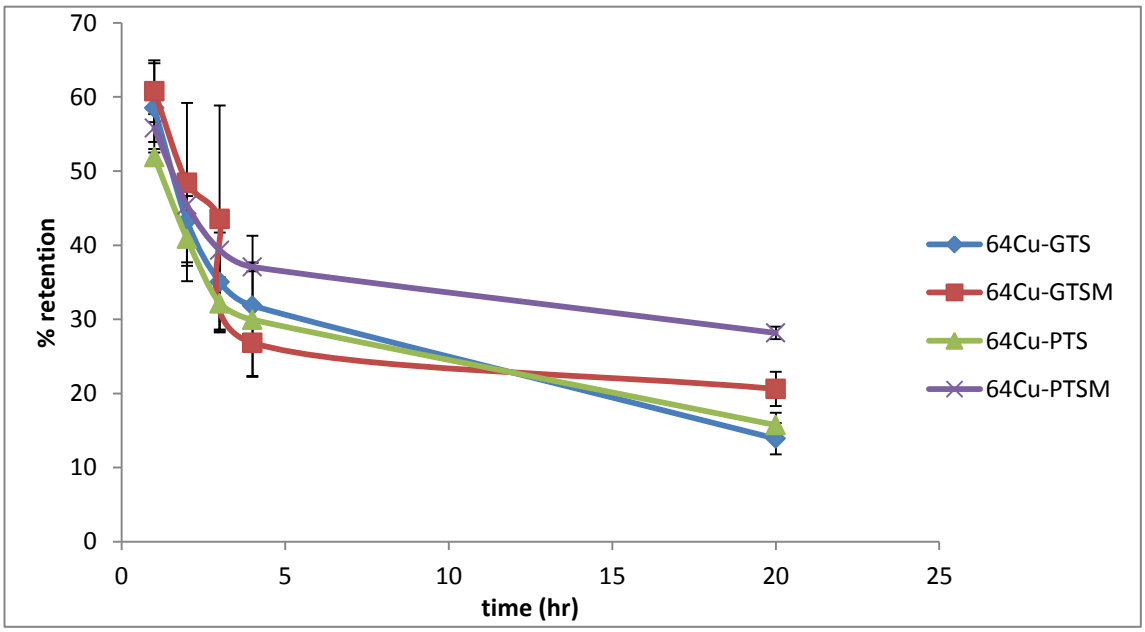

Figure 2.21: Percentage retention of the complexes of ^{64}Cu (BTSC)s within J774 cells, are compared after incubation in radioactivity-free medium for 1 hr, 2 hr, 3 hr, 4 hr and 20 hr.

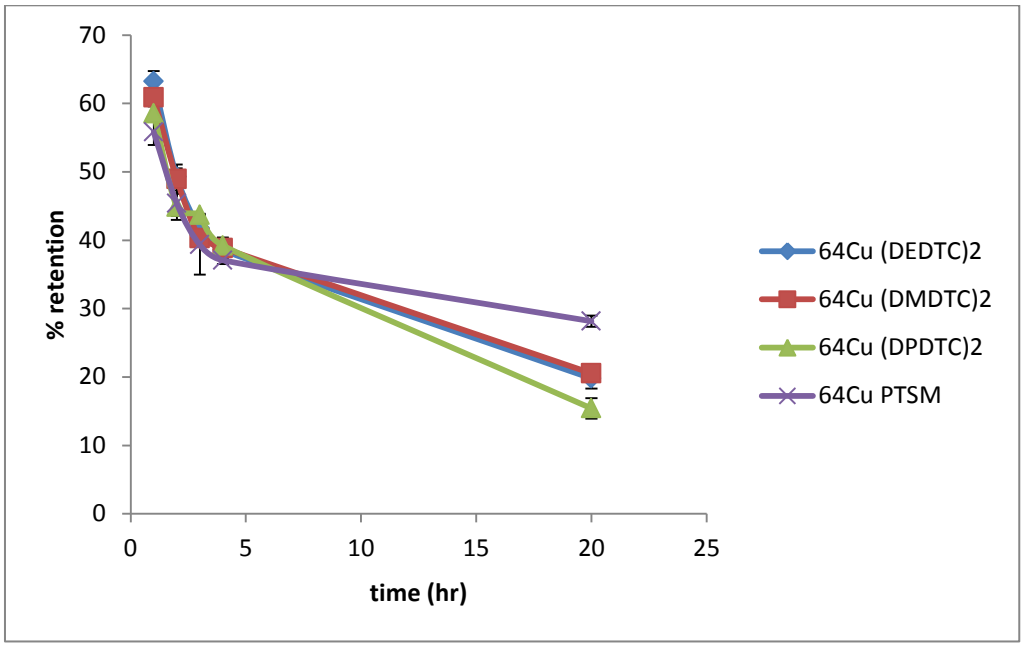

Figure 2.22: Percentage retention of the complexes of $^{64}Cu(DTC)_2$ complexes and ^{64}Cu-PTSM within J774 cells after incubation in radioactivity-free medium for 1 hr, 2 hr, 3 hr, 4 hr and 20 hr.

In eGFP-5T33 efflux was only measured up to 4 hr after completion of cell labelling. The results showed that greater than 60% of the activity had leaked from the cells by 4 hr post incubation with the fresh medium as shown in Figure 2.23.

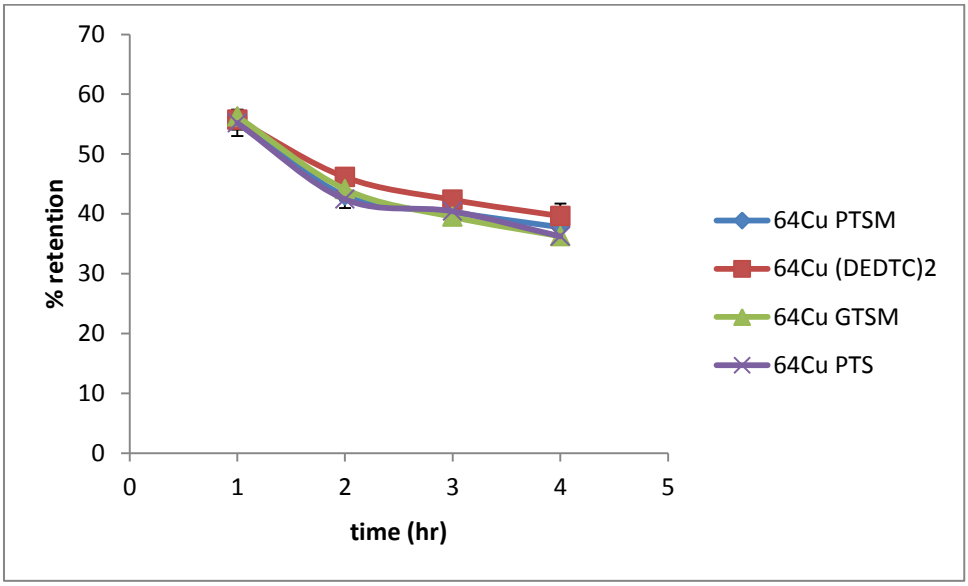

Figure 2.23: Percentage retention of the complexes of ^{64}Cu (BTSC) complexes and ^{64}Cu (DEDTC)$_2$ within eGFP-5T33 cells, are compared after incubating for 1 hr, 2 hr, 3 hr and 4 hr in radioactivity-free medium. The data values are mean ± SD of triplicate samples from 1 experiment.

2.5 Discussion

The TLC radiochromatogram results of ^{64}Cu-PTSM showed high purity (100%) which was reproducible in every preparation, showing that the preparation of the labelled complex is simple and reliable. Nevertheless, quality control by TLC was performed before starting new biological experiment to ensure that there would be no interference from some impurity.

In order to validate the result of radiolabelling of novel radiotracers, the TLC and HPLC chromatogram of all synthesised radiotracers have to be compared with the corresponding cold complex and cold copper salt. The TLC chromatogram of copper sulphate and Cu $(DEDTC)_2$ complex showed the R_f values of free copper and the complex were zero and 0.6, respectively. Radiochromatograms of ^{64}Cu $(DEDTC)_2$ (20 μg of DEDTC) in the same TLC system were analysed. The single radioative peak showed the same R_f of 0.6 as cold copper complex. No peak corresponding to free copper (R_f = 0) was observed suggesting a radiochemical purity of 100% for ^{64}Cu $(DEDTC)_2$. In addition, this complex has a shelf life up to 24 hr after preparation as verified by TLC.

The TLC chromatogram of ^{64}Cu $(DEDTC)_2$ showed high labelling yield, however, radiochemical impurities were demonstrated when the amount of DEDTC decreased to 2 μg. A mass of DEDTC less than 2 μg (0.2 and 0.02 μg) was not enough to label efficiently with radiocopper as shown in Figure 2.6. Therefore, the optimum amount of sodium diethyldithiocarbamate selected for production of ^{64}Cu $(DEDTC)_2$ was 20 μg.

Apart from TLC, HPLC analysis of sodium diethyl DTC and the cold and hot copper DTC complex was performed. The HPLC chromatogram using the UV detector (at 220 nm) showed the retention time of sodium diethyldithiocarbamate and copper complex at 11 and 15.5 min, respectively. The hot copper complex exhibited only one radioactive peak at 16 min while no obvious UV peak was detected at 220 nm. It is likely that of the amount of the radiocomplex is lower than detectable by the UV detector. The gamma detector detects the activity peak of radioactive product about 10 sec later than the UV detector because of the distance between the detectors.

Therefore, the peak in gamma detector was related to peak of cold Cu $(DEDTC)_2$ in UV detector (at 15.5 min) suggesting that this peak was ^{64}Cu $(DEDTC)_2$.

TLC is suggested as the routine QC method to analyse the radiopharmaceutical product in every preparation rather than HPLC because of reliable determination results and rapid procedure that is suitable for routine studies.

Uptake experiments in 24 well plates were performed with $^{64}CuCl_2$, ^{64}Cu-PTSM and ^{64}Cu $(DEDTC)_2$ in J774 and HCT116 cells. $^{64}CuCl_2$ was used as a control to determine the uptake of free ^{64}Cu by the cells. In both cell types, an insignificant percentage uptake of $^{64}CuCl_2$ was observed over the first hour of incubation before slightly increasing by two hours to around 15% and 7% for J774 and HCT 116, respectively. This was unexpected because $^{64}CuCl_2$ is not lipophilic and should not diffuse non-specifically through cell membranes. Thus, there is a possibility that free copper only associates outside the targeted cells not uptake inside the cells, or is taken up by specific transporter systems. On the other hand, ^{64}Cu-PTSM and ^{64}Cu $(DEDTC)_2$ were very efficiently extracted into both cell lines. Thus, when compared to other tracers, $^{64}CuCl_2$ showed lowest uptake. The uptake results of ^{64}Cu-PTSM support the previous studies which suggest that it has potential as a tracer for labelling cells (101, 103). Nonetheless, ^{64}Cu $(DEDTC)_2$ showed even greater influx into the cells, up to 60% within 1 hr. Because slightly different uptake rate of the same tracer between two cells lines were observed uptake of radiotracer is somewhat cell type specific. Possibly cell size and surface area may account for this, or the rate of bioreduction of Cu(II) (which, followed by ligand dissociation, is believed to be the primary mechanism of intracellular trapping within the cell).

However, experiments indicated a high degree of interaction between ^{64}Cu $(DEDTC)_2$ and plastic ware, up to 80% at 120 min after incubation. More importantly,

approximately 50% of attached activity on the plate can be detached by NaOH at the same time point. Therefore, the apparent percentage uptake of ^{64}Cu (DEDTC)$_2$ in the previous experiments were not only activity uptake by cells but also activity that had bound to the plate and was subsequently removed by washing. Therefore, the reaction between tracer and plastic containers should be investigated to validate the uptake results; based on these preliminary results, the rate of tracers extracted into the cells cannot be analysed accurately. Therefore we investigated the intracellular accumulation and the retention of the radiocopper tracers using glass tubes instead of plastic plates, with the cells in suspension. All of the radiotracers used in these experiments were also the subject of cell-free controls to determine the degree of binding to the reaction tubes. All of the radiocopper tracers showed negligible binding to the tube expect for ^{64}Cu (DMDTC)$_2$ and ^{64}Cu (DPDTC)$_2$ which bound to tubes to the extent of about 3% and 5%, respectively. For intracellular uptake and retention studies, because the same number of cells were seeded into the tubes on the day of experiment, leading to normalisation among the samples, the protein assay was unnecessary in these experiments. The cellular uptake of ^{64}Cu BTSC complexes (PTS, PTSM, GTS and GTSM) in J774 cells showed time-dependent accumulation of the tracers. The highest uptake at 60 min was over 50% for all radiocopper BTSC complexes. The % uptake in J774 cells increased in the order ^{64}Cu-GTSM> ^{64}Cu-PTS> ^{64}Cu-GTS> ^{64}Cu-PTSM. A similar pattern was also observed in eGFP-5T33 cells which gave % uptake in the order ^{64}Cu-GTSM> ^{64}Cu-PTS> ^{64}Cu-PTSM. The efficient and very rapid uptake of ^{64}Cu-GTSM into both of cell types was expected owing to the relatively high reduction potential of this complex, which results in very rapid non-selective bioreductive trapping in cells, as reported by Dearling and colleagues (107). The complexes of ^{64}Cu DTCs, ^{64}Cu (DEDTC)$_2$ and ^{64}Cu (DPDTC)$_2$ showed efficient extraction into J774 cells after incubation for 30 min whereas slightly lower uptake

with ^{64}Cu (DMDTC)$_2$ was observed. However, the accumulated activity of ^{64}Cu (DMDTC)$_2$ in eGFP-5T33 cells was greater than ^{64}Cu (DEDTC)$_2$ over the period of study. This finding suggests cell type dependence.

When comparing the complexes of BTSCs and DTCs in eGFP-5T33 cells, although the influx of ^{64}Cu (DTC) complexes were higher than that of ^{64}Cu (BTSC) complexes in the cells, a plateau of uptake of ^{64}Cu (BTSC) complexes was not clearly observed especially for ^{64}Cu-PTS and ^{64}Cu-PTSM. Therefore longer incubation time might be considered. According to the study of Griessinger and colleagues, the optimum time to labelled murine Th1 cells with ^{64}Cu-PTSM was up to 3 hr in order to reach the cell labelling efficiency between 6.5% - 9% (106). From another study, C6 rat glioma cells, were incubated for 5 hr to achieve 70% - 85% cell uptake and it was necessary to take up ^{64}Cu-PTSM for 90 min before performing subsequent efflux experiments (101). These combined observations suggest that longer incubation with ^{64}Cu-PTSM (longer than 1 hr) might be necessary to achieve a higher labelling efficiency.

Once radiolabelling efficiency and rates had been determined in 24 well plates, efflux of ^{64}Cu from cells labelled with the tracers ^{64}Cu-PTSM and ^{64}Cu (DEDTC)$_2$ was performed (in 24 well plate) and compared in J774 and HCT 116 cells. ^{64}Cu-PTSM was rapidly washed out from the labelled cells; up to 30-40% leakage occurred after incubation for 1 hr after the end of labelling in both cell types. At 24 hr, only 40% and 50% of the activity remained in J774 and HCT 116 cells, respectively. The associated activity of ^{64}Cu (DEDTC)$_2$ in J774 and HCT 116 cells was around 30% and 70%, respectively, 24 hr after labelling. Based on the observation that ^{64}Cu (DEDTC)$_2$ was absorbed and leached from the multiwell plates, these retention results could be

affected by leaching activity from the multiwell plates which were used for the previous uptake experiments.

In addition, therefore, the retention of activity of various ^{64}Cu BTSC complexes and ^{64}Cu DTC complexes in J774 cells were determined in glass test tubes. The results showed rapid wash out of the radio tracers from the labelled cells with less than 30% of initial activity remaining in the cells after incubation for 20 hr with all the ^{64}Cu complexes. In the different cell type, eGFP-5T33 cells, the efflux of ^{64}Cu BTSC complexes (PTS, PTSM and GTSM) and ^{64}Cu $(DEDTC)_2$ in the first four hours was significant with up to 60% released from the cells. Wash out of the lipophilic complexes of ^{64}Cu either with BTSC or DTC ligands was remarkably similar in different cell types and different ligands. These finding are similar to previous studies from several groups which showed high efflux rate of lipophilic radiocopper complex in various types of cells (101, 106). This suggests that although different complexes lead to different rates and efficiencies of labelling, the efflux of ^{64}Cu from cells is unrelated to the ligand. This is consistent with the hypothesis that dissociation of the complex is a common step in the intracellular trapping of the copper and that after this, efflux of copper by cellular homeostatic pathways specific to copper is likely to be responsible for removing copper from the cells. As previously described, copper generally binds to proteins (such as copper-dependent apoenzymes, ceruloplasmin and metallothionein) resulting in delivery of copper to the target molecules or proteins as well as keeping copper in the form of free ion to a minimum. This homeostasis might support the rapid wash out of radiocopper complexes from the labelled cells. However, the species of copper isotope that is dissociated from labelled cells has not been identified. Thus, it should be advantageous to identify the chemical form in which the radiotracer is exported. This knowledge would assist in the design of methods and mechanisms to label cells.

2.6 Conclusion

The complexes of ^{64}Cu (DEDTC)$_2$ and ^{64}Cu-PTSM were successfully synthesised by a method that proved to be simple, quick, reliable and reproducible. The amount of DEDTC ligand was optimised to achieve the radiolabelling efficiency with the lowest amount of the ligand, showing that 20 μg of DEDTC is enough for the production of ^{64}Cu (DEDTC)$_2$. ^{64}Cu (DEDTC)$_2$ was characterised against its cold complex analogue using HPLC. Quality control of the complexes was performed by TLC. The results showed that the quality of ^{64}Cu (DEDTC)$_2$ and ^{64}Cu PTSM are acceptable for further experiments.

The procedures for time course of the uptake and efflux in this study were developed and validated. The most reliable method was to ensure that the same number of cells were freshly seeded before the experiments and carrying out the cell labelling in the test tube instead of in the plastic plate. This procedure can overcome the problem of the variation from the protein measurement and the differences of cell size as well as eliminating the problem of the tracers binding to the plastic reaction containers and multi-well plates.

The ^{64}Cu BTSC complexes, especially ^{64}Cu-GTSM, were efficiently accumulated in various cell types. Similarly, ^{64}Cu complexes of DTC showed very efficient extraction into the cells, especially ^{64}Cu (DEDTC)$_2$ which showed very rapid influx into the cells a few minutes after incubation. On the other hand, high efflux rate of radiocopper from cells labelled with either the ^{64}Cu BTSC or ^{64}Cu DTC complexes was observed, and the retained activities of ^{64}Cu were lower than 30% at 24 hr post labelling for all of lipophilic radiocopper complexes.

Our results indicate that while the lipophilic ^{64}Cu complexes of either BTSCs or DTCs are able to label cells remarkably quickly and efficiently, they lack the important property of prolonged retention in the labelled cells for a period compatible with the half life of the radionuclide. Therefore these complexes are not suitable radiotracers for direct labelling and tracking the labelled cells for a long period of time; indeed, it is possible that copper radionuclides in general are unsuitable as cell tracking agents for this reason. Further work is needed to identify suitable PET tracers for prolonged *in vivo* tracking of cells.

Chapter 3: Synthesis of lipophilic complexes of ^{89}Zr and *in vitro* studies of [^{89}Zr]-Zr(oxinate)$_4$

3.1 Introduction

In recent years, a non-standard long lived positron emitteing radionuclide, zirconium-89 has been increasingly available. ^{89}Zr emits a positron in 23 % of its decays (maximum energy = 897 keV) and high energy gamma emission at 909 keV (99% abundance). Its physical half life is 78 hour (3.2 d) (134). Owing to ^{89}Zr decay characteristics, it has been increasingly considered as a label for molecules which have slow pharmacokinetic clearance in the blood circulation such as antibodies, proteins or nanoparticles (135, 136). Desferrioxamine (DFO) has been widely used as a bifunctional chelator to form stable complexes between ^{89}Zr and these molecules (137). Because of the long accumulation period to the targets (tissues or tumours) and slow clearance process of antibodies leading to delays in achieving high target to background ratios (e.g. a few days), the long half life of ^{89}Zr is useful for *in vivo* antibody imaging to allow sequential PET imaging and ^{89}Zr has been mainly employed for immuno-PET. Although ^{89}Zr properties are striking as a potential of cell labelling radioisotope (especially for application in cell based therapy), it has not been used for direct labelling of cells. It is therefore a challenge to label cells with zirconium-89 complex for *in vivo* imaging and cell tracking. Its dominant oxidation number is 4+, compared to 3+ in the case of ^{111}In. The ligands which can be complexed with ^{111}In might also react with ^{89}Zr in the similar manner. As both of them are radiometals, the mechanism to exploit cell labelling should be similarly applied using the lipophilic property of the radiocomplexes which are able to passively across cell membrane before dissociation of the complexes in the cells leading to released radiometals

becoming trapped by biomolecules inside the cells. Therefore the potential of lipophilic ^{89}Zr radiotracers for cell labelling needs to be investigated.

^{89}Zr can be produced by cyclotron bombardment via 2 nuclear reactions. The reaction mostly used to produce ^{89}Zr is the ^{89}Y(p,n)^{89}Zr reaction. The target, natural yttrium (^{89}Y) is bombarded with a photon beam (energy 14-14.5 MeV) for 2-3 hr to get the product of ^{89}Zr (138). Another reaction uses a 16 MeV deuteron beam to irradiate the yttrium pellet by the reaction of ^{89}Y(d,2n)^{89}Zr (139). The ^{89}Zr from both reactions is dissolved in hydrochloric acid HCl) and then ^{89}Zr in the acid solution is separated from its starting material and purified by ion exchange chromatography (140). HCl is used to elute impurities while ^{89}Zr is strongly bonded to the column. Then ^{89}Zr is successfully transchelated from the column by oxalic acid (at least 0.5 M) (140).

In order to label cells with ^{89}Zr radiotracer, it is proposed that zirconium-89 should be considered in the form of a lipophilic complex, based on knowledge of mechanisms of other radiotracers (e.g. ^{111}In-oxine) currently used to label cells. It is know that tetravalent zirconium can form complexes with monobasic bidentate ligands such as oxinate (141), tropolonate (142) and hydroxamates (143) of the stoichiometry ZrL_4 which should be parallel to those of InL_3.

3.2 Aims

In this section we aimed to synthesise a lipophilic complex of ^{89}Zr with 8-hydroxyquinoline (oxine). The production procedure (time and concentration of ligand) was investigated to determine the optimum conditions. We also aimed to evaluate the *in vitro* uptake and efflux of [^{89}Zr]-Zr(oxinate)$_4$ in different cell types including human white blood cells. In addition, labelling of multiple myeloma cells with [^{89}Zr]-Zr(oxinate)$_4$ was performed prior to *in vivo* imaging.

3.3 Materials and Methods

^{89}Zr used in the following studies was purchased from Perkin-Elmer (Seer Green, UK) in the form of ^{89}Zr in 0.1 M oxalic acid. 8-hydroxyquinoline (oxine) from Sigma, USA was used. Radioactivity and count rate of radioactivity was measured and counted in a dose calibrator (Capintec CRC-25) and a gamma counter (Wallac 1282 Compugamma Universal Gamma counter), respectively. Radiochromatograms of ITLC strips were scanned with a TLC scanner (LabLogic, UK) fitted with a $\beta^{-/+}$ detector (B-FC-3600) using Laura (v. 4.0.3.75) software (LabLogic, UK).

Mouse macrophage cell line (J774), breast adenocarcinoma cell line (MDA-MB-231) and murine multiple myeloma cell line (eGFP-5T33) were used for the *in vitro* experiments. Numbers of cells were counted with a cell counting machine (Countess automated cell counter, Invitrogen, USA).

3.3.1 Synthesis of [^{89}Zr]-Zr(oxinate)$_4$ complex

In order to synthesise [^{89}Zr]-Zr(oxinate)$_4$ complex, a solvent extraction technique was applied using one-to-one (volume) ratio of chloroform and water

(organic phase and aqueous phase, respectively, *vide infra*). The lipophilic ligand was in the organic solvent prior to combining with the neutralised ^{89}Zr (^{89}Zr oxalate) in the aqueous phase and then the lipophilic complex of [^{89}Zr]-Zr(oxinate)$_4$ dissolved in the organic phase. Neutralised ^{89}Zr was ^{89}Zr oxalate prepared from 1 volume of ^{89}Zr in 0.1 M oxalic acid neutralised with approximately 0.5 equivalent volume of 1 M sodium carbonate (Na_2CO_3) to pH 7. To find the best conditions (i.e. those resulting in the best radiolabelling yield), reaction time and amount (concentration) of ligand were varied as follows.

3.3.1.1 Optimisation of the reaction time

In this set of experiment, labelling efficiencies were assessed as a function of the reaction times (15 min, 45 min and 60 min) in duplicate for each time point. One to two MBq of ^{89}Zr in 0.1 M oxalic acid was neutralised with approximately 0.5 equivalent volume of 1 M sodium carbonate (Na_2CO_3) to pH 7 before adding water to bring the volume to 100 μl as a stock solution. Ten μl of neutralised ^{89}Zr stock solution was dispensed into 15 ml Falcon tube then water was added to make the final volume to 500 μl. Five hundred micrograms of 8-hydroxyquinoline (oxine) dissolved in 500 μl chloroform were added to neutralised ^{89}Zr in the tube. The mixture was continuously vortexed for 15 min, 45 min and 60 min then allowed to stand for 5 minutes to achieve complete separation of chloroform phase and water. 300 μl of each phase were transferred into 1.5 ml microcentrifuge tubes separately. Radioactivities were counted by gamma counter (Wallac 1282 Compugamma Universal Gamma counter). The count rates (count per minute (cpm)) of the paired samples between two phases from their original reactions were calculated for labelling efficiency. The equation was defined as follows,

$$\text{Labelling efficiency} = (CPM_{chlo} * 100)/ (CPM_{chlo} + CPM_{aq})$$

where CPM_{chlo} = count rate in chloroform phase

CPM_{aq} = count rate in aqueous (water) phase

3.3.1.2 Optimisation amount of oxine

In this experiment we sought to determine the lowest amount of oxine which can be used to achieve acceptable labelling efficiency (N.B. oxine is cytotoxic (144). Oxine quantities of 100 μg, 300 μg and 500 μg (1.4 mmol, 4.2 mmol and 7.0 mmol, respectively) were used to synthesise [^{89}Zr]-Zr(oxinate)$_4$. The procedures to synthesise ^{89}Zr complex were the same as described above with mixing time kept at 15 min for every reaction. The mixture was allowed to fully separate for 3 min. Subsequently, 2 μl of the chloroform phase were used to determine the labelling efficiency using solvent extraction which was the mixture between 0.5 ml of PBS and 0.5 ml chloroform to be used. Reactions were mixed with a vortexer for 5 min and left to separate for 3 min then 100 μl of each phase was collected into new 1.5 ml microcentrifuge tubes separately. Radioactivity in the PBS phase and chloroform phase was measured in the gamma counter. At the end, radiolabelling efficiencies were determined using the same equation as shown previously in the section 3.3.1.1 on time optimisation.

3.3.1.3 Synthesis of [^{89}Zr]-Zr(oxinate)$_4$ complex for *in vitro* biological evaluation

For the following experiments to label cells for *in vitro* studies, [^{89}Zr]-Zr(oxinate)$_4$ was synthesised using the following (optimised) protocols. Five to ten MBq of neutralised ^{89}Zr (pH 7) was prepared as described in section 3.3.1.1 and diluted to a final volume of 500 μl with distilled water. A 5 ml heart shaped glass flask was

used instead of Falcon tubes to avoid losses due to adsorption reactions between organic solvent and plastic material. Five hundred μg of oxine in 500 μl of chloroform were added to neutralised ^{89}Zr in the glass flask. The mixture was continuously vortexed for 15 min prior to transferring the contents to 1 ml glass vial with a v-shaped bottom using a glass pasteur pipette. The two solution phases were left to separate completely (ca. 5 min) then the chloroform phase containing [^{89}Zr]-Zr(oxinate)$_4$ was collected and transferred into a new small glass vial. Chloroform was completely evaporated by heating at around 60^{o}C using a heating block. The residue complex was redissolved in 10-20 μl of DMSO to obtain [^{89}Zr]-Zr(oxinate)$_4$. In order to use [^{89}Zr]-Zr(oxinate)$_4$ the DMSO was diluted with serum free medium or normal saline for use in uptake and efflux studies with myeloma cells and white blood cells.

[^{89}Zr]-Zr(oxinate)$_4$ used for *in vivo* studies was synthesised in the same procedures as for *in vitro* study but the starting activity of ^{89}Zr was increased to around 45 MBq or more in order to obtain enough activity for PET imaging. After the first run of synthesising [^{89}Zr]-Zr(oxinate)$_4$ in which [^{89}Zr]-Zr(oxinate)$_4$ in chloroform phase was completely removed from the V-shape bottom glass vial, the remaining aqueous phase containing unreacted neutralised ^{89}Zr solution was reused in further extractions of [^{89}Zr]-Zr(oxinate)$_4$ by transferring to 5 ml reaction glass flask, adding 500 μl of 1 mg/ml oxine in chloroform and repeating all the procedures for synthesising [^{89}Zr]-Zr(oxinate)$_4$. Activities of initial neutralised ^{89}Zr and [^{89}Zr]-Zr(oxinate)$_4$ were measured with a dose calibrator. Labelling efficiencies were calculated using equation as follows:

$$\text{Labelling efficiency} = (\text{Act}^{89}\text{Zr}_{\text{oxine}} * 100) / \text{Act}_{\text{int}}$$

where $\text{Act}^{89}\text{Zr}_{\text{oxine}}$ = Activity of produced [^{89}Zr]-Zr(oxinate)$_4$

Act_{int} = Activity of initial neutralised ^{89}Zr solution

However, to determine labelling efficiency, only the first synthesising extraction can be precisely calculated because activities of subsequently reuse ^{89}Zr solutions were not actually measured. Those activities could be estimated as follows. The initial activity of neutralised ^{89}Zr in each synthesis which was measured with the dose calibrator was subtracted with the activity of produced [^{89}Zr]-Zr(oxinate)$_4$ in the correspondent extraction. The rest of the activity became the initial activity of the subsequent extraction. Then calculations were repeated in the same manner for the following production and applied to all of 5 syntheses.

3.3.2 Quality control of [^{89}Zr]-Zr(oxinate)$_4$

In this study two techniques were used to determine radiochemical purity of [^{89}Zr]-Zr(oxinate)$_4$ complex, instant thin layer chromatography (ITLC) and solvent extraction. For ITLC, instant thin layer chromatography strips impregnated with silica gel (ITLC-SG) were cut into 1 cm X 8 cm strips, the origin and solvent front were marked with pencil at 1 cm and 7.5 cm, respectively, from the edge of strip. In order to verify the Rf of [^{89}Zr]-Zr(oxinate)$_4$ in thin layer chromatography system, cold zirconium oxine complex Zr(oxinate)$_4$ of verified formula and purity was provided from Mr. Trevor J Ferris, School of Physical Sciences, University of Kent, UK. A small amount of Zr(oxinate)$_4$ (yellow powder) was dissolved in DMSO. Then 1 μl of this solution was spotted on ITLC-SG strip. The separation was developed in mobile phase, ethyl acetate, until the solvent reached the solvent front line. The zirconium complex was visualised and marked in UV box with a short wavelength. The Rf of neutralised ^{89}Zr was determined in the same system. Using this method [^{89}Zr]-Zr(oxinate)$_4$ dissolved in DMSO prior to dilution with saline was verified against with cold complex and compared with neutralized ^{89}Zr. Radiochromatograms were scanned with a TLC scanner (LabLogic, UK) using Laura (v. 4.0.3.75) software (LabLogic, UK).

For solvent extraction technique, the two-phase system was prepared prior to the experiment. A one to one volume by volume (50 ml for each phase) mixture of PBS and chloroform was mixed and left to equilibrate for around 2-3 hours before using. Preferential solubility of free ^{89}Zr and [^{89}Zr]-Zr(oxinate)$_4$ between two phases was determined so that we could calculate percentage of labelling yield in any following samples. 0.5 ml of each phase was transferred into 15 ml Falcon tubes. 0.5 μl of neutralised ^{89}Zr or [^{89}Zr]-Zr(oxinate)$_4$ (dissolved in DMSO) was added into this mixture then it was continuously vortexed for 1 minute and left to stand for 3 min. One hundred μl of each phase were transferred to 1.5 ml eppendorff tubes and count rate (count per minute) was measured in the gamma counter. Then to calculate radiochemical purity of [^{89}Zr]-Zr(oxinate)$_4$ complex, count rate of ^{89}Zr in the organic phase was divided by total count rate in both phases and multiply by one hundred as shown in equation below.

Radiochemical purity = (CPM $_{\text{organic phase}}$) * 100/ (CPM $_{\text{organic phase}}$ + CPM $_{\text{aqueous phase}}$)

3.3.3 Cell culture

Mouse macrophages (J774), breast adenocarcinoma cells (MDA-MB-231) and mouse myeloma eGFP-5T33 were used to investigate the rate and percentage of uptake and efflux of [^{89}Zr]-Zr(oxinate)$_4$. J774 cell line was kindly provided by Dr. Helen Collins, Department of Infectious Diseases, King's College London. Cells were cultured in adhesion semi-continuous culture in high glucose (4.5 g/l glucose) DMEM supplemented with 10% foetal bovine serum, 2 mM L-glutamine, penicillin/streptomycin (5 ml of 5000U pen/ 5000 μg/ml strep), 1 mM sodium pyruvate and 10 mM HEPES. MDA-MB-231 cell line was provided from University of Manchester (ATCC-HTB-26). MDA-MB-231 were semi-continuously grown as adhesion culture in medium containing 10% fetal bovine serum, 2mM L-glutamine and

25000 U penicillin/25 mg streptomycin. All cell lines were cultured under a humidified atmosphere at 37^{o}C with 5% CO_2.

On the experiment day, culture medium of J774 cells was removed and the J774 adhesion cells were washed twice with PBS (10 ml and 20 ml in 75 cm^2 and 175 cm^2 flask, respectively). Serum-free medium was added and cells were scraped from the culture flask and gently mixed before counting. For MDA-MB-231 cells, after removing culture medium and washing the cells with PBS, trypsin (1 ml and 2 ml for 75 cm^2 and 175 cm^2 culture flask, respectively) was added into pre-washed cells and further incubated in 37^{o}C incubator for 5 min to detach cells from the flask. Medium was added to stop the reaction and cells were counted in a cell counting machine (Countess automated cell counter, Invitrogen, USA). Both cell types were diluted to a final concentration of $1x10^6$ cells in 450 μl of serum free medium then dispensed into glass test tubes for labelling experiments.

The eGFP-5T33 murine multiple myeloma cell line was provided by Dr Yolanda Calle (University of Roehampton) and used for *in vitro* studies and *in vivo* cell tracking. Cells were grown in suspension culture in RPMI 1640 supplemented with 10% foetal bovine serum, L-glutamine and penicillin/streptomycin semi-continuously in humidified 37^{o}C with 5% CO_2. Cells were subcultured by transferring the cell suspension to a new 50 ml falcon tube followed by centrifugation at 2000 RPM for 5 min. The supernatant was discarded and the cell pellet was resuspended in fresh culture medium and transferred to new culture flask. In order to prepare cells for particular experiments, the cell pellet was washed with PBS twice before counting cell numbers for preparing the required cell concentration.

3.3.4 Uptake and efflux experiments

In order to investigate in vitro uptake of tracer, [^{89}Zr]-Zr(oxinate)$_4$ and neutralized ^{89}Zr were diluted to 0.05 MBq per 50 μl serum free medium before adding to each glass reaction tube containing with 1x10^6 cells (J774, MDA-MB-231 or eGFP-5T33) in 450 μl serum free medium. The percentages of ^{89}Zr tracer taken up by all three cell types were determined at 5 time points (1, 15, 30, 45 and 60 min) during incubation at room temperature. At each point, the reaction tubes were centrifuged at 2000 RPM for 5 min. Four hundred and fifty microlitres of supernatant were transferred into a new tube. Cell pellets (including residual supernatant) and their corresponding supernatants were counted in gamma counter to calculate the percentage of radioactivity in labelled cells in each time point. The percentage of radiotracers taken up in the cells was calculated as shown in the equation as follows:

$$\% \text{ uptake in the cells} = (CPM_{act\ cell} * 100) / (CPM_{cell} + CPM_{sup})$$

$$CPM_{act\ cell} = CPM_{cell} - ((CPM_{sup} * 50)/450)$$

where $CPM_{act\ cell}$ = actual count rate of the cell pellet corrected with the count rate of 50 ml residual of supernatant

CPM_{cell} = count rate of the cell pellet

CPM_{sup} = count rate of the supernatant

The experiments were repeated 3 times. [^{111}In]-In(oxinate)$_3$ was also used as a radiolabel, for comparison, using similar procedures, in the case of the J774 cell line. 0.1 MBq of [^{111}In]-In(oxinate)$_3$ (GE Healthcare, UK) was added per cell sample and then the experiments were performed as described for zirconium tracers. In addition,

cell free controls were analysed in the same way at the same time points to determine degree of binding of tracers to the glass reaction tubes.

For the efflux study, cells were incubated with the tracer for 30 min using the same conditions as in the uptake study described above. After removing the supernatant, cell pellets were washed with 500 μl of PBS twice to remove excess radiotracer. Five hundred microlitres of fresh medium supplemented with 10% FBS were added into each tube. Tracer retention was determined at 1, 2, 3, 20 and 24 hr post labelling for J774 and MDA-MB-231 cells with [^{89}Zr]-Zr(oxinate)$_4$ and [^{111}In]-In(oxinate)$_3$ whereas the retention of eGFP-5T33 cells with [^{89}Zr]-Zr(oxinate)$_4$ was determined at 1, 20 and 24 hr after labelling. At each time point, samples were centrifuged at 2000 RPM for 5 min to pellet the cells. Five hundred microlitres of supernatant were removed to a new tube. Radioactivity in the cell pellets and corresponding supernatants were counted in gamma counter. Percentage retention of tracers in the labelled cells was calculated from activity in the cell pellets compared to total activity in cells and supernatants.

3.3.5 Labelling the eGFP-5T33 myeloma cell line

The 5T33 is a syngeneic murine multiple myeloma model that originates from the C57Bl/KaLwRij (immunocompetent) strain. Cells can be maintained *in vitro* and disease can be induced by i.v. inoculation. The model has been used for 3 years in our laboratories, and based on our previous experience (in which cell tracking with In-111 had been used to characterise the model) we decided to evaluate the radiotracer in this model for comparison. Therefore, before *in vivo* study was performed, the percentage of [^{89}Zr]-Zr(oxinate)$_4$ taken up by eGFP-5T33 cells was determined. Because [^{111}In]-In(oxinate)$_3$ is one of the standard radiopharmaceuticals for labelling white blood cells in nuclear medicine then in this part of study eGFP-5T33 was labelled with [^{111}In]-

In(oxinate)$_3$ to compare with [^{89}Zr]-Zr(oxinate)$_4$. Since for *in vivo* imaging of labelled cells a higher activity of labelled cells is needed compared with *in vitro* uptake studies, higher activities of [^{89}Zr]-Zr(oxinate)$_4$ and [^{111}In]-In(oxinate)$_3$ were used. In this experiment, eGFP-5T33 cells were labelled with neutralised ^{89}Zr, [^{89}Zr]-Zr(oxinate)$_4$ and [^{111}In]-In(oxinate)$_3$, as follows.

Twenty microlitres of eGFP-5T33 cells suspension was dispensed from the culture flask to count cells using automated cell counter. Approximately 10^7 cells were transferred from the culture flask into a 50 ml falcon tube and centrifuged at 2000 RPM for 5 min. The supernatant was discarded and the cell pellet was washed twice with 15 ml PBS. After washing, cell pellets were resuspended in serum-free medium and cell concentration and viability was determined in the Invitrogen cell counter based on trypan blue exclusion. The cell suspension was diluted to a final cell concentration of 4.0 x 10^6 to 7.5 x 10^6 cells per ml. Then 7.5 x 10^6- 1.5 x 10^7 eGFP-5T33 cells were transferred to 50 ml Falcon tube and then serum-free medium was added to reach a final volume of 2 ml.

Then radiotracers [^{89}Zr]-Zr oxalate, [^{111}In]-In(oxinate)$_3$ and [^{89}Zr]-Zr(oxinate)$_4$, were diluted to 1 ml in serum-free cell culture medium. For neutralised ^{89}Zr, activity around 1.7-1.9 MBq was added to the cell suspensions. Labelling with [^{111}In]-In(oxinate)$_3$ and [^{89}Zr]-Zr(oxinate)$_4$ were performed both with higher (7 and 5 MBq) and lower (2 and 0.3 MBq) activities. Diluted radiotracers were added dropwise to the cell suspensions in the 50 ml Falcon tubes. Actual added activities in the tubes were measured in dose calibrator. The suspensions were incubated at room temperature for 30 min and gently shaken occasionally. After incubation, 7 ml of PBS were added and then centrifuged at 2000 RPM for 5 min. The supernatant (SN) was removed and cell pellets were washed twice with 10 ml PBS (1st and 2nd wash). Supernatants and

washing solutions in every step were collected in the same tube; the radioactivities of supernatants were measured in the dose calibrator prior to pooling washing solutions. After the second washing step, cell pellets were resuspended in 12-15 ml of cell culture medium then activities in the labelled cells were measured. Cell viabilities and concentrations were measured in the Invitrogen cell counter using trypan blue exclusion.

3.3.6 Labelling human white blood cells with [^{89}Zr]-Zr(oxinate)$_4$

The routine clinical procedure developed for white blood cell labelling at the Department of Nuclear Medicine, Guy's Hospital, was followed in this study (details below). Human WBCs were labelled with [^{89}Zr]-Zr(oxinate)$_4$ instead of [^{111}In]-In(oxinate)$_3$ or Tc-99m HMPAO which were commercial available and widely used in Nuclear Medicine using similar SOPs for radiolabelling white blood cells.

[^{89}Zr]-Zr(oxinate)$_4$ was synthesised from ^{89}Zr oxalate and oxine as described previously. After chloroform was completely evaporated from the organic phase of [^{89}Zr]-Zr(oxinate)$_4$ solution, residual [^{89}Zr]-Zr(oxinate)$_4$ was redissolved in 15 µl of DMSO then transferred to a small glass vial. QC of tracer was performed as described above (i.e. solvent extraction in PBS and chloroform mixture and ITLC). Radiochemical purity of the tracer was higher than 95%. Activity of [^{89}Zr]-Zr(oxinate)$_4$ in DMSO was measured in the dose calibrator.

The syringe for blood collection was prepared as follows. A fifty ml syringe containing 500 U of heparin (heparin 1000 units/ml in ampoule), was prepared. A 20 gauge scalp-vein cannula (chosen because the extension cannula in its set offers more efficient and flexible handling and reduced risk of dislodging when drawing high volume of blood from peripheral vein) was attached to the heparinised syringe and 55

ml blood was withdrawn from a peripheral vein of a volunteer, slowly to avoid red blood cell haemolysis. The cannula was replaced on the syringe by a red luer lock syringe cap. The syringe was gently inverted 4-5 times to complete mixing of blood with heparin. The blood filled syringe was carefully handled and wiped with 70% IMS to avoid contamination from blood infection.

The entire WBCs labelling procedure was performed inside a laminar flow cabinet as follows. Two ml of Methocel 2% (to help red blood cells to sediment from white blood cells efficiently) were added into a 50 ml Falcon tube. 45 ml of the anticoagulant-blood mixture were transferred into the prepared 50 ml Falcon tube labelled as sample A. The tube was sealed then contents were mixed very gently. The remaining 10 ml of the anticoagulant blood mixture were transferred to a new 15 ml Falcon tube labelled as sample B. Both tubes were placed upright in a plastic rack. To separate white blood cells for subsequent labelling with the radiotracer, the 50 ml Falcon tube, sample A, was centrifuged at 210 RPM for 15 min. After centrifugation, the upper layer (supernatant) contained white blood cells, platelets and leukocyte rich plasma (LRP). A 20 ml syringe attached to kwill tube (a plastic cannula used instead of a needle, to reduce damage to cells) was used to withdraw the supernatant without disturbing the packed red blood cell layer. The supernatant was transferred into a new 50 ml Falcon tube then centrifuged at 900 RPM for 5 min. After centrifugation, white blood cells formed a pellet at the bottom of the tube, and the supernatant layer was platelet-rich plasma (PRP). The supernatant was gently removed to avoid disturbing packed of white blood cells by using syringe attached to a kwill. The pellet was then washed in 10 ml of isotonic saline (sodium chloride 0.9% w/v) to remove plasma residues. The tube was centrifuged at 900 RPM for 5 min then the supernatant was discarded. The pellet was gently resuspended in 1 ml of saline then transferred into a glass test tube. [^{89}Zr]-Zr(oxinate)$_4$ in 15 µl DMSO was diluted with 1 ml normal saline

then added to the above cell suspension and mixed very gently. The tracer was incubated with white blood cells at room temperature for 15 min. In the meantime platelet-poor plasma (PPP) was prepared from sample B by centrifuging the sample at 2000 RPM for 5 min. The supernatant layer consisting of PPP was collected in a new 15 ml Falcon tube. This solution was kept and used to dilute and resuspend WBCs after labelling with radiotracer to simulate physiological conditions. After incubating WBCs with [^{89}Zr]-Zr(oxinate)$_4$ for 15 min, the cell suspension containing the labelled cells was withdrawn with auto-pipette and transferred back to the original 50 ml Falcon tube. Three ml of PPP were added to radioactive white blood cell suspension and saline was used to dilute the solution to 10 ml. The mixture was then centrifuged at 900 RPM for 5 min. Then supernatant containing unbound [^{89}Zr]-Zr(oxinate)$_4$ was carefully withdrawn without disturbing the white cell pellet and collected into a new 50 ml Falcon tube. The radiolabelled white blood cell pellet was gently re-suspended in 3 ml of PPP. Activities in the labelled cells and supernatant were measured in the dose calibrator. Cell labelling yield was calculated as activity in the labelled white cells divided by the sum of activity in the labelled cells and supernatant then multiplied by one hundred shown in the equation as follows.

$$\text{Cell labelling yield} = (\text{Act}_{\text{cell}}) * 100 / (\text{Act}_{\text{cell}} + \text{Act}_{\text{sup}})$$

where Act_{cell} = Activity of the labelled white blood cells

Act_{sup} = Activity of the supernatant

The cells suspension was incubated in a tissue culture incubator (37^{o}C, 95% air/5% CO_2 humidified atmosphere). Retention of radioactivity was determined at 24 hours after labelling. At the time point, the tube was taken from the incubator and processed as follows. Cells suspensions were centrifuged at 2000 RPM for 5 min. The

supernatant was carefully collected and transferred to another glass tube. Activities in labelled WBCs and in supernatant were measured and percentage of activity in the cells calculated.

3.4 Results

3.4.1 Optimisation of reaction time for [^{89}Zr]-Zr(oxinate)$_4$ synthesis (low activity)

To determine the optimal reaction time to synthesise [^{89}Zr]-Zr(oxinate)$_4$, 1 - 2 MBq neutralised ^{89}Zr (aqueous phase) was incubated and agitated with 500 μg oxine (chloroform phase) for 15, 45 and 60 min. (Upon separation the two phases were collected separately, [^{89}Zr]-Zr(oxinate)$_4$ and free ^{89}Zr in chloroform phase and aqueous phase, respectively, were collected and counted to determine the labelling efficiency.) Labelling efficiency was above 95% at each time point (results shown in Table 3.1).

Time (min)	Labelling yield (%)
15	95.3 ± 1.3
45	97.0 ± 0.4
60	95.5 ± 0.4

Table 3.1: Labelling yield of [^{89}Zr]-Zr(oxinate)$_4$ with 500 μg of oxine using solvent extraction technique with a range of reaction times for 15 min, 45 min and 60 min.

3.4.2 Optimisation of amount of oxine (low activity)

After synthesising [^{89}Zr]-Zr(oxinate)$_4$ in presence of various amount of oxine ligand (using a 15 minute reaction time based on results above), radiolabelling efficiencies were determined, results are shown in Table 3.2.

Amount of oxine (μg)	Labelling yield (%)
100	81.7 ± 2.5
300	92.4 ± 8.9
500	96.9 ± 2.1

Table 3.2: Labelling yield of [^{89}Zr]-Zr(oxinate)$_4$ with varied amount of oxine (n=4, 3 and 4, respectively)

3.4.3 Quality control of [^{89}Zr]-Zr(oxinate)$_4$ complex

Chromatography of cold zirconium oxine was performed with ITLC-SG with ethyl acetate mobile phase, and showed the Rf of zirconium complex to be 0.9, detected under short wavelength UV.

After synthesis of [^{89}Zr]-Zr(oxinate)$_4$ dissolved in DMSO, the radiochemical purity of [^{89}Zr]-Zr(oxinate)$_4$ was determined by using ITLC-SG with ethyl acetate mobile phase. Neutralised ^{89}Zr (^{89}Zr oxalate) was also analysed in the same system. R_f values of ^{89}Zr oxalate and [^{89}Zr]-Zr(oxinate)$_4$ were 0 and 0.9, respectively, as shown in Figure 3.1.

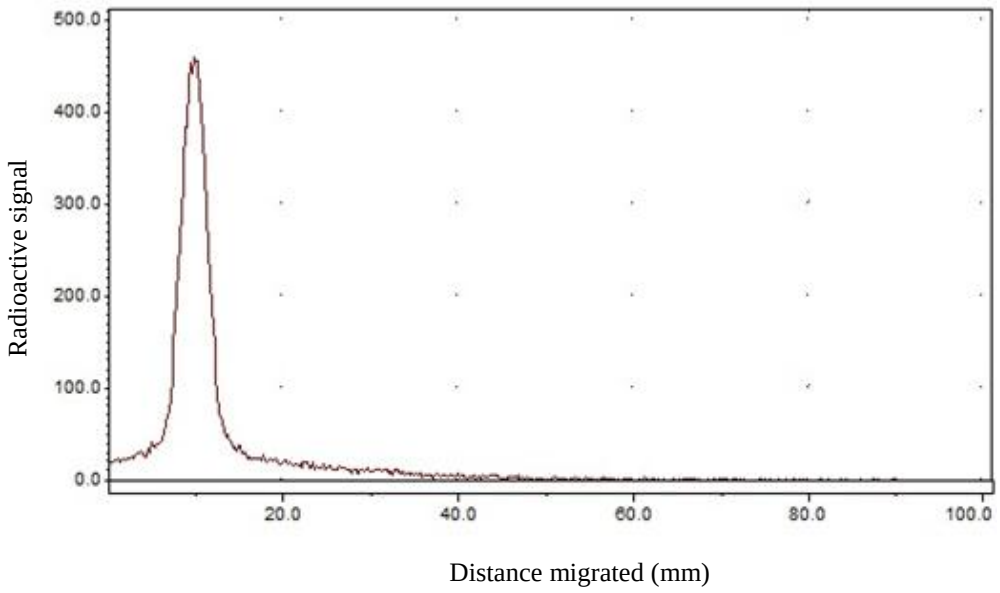

(A)

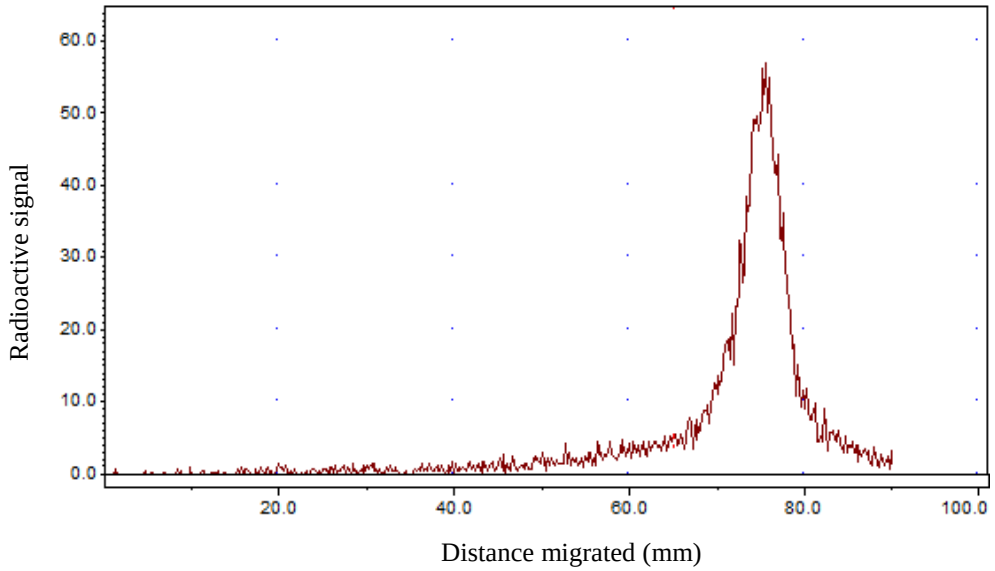

(B)

Figure 3.1: Radiochromatograms of ^{89}Zr oxalate (A, Rf = 0) and [^{89}Zr]-Zr(oxinate)$_4$ (B, R_f = 0.9) in ITLC/SG-ethyl acetate system.

Solvent extraction results showed that ^{89}Zr oxalate ("free ^{89}Zr") was extracted in the aqueous phase whereas [^{89}Zr]-Zr(oxinate)$_4$ was dissolved in the chloroform phase. Radiochemical purity of [^{89}Zr]-Zr(oxinate)$_4$ (dissolved in DMSO) used subsequently for cell labelling was over 95%.

3.4.4 Labelling efficiency of synthesis of [^{89}Zr]-Zr(oxinate)$_4$ for *in vivo* studies (high activity)

Results of 5 syntheses of [^{89}Zr]-Zr(oxinate)$_4$ by the solvent extraction technique are summarised in Table 3.3. Radiochemical yields were much lower than with the low activity experiments described above.

Starting activity (MBq)	Sequence of extraction	Activity of ^{89}Zr oxine (MBq)	Labelling efficiency (%)
47.5	1st	3.7	7.79
	2nd	23.1	52.74
77.6	1st	0.7	0.90
	2nd	5.5	7.15
	3rd	12.7	17.79
	4th	27.8	47.36
50.7	1st	10.0	19.70
	2nd	17.5	43.00
	3rd	9.0	38.79
66.0	1st	1.7	2.58
	2nd	24.8	38.57
	3rd	21.9	55.44

Starting activity (MBq)	Sequence of extraction	Activity of ^{89}Zr oxine (MBq)	Labelling efficiency (%)
84.0	1st	22.3	26.55
	2nd	23.2	37.60
	3rd	16.8	43.64
	4th	12.5	57.60
	5th	8.0	86.96

Table 3.3: Results of five independent attempts to synthesise [^{89}Zr]-Zr(oxinate)$_4$ for *in vivo* imaging using solvent extraction technique. "Starting activity" is the activity (i.e. activity added to the first 500 μg of oxine) of neutralised ^{89}Zr which was used to synthesise the first extraction of [^{89}Zr]-Zr(oxinate)$_4$. The first extraction of [^{89}Zr]-Zr(oxinate)$_4$ in chloroform phase was then separated. The activity of the chloroform phase (i.e. [^{89}Zr]-Zr(oxinate)$_4$) was measured as shown in the column of activity of [^{89}Zr]-Zr(oxinate)$_4$ (refer to Table 3.3) prior to evaporating chloroform before using for *in vivo* studies. Neutralised ^{89}Zr was transferred to the glass flask and reused. A fresh 500 μg of oxine in 500 μl chloroform was added and the procedures for extracting were repeated to produce the subsequent extractions of [^{89}Zr]-Zr(oxinate)$_4$ as shown in the sequence of synthesis for the second, third, fourth and fifth sequences (refer to Table 3.3). The starting activity in each extraction was the left over activity of ^{89}Zr from the previous sequence (i.e. the aqueous phase was re-used with a new aliquot of oxine in chloroform).

3.4.5 *In vitro* uptake and efflux of [^{89}Zr]-Zr(oxinate)$_4$ in cell lines

[^{89}Zr]-Zr(oxinate)$_4$ uptake studies were carried out in J774 and MDA-MB-231 cell lines. Neutralised ^{89}Zr was used as a control. The accumulation of [^{89}Zr]-

$Zr(oxinate)_4$ in both cell lines increased with time over an incubation period of 60 min (refer to Figure 3.2 and 3.3). The percentage of tracer uptake was similar in both cell lines. Neutralised ^{89}Zr (in the form of ^{89}Zr oxalate) exhibited relatively low uptake in both cell lines. The highest percentage of uptake of $[^{89}Zr]$-$Zr(oxinate)_4$ in J774 and MDA-MB-231 cells after 60 min of incubation was 23% and 20%, respectively, as shown in Figure 3.2 and 3.3. A slight uptake of neutralised ^{89}Zr was observed in both cell lines however this was significantly lower than that of $[^{89}Zr]$-$Zr(oxinate)_4$ (Figure 3.2 and 3.3). The uptake of $[^{89}Zr]$-$Zr(oxinate)_4$ was also determined in eGFP-5T33 multiple myeloma cells. Results show that for 1 x 10^6 cells, around 10% of the radiotracer was taken up after 60 minutes as shown in Figure 3.4. Meanwhile cellular uptake of $[^{111}In]$-$In(oxinate)_3$ was determined in J774 cells, the result was shown in Figure 3.5 which showed extracted activity into the cells between 11% and 42% over 60 min.

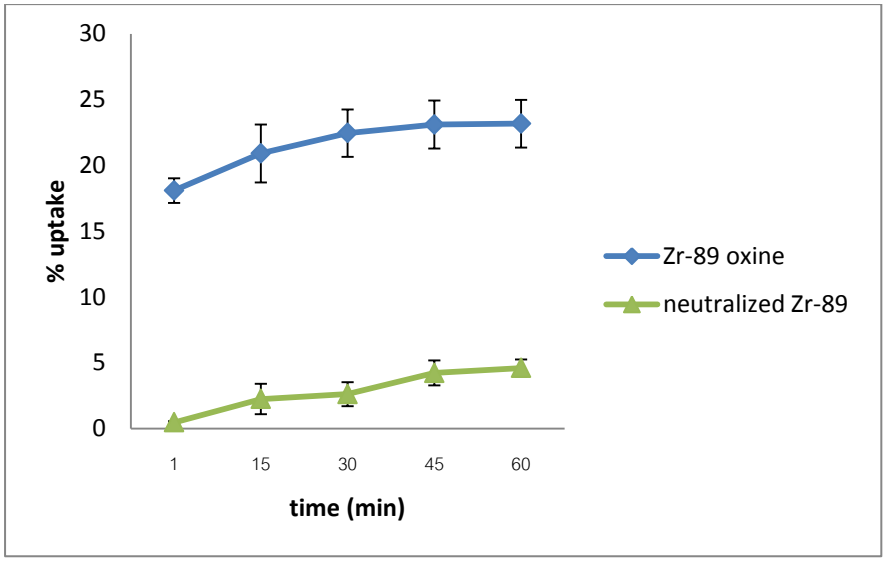

Figure 3.2: Comparison of uptake of $[^{89}Zr]$-$Zr(oxinate)_4$ and neutralised ^{89}Zr in J774 cells as a function of incubation time.

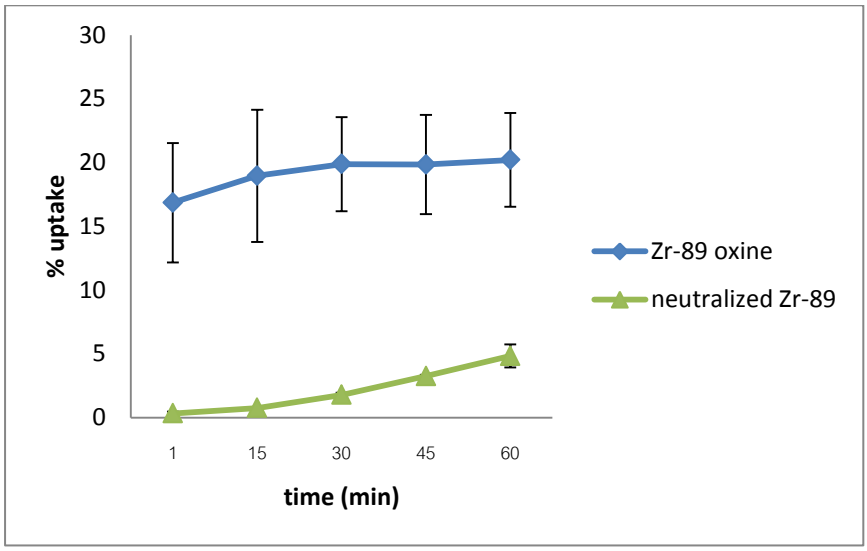

Figure 3.3: Comparison of [^{89}Zr]-Zr(oxinate)$_4$ and free ^{89}Zr uptake in MDA-MB-231 cells.

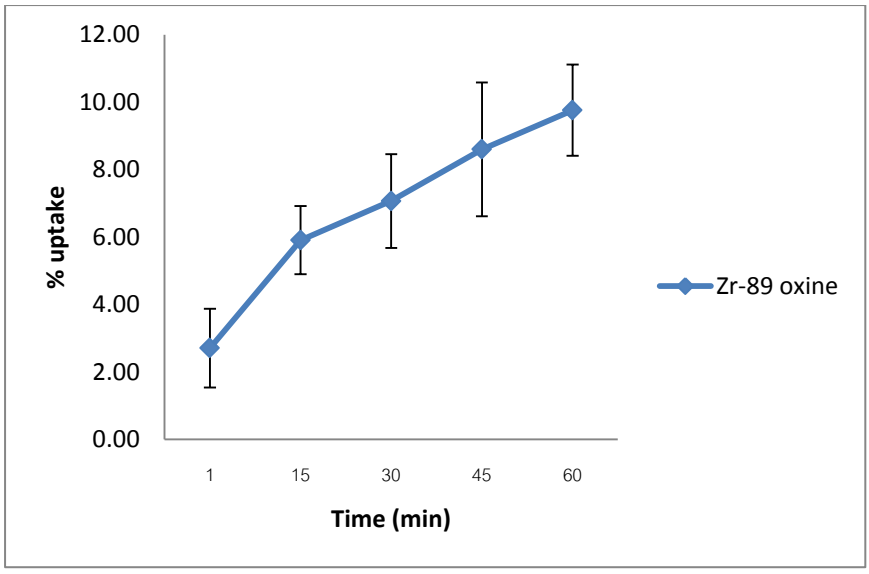

Figure 3.4: Graph showing cellular uptake of [^{89}Zr]-Zr(oxinate)$_4$ in multiple myeloma cells, eGFP-5T33, over 60 min.

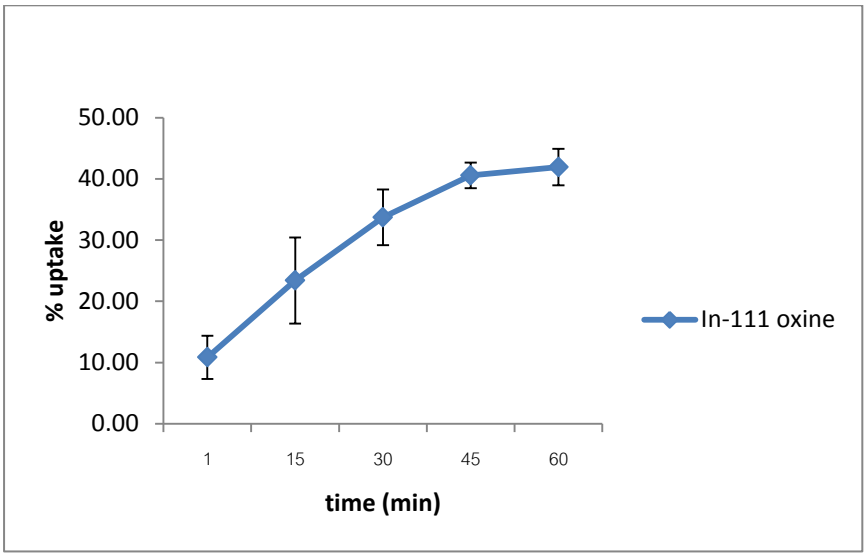

Figure 3.5: Graph showing cellular uptake of [^{111}In]-In(oxinate)$_3$ in mouse macrophages cells, J774, over 60 min.

We also determined the extent of non-specific binding of [^{89}Zr]-Zr(oxinate)$_4$ to the glass reaction tubes. Results shown in Table 3.4 suggest that this was negligible.

Time (min)	Percentage of ^{89}Zr oxine binding to glass tube
1	0.13 ± 0.04
15	0.38± 0.19
30	0.24 ± 0.14
45	0.25 ± 0.11
60	0.29 ± 0.09

Table 3.4: Degree of binding between [^{89}Zr]-Zr(oxinate)$_4$ and glass tube. The activity bound to glass tube was carried out in cell-free reaction in the same manner as cell uptake experiments.

Examination of the efflux kinetics of [^{89}Zr]-Zr(oxinate)$_4$ in labelled cells showed that in J774 and MDA-MB-231 cell lines wash out from labelled cells was minimal: around 94% to 96% of tracer was retained in labelled cells in first 3 hours after labelling and around 91% and 82% was still associated with the J774 and MDA-MB-231 cells, respectively, after 24 hours (Figure 3.6). [^{89}Zr]-Zr(oxinate)$_4$ in eGFP-5T33 showed greater than 70% retention within the cells after 1 day post-labelling (Figure 3.7). [^{111}In]-In(oxinate)$_3$ was also examined to determine the percentage of retention in the labelled J774 and MDA-MB-231 cells; activity between 89% and 52% remained associated with J774 cells from 1 hr to 24 hr post labelling and similarly, 90% to 44% activity was retained in the MDA-MB-231 cells at 1 hr and 24 hr post-labelling (Figure 3.8).

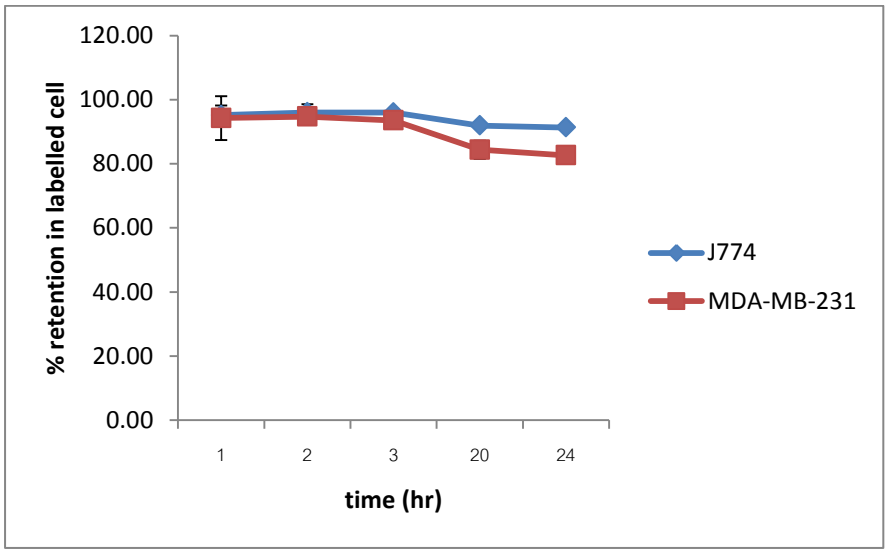

Figure 3.6: Percentage of ^{89}Zr retained over a period of 24 hr in 1 x 10^6 J774 cells and MDA-MB-231cells, after labelling with [^{89}Zr]-Zr(oxinate)$_4$.

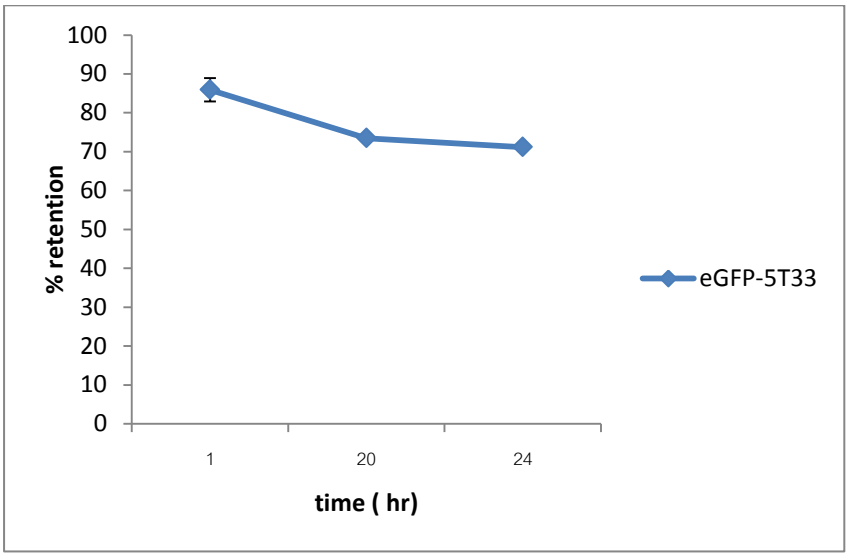

Figure 3.7: Graph shows the efflux of ^{89}Zr from labelled eGFP-5T33 cells over 24 hr post labelling.

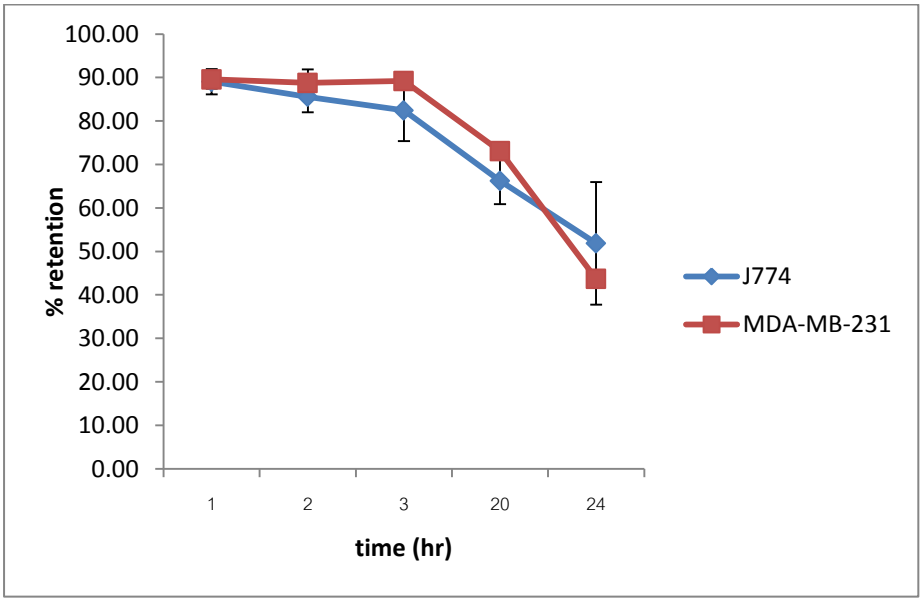

Figure 3.8: Percentage of ^{111}In retained over a period of 24 hr in 1 x 10^6 labelled J774 cells and MDA-MB-231cells, after labelling with [^{111}In]-In(oxinate)$_3$.

3.4.6 Results of radiolabelling eGFP-5T33 cells

Labelling with [^{89}Zr]-Zr(oxinate)$_4$ and [^{111}In]-In(oxinate)$_3$ were studied and compared in the eGFP-5T33 cell line. Results are shown in Tables 3.5-3.7.

	Tube 1	Tube 2	Tube 3	Tube 4
Number of cells	7.5 x 10^6	7.5 x 10^6	7.5 x 10^6	7.5 x 10^6
Viability$_i$	98%	98%	98%	98%
Neutralised ^{89}Zr added	1.8 MBq	1.7 MBq	1.9 MBq	1.9 MBq
Activity of SN + 1st and 2nd wash	1.8 MBq	1.6 MBq	1.9 MBq	1.83 MBq
Activity of cell pellet	0.1 MBq	0.1 MBq	0.1 MBq	0.1 MBq
Viability$_a$	75%	75%	75%	75%
Number of labelled cells	5 x 10^6	5 x 10^6	5 x 10^6	5 x 10^6
Labelling yield	0%	5.0%	0%	3.68%

Table 3.5: Neutralised ^{89}Zr-oxalate labelling of eGFP-5T33 cells. Tubes 1-4 represent labelling with neutralised ^{89}Zr with eGFP-5T33 cells in four replicates. "Number of cells" refers to the initial number of cells used in the labelling procedure and number of labelled cells refers to the total number of cells after labelling. Viability$_i$ is the initial cell viability before starting the labelling process and viability$_a$ is the cell viability after the labelling procedure had been completed. Activity of SN is the activity of supernatant which was removed from the cell pellets after labelling and centrifugation, 1st and 2nd wash are activities of the supernatants discarded after 1st and 2nd washing steps. Activity of cell pellet is the final activity of labelled cells. Labelling yield was calculated as the ratio of 'activity of cell pellet' and added activity of tracer (neutralised ^{89}Zr, [^{89}Zr]-Zr(oxinate)$_4$ and [^{111}In]-In(oxinate)$_3$).

In several columns in Tables 3.5-3.7, the sum of activity of cell pellet, activity of supernatant and activity from washing steps is higher than the activity added to the tube. These (minor) differences can be accounted for by an instrument error (low accuracy of dose calibrator when measuring low activities). Cell labelling yield therefore was calculated based on the added activity and activity in supernatant including activity in washing buffer. Based on these calculations the uptake of neutralised ^{89}Zr was very low.

	Tube 1	Tube 2	Tube 3	Tube 4
Number of cells	8.5×10^6	8.5×10^6	8.5×10^6	8.5×10^6
$Viability_i$	97%	97%	97%	97%
^{89}Zr oxine added	5.50 MBq	0.33 MBq	0.30 MBq	0.30 MBq
Activity of SN	2.47 MBq	0.2 MBq	0.2 MBq	0.2 MBq
Activity of SN + 1st wash	3.62 MBq	0.2 MBq	0.2 MBq	0.2 MBq
Activity of SN + 1st wash + 2nd wash	3.68 MBq	0.2 MBq	0.3 MBq	0.2 MBq
Activity of cell pellet	1.6 MBq	0.1 MBq	0.1 MBq	0.1 MBq
$Viability_a$	70%	70%	70%	70%
Number of labelled cells	6×10^6	6×10^6	6×10^6	6×10^6
Labelling yield	29.09%	30.00%	33.00%	33.00%

Table 3.6: Results of [^{89}Zr]-Zr(oxinate)$_4$ labelling with eGFP-5T33 cells. In tube 1 and tube 2-4, eGFP-5T33 cells were labelled with high and low activities of [^{89}Zr]-Zr(oxinate)$_4$, respectively.

Uptake of [^{89}Zr]-Zr(oxinate)$_4$ was between 29-33%; the percentage uptake was not affected by the activity (Table 3.6 and 3.7) (which is higher than that of neutralised ^{89}Zr). Measurements of low activity also shows inaccuracy as in the previous experiment.

	Tube 1	Tube 2	Tube 3	Tube 4
Number of cells	1.3 x 10^7	1.3 x 10^7	1.3 x 10^7	1.3 x 10^7
Viability$_i$	97%	97%	97%	97%
^{111}In oxine added	7.10 MBq	2.32 MBq	2.36 MBq	2.37 MBq
Activity of SN	0.40 MBq	0.3 MBq	0.4 MBq	0.4 MBq
Activity of SN + 1st wash	0.50 MBq	0.4 MBq	0.4 MBq	0.5 MBq
Activity of SN + 1st wash + 2nd wash	0.7 MBq	0.4 MBq	0.4 MBq	0.6 MBq
Activity of cell pellet	5.95 MBq	1.78 MBq	1.84 MBq	1.72 MBq
Viability$_a$	80%	80%	80%	80%
Number of labelled cells	8.5 x 10^6	8.5 x 10^6	8.5 x 10^6	8.5 x 10^6
Labelling yield	83.80%	76.72%	77.97%	72.57%

Table 3.7: Labelling of eGFP-5T33 cells with [^{111}In]-In(oxinate)$_3$. In tube 1 and tube 2-4, eGFP-5T33 cells were labelled with high and low activities of [^{111}In]-In(oxinate)$_3$, respectively.

When labelling eGFP-5T33 cells with [^{111}In]-In(oxinate)$_3$, a greater percentage of tracer was taken up by the cells (up to about 84%) when compared to cells labelled with [^{89}Zr]-Zr(oxinate)$_4$.

3.4.7 Results of human white blood cells labelled [^{89}Zr]-Zr(oxinate)$_4$

Human leukocytes were separated according to SOPs for [^{111}In]-In(oxinate)$_3$ labelling white blood cells. Labelling yields in 3 independent experiments are

summarised in Table 3.8 for [^{89}Zr]-Zr(oxinate)$_4$ labelling and in Table 3.9 for the percentage of retention activity in the cells at 24 hr after labelling is shown. In the second efflux experiment of labelled white blood cells, due to low activity the retention at 24 hr was not determined and only 2 independent experiments were carried out.

Labelling	Added ^{89}Zr oxine (MBq)	Activity in cells (MBq)	Activity in supernatant (MBq)	Total activity (MBq)	Labelling yield (%)
1st	11.10	1.8	9.10	10.90	16.50
2nd	3.05	0.5	2.33	2.83	17.67
3rd	16.20	2.5	13.55	16.05	15.58

Table 3.8: [^{89}Zr]-Zr(oxinate)$_4$ labelling of human white blood cells

Labelling	Activity in labelled WBCs @ 24 hr (MBq)	Activity in supernatant @ 24 h (MBq)	% retention activity in labelled WBCs @ 24 hr
1st	1.15	0.20	85.19
3rd	1.65	0.25	86.85

Table 3.9: Retained activity of [^{89}Zr]-Zr(oxinate)$_4$ in human white blood cells 24 hr post labelling

3.5 Discussion

In order to synthesise [^{89}Zr]-Zr(oxinate)$_4$ complex, a solvent extraction technique was used. The problem of low labelling yield when plastic containers were used in the synthesis process might be due to reaction of organic solvent with plastic containers leading to contamination by the eluted impurity in the reaction (data not shown). To overcome the problem, glass devices and glass containers were chosen in the synthesis process especially for [^{89}Zr]-Zr(oxinate)$_4$ which was further investigated in both *in vitro* and *in vivo* experiments.

The results from optimisation of time of synthesis of [^{89}Zr]-Zr(oxinate)$_4$ with low activities of ^{89}Zr showed that a reaction time of only 15 min was sufficient to produce [^{89}Zr]-Zr(oxinate)$_4$ with labelling efficiency greater than 95%. Results of experiments to determine the effect of varying the quantity of oxine indicated that labelling yield was correlated to the amount of oxine. Using 500 μg of oxine showed the highest labelling yield, around 97% compared to 300 μg and 100 μg (about 92% and 82%, respectively). The optimal conditions therefore selected were 500 μg of oxine with incubation for 15 min. Under these condition, with low activities of ^{89}Zr (i.e. low volumes of the supplied ^{89}Zr in oxalic acid) the radiochemical yield is excellent. Therefore in the following experiments, a protocol to synthesise [^{89}Zr]-Zr(oxinate)$_4$ was adopted with these conditions. However, the quantity of oxine used may need to be increased further for larger activity labelling, in light of experiments described below.

Determination of radiochemical purity of [^{89}Zr]-Zr(oxinate)$_4$ can be done by ITLC or solvent extraction. ITLC-SG (stationary phase) and ethyl acetate (mobile phase) were used to develop the radio-chromatogram of [^{89}Zr]-Zr(oxinate)$_4$ which

demonstrated an Rf of 0.9 whereas the Rf of free ("neutralised") ^{89}Zr was 0. Rf of [^{89}Zr]-Zr(oxinate)$_4$ was compared with cold zirconium oxine complex (dissolved in DMSO) which gave a corresponding Rf value of 0.9. In the solvent extraction procedure, chloroform and PBS were used as organic solvent and aqueous solution, respectively, to examine the percentage of hydrophilic impurity. The lipophilic complex, [^{89}Zr]-Zr(oxinate)$_4$ can be determined from the activity found in the chloroform fraction whereas activity of the other impurities can be determined from the PBS fraction. For the (previously) commercially available [^{111}In]-In(oxinate)$_3$, solvent extraction is a standard procedure to determine labelling efficiency of the complex in the U.S. and European pharmacopeia. Acceptable radiochemical purity of [^{111}In]-In(oxinate)$_3$ used in clinical work according to the pharmacopeia is not less than 90%. However, [^{111}In]-In(oxinate)$_3$ complex is commercially available and ready to use so the process to determine labelling efficiency and shelf life of product is the responsibility of the manufacturers. Although high performance liquid chromatography (HPLC) has been widely used to carry out radiochemical purity testing for a range of radiopharmaceuticals especially in research, for the lipophilic complexes of oxine it has never been reported. HPLC might not be suitable for determining radiochemical purities of the radiotracers oxine complex due to dissociation and hence separation of oxine from indium during passage down the column leading to unreliability.

Oxine is well known as a chelator for metal ions. Lipophilic complexes of oxine have been investigated with a number of radionuclides such as Co-57 (145), Fe-59 (145), Ga-67 (145), Tl-201 and Ga-68 (97) as tracers for labelling cells. Different amounts of oxine have been utilised to complex with radionuclides. For instance in the early research on [^{111}In]-In(oxinate)$_3$, 150 μg of oxine in ethanol was used to complex with [^{111}In]-InCl$_3$ (146); currently commercial available of [^{111}In]-In(oxinate)$_3$ is

prepared with 50 μg of oxine. In other research 150 μg oxine was used to complex with ^{68}Ga (97). Since oxine has antimicrobial properties then it might be toxic to the cells and possible damage the labelled cells would correlate with the amount of oxine. To avoid this effect therefore researchers have been attempted to keep the quantity of oxine as low as possible. In our solvent extraction technique 500 μg of oxine was needed to complex with ^{89}Zr to achieve adequate labelling yield. This amount of oxine is higher than in [^{111}In]-In(oxinate)$_3$ commercially. Therefore an alternative procedure to do the reaction in aqueous solution might be able to reduce quantity of oxine, similar to the commercial [^{111}In]-In(oxinate)$_3$. However, the chemical form of ^{89}Zr is different from that of ^{111}In and the ligand metal affinity is likely to be different, so further optimisation is needed.

The production of [^{89}Zr]-Zr(oxinate)$_4$ by using solvent extraction technique was reproducibly above 75% when lower activity was used in the experiments of method development (1–2 MBq) or for *in vitro* biological evaluation (around 5-10 MBq) was initially used. However, the results of synthesis [^{89}Zr]-Zr(oxinate)$_4$ for the *in vivo* studies using larger activities (40-80 MBq) showed significantly lower radiochemical yields were obtained. From Table 3.3 labelling efficiency of [^{89}Zr]-Zr(oxinate)$_4$ was significantly less than expected and was variable. Among many productions, a similar pattern was observed. Typically the first extraction of [^{89}Zr]-Zr(oxinate)$_4$ gave lower activity compared to activities of the complex produced from the subsequent extractions. This could be explained by the increased quantity of oxalate present in larger volumes, possibly acting as a competing ligand. Initial extractions with chloroform may remove some of the oxalic acid allowing more efficient complexation by oxine in subsequent extractions. From these results, although the synthesis

successfully produced [^{89}Zr]-Zr(oxinate)$_4$ with acceptable quality, labelling efficiency of the high initial activity is still problematic.

A different procedure to synthesise oxine complexes in the aqueous phase with oxine in ethanol instead of chloroform were reported (97, 147). In that procedure, the lipophilic oxine complex was precipitated and then separated from the mixture. Subsequently, organic solvent was used to extract the oxine complex from the precipitate (145). This alternative procedure might improve labelling efficiency of [^{89}Zr]-Zr(oxinate)$_4$ however further investigation is required.

Junfeng Yu *et al*. reported that to prepare ^{90}Y oxine-ethiodol, a therapeutic tracer for liver cancer, ^{90}Y oxine was labelled by reaction between buffered yttrium-90 chloride and oxine in either ethanol or chloroform prior to extracting the ^{90}Y oxine complex in chloroform or dichloromethane (148). The results showed that radiolabelling efficiency depended on the solvent used to dissolve oxine; while chloroform was not able to produce ^{90}Y oxine, about 36% of ^{90}Y oxine could be produced when ethanol was used as a solvent with the same concentration of oxine. This suggests we could apply to our [^{89}Zr]-Zr(oxinate)$_4$ production a procedure to replace the solvent in which oxine is dissolved from chloroform to ethanol to improve radiolabelling efficiency. However alteration of solvents will required further investigation.

Another issue relates to the solvent (DMSO) which is used to dissolve [^{89}Zr]-Zr(oxinate)$_4$ complex after evaporation of the chloroform. It would be preferable to avoid use of DMSO. In case of standard tracer for labelling cells, [^{111}In]-In(oxinate)$_3$, in early research it was produced with solvent extraction technique and the final product [^{111}In]-In(oxinate)$_3$ was dissolved in ethanol. With this procedure, the toxicity of ethanol to the labelled cells was a problem and in addition it was time consuming.

Moreover, this complex was bound to the container so the final product was obtained in lower yield than expected. However, researchers were subsequently able to overcome these problems with a procedure to synthesise [^{111}In]-In(oxinate)$_3$ in an aqueous phase, which was successfully patented in France and USA in the 1980s. This formula contained a surfactant which reduced amount of tracer adsorbed to its containing glass vial. The aqueous solution can be autoclaved to give sterile [^{111}In]-In(oxinate)$_3$ product suitable for autologous blood cell labelling. Labelling efficiency to blood cells was also increased compared with those labelled with [^{111}In]-In(oxinate)$_3$ in ethanol solution.

The time-course and efficiency of uptake of the synthesised [^{89}Zr]-Zr(oxinate)$_4$ into 3 different cell lines including mouse macrophage J774, human breast cancer MDA-MB-231 and human multiple myeloma eGFP-5T33 was investigated. The intracellular transport of [^{89}Zr]-Zr(oxinate)$_4$ was monitored using eGFP-5T33 cells.

Currently, the imaging of labelled cells is used clinically for diagnosis and localisation of infection and inflammation lesions. Infection/inflammation in animals is therefore an appropriate model in which to demonstrate new radiolabelling methods. However to obtain an adequate amount of white blood cells (WBCs) for radiolabelling, 10 ml of whole blood from many animal donors is needed. Due to the rapid growth eGFP-5T33 cells, compatible with multiple myeloma mouse model (C57BL/KaLwRij), and because it has been investigated in our group for the other purposes and they have been genetically modified to express eGFP, these cells offer an advantage for use as a model system in the present context.

The uptake rate of [^{89}Zr]-Zr(oxinate)$_4$ showed a similar pattern in all three cell lines used. The radiotracer was moderately transported into the 1 x 10^6 J774 and MDA-MB-231 cells and reached the highest percentage of 23% and 20%, respectively,

while 1 x 10^6 eGFP-5T33 cells showed lower uptake rate at approximately 10%. Meanwhile, the uptake of neutralised ^{89}Zr was determined in order to determine whether lipophilic [^{89}Zr]-Zr(oxinate)$_4$ was required or non-lipophilic neutralised ^{89}Zr (free ^{89}Zr) could be taken up by the cells. As expected, relatively low uptake of free ^{89}Zr into J774 and MDA-MB-231 cells was observed. Although the uptake of free ^{89}Zr into eGFP-5T33 was not determined, low uptake rate was expected, although different uptake rates among cell lines might be cell type dependent which is similar to other radiotracers for labelling cells.

Non-specific binding of [^{89}Zr]-Zr(oxinate)$_4$ to materials used in the vessels and equipment was determined in parallel with cellular uptake experiments, because preliminary work of lipophilic ^{64}Cu complexes had identified problems with adsorption to plasticware. Tracer was found to negligibly bind to the glass reaction tubes and the apparent percentage of tracer taken up by the cells was not affected by non-specific binding. Therefore the results indicated that [^{89}Zr]-Zr(oxinate)$_4$ was successfully taken up in a range of cell types, although the efficiency of uptake (percent) was in general lower than observed for [^{111}In]-In(oxine)$_3$ in parallel cell samples.

The efflux rate of [^{89}Zr]-Zr(oxinate)$_4$ in 3 cell lines after labelling was also investigated. At 24 hr after labelling, the retained activity in J774, MDA-MB-231 and eGFP-5T33 cells was found to be 91%, 83% and 72%, respectively. The retention activity of [^{111}In]-In(oxinate)$_3$ in the labelled cells in both cell lines, J774 and MDA-MB-231, was significantly lower at approximately 52% and 44% in the labelled cells 24 hr post labelling. At 24 hr, the retention of [^{89}Zr]-Zr(oxinate)$_4$ labelled J774 and MDA-MB-231 cells was statistically significantly greater than that of [^{111}In]-In(oxinate)$_3$ with p-values of 0.008 and < 0.001, respectively.

Prolonged retention of activity by labelled cells is advantageous because it allows imaging to follow the labelled cells for longer period of time, and the images are less impaired by the presence of radioactivity that is not bound to the administered cells. This is important especially in the application of tracking labelled therapeutic cells or stem cells where it is desirable to track the cells over a longer periods compared to autologous white blood cell labelling.

For labelling eGFP-5T33 experiment, the labelling procedure was modified to minimise differences of geometry among the samples before measuring with dose calibrator. As shown in Table 2-4, the cell pellets were resuspended with culture medium to a volume of 12-15 ml prior to measuring the activities instead of directly measuring the activities of only the cell pellets compared to the activity in the supernatant (including washing buffer). The eGFP-5T33 cells were labelled with [^{89}Zr]-Zr(oxinate)$_4$ and [^{111}In]-In(oxinate)$_3$ with either high or low activity in order to study the effect of radioactivity levels on labelling yield. The percent labelling yields of both tracers were similar despite using different activities. Taken together, it was found that the initial activity of [^{89}Zr]-Zr(oxinate)$_4$ and [^{111}In]-In(oxinate)$_3$ did not affect the labelling yield in eGFP-5T33 cells. However, the number of cells was an influence on labelling yield. By increasing the number of cells from 1 x 10^6 to around 8.5 x 10^6 and 1.3 x 10^7, the labelling yield was improved with both [^{89}Zr]-Zr(oxinate)$_4$ or [^{111}In]-In(oxinate)$_3$. Therefore these finding suggest, predictably, that labelling yields should be enhanced by increasing the number of cells but not by varying the initial amount of radioactivity.

From the results of white blood cell labelling, WBCs were consistently labelled with [^{89}Zr]-Zr(oxinate)$_4$ in the range of 15.58% and 17.67% (mean 16.58 ± 1.05 %). These cell labelling efficiencies are lower than those of [^{111}In]-In(oxinate)$_3$. 24 hr after

labelling, [^{89}Zr]-Zr(oxinate)$_4$ showed higher retention in the labelled cells than [^{111}In]-In(oxinate)$_3$. Greater than 85% of [^{89}Zr]-Zr(oxinate)$_4$ was retained in the labelled cells whereas retention in [^{111}In]-In(oxinate)$_3$ labelled WBCs was around 75% (based on package insert of [^{111}In]-In(oxinate)$_3$, Amersham Healthcare) at the same time point.

The uptake in the other cell types related to the applications of tracking labelled cells such as T-cells, dendritic cells and stem cells should be further investigated. Another aspect that needs further study prior to translating this method to clinical application is whether [^{89}Zr]-Zr(oxinate)$_4$ can alter cell proliferation and function, including perturbation of genotype and phenotype of the labelled cells, compared to [^{111}In]-In(oxine)$_3$.

3.6 Conclusion

From our study, the production of ^{89}Zr lipophilic complex, [^{89}Zr]-Zr(oxinate)$_4$, was successfully accomplished using a solvent extraction technique. According to the results of optimisation of the amount of oxine and reaction time, 500 μg of oxine was chosen to reach the highest labelling yield and the reaction was performed for 15 min, generating radiotracer with acceptable labelling yield if low activities were used. The quality of [^{89}Zr]-Zr(oxinate)$_4$ was adequate to use in either *in vitro* or *in vivo* studies. However, radiolabelling efficiency when high activity (>40 MBq) is required for *in vivo* imaging, yields are lower and the quantity of oxine, the choice of solvent and overall production procedures need to be improved and opportunities to improve these in future have been identified.

[^{89}Zr]-Zr(oxinate)$_4$ is moderately taken up by several cell types such as macrophages, breast cancer cells and multiple myeloma cells including human white

blood cells. High retention of [^{89}Zr]-Zr(oxinate)$_4$ within the labelled cells (compared to[^{111}In]-In(oxine)$_3$) was shown over all cell types evaluated. It is therefore suggested that [^{89}Zr]-Zr(oxinate)$_4$ is a promising tracer for labelling cells due to consistent higher retention within the labelled cells than the standard radiotracer ([^{111}In]-In(oxinate)$_3$), and other PET radiotracers (^{18}F-FDG and ^{64}Cu-PTSM). Moreover, translation of [^{89}Zr]-Zr(oxinate)$_4$ to be used in the clinical practice would be possible and with low regulatory barriers because the ligand, oxine, is established as a gold standard radiotracer for cell labelling and cell tracking in nuclear medicine.

Chapter 4: *In vivo* study of [^{89}Zr]-Zr(oxinate)$_4$

4.1 Introduction

Zirconium-89, a long-lived PET radionuclide, has been the subject of increased interest in recent years for use in the field of immuno-PET imaging. The physical properties of ^{89}Zr offer advantages for molecular imaging using antibodies which require long periods of time for accumulation into the targets and also to achieve optimum ratio between target (tissue or organ lesions) and background.

In the same period, Heuveling *et al*. and Keliher *et al*. reported on the feasibility of ^{89}Zr labelled nanocolloidal albumin and dextran nanoparticles to detect sentinel lymph node and macrophages homing tissues, respectively, in animals (149, 150). Subsequently, a preliminary study in patients was presented from the same group. The sentinel lymph node detection in cancer patients with ^{89}Zr labelled nanocolloidal albumin with PET illustrated superior sensitivity and the resolution compared to ^{99m}Tc labelled nanocolloidal albumin with SPECT (151). The potential advantages of this superior imaging capability of ^{89}Zr in the field of cell tracking have not yet been exploited for cell tracking.

In the late 1980's Radl *et al.* reported that multiple myeloma (MM) spontaneously arises in ageing C57Bl/KaLwRij mice; they subsequently described and characterised different subtypes of MM such as 5T2, 5T33 cells (152). Disease can be induced and also transferred to another C57Bl/KaLwRij mouse by simple intravenous inoculation with 5T MM cells. In the 5T models of MM myeloma cells are localised in the bone marrow (BM), spleen and liver (haematopoietic organs) of inoculated mice. In 2000, Vanderkerken and colleagues found that radiochromium (Cr-51) labelled 5T2 cells predominantly accumulated in the liver, spleen and BM while activity released by

radiolabelled cells was observed in the kidneys and urine (153). Alici *et al.* established an enhanced green fluorescent protein (eGFP) transfected 5T33 cell line that could be maintained *in vitro* (154). The homing pattern of eGFP-5T33 cells could then be studied by FACS analysis of organ homogenates (and detection of the endogenous eGFP signal) which proved to be a more convenient method than previous approaches relying on immunostaining and subsequent FACS analysis. Tissue distribution of eGFP-5T33 cells confirmed that BM, spleen and liver were the main target tissues for 5T33 MM cells. [^{89}Zr]-Zr(oxinate)$_4$ labelled eGFP-5T33 cells are expected to present an identical homing pattern in C57BL/KaLwRij mice.

4.2 Aims

The aims of this set of experiments were to build on the radiochemical and *in vitro* studies in the previous chapter to track the fate of [^{89}Zr]-Zr(oxinate)$_4$ labelled eGFP-5T33 cells in the murine multiple myeloma model, C57BL/KaLwRij, comparing with those of [^{111}In]-In(oxinate)$_3$ labelled cells, and thereby evaluate the ^{89}Zr-method as a PET approach to cell tracking. We also set out to determine the viability of labelled cells *in vivo* and their retention of the radiolabel, using *ex vivo* tissue counting of mice injected with labelled cells. The *in vivo* stability of and radioactivity counting in FACS-sorted [^{89}Zr]-Zr(oxinate)$_4$ labelled cells *ex vivo*, a new technique to determine the survival or radiolabelled cells *in vivo*, was demonstrated.

4.3 Methods

4.3.1 *In vivo* tracking of labelled eGFP-5T33 in multiple myeloma model

Throughout this section, *in vivo* imaging and *ex vivo* tissue counting was carried out in murine multiple myeloma model, C57BL/KaLwRij strain, in which myeloma can be induced with 5T33 cells via intravenous injection. 5T33 cells, transfected with enhanced green fluorescent protein to give a new cell line derivative eGFP-5T33, used in our experiments was provided by Dr Yolanda Celle (University of Roehampton) (originally provided by Dr. Abedi-Valugerdi, Division of Haematology, Department of Medicine, Karolinska Institute at Karolinska University Hospital, Stockholm, Sweden). This cell line has been used for a number of studies at the Department of Haematological Medicine, King's College London. A report from Alici and colleagues indicated that eGFP-5T33 cells home to the bone marrow, spleen and liver (154). Therefore in this study these cells were labelled with the ^{89}Zr tracer, [^{89}Zr]-Zr(oxinate)$_4$, to carry out *in vivo* biodistribution with both imaging and tissue distribution counting, in comparison with ^{111}In labelling.

4.3.1.1 *In vivo* study, Series 1

In this part of the study we aimed to track [^{89}Zr]-Zr(oxinate)$_4$ labelled cells *in vivo* in the 5T33 murine multiple myeloma model in C57BL/KaLwRij mice and compare these results to *in vivo* tracking of [^{111}In]-In(oxinate)$_3$ labelled cells in the same model. [^{111}In]-In(oxinate)$_3$ is a well-established clinical standard radiotracer for cell tracking. The tissue distribution of labelled cells was also determined (*ex vivo* tissue counting). The fate of lysed (dead) eGFP-5T33 cells that had previously been labelled with either [^{89}Zr]-Zr(oxinate)$_4$ or [^{111}In]-In(oxinate)$_3$ was also investigated.

eGFP-5T33 cells were dispensed from the culture flask, and cell concentrations and viabilities were measured as described in Chapter 3. Cell suspensions containing 4 x 10^7 cells and 2.5 x 10^7 cells were aliquoted into 50 ml Falcon tubes (one tube with 4.0 x 10^7 cells and two tubes with 2.5 x 10^7 cells). Cells were washed with PBS twice (*vide supra*). After the last washing step, supernatants were discarded and cell pellets were resuspended in 1 ml of serum free medium. 20 MBq of [^{111}In]-In(oxinate)$_3$ was used to label 4.0 x 10^7 cells and 19 MBq and 21 MBq of [^{89}Zr]-Zr(oxinate)$_4$ were used to label each of 2.5 x 10^7 cells. Both radiotracers were diluted in 2 ml of serum free medium and added dropwise to the cell suspensions followed by swirling every 10 min. After incubation (room temperature) with radiotracers for 30 min, labelled cells were washed following the same procedure as described in Chapter 3 to eliminate radioactivity weakly bound or released by radiolabelled cells.

Labelled cells were resuspended in sterile PBS for injection. At this stage ^{89}Zr labelled cells from different extractions of [^{89}Zr]-Zr(oxinate)$_4$ were pooled then activity retained in the labelled cells was measured in the dose calibrator as well as for [^{111}In]-In(oxinate)$_3$ labelled cells. Meanwhile cell viabilities and cell concentrations were determined; washed labelled cells were diluted with PBS to get the final cell concentration of around 10^7 viable cells/100 μl for administration into animals. ^{89}Zr labelled cells prepared in this experiment were used for *in vivo* PET tracking of live labelled cells and dead labelled cells and for *ex vivo* organ biodistribution in 4 mice while cells labelled with ^{111}In were only used to carry out SPECT tracking of live cell and *ex vivo* tissue counting experiments. [^{111}In]-In(oxinate)$_3$ labelled lysed (dead) eGFP-5T33 cells was separately labelled. 6 MBq of [^{111}In]-In(oxinate)$_3$ was an initial activity added into around 7 x 10^6 washed eGFP-5T33 cells for labelling. The labelling procedure was same as described above.

The study of radiolabelled cell lysates was assessed as a model for radioactivity released from dead and dying cells *in vivo*. In order to study fate of radiotracers in the dead labelled eGFP-5T33 cells, labelled cells (either with [^{111}In]-In(oxinate)$_3$ or [^{89}Zr]-Zr(oxinate)$_4$) were aliquoted into microcentrifuge tubes. In order to lyse the cells, labelled cells were centrifuged, supernatant discarded and cells subsequently underwent a repeated process of freezing in liquid nitrogen, thawing at 37^{o}C and vortexing. This procedure was repeated three times. PBS was used to re-suspend the lysed (dead) labelled cells. To avoid cell debris aggregation, cell lysates were repeatedly withdrawn into an insulin syringe fitted with a 29 gauge needle several times. Lysates were then carefully withdrawn into a 1 ml syringe, with extra care taken to eliminate air bubbles.

Re-suspended [^{111}In]-In(oxinate)$_3$ and [^{89}Zr]-Zr(oxinate)$_4$ labelled cell samples were withdrawn in insulin syringes fitted with a 29 g needle (for *ex vivo* tissue counting) or into a 1 ml syringe (for imaging). Cannulae fitted with 27 gauge needles were altered so that they could be used for injecting small animals. The original tubing was removed and replaced by extended tubing. Tubing was filled with saline for injection and air bubbles eliminated.

In vivo experiments in this chapter were performed under project licence (PPL) 70/7238 (*in vivo* imaging in cancer models) and personal investigator licence (PIL) 70/23500, held by Prof. Philip Blower and Dr. Levente Meszaros, respectively. Experimental protocols and animal handling fully complied with the corresponding PPL, PIL and Home Office guidelines. Seven weeks old male C57BL/KaLwRij mice were purchased from Harlan UK. For each tracer one mouse was used for *in vivo* imaging of labelled cells, 4 mice for *ex vivo* tissue counting and 1 mouse was used for imaging dead radiolabelled cells (n=6/tracer, 12 mice in total). Mice had *ad libitum* access to water and diet throughout the study.

Mice were transferred from biological services unit (BSU) to the pre-clinical laboratory 15-30 min before the experiments to let them acclimatise.

4.3.1.1.1 Injection of labelled cells for imaging

In vivo images throughout this chapter were acquired in nanoSPECT/CT Plus system (Mediso, Hungary) and nanoScan PC in vivo pre-clinical PET/CT imager (Mediso, Hungary).

Mice were anaesthetised with 2-3% isoflurane in O_2 in an induction box then transferred to the scanner bed where anaesthesia was maintained (isoflurane, 1.5-2.0% in O_2). Mice were monitored using a respiratory pad. The injection site was wiped with a tissue impregnated in 70% ethanol. One of the lateral tail veins was cannulated. A PET or SPECT scan was started and ca. 1 minute later the labelled cells or cell lysate were injected. Injected activities of [^{111}In]-In(oxinate)$_3$ labelled live cells, dead cells and ^{89}Zr labelled live cells and lysed cells were 10 MBq, 3.5 MBq, 6 MBq and 2.0 MBq, respectively. PET scans were acquired continuously for 4 hr for [^{89}Zr]-Zr(oxinate)$_4$ labelled live eGFP-5T33 cells and 2 hr for [^{89}Zr]-Zr(oxinate)$_4$ labelled lysed eGFP-5T33 cells. Mice injected with [^{111}In]-In(oxinate)$_3$ labelled live cells and lysed cells were scanned continuously for 3.5 hr and 30 min respectively. Each SPECT and PET scan was followed by a whole-body CT scan (55 kV X-ray source, 1000 ms exposure time and 180 projections). At the end of the scanning session each mouse was transferred to a recovery cage. After recovery, imaged mice were transferred to their home cage and returned to the BSU. Subsequent scanning sessions were performed as follows: 24 hr, 48 hr, and 168 hr post-inoculation for both of radiotracers (live cells). In the studies with radiolabelled "lysed (dead) cells", the mouse injected with ^{89}Zr labelled lysed cells was scanned at 1 day and 2 days after injection. The mouse

inoculated with [^{111}In]-In(oxinate)$_3$ labelled lysed cells was only imaged one day post injection. At the end of last scan all injected mice were culled by cervical dislocation.

For the *ex vivo* tissue biodistribution study, each radiotracer was evaluated in 3 mice at day 7 after inoculation of the labelled cells. Cells radiolabelled with either [^{111}In]-In(oxinate)$_3$ or [^{89}Zr]-Zr(oxinate)$_4$ were withdrawn in insulin syringes fitted with a 29 gauge needle. 1.7 MBq of [^{111}In]-In(oxinate)$_3$ and 0.9 MBq of [^{89}Zr]-Zr(oxinate)$_4$ were used per mouse. Due to the rapid sedimentation of labelled cells cell suspensions were mixed well before dispensing. This way we could make sure that activity of each radiotracer in each syringe was nearly identical. Activities in the syringes were measured in the dose calibrator. In addition before and after injection all syringes were weighed. Four syringes per compound were used to inoculate mice for biodistribution study and one syringe for each compound (prepared the same way as those used for inoculations) was kept as a calibration standard for the gamma counter. For inoculations mice were placed in a heating box (T=37^{o}C) for 5-10 minutes to evoke vasodilation then placed in a restrainer for inoculation. The tails were wiped with an ethanol-impregnated tissue, then labelled cells were injected via a lateral tail vein. Mice were released then, once bleeding at the injection site had stopped, placed in their home cage and subsequently transferred to the BSU.

Calibration standards were prepared as follows. Labelled cells in the standard syringe were injected into a tube and diluted to a final volume of 1 ml in PBS. Then this solution was dispensed into scintillation vials as follows: 250 μl, 125 μl, 62.5 μl, 31.25 μl, 15.63 μl, 7.81 μl, 3.90 μl and 1.95 μl. In order to avoid measurement error from geometry, PBS was added into each tube to make up solutions to 500 μl in each tube. These standard solutions were kept and gamma counted together with tissue samples.

In order to determine tissue distribution of radioactivity in the inoculated mice, 7 days post inoculation, mice were culled by CO_2 asphyxiation. Mice were dissected and the following organs collected: heart, lungs, liver, spleen, stomach, small intestine, large intestine, kidneys, muscle, femur, salivary glands, tail and 50-150 μl of blood. Organs were weighed and gamma counted, %ID and %ID/g were calculated. To ensure measurement accuracy, samples with a measurement dead time exceeding 20% were left to decay and measured later. The organ-to-organ uptake ratios were calculated among the main target organs (the liver, the spleen, the femur and the kidneys).

4.3.1.2 *In vivo* study, Series 2

Due to a fatal thermal injury of a mouse injected with [^{89}Zr]-Zr(oxinate)$_4$ labelled cells in the previous section, the study had to be repeated. In this series the imaging protocol was extended to 14 days.

Based on the images we obtained with the mice injected with radiolabelled and subsequently lysed cells we suspected that cell lysis in those studies (reported in Series 1) was incomplete. Therefore we decided to repeat these experiments; with an improved protocol to lyse the labelled cells.

[^{89}Zr]-Zr(oxinate)$_4$ in this study was synthesised using the protocol for *in vivo* experiments (described in Chapter 3). 2 x 10^7 cells, 3.5 x 10^7 cells and 2 x 10^7 cells of eGFP-5T33 cells were added with 8.4 MBq, 15.9 MBq and 8.3 MBq of [^{89}Zr]-Zr(oxinate)$_4$, respectively, to obtain the radiolabelled cells. The procedures for washing myeloma cells and labelling the cells were the same as described in series 1. Subsequently, 3 batches of labelled cells were pooled before measuring the activity, cell concentration and viability. [^{89}Zr]-Zr(oxinate)$_4$ labelled eGFP-5T33 cells were

diluted with PBS and withdrawn into a 1 ml syringe for subsequent injection via cannula.

To prepare the ^{89}Zr labelled cell lysates the following process was adopted. eGFP-5T33 cells labelled with [^{89}Zr]-Zr(oxinate)$_4$ were flash frozen in liquid N_2 then subsequently incubated at 95^{o}C for 5 min in a heatable shaker. The cell pellet was then vigorously mixed with a vortex mixer. The process was repeated 3 times. The resulting "cell lysate" was dispensed in a 1 ml syringe for subsequent injection via cannula.

In vivo imaging of labelled live cells was performed for the first 2 hr, 24 hr, 48 hr, 72 hr, 168 hr (7days) and 336 hr (14 days) post inoculation. Mice injected with labelled cell lysate were imaged for 2 hr after injection then at 24 hr post-injection.

4.3.1.3 *In vivo* study, Series 3

Further to unsuccessful (to completely lyse the labelled cells) of imaging lysed (dead) [^{89}Zr]-Zr(oxinate)$_4$ labelled eGFP-5T33 cells in the *in vivo* study Series 2, in this experiment we took extra care for the preparation and injection of radiolabelled lysed cells. 7 x 10^6 multiple myeloma cells were dispensed for labelling with radiotracer. Following washing steps as described previously, 7.2 MBq of [^{89}Zr]-Zr(oxinate)$_4$ was used to label the cells as described above. The labelled cell pellet (3 x 10^6 cells for 2.6 MBq) was frozen in liquid nitrogen and thawed at 95^{o}C 3 times. The [^{89}Zr]-Zr(oxinate)$_4$ labelled cell lysate (in PBS) was repeatedly withdrawn into a 1 ml syringe fitted with an 18 gauge needle. This was then repeated using decreasing needle width (21 gauge, 26 gauge and 27 gauge respectively). With this process we aimed to disintegrate aggregates present in the suspension. After this process, the cell lysate was withdrawn in an insulin syringe before injection into the mouse. Around 1 MBq of dead labelled cell lysate were injected i.v. via the tail vein. PET/CT images were acquired after injection for 30 min and 1 day post injection.

Moreover in this study, biodistribution of ^{89}Zr labelled cells was investigated at earlier time points to investigate any change in initial tissue distribution with time. 45 x 10^6, 45 x 10^6 and 25 x 10^6 eGFP-5T33 cells were withdrawn from the culture flask into 50 ml Falcon tubes. Cells were washed and 16.5 MBq, 14.8 MBq and 6.98 MBq of [^{89}Zr]-Zr(oxinate)$_4$ were added to label cells, respectively, as described above. Pooled radiolabelled cells in PBS were measured in a dose calibrator and then drawn up into insulin syringes which then contained approximately 2.5 x 10^6 cells labelled with 0.9 MBq ^{89}Zr. Tissue distribution of labelled cells was determined in 3 or 4 mice for each time point. Injected mice were sacrificed at 9 hr, 24 hr and 48 hr after intravenous injection. The desired tissues or organs were dissected and counted in the gamma counter (together with their injected activity standard).

4.3.1.4 *In vivo* study, Series 4

Cell sorting technique is a useful tool to separate cell samples depending on their phenotypes. In this section, fluorescence activated cell sorting (FACS) was used to assess whether the radiolabel *in vivo* remained in the labelled cells or was released into the organ homogenate cells. Based on the previous study for *in vivo* biodistribution of [^{89}Zr]-Zr(oxinate)$_4$ labelled eGFP-5T33 cells, the main accumulation organs were liver, spleen and skeleton. Therefore, these organs of mice injected with [^{89}Zr]-Zr(oxinate)$_4$ labelled cells were homogenised to obtain the cells for subsequent FACS sorting.

[^{89}Zr]-Zr(oxinate)$_4$ was synthesised and radiochemical purity was determined before using in the study. eGFP-5T33 cells were labelled with [^{89}Zr]-Zr(oxinate)$_4$ in the same manner described in the Series 1. Six multiple myeloma mice were used in this study and prepared for the injection as described above. An aliquot of 1.5 MBq of [^{89}Zr]-Zr(oxinate)$_4$ labelled cells (1 x 10^7 cells) was diluted to 200 µl with sterile PBS

and injected intravenously (lateral tail vein). Then injected mice were allowed to recover and returned to BSU. At 2 days and 7 days after inoculation, for each time point 3 mice were culled by CO_2 asphyxiation. The liver, spleen and femora were harvested. Each liver and spleen was homogenised by using syringe puncture and gently filtered through a 40 μm cell strainer (BD, USA) in order to remove larger cell aggregations. The organ homogenates were diluted in ice-cold FACS buffer (PBS with 1% v/v FCS, 2 μM EDTA). Femora were cleaned of muscle and joints were cut off. The bone marrow cells were flushed with ice-cold FACS buffer and filtered through a 40 μm cell strainer. Cells were counted by staining with trypan blue in a haemocytometer before diluting with FACS buffer to a concentration of 10^7 cells/ml. Samples were kept on ice in FACS buffer and sorting experiments were performed within 6 hr after preparation.

The samples were analysed and sorted on a BD FACSAria III cell sorter (BD, USA). The samples were monitored for the expression of green fluorescence protein on FITC channel in order to discriminate between injected eGFP-5T33 cells and organ homogenate cells. To confirm the GFP expression by eGFP-5T33 cells (which had undergone semi-continuous culturing in our lab), cells were made into suspension using FACS buffer for a concentration of 1 x 10^5 cells/ml and analysed with flow cytometer in comparison to those of negative GFP expression cells, J774 cells, to show contrast with the GFP cells and hence the validity of the FACS experiments. Then each sample was sorted based on GFP expression to collect either 10,000 or 25,000 GFP positive cells and an equal number of GFP-negative cells in the same sample were also sorted, with the positive and negative samples collected in separate tubes. The count rate of each sample was measured in gamma counter.

4.3.1.5 *In vivo* study, Series 5

In order to study the biodistribution pattern of the tracer itself (i.e. not incorporated into cells), the injection of [^{89}Zr]-Zr(oxinate)$_4$ in the multiple myeloma mouse was conducted. [^{89}Zr]-Zr(oxinate)$_4$ was synthesised using the protocol described in Chapter 3. Four MBq of [^{89}Zr]-Zr(oxinate)$_4$ was diluted in 100 μl sterile PBS and placed in an insulin syringe for the injection. A mouse was prepared for the injection as for Series 1-4. The radiotracer was intravenously injected via the tail vein prior to PET/CT imaging with nanoScan PC for 30 min. After imaging, the mouse was allowed to recover and returned to the BSU. Further imaging was performed at 24 hr post administration.

4.3.1.6 *In vivo* study, Series 6

The biodistribution of neutralised ^{89}Zr (^{89}Zr oxalate) accumulation in organs of C57BL/6J mice was determined for comparison with that of labelled cells and oxine complex. *Ex vivo* tissue counting of the mice was determined at day 2 and day 7 after inoculation.

In this set of studies, to prepare the tracer, 5 MBq of ^{89}Zr in oxalic acid was neutralised with 1 M sodium carbonate and 0.1 M ammonium acetate was added to adjust pH to around 7-8. The volume of neutralised ^{89}Zr was adjusted to 100 μl with 0.9% normal saline before dispensing into an insulin syringe. Then the mouse was anaesthetised (*vide supra*) and injected with 5 MBq of neutralised ^{89}Zr in a lateral tail vein then transferred to the nano-PET scanner bed and scanned for 30 min. Further *in vivo* imaging was carried out at 24 hr post-injection.

For *ex vivo* tissue counting, approximately 9 MBq of ^{89}Zr in oxalic acid was neutralised with 1 M sodium carbonate to (reach pH around 7) and 0.1 M ammonium

acetate was added to get the final activity concentration of 1 MBq/100 μl. 100 μl of the above solution was injected into each mouse (n = 3 for each time point) as described for Series 1 above. Three mice were sacrificed at each time point (day 2 and day 7 after tracer injection) by CO_2 asphyxiation, mice were dissected, relevant organs collected, weighed and gamma counted and uptake was calculated.

4.4 Results of the *in vivo* tracking of radiolabelled cells

4.4.1 *In vivo* study, Series 1

Initial activities added to cells to label them in two batches were 19 MBq and 21 MBq. The washed radiolabelled cells from these 2 separate labellings were pooled together. The final activity was 14 MBq (in 2.4 x 10^7 cells) so cell labelling yield was around 35% while viability of labelled cells was 90%. After labelling these eGFP-5T33 cells with [^{89}Zr]-Zr(oxinate)$_4$ the cells were dispensed as follows: 6 MBq/1.0 x 10^7 cells were injected for PET imaging, 2 MBq/3 x 10^6 cells for were treated for imaging dead cells and 0.6 MBq/ 1 x 10^6 cells were used for *ex vivo* tissue counting in 4 mice. The activity of [^{111}In]-In(oxinate)$_3$ labelled cells was 18.8 MBq (94% cell labelling yield), and 10 MBq/1 x 10^7 cells and 1.7 MBq/1.7 x 10^6 cells were injected for *in vivo* imaging and *ex vivo* tissue counting, respectively. For the study with [^{111}In]-In(oxinate)$_3$ labelled lysed cells another batch of cells were labelled. The labelling yield was 78%; 5 MBq of [^{111}In]-In(oxinate)$_3$ labelled cells were obtained. After the labelled cells had been lysed, 3.5 MBq/2.1 x 10^6 cells were dispensed into an insulin syringe fitted with a 29 g needle and subsequently injected i.v. into a mouse for imaging. All labelled cells whether with [^{89}Zr]-Zr(oxinate)$_4$ or [^{111}In]-In(oxinate)$_3$ showed cell viability over 90% using trypan blue staining for lived-cells experiment.

The mouse injected with [^{89}Zr]-Zr(oxinate)$_4$ labelled eGFP-5T33 cells was imaged for 30 min after injection; subsequent scans were acquired at 24 hr and 48 hr, after inoculation. At 4 days post-injection a serious injury unrelated to the cell inoculation was discovered hence the mouse had to be culled and the study was terminated. For the early time point, [^{89}Zr]-Zr(oxinate)$_4$ labelled eGFP-5T33 cells were transiently accumulated in the lungs, heart and in blood pool. Soon after that, activity began to clear from the lungs to the liver and spleen and some was also detected in the skeleton. On the subsequent images at 24 hr, activity had completely cleared from the lungs whereas high activity remained localised in liver, spleen and bone. Due to the injury affecting the right hand side of the animal activity distribution was asymmetric (Figure 4.1) suggesting that progressed tissue necrosis occurred; this was later confirmed by necropsy. The experiment therefore had to be repeated (*vide infra*).

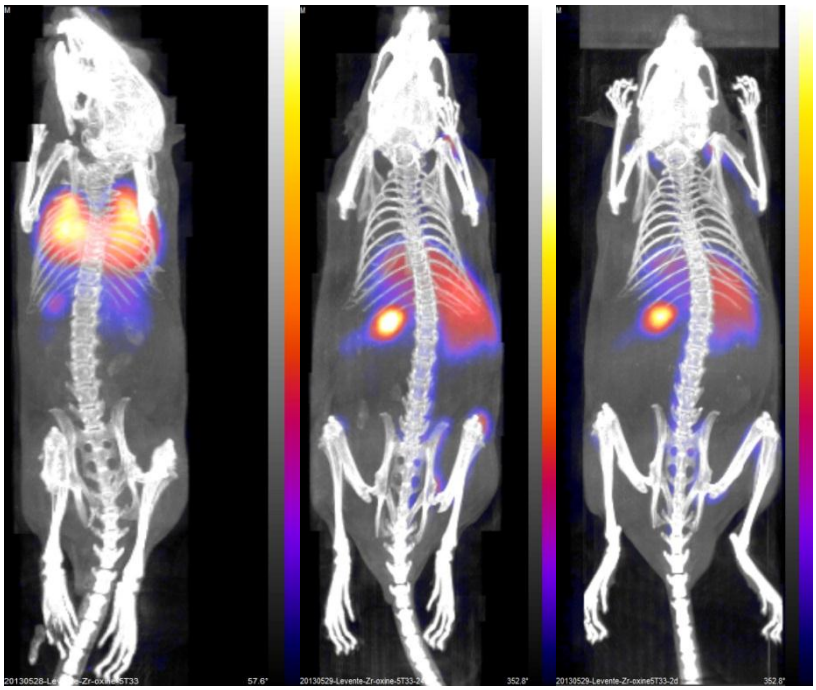

30 min 24 hr 48 hr

Figure 4.1: Biodistribution of [^{89}Zr]-Zr(oxinate)$_4$ labelled eGFP-5T33 cells after injection into multiple myeloma mouse model, at 30 min, 24 hr and 48 hr post administration. Asymmetry of the biodistribution was observed since 24 hr after injection.

After injection of [^{111}In]-In(oxinate)$_3$ labelled eGFP-5T33 cells the mouse was scanned for the first 30 min. Subsequent images were acquired at 2 hr, 24 hr, 48 hr and 168 hr after injection as shown in Figure 4.2. Most of the injected activity in the early hours was retained in the lungs and blood pool before clearing to the liver and spleen. After 24 hr accumulation activity in the bones was observed. At day 7 after injection, activity still remained in the liver, spleen and bones. Some activity was detected in the kidneys which might be caused by excretion of ^{111}In from the dying labelled cells. Images suggested that the radiolabel was mostly retained by the cells for at least 7 days.

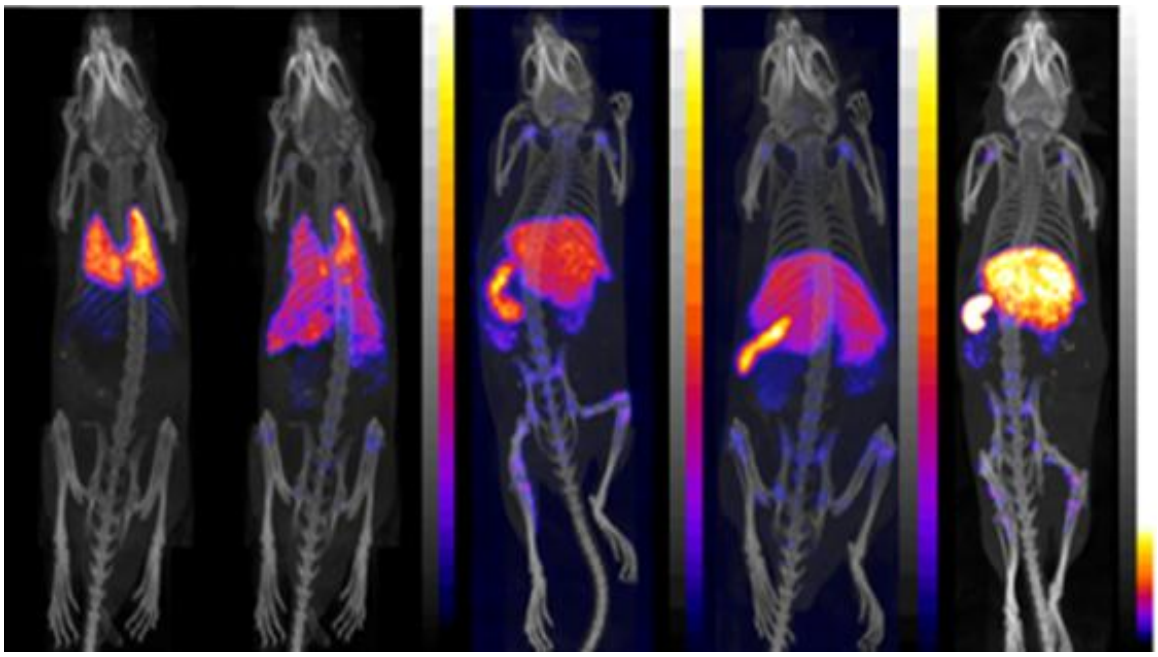

30 min 2 hr 24 hr 48 hr 168 hr

Figure 4.2: Tissue distribution of [^{111}In]-In(oxinate)$_3$ labelled eGFP-5T33 cells in C57BL/KaLwRij mouse. SPECT/CT images were obtained at 30 min, 2 hr, 24 hr, 48 hr and 168 hr after i.v. inoculation.

The images obtained with lysed [^{111}In]-In(oxinate)$_3$ labelled eGFP-5T33 cells 24 hr after injection exhibited similar pattern to images obtained with live cells. Activity mainly accumulated in the liver, spleen and skeleton. However significantly more activity in the kidneys was observed (Figure 4.3).

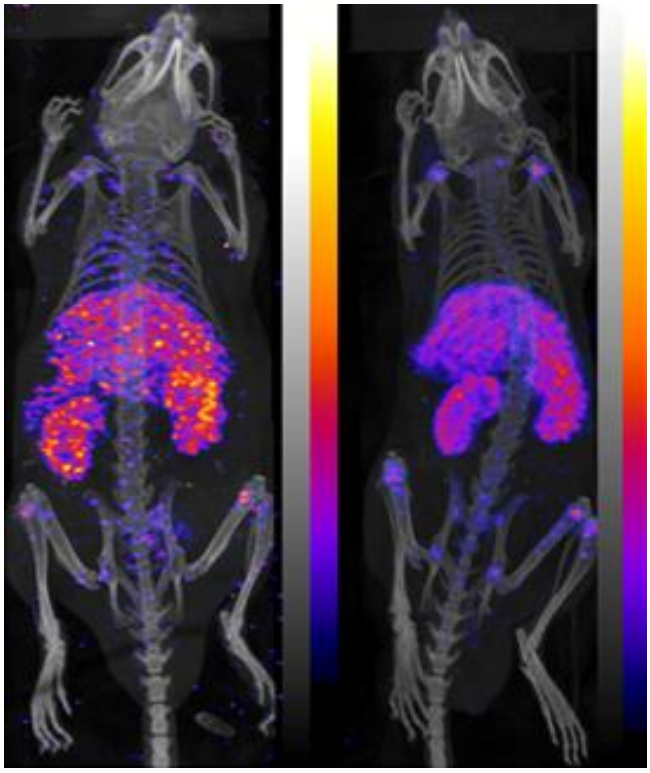

1 hr 24 hr

Figure 4.3: Biodistribution of [^{111}In]-In(oxinate)$_3$ labelled eGFP-5T33 cell lysate in multiple myeloma mouse at 1 hr and 24 hr after i.v. inoculation.

Lysed [^{89}Zr]-Zr(oxinate)$_4$ labelled cells were imaged similarly. Images (Figure 4.4) acquired 1 day post-injection the activity showed activity in the liver, spleen and bone marrow and also elevated activity in the kidneys was observed compared to injected live cells. This was similar to that of lysed [^{111}In]-In(oxinate)$_3$ labelled cells.

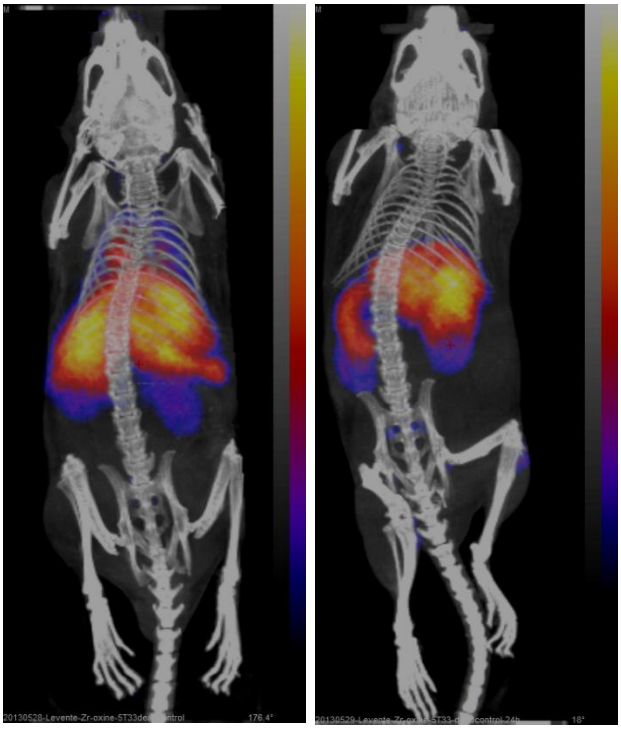

30 min 24 hr

Figure 4.4: Biodistribution of [^{89}Zr]-Zr(oxinate)$_4$ labelled lysed eGFP-5T33 in a C57BL/KalwRij mouse after inoculation for 30 min and 24 hr.

For *ex vivo* tissue counting, 0.9 MBq of ^{89}Zr oxine or 1.7 MBq of [^{111}In]-In(oxinate)$_3$ labelled cells were injected intravenously into C57BL/KaLwRij mice. Seven days after injection mice were culled, major thoraco-abdominal organs, a femur and thigh muscle was dissected for subsequent gamma counting. Biodistribution results of [^{89}Zr]-Zr(oxinate)$_4$ and [^{111}In]-In(oxinate)$_3$ labelled cells are summarised in Table 4.1.

Biodistribution of radiolabelled eGFP-5T33 cells in multiple myeloma mouse model 7 days post injection				
organs	^{89}Zr oxine labelled eGFP-5T33 cells (n=3)		^{111}In oxine labelled eGFP-5T33 cells (n=3)	
	% ID	% ID/g	% ID	% ID/g
Heart	0.04 ± 0.01	0.24 ± 0.04	0.11 ± 0.02	0.71 ± 0.12
Lungs	0.10 ± 0.01	0.35 ± 0.04	0.20 ± 0.01	0.66 ± 0.05
Liver	59.83 ±5.97	50.58 ± 8.87	44.94 ± 3.41	33.43 ± 2.09
Spleen	7.93 ± 0.79	129.5 ± 26.5	4.44 ± 0.34	71.65 ± 6.85
Stomach	0.13 ± 0.05	0.43 ± 0.12	0.19 ± 0.03	0.66 ± 0.14
Small intestine	0.17 ± 0.07	0.17 ± 0.07	0.43 ± 0.11	0.43 ± 0.11
Large intestine	0.18 ± 0.09	0.17 ± 0.08	0.56 ± 0.15	0.45 ± 0.07
Kidneys	0.97 ± 0.05	2.64 ± 0.39	4.03 ± 0.41	9.89 ± 0.64
Muscle	0.02 ± 0.002	0.15 ± 0.02	0.05 ± 0.01	0.43 ± 0.05
Femur	0.89 ± 0.13	10.84 ± 2.54	0.53 ± 0.05	6.01 ± 0.50
Salivary glands	0.06 ± 0.01	0.39 ± 0.03	0.34 ± 0.09	1.96 ± 0.24
Blood	0.02 ± 0.003	0.23 ± 0.10	0.02 ± 0.003	0.22 ± 0.06

Table 4.1: Whole body biodistribution of [^{89}Zr]-Zr(oxinate)$_4$ and [^{111}In]-In(oxinate)$_3$ labelled eGFP-5T33 cells in multiple myeloma mice, in terms of percentage of injected dose (%ID) and percentage of injected dose normalised with weight of organs (%ID/g) post inoculation 7 days.

From the *in vivo* study Series 1, Table 4.2 shows *ex vivo* tissue distribution results for %ID/g of [^{89}Zr]-Zr(oxinate)$_4$ and [^{111}In]-In(oxinate)$_3$ labelled eGFP-5T33 cells and compares organ-to-organ uptake ratios. A broadly similar pattern of the accumulation of the activity in the main organs was noticed for the two radiolabels. [^{111}In]-In(oxinate)$_3$ was consistently and significantly lower than that of ^{89}Zr in liver, spleen and femur by factors of 1.5, 1.8 and 1.8, respectively (with $p = 0.03$, $p = 0.02$ and $p = 0.03$, respectively). On the other hand activity of ^{111}In in the kidneys was significantly higher than that of ^{89}Zr by a factor of 3.75, $p < 0.0001$).

Biodistribution %ID/g of radiotracers incorporated into eGFP-5T33 cells in multiple myeloma mouse model 7 days post injection		
Organ	^{89}Zr oxine (n=3)	^{111}In oxine (n=3)
Liver : spleen	0.39 ± 0.11	0.47 ± 0.05
Liver : femur	4.69 ± 1.36	5.57 ± 0.58
Spleen : femur	12.0 ± 3.71	11.9 ± 1.52
Liver : kidneys	19.2 ± 4.4	3.4 ± 0.4
Spleen : kidneys	49.1 ± 12.4	7.23 ± 0.8
Femur : kidneys	4.1 ± 1.1	0.61 ± 0.06

Table 4.2: Tissue distribution of [^{89}Zr]-Zr(oxinate)$_4$ and [^{111}In]-In(oxinate)$_3$ labelled eGFP-5T33 cells, compared organ-to-organ ratio in C57BL/KaLwRij mice at day 7 after injection

Comparison of the activity accumulated in haematopoietic tissues and the kidneys, between eGFP-5T33 cells labelled [^{89}Zr]-Zr(oxinate)$_4$ and [^{111}In]-In(oxinate)$_3$ 7 days post injection is illustrated in Figure 4.5.

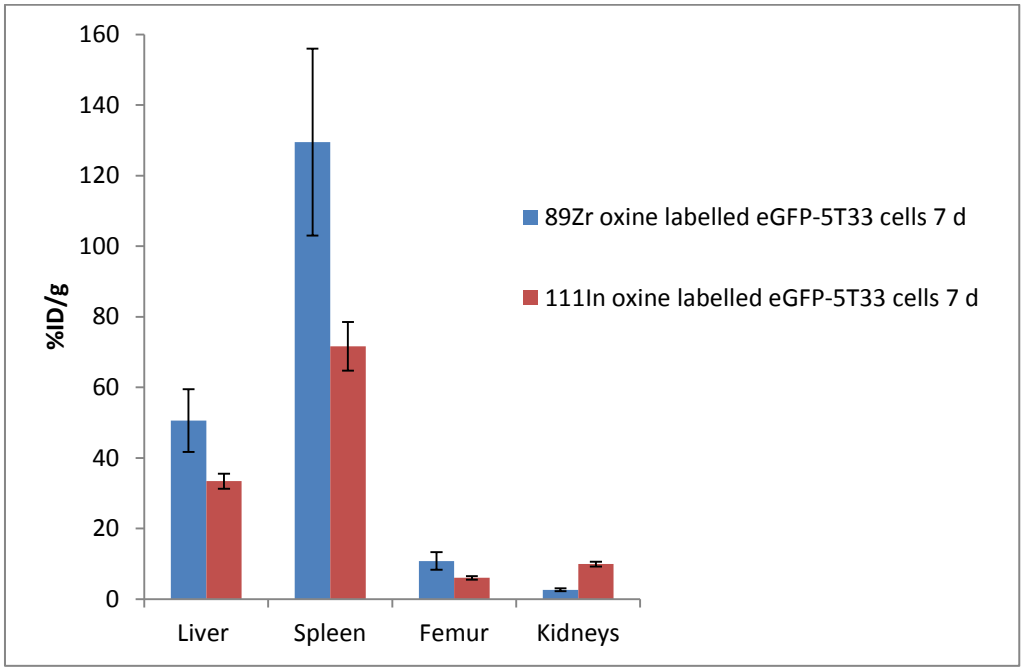

Figure 4.5: Graph showing the accumulation of [^{89}Zr]-Zr(oxinate)$_4$ and [^{111}In]-In(oxinate)$_3$ labelled eGFP-5T33 cells, 7 days after i.v. administration in haematopoietic tissues and kidneys in C57BL.KaLwRij mice

4.4.2 *In vivo* study, Series 2

After finishing the procedures to label 3 separated tubes of eGFP-5T33 cells with [^{89}Zr]-Zr(oxinate)$_4$ (8.4 MBq, 15.9 MBq and 8.3 MBq), the labelled cell samples were pooled, the resulting 3.4 x 10^7 labelled cells contained 14.7 MBq of [^{89}Zr]-Zr(oxinate)$_4$ (cell labelling yield 45%), with cell viability 87%. 4.2 MBq of [^{89}Zr]-Zr(oxinate)$_4$ labelled cells (9.7 x 10^6 cells) was administered into a mouse for cell tracking by PET imaging. The PET images were shown in Figure 4.6 and 4.7.

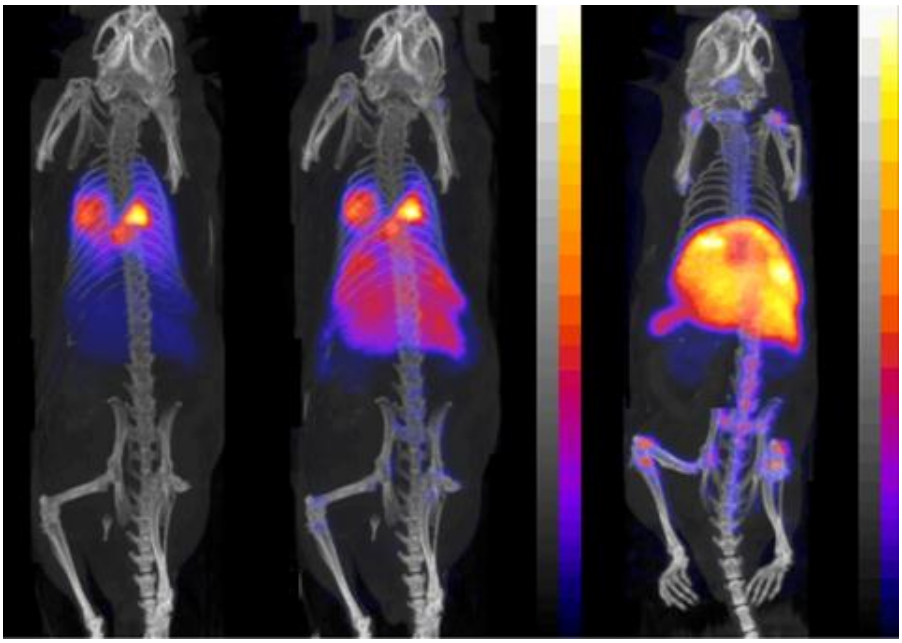

30 min 2 hr 24 hr

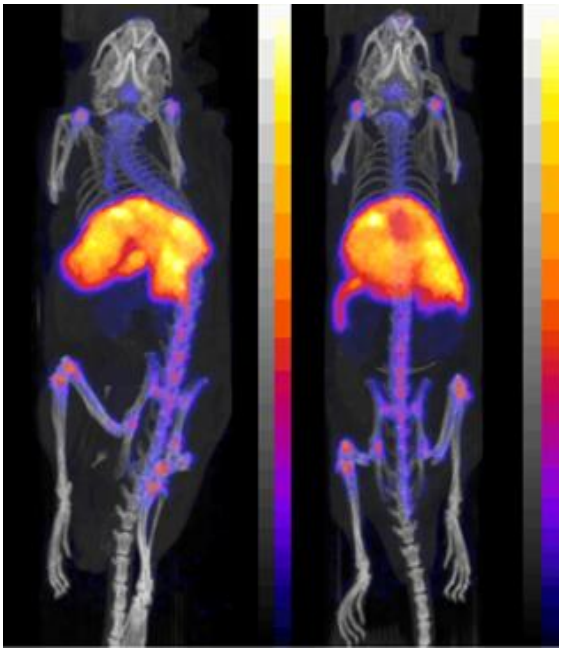

48 hr 168 hr

Figure 4.6: Whole body images of multiple myeloma mouse injected with [^{89}Zr]-Zr(oxinate)$_4$ labelled eGFP-5T33 cells, at 30 min, 2 hr, 24 hr, 48 hr, 168 hr (7 days)

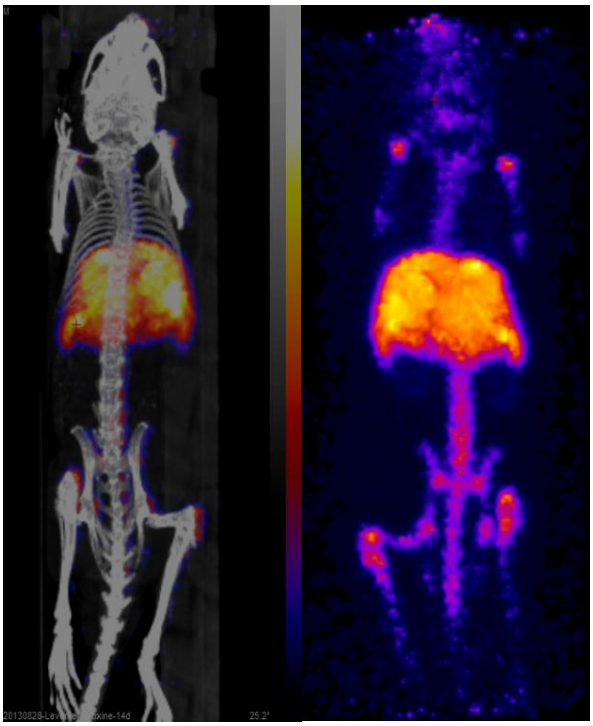

336 hr with CT 336 hr without CT

Figure 4.7: Whole body images of multiple myeloma mouse injected with [^{89}Zr]-Zr(oxinate)$_4$ labelled eGFP-5T33 cells, 336 hr (14 days, with CT and without CT) post inoculation.

Unfortunately, the mouse injected with the labelled cell lysate died ca. 5 min after injection. It is possible that labelled cells lysates were aggregated and blocked pulmonary capillaries.

4.4.3 *In vivo* study, Series 3

PET/CT imaging of dead/lysed [^{89}Zr]-Zr(oxinate)$_4$ labelled eGFP-5T33 cells was performed and images were analysed at 30 min and 1 day after injection (Figure 4.8).

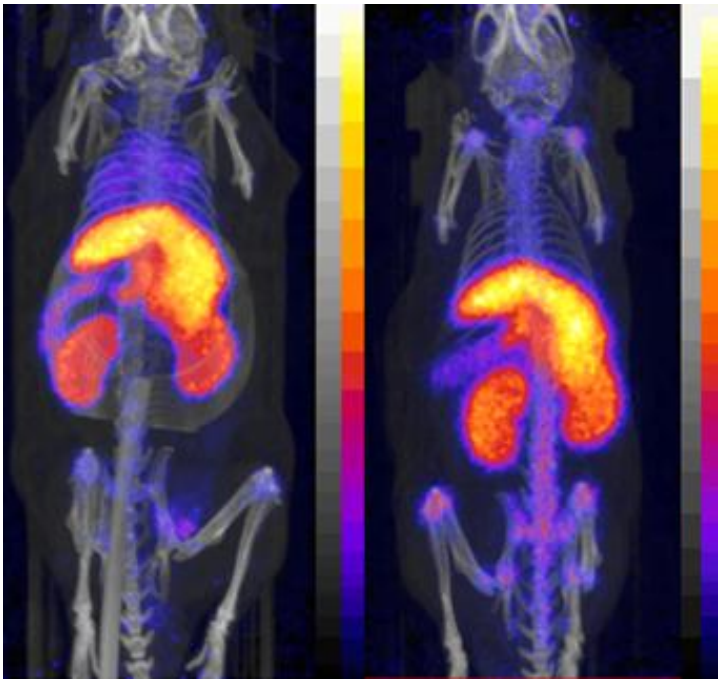

30 min 24 hr

Figure 4.8: PET/CT whole body images of dead/lysed labelled [^{89}Zr]-Zr(oxinate)$_4$ eGFP-5T33 cells in multiple myeloma mouse, at 30 min and 24 hr post injection.

The results of *ex vivo* tissue counting of mice injected [^{89}Zr]-Zr(oxinate)$_4$ labelled eGFP-5T33 at 9 hr, 24 hr and 48 hr post inoculation are shown in Tables 4.3-4.4 and Figure 4.9. The liver was the organ with the highest levels of activity from a couple of hours post-injection for up to 2 days. Spleen also retained activity but less than in the liver, higher than in kidneys. However percentage of activity normalised to the mass of the spleen was higher than that in the liver. Greater activity was obtained

when mass of the bone (femur) was used to calculate % ID/g compared to the activity per tissue (femur) (% ID).

% ID of ^{89}Zr oxine labelled eGFP-5T33 cells in multiple myeloma mouse model			
organs	9 hr post Injection (n=3)	24 hr post injection (n=4)	48 hr post injection (n=3)
Heart	0.18 ± 0.02	0.09 ± 0.02	0.08 ± 0.02
Lungs	0.59 ± 0.11	0.45 ± 0.08	0.21 ± 0.04
Liver	69.26 ± 6.17	69.28 ± 11.93	57.58 ± 5.35
Spleen	5.82 ± 0.85	7.10 ± 0.96	4.74 ± 0.52
Stomach	0.14 ± 0.01	0.17 ± 0.06	0.12 ± 0.01
Small intestine	0.34 ± 0.05	0.31 ± 0.06	0.32 ± 0.04
Large intestine	0.36 ± 0.04	0.30 ± 0.09	0.26 ± 0.10
Kidneys	1.80 ± 0.15	1.75 ± 0.18	1.42 ± 0.21
Muscle	0.03 ± 0.01	0.03 ± 0.01	0.02 ± 0.01
Femur	0.63 ± 0.08	0.82 ± 0.12	0.52 ± 0.04
Salivary glands	0.12 ± 0.004	0.11 ± 0.02	0.10 ± 0.03
Blood	0.39 ± 0.10	0.18 ± 0.10	0.10 ± 0.03

Table 4.3: Whole body biodistribution of [^{89}Zr]-Zr(oxinate)$_4$ labelled eGFP-5T33 cells in multiple myeloma mice, presented in terms of percentage of the injected dose in each tissue at 9 hr, 24 hr and 48 hr post injection.

% ID/g of ^{89}Zr oxine labelled eGFP-5T33 cells in multiple myeloma mouse model			
organs	9 hr post Injection (n=3)	24 hr post injection (n=4)	48 hr post injection (n=3)
Heart	0.85 ± 0.09	0.50 ± 0.13	0.32 ± 0.07
Lungs	2.28 ± 0.41	1.35 ± 0.07	0.68 ± 0.06
Liver	44.63 ± 10.59	42.17 ± 9.13	30.90 ± 4.2
Spleen	74.95 ± 13.17	99.47 ± 10.95	54.90 ± 1.2
Stomach	0.29 ± 0.08	0.45 ± 0.17	0.28 ± 0.07
Small intestine	0.35 ± 0.01	0.34 ± 0.02	0.27 ± 0.07
Large intestine	0.35 ± 0.04	0.27 ± 0.02	0.21 ± 0.04
Kidneys	3.94 ± 0.45	4.01 ± 0.44	3.00 ± 0.43
Muscle	0.19 ± 0.03	0.21 ± 0.05	0.13 ± 0.03
Femur	7.12 ± 1.41	8.390± 0.47	5.30 ± 0.85
Salivary glands	0.54 ± 0.06	0.52 ± 0.14	0.44 ± 0.04
Blood	1.77 ± 0.1	1.03 ± 0.18	0.53 ± 1.68
Liver : spleen	0.60 ± 0.18	0.42 ± 0.10	0.56 ± 0.08
Liver : femur	6.28 ± 1.94	5.02 ± 1.12	5.83 ± 1.23
Spleen : femur	10.6 ± 2.78	11.9 ± 1.47	10.4 ± 1.68
Liver : kidneys	11.4 ± 3.0	10.6 ± 2.6	10.3 ± 2.0
Spleen : kidneys	19.2 ± 4.2	24.9 ± 3.9	18.3 ± 2.7
Femur : kidneys	1.8 ± 0.42	2.1 ± 0.26	1.8 ± 0.38

Table 4.4: Whole body biodistribution of [^{89}Zr]-Zr(oxinate)$_4$ labelled eGFP-5T33 cells in multiple myeloma mice presented in terms of percentage of the injected dose normalized with weight of organs at 9 hr, 24 hr and 48 hr post injection.

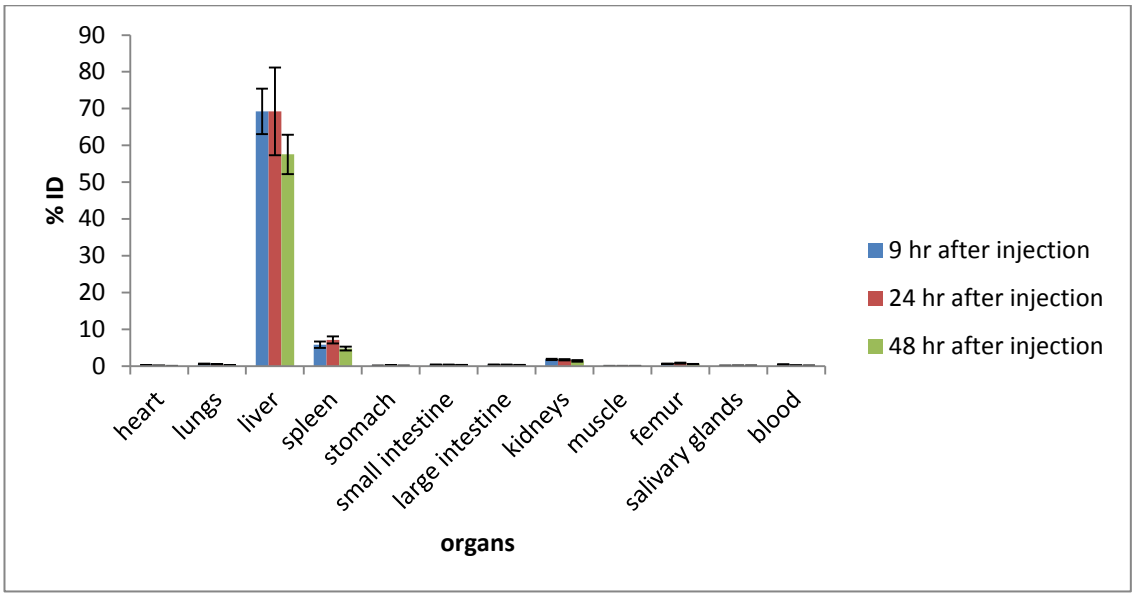

(A)

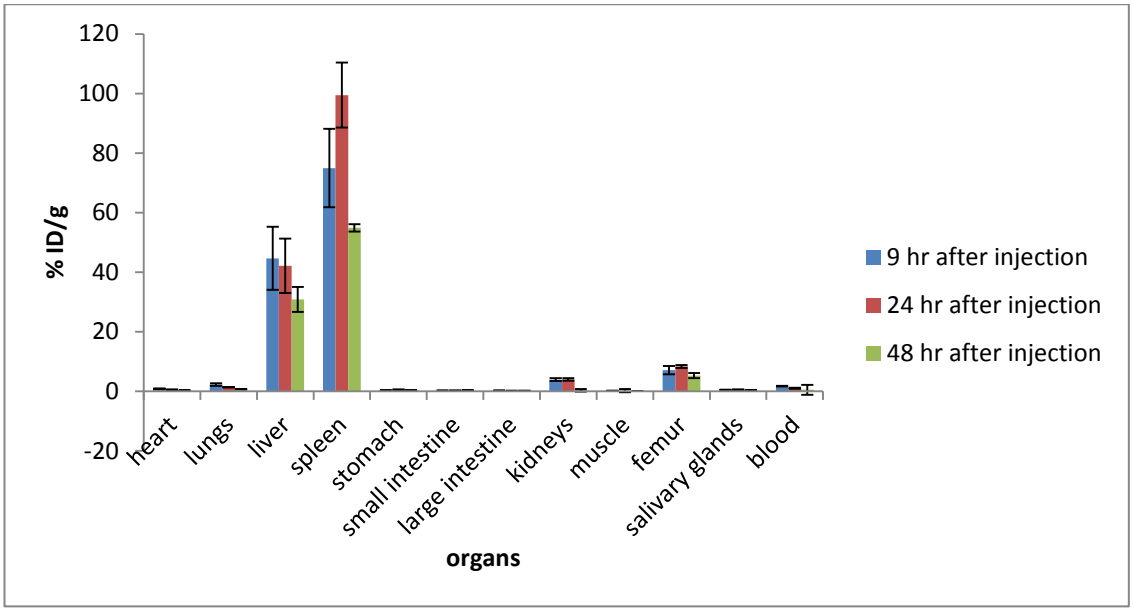

(B)

Figure 4.9: Graphs of whole body biodistribution of [^{89}Zr]-Zr(oxinate)$_4$ labelled eGFP-5T33 cells in multiple myeloma mice, presented as (A) % ID and (B) % ID/g at 9 hr, 24 hr and 48 hr post injection.

4.4.4 *In vivo* study, Series 4

FACS analysis of *in vitro* cultured J774 cells (negative for GFP) and eGFP-5T33 cells are shown in Figure 4.10.

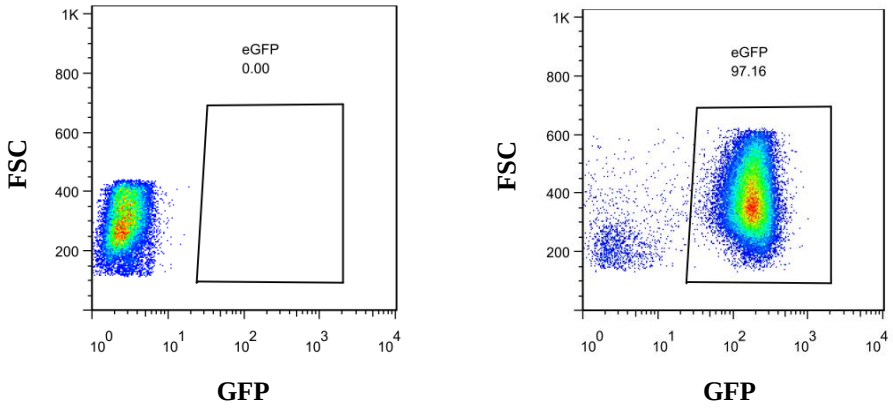

Figure 4.10: Results of the FACS analysis comparing J774 cells (GFP negative, A) and eGFP-5T33 (GFP positive, B).

The liver, spleen and bone marrow were harvested from [^{89}Zr]-Zr(oxinate)$_4$ labelled cells injected mice at day 2 and day 7 post inoculation. The organs were homogenised and analysed by FACS as shown in Figure 4.11 and 4.12 for the organs of mice culled on day 2 and day 7 after administration, respectively.

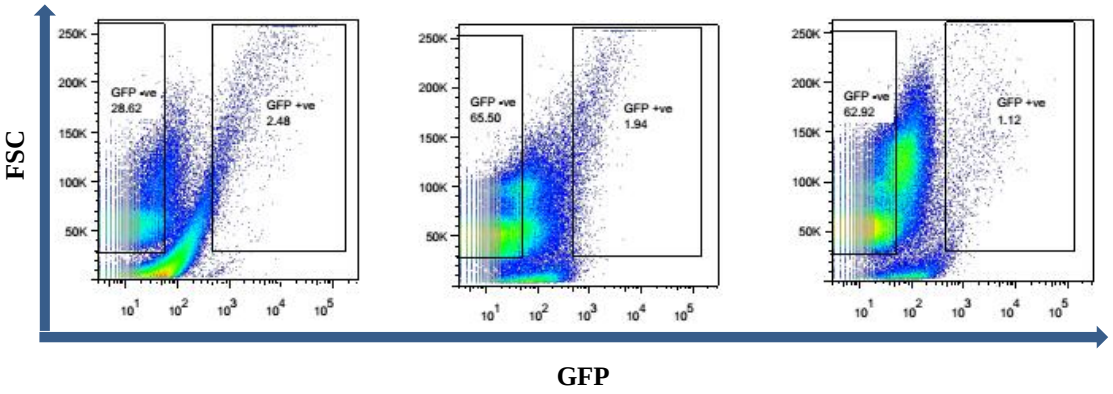

(A) (B) (C)

Figure 4.11: Representative FACS results of organ homogenates of MM model injected [^{89}Zr]-Zr(oxinate)$_4$ labelled eGFP-5T33 cells 2 days after injection, in A= liver, B=spleen and C=bone marrow. (n=3 for each organ)

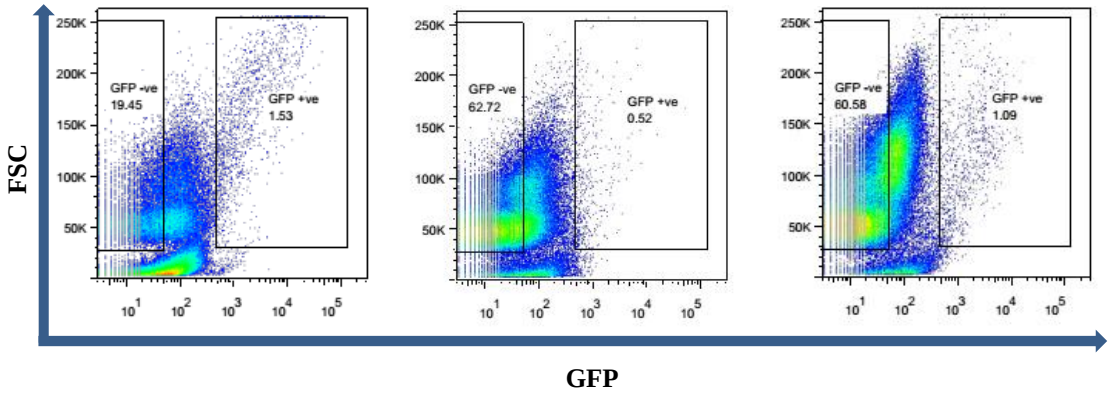

(A) (B) (C)

Figure 4.12: Representative FACS results of organ homogenates of MM model injected [^{89}Zr]-Zr(oxinate)$_4$ labelled eGFP-5T33 cells 7 days after injection, in A= liver, B=spleen and C=bone marrow. (n=3 for each organ)

After FACS sorting of organ homogenates based on eGFP expression from injected [^{89}Zr]-Zr(oxinate)$_4$ labelled eGFP-5T33 mouse culled after inoculation for 2 days and 7 days, most of the activity was present in the GFP+ cells compared to GFP- cell in the same organ homogenates (Figure 4.13). The GFP+ cell populations contained significantly higher activity per cell by a factor of > 23 and > 12 at day 2 and day 7, respectively, than GFP- samples.

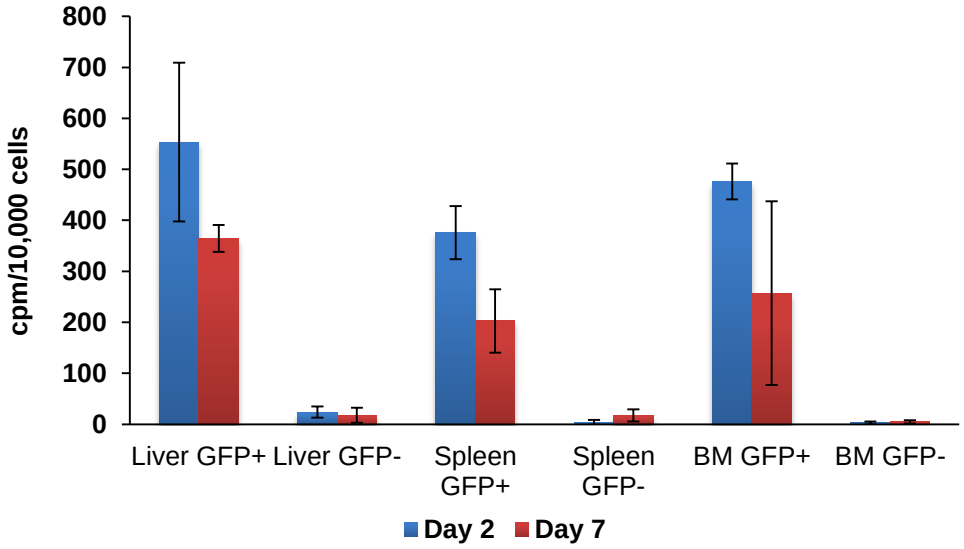

Figure 4.13: Activities in GFP positive and GFP negative cell populations sorted from the livers, spleens and femoral marrow (BM) organ homogenates harvested from mice 2 and 7 days after intravenous injection with [^{89}Zr]-Zr(oxinate)$_4$ labelled eGFP-5T33 cells (n=3/group, values decay corrected to day 2)

4.4.5 *In vivo* study, Series 5

Biodistribution of [^{89}Zr]-Zr(oxinate)$_4$ in MM mouse was investigated by PET imaging for 30 min after intravenous injection of 4 MBq [^{89}Zr]-Zr(oxinate)$_4$ and again at 24 hr as shown in Figure 4.14. For the early time point, the activities were observed in the heart, lungs, liver, spleen and faint activity in the kidneys. After 24 hr, the activity remained in those organs while increased activity in the spleen was observed.

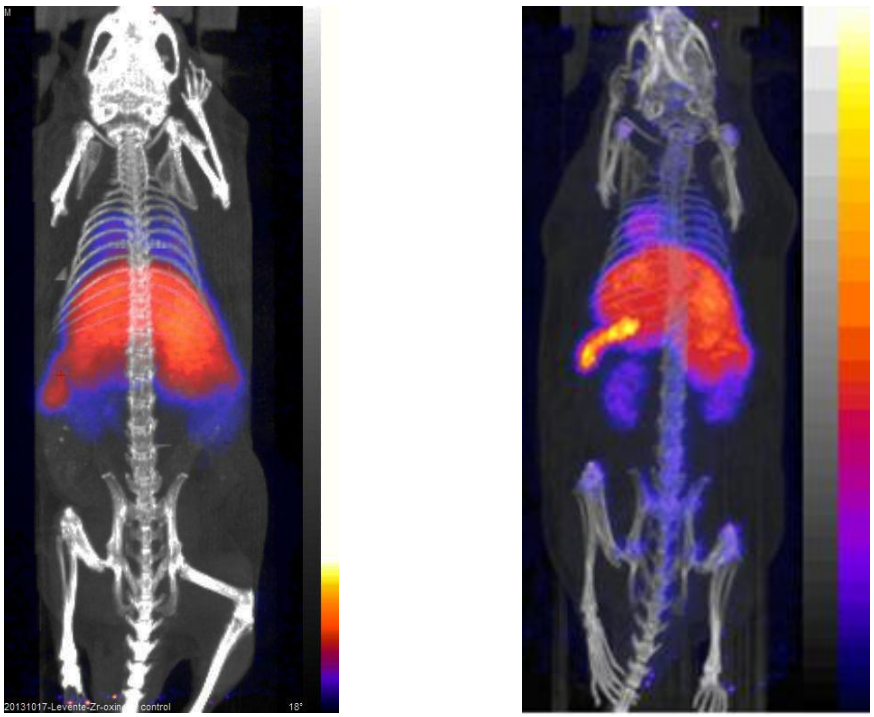

30 min 1 day

Figure 4.14: Distribution of [^{89}Zr]-Zr(oxinate)$_4$ in a C57BL/KaLwRij mouse, PET/CT images were obtained at 30 min and 24 hr after i.v. injection.

4.4.6 *In vivo* study, Series 6

Biodistribution of neutralised ^{89}Zr in the form of ^{89}Zr oxalate in C57BL/6J mouse was investigated by intravenous injection of 5 MBq of neutralised ^{89}Zr via tail vein then scanning for 30 min, with further imaging at 24 hr post administration. The images are shown in Figure 4.15.

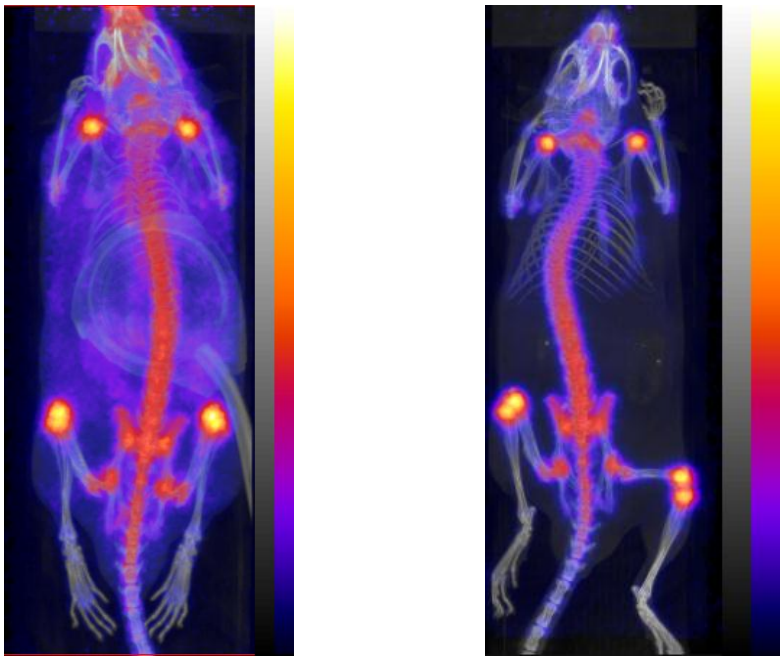

4 hr 24 hr

Figure 4.15: Biodistribution of neutralised ^{89}Zr (^{89}Zr oxalate) in a C57BL/6J mouse, the images were obtained 4 hr and 24 hr after injection.

The results of biodistribution of neutralised ^{89}Zr, determined by ex vivo organ counting, are summarised and represented as a percentage of injected dose per organs and with those normalised with mass of the organs in Table 4.5 and 4.6, respectively.

% ID of neutralised ^{89}Zr in C57BL/6J mouse		
organs	2 days post Injection (n=3)	7 days post Injection (n=3)
Heart	0.34 ± 0.03	0.19 ± 0.01
Lungs	1.29 ± 0.09	0.32 ± 0.04
Liver	5.18 ± 0.97	6.18 ± 0.10
Spleen	0.28 ± 0.04	0.32 ± 0.05
Stomach	0.32 ± 0.05	0.19 ± 0.02
Small intestine	1.26 ± 0.09	0.41 ± 0.05
Large intestine	0.80 ± 0.15	0.49 ± 0.08
Kidneys	1.20 ± 0.07	0.83 ± 0.04
Muscle	0.09 ± 0.02	0.09 ± 0.01
Femur	2.32 ± 0.20	1.97 ± 0.21
Salivary glands	0.45 ± 0.07	0.37 ± 0.04
Blood	0.47 ± 0.04	0.04 ± 0.01

Table 4.5: Whole body biodistribution of neutralised ^{89}Zr in C57BL/6J mice, presented in terms of % ID, (percentage of the injected dose) at day 2 and day 7 post injection.

% ID/g of neutralised ^{89}Zr in C57BL/6J mouse		
organs	2 days post Injection (n=3)	7 days post Injection (n=3)
Heart	1.34 ± 0.04	0.73 ± 0.03
Lungs	2.54 ± 0.40	0.70 ± 0.03
Liver	3.16 ± 0.28	3.15 ± 0.22
Spleen	3.01 ± 0.25	3.05 ± 0.34
Stomach	0.51 ± 0.05	0.34 ± 0.10
Small intestine	0.91 ± 0.08	0.28 ± 0.03
Large intestine	0.68 ± 0.10	0.31 ± 0.04
Kidneys	2.37 ± 0.20	1.74 ± 0.20
Muscle	0.52 ± 0.05	0.66 ± 0.01
Femur	22.82 ± 2.70	23.22 ± 0.74
Salivary glands	1.86 ± 0.20	1.81 ± 0.14
Blood	2.19 ± 0.12	0.22 ± 0.01

Table 4.6: Whole body biodistribution of neutralised ^{89}Zr in C57BL/6J mice presented in terms of % ID/g, (percentage of the injected dose normalized with weight of organs) 2 day and 7 day post injection.

4.5 Discussion

To obtain labelled eGFP-5T33 cells for *in vivo* studies, cells were labelled with each extraction of [^{89}Zr]-Zr(oxinate)$_4$. In order to investigate either *in vivo* imaging or *ex vivo* tissue counting, relatively high activity of radiolabelled cells was required compared to *in vitro* studies. Altogether, 2-3 extractions of [^{89}Zr]-Zr(oxinate)$_4$ were required to separately label separate aliquots of cells and then radiolabelled cells were washed and pooled together to achieve the adequate activity of radiolabelled cells for *in vivo* studies or *ex vivo* tissue counting experiments.

Cell labelling yields for *in vivo* studies provide additional data supporting the results in Chapter 3. eGFP-5T33 cells were labelled with [^{89}Zr]-Zr(oxinate)$_4$ with a labelling efficiency of 43.16% ± 6.39 (between 35% and 52.30%) whereas the labelling efficiency with [^{111}In]-In(oxinate)$_3$ was 82.86% and 94%, with more than 10^7 cells being labelled for both of tracers. Comparing to the labelling of [^{111}In]-In(oxinate)$_3$, cell labelling yields of [^{89}Zr]-Zr(oxinate)$_4$ were lower than with [^{111}In]-In(oxinate)$_3$ but still sufficiently promising as a basis for further optimisation.

For the *in vivo* tracking of labelled eGFP-5T33 cells with either [^{89}Zr]-Zr(oxinate)$_4$ or [^{111}In]-In(oxinate)$_3$, the labelled cells were in the blood circulation and transiently accumulated in the lungs and heart before rapidly migrating to the liver, spleen and skeleton. Radioactivity largely remained in those organs for at least 7 days. These data confirm that 5T33 cells home to haematopoietic organs (liver and spleen) and skeleton with high affinity in the multiple myeloma mouse model. Comparing our results to another multiple myeloma cell line, 5T2, the biodistribution of which was investigated by labelling with ^{51}Cr, similar biodistribution was observed to that reported by Vanderkerken and colleagues (153).

Apart from these main target organs, we also observed faint activity in the kidneys at the early time points in mice injected with [^{89}Zr]-Zr(oxinate)$_4$ labelled cells and to a much higher level with [^{111}In]-In(oxinate)$_3$ labelled cells. According to radiolabelled cell lysates experiments these might be due to released activity of [^{111}In]-In(oxinate)$_3$ and [^{89}Zr]-Zr(oxinate)$_4$ from living or dead labelled cells *in vivo*. This was consistent with the results of the control experiments in which the lysate of radiolabelled eGFP-5T33 cells was investigated in order to determine the fate of released activity in the dead labelled cells *in vivo*. The results may thus be interpreted as indicating that the retention of ^{89}Zr in the labelled cells *in vivo* was much better than that of ^{111}In.

However in the first series of imaging, the results of tissue distribution of [^{89}Zr]-Zr(oxinate)$_4$ and [^{111}In]-In(oxinate)$_3$ labelled cell lysates 24 hr after injection, the activity was mainly accumulated in the liver, spleen and skeleton, a pattern similar to the imaging of live radiolabelled cells. Meanwhile activity in the kidneys was faintly detected. According to a previous study that had been carried out in our group by Dr. Levente Meszaros, lysed [^{111}In]-In(oxinate)$_3$ labelled eGFP-5T33 cells clear rapidly via kidneys 24 hr after inoculation, this is likely to be due to "In-111-labelled" proteins released by cells. Thus results obtained in this experiment indicate that live or viable labelled cells were still present in the suspension after repeated flash-freezing and thawing. Also the images of lysed [^{89}Zr]-Zr(oxinate)$_4$ labelled cells showed similar organ accumulation to that of lysed [^{111}In]-In(oxinate)$_3$ labelled cells. This indicated that some of the labelled cells remained viable according to the significant levels of radioactivity present in the liver, spleen and bone marrow, but renal uptake (to a much greater extent than with live cells) was also observed. So the results were very similar to what we observed with both the [^{111}In]-In(oxinate)$_3$ and [^{89}Zr]-Zr(oxinate)$_4$ labelled cell lysate.

Therefore we repeated the control experiment in the second series study with an improved procedure to kill the labelled cells by repeatedly freezing the cells in liquid N_2 and thawing at 95^{o}C. In this case the injected mouse was dead several minutes after administration of lysate [^{89}Zr]-Zr(oxinate)$_4$ labelled cells. This may have been caused by aggregation of the cell lysates resulting in suspected pulmonary embolus. So we improved the procedure for preparation of the cells lysates using subsequent passage through different gauges of needle to disintegrate aggregation of the cell lysates before administration to the mouse in the third series of imaging. This improved procedure was able to overcome the problem.

Data obtained in the third series of imaging of labelled cell lysates showed accumulation in the liver, spleen and skeleton as well as in the kidneys both for [^{89}Zr]-Zr(oxinate)$_4$ and [^{111}In]-In(oxinate)$_3$. The activities in the bones might indicate that a small amount of live radiolabelled cells presented in the suspension injected to the mouse, or may be due to other reasons. There was more uptake in the kidneys at 24 hr post inoculation compared to the early time point at 30 min after administration. These findings suggest that fate of radioactivity released from the labelled cells can be possibly in different forms which were trapped by the liver and kidneys. For example ^{89}Zr and ^{111}In bound to large proteins from the cytoplasmic components in the labelled cells could be accumulated in the liver whereas the fractions bound to smaller proteins or peptides may be trapped in the kidneys. Radiolabelled molecules metabolised in the liver may subsequently be released and then trapped in the kidneys.

Table 4.1 shows that activity from liver, spleen and bone marrow of mice inoculated [^{111}In]-In(oxinate)$_3$ labelled cells was significantly less than that of eGFP-5T33 cells labelled with [^{89}Zr]-Zr(oxinate)$_4$ at 7 days after administration (Figure 4.5). In contrast, the activity in the kidneys was significant greater with [^{111}In]-In(oxinate)$_3$

than [^{89}Zr]-Zr(oxinate)$_4$ labelled cells. The observation that when imaging cell lysates of labelled [^{89}Zr]-Zr(oxinate)$_4$ and [^{111}In]-In(oxinate)$_3$, higher activities were accumulated in the kidneys 24 hr after inoculation, is consistent with the hypothesis that any Zr-89 released from labelled cells *in vivo* is slower for Zr-89 than for In-111. This is an important observation as it indicates that Zr-89 shows great promise for tracking cells *in vivo* over long periods.

Results of FACS analysis of *in vitro* culture of eGFP-5T33 cells confirmed that the cells strongly express GFP (more than 97% of cells) as expected, compared to negative control J774 cells, which do not express GFP. This result suggests that eGFP-5T33 cells could be used for sorting cells isolated from mice based on GFP expression followed tracking labelled cells *in vivo*. The results of *ex vivo* FACS sorting of GFP positive and GFP negative populations from organ homogenates (liver, spleen, bone marrow) prove that GFP positive cells contained significantly higher activity than GFP negative cells. In other words [^{89}Zr]-Zr(oxinate)$_4$ labelled cells retained the radiolabel *in vivo* at least for a week, and do not transfer a significant fraction of their radioactivity to other cells. In addition, these results would prove that eGFP-5T33 cells labelled with [^{89}Zr]-Zr(oxinate)$_4$ were alive *in vivo* for up to 7 days because only live cells are able to express GFP.

The biodistribution results of [^{89}Zr]-Zr(oxinate)$_4$ in the multiple myeloma mouse show accumulation of activity in the organs with a high blood supply including heart, lungs, liver and spleen at 30 min after injection. On the following day, activity still remained in those organs but the activity in the lungs was decreased whereas increased activity was observed in the spleen at 24 hr after administration. This biodistribution pattern of [^{89}Zr]-Zr(oxinate)$_4$ is similar to that of [^{111}In]-In(oxinate)$_3$ in glioma bearing nude rat which was reported by Varma *et al*. (155). The biodistribution

of [^{89}Zr]-Zr(oxinate)$_4$ within the high blood flow organs might be due to potential to label red blood cells in the similar manner to gallium-68 oxine labelling red blood cells (97) or to uptake in cells of the well-perfused organs.

According to the information obtained from the biodistribution of [^{89}Zr]-Zr(oxinate)$_4$ labelled eGFP-5T33 cells and [^{89}Zr]-Zr(oxinate)$_4$ in multiple myeloma mouse, liver, spleen and bone marrow were the main accumulation activity organs for both of radiotracers. However the presented activities in those organs of mouse injected [^{89}Zr]-Zr(oxinate)$_4$ labelled eGFP-5T33 cells were not related to [^{89}Zr]-Zr(oxinate)$_4$. This conclusion was confirmed by the results of the *ex vivo* FACS sorting cells which the detected radioactivity was associated with the GFP positive cells rather than free radiotracer unbound to the cells or bound to other cells.

Comparing our *in vivo* imaging of neutralised ^{89}Zr (which is in the form of ^{89}Zr oxalate) in C57BL/6J mouse with those in NIH Swiss mouse reported by D.S. Abou *et al*., the biodistribution of the tracer was similar (156). At the early time point, for 30 min post injection, radioactivity in the blood pool was observed with significant activity also localised in the bones and joints. After 24 hr, activity was completely cleared from blood pool, only accumulation activity in the skeleton and joints remained. This result was concordant with the results of the *ex vivo* tissue counting which showed that activity in the circulation and in the vascular organs was decreased between 2 days to 7 days post injection in contrast with the persistent activity in the bones up to 7 days. Altogether these results of ^{89}Zr oxalate biodistribution in C57BL/6J mouse suggest high affinity between ^{89}Zr oxalate and skeletons and joints.

4.6 Conclusion

eGFP-5T33 cells were successfully labelled with [^{89}Zr]-Zr(oxinate)$_4$ and used for *in vivo* tracking of labelled cells in a multiple myeloma mouse model, C57BL/KaLwRij, for up to two weeks. Comparing [^{89}Zr]-Zr(oxinate)$_4$ and [^{111}In]-In(oxinate)$_3$ labelled eGFP-5T33 cells showed no qualitative difference in the homing organs of the radiolabelled cells. Although the tissue biodistribution of [^{89}Zr]-Zr(oxinate)$_4$ labelled cells was similar to that of [^{111}In]-In(oxinate)$_3$, a standard radiotracer for labelling cells, *in vivo* stability of [^{89}Zr]-Zr(oxinate)$_4$ labelled cells was greater than those of [^{111}In]-In(oxinate)$_3$ after longer periods of tracking the cells. [^{89}Zr]-Zr(oxinate)$_4$ labelled eGFP-5T33 cells were also proved to retain the radiolabel and remain viable in *in vivo* for at least a week according to the results of *ex vivo* FACS sorting based on GFP expression. Therefore, the lipophilic complex of [^{89}Zr]-Zr(oxinate)$_4$ is a very promising long lived PET radiotracer to label and track cells especially for applications that require tracking the labelled cells for weeks.

Chapter 5: Summary and future work

The studies in this thesis reported on the production and characterisation of complexes of ^{64}Cu, a relatively long lived PET isotope, with dithiocarbamates (DTC) and bis(thiosemicarbazones) (BTSCs). The synthesis protocol was simple, fast and efficient to produce radiocopper complexes with either DTC or BTSC ligand. Copper-64 complexes of DTCs and BTSCs were shown the acceptable quality for further *in vitro* studies.

Intracellular uptake studies of the lipophilic ^{64}Cu tracers, ^{64}Cu (DEDTC)$_2$ and ^{64}Cu GTSM showed rapid and high extraction into various cell types. Although both types of tracers were able to efficiently influx into the cells, the retention of the activity in the labelled cells decreased rapidly after labelling. Less than 30 % of ^{64}Cu activities were retained in the cells 24 hr post labelling for all the lipophilic complexes of ^{64}Cu. Based on the results, therefore, those lipophilic complexes of copper are not suitable for long period tracking of the labelled cells especially in the application of cell based therapy and alternative PET labels were sought.

The physical half life of ^{89}Zr (3.2 days) offers opportunity for sequential imaging studies longer period of time and its decay properties are good for PET imaging. Therefore the later part of this thesis describes synthesis and characterisation of a new ^{89}Zr lipophilic complex, [^{89}Zr]-Zr(oxinate)$_4$, to label cells. Although the quality of [^{89}Zr]-Zr(oxinate)$_4$ was suitable for the following experiments either *in vitro* or *in vivo*, the quantity of the radiotracer was lower than expected when high initial activity was used (in order to use in *in vivo* studies). The issue of suboptimal production for required high activity of [^{89}Zr]-Zr(oxinate)$_4$ will need to be addressed for further improvement.

In vitro studies of intracellular uptake and efflux of [^{89}Zr]-Zr(oxinate)$_4$ by several cell types (macrophages (J774), breast cancer cells (MDA-MB-231) and mouse multiple myeloma cells (eGFP-5T33)) were performed. [^{89}Zr]-Zr(oxinate)$_4$ was moderately taken up by the cell lines including human white blood cells. However, high retention activity in the labelled cells 24 hr post labelling compared to that of [^{111}In]-In(oxinate)$_3$ (which is and approved radiotracer for labelling cells in clinical practice) was exhibited. This finding suggested that [^{89}Zr]-Zr(oxinate)$_4$ could be beneficially used to label cells for tracking over longer time periods because greater stability of the radiotracer in the labelled cells can be achieved.

This project also achieved the successful labelling of eGFP-5T33 cells with [^{89}Zr]-Zr(oxinate)$_4$ for both *in vitro* experiments and *in vivo* tracking of labelled cells in a multiple myeloma mouse model, C57BL/KaLwRij. *In vivo* cell tracking and *ex vivo* biodistribution of [^{89}Zr]-Zr(oxinate)$_4$ labelled cells were compared to those of [^{111}In]-In(oxinate)$_3$ labelled eGFP-5T33 cells showed the similar main organs of homing: liver, the spleen and the skeleton. The experiment of imaging lysates of cells labelled with [^{89}Zr]-Zr(oxinate)$_4$ and [^{111}In]-In(oxinate)$_3$ suggested that the released activity from the labelled cells *in vivo* could subsequently taken up or excreted via the kidneys. At the longer period of tracking labelled cells, *in vivo* stability of [^{89}Zr]-Zr(oxinate)$_4$ labelled cells was superior to that of cells labelled with [^{111}In]-In(oxinate)$_3$ as less accumulation of released activity in the kidneys was observed. [^{89}Zr]-Zr(oxinate)$_4$ labelled eGFP-5T33 cells were also confirmed to retain the radiolabel, and to remain viable *in vivo* for at least a week, according to the results of FACS sorting of organ homogenates based on GFP expression. *In vivo* imaging of [^{89}Zr]-Zr(oxinate)$_4$ labelled cells was successful in tracking the labelled for up to two weeks.

In order to improve synthesising yield and cell labelling yield, alternative ligands such as tropolone or MPO (2-mercaptopyridine-N-oxide) should undergo investigations since those ligands have shown the possibility to label cells with a range of radionuclides and radiocomplexes.

Based on the half life of ^{89}Zr, this novel lipophilic PET tracer should be useful for the application of tracking cells especially for stem cell or immune cell therapy where longer tracking of labelled cells is required. This would offer superior observation of the retention of labelled stem cells in homing tissues or organs and also lead to better understanding the mechanism of labelled cells in cell based therapy. Therefore further investigation of labelling [^{89}Zr]-Zr(oxinate)$_4$ with those cells will be considered.

Although this work described the promise of [^{89}Zr]-Zr(oxinate)$_4$ as a PET tracer for labelling cells and prolong tracking radiolabelled cell *in vivo*, the aspect of radiation biology and toxicity of this tracer to the labelled cells has not been yet investigated. Comparison of toxicity to radiolabelled cells and alteration of labelled cell function between ^{89}Zr and ^{111}In will be need to be done. There is not only radiation affect to labelled cells to consider but also the radiation dosimetry and radiation protection for related working staff, other people and environment should be determined.

Publication

Eur J Nucl Med Mol Imaging
DOI 10.1007/s00259-014-2945-x

ORIGINAL ARTICLE

[^{89}Zr]Oxinate$_4$ for long-term in vivo cell tracking by positron emission tomography

Putthiporn Charoenphun · Levente K. Meszaros · Krisanat Chuamsaamarkkee · Ehsan Sharif-Paghaleh · James R. Ballinger · Trevor J. Ferris · Michael J. Went · Gregory E. D. Mullen · Philip J. Blower

Received: 15 June 2014 / Accepted: 16 October 2014

Abstract
Purpose ^{111}In (typically as [^{111}In]oxinate$_3$) is a gold standard radiolabel for cell tracking in humans by scintigraphy. A long half-life positron-emitting radiolabel to serve the same purpose using positron emission tomography (PET) has long been sought. We aimed to develop an ^{89}Zr PET tracer for cell labelling and compare it with [^{111}In]oxinate$_3$ single photon emission computed tomography (SPECT).
Methods [^{89}Zr]Oxinate$_4$ was synthesised and its uptake and efflux were measured in vitro in three cell lines and in human leukocytes. The in vivo biodistribution of eGFP-5T33 murine myeloma cells labelled using [^{89}Zr]oxinate$_4$ or [^{111}In]oxinate$_3$ was monitored for up to 14 days. ^{89}Zr retention by living radiolabelled eGFP-positive cells in vivo was monitored by FACS sorting of liver, spleen and bone marrow cells followed by gamma counting.
Results Zr labelling was effective in all cell types with yields comparable with ^{111}In labelling. Retention of ^{89}Zr in cells in vitro after 24 h was significantly better (range 71 to >90 %) than ^{111}In (43–52 %). eGFP-5T33 cells in vivo showed the same early biodistribution whether labelled with ^{111}In or ^{89}Zr (initial pulmonary accumulation followed by migration to liver, spleen and bone marrow), but later translocation of radioactivity to kidneys was much greater for ^{111}In. In liver, spleen and bone marrow at least 92 % of ^{89}Zr remained associated with eGFP-positive cells after 7 days in vivo.
Conclusion [^{89}Zr]Oxinate$_4$ offers a potential solution to the emerging need for a long half-life PET tracer for cell tracking in vivo and deserves further evaluation of its effects on survival and behaviour of different cell types.

Keywords PET · Cell labelling · Cell tracking · ^{89}Zr · Leukocyte labelling

Introduction

Cell tracking by scintigraphy with radionuclides has been routine in nuclear medicine for 30 years [1] for tracking autologous leukocytes to detect sites of infection/inflammation [2, 3]. The standard radiolabelling methodology has been non-specific assimilation of lipophilic, metastable complexes of ^{111}In (with oxine [4], tropolone [5] and occasionally other bidentate chelators [6]), and later ^{99m}Tc [7].

New insight in immunology is creating interest in imaging the migration of individual immune cell types (e.g. eosinophils [8, 9], neutrophils [8, 9], T-lymphocytes [10–12], and dendritic cells [13]) in cancer, atherosclerosis, stroke, transplant and asthma. Regenerative medicine and cell-based therapies are creating new roles for tracking stem cells and chimeric antigen receptor-expressing T-lymphocytes [14, 15]. Conventional labelling methods have been applied in some of these areas, but for clinical use some of these new applications

Putthiporn Charoenphun and Levente K. Meszaros contributed equally to this work and are joint first authors.

Electronic supplementary material The online version of this article (doi:10.1007/s00259-014-2945-x) contains supplementary material, which is available to authorized users.

P. Charoenphun · L. K. Meszaros · K. Chuamsaamarkkee · E. Sharif-Paghaleh · J. R. Ballinger · G. E. D. Mullen · P. J. Blower
King's College London, Division of Imaging Sciences and Biomedical Engineering, 4th Floor Lambeth Wing, St Thomas' Hospital, London SE1 7EH, UK

T. J. Ferris · M. J. Went
School of Physical Sciences, University of Kent, Canterbury CT2 7NH, UK

P. J. Blower (✉)
Division of Chemistry, King's College London, Britannia House, 7 Trinity St, London SE11DB, UK
e-mail: Philip.Blower@kcl.ac.uk

Published online: 31 October 2014

will require detection of small lesions and small numbers of cells beyond the sensitivity of gamma camera imaging with ^{111}In (e.g. coronary artery disease, diabetes, neurovascular inflammation and thrombus), creating a need for positron-emitting radiolabels to exploit the better sensitivity, quantification and resolution of clinical positron emission tomography (PET).

So far the search for positron-emitting radiolabels for cells has met with limited success. The near-ubiquitous presence of glucose transporters allows labelling with [^{18}F]fluorodeoxyglucose (FDG), but labelling efficiencies are highly variable, the radiolabel is prone to rapid efflux and the short half-life (110 min) of ^{18}F allows only brief tracking [16–18]. ^{68}Ga can be used to label cells [19] but it too has a short half-life (68 min). ^{64}Cu offers a longer (12 h) half-life and efficient cell labelling using lipophilic tracers (complexes of PTSM [11, 20–22], GTSM [23], diethyldithiocarbamate [24] and tropolonate [25]), but rapid efflux of label from cells is a persistent problem and a still longer half-life would be preferred. A "PET analogue" of [^{111}In]oxinate$_3$, capable of cell tracking over 7 days or more, would be highly desirable but is not yet available.

^{89}Zr is a long half-life positron emitter that could meet this need [26, 27]. The favoured oxidation state of zirconium is 4+ (compared to 3+ for indium), but the parallels between the two metals in reactivity and preferred ligand types suggest that the mechanism exploited to label cells with ^{111}In (i.e. lipophilic metastable chelates entering cells and subsequently dissociating) might be exploited in the case of ^{89}Zr. Tetravalent zirconium forms ZrL_4 complexes with monobasic bidentate ligands such as oxinate [28], tropolonate [29] and hydroxamates [30], analogous to InL_3 [31, 32]. Here we describe the first synthesis of [^{89}Zr]oxinate$_4$ and comparison with [^{111}In]oxinate$_3$ for labelling several cell lines and tracking eGFP-5T33 cells in mice. eGFP-5T33 is a syngeneic murine multiple myeloma model originating from the C57Bl/KaLwRij strain [33], engineered to express enhanced green fluorescent protein (eGFP). It was chosen for this work because the fate of the cells after i.v. inoculation is known from the literature [34–36] and prior work in our laboratory. Like human multiple myeloma, 5T33 develops elevated serum immunoglobulin levels and osteolytic disease [33, 37]. Intravenously injected cells migrate exclusively to the liver, spleen and bone marrow [37].

Materials and methods

Radiochemistry

^{89}Zr was supplied as Zr^{4+} in a 0.1 M oxalic acid (PerkinElmer, Seer Green, UK), brought to pH 7 with 1 M Na_2CO_3 and diluted to 500 μl with water. This "neutralised [^{89}Zr]oxalate" was used as a control in cell labelling experiments in vitro. To prepare [^{89}Zr]oxinate$_4$ the above neutralised [^{89}Zr]oxalate solution (typically 20–90 MBq) was added to a glass reaction vessel containing 500 μl of a 1 mg/ml 8-hydroxyquinoline solution in chloroform. The vessel was shaken for 15 min and the product [^{89}Zr]oxinate$_4$ was recovered from the chloroform phase by evaporation, redissolved in dimethyl sulfoxide (DMSO, 10–20 μl) and diluted with phosphate-buffered saline (PBS, 1–3 ml) or cell culture medium. Full details are provided in the Electronic Supplementary Material (ESM).

Cell labelling initial evaluation

[^{89}Zr]Oxinate$_4$ was evaluated in vitro in three cell lines: cultured J774 mouse macrophages [38], MDA-MB-231 breast cancer cells [39] and eGFP-5T33 murine myeloma cells [40]; and in leukocytes from healthy volunteers. Studies were approved by an independent UK National Research Ethics Committee and complied with the Declaration of Helsinki. Culture methods and leukocyte preparation and labelling are described in the ESM. Labelling of cell lines was initially evaluated as follows: To triplicate suspensions of 10^6 cells in 450 μl of serum-depleted [i.e. not supplemented with foetal bovine serum (FBS)] culture medium in glass tubes were added 0.05 MBq of [^{89}Zr]oxinate$_4$ (or neutralised [^{89}Zr]oxalate) in 50 μl of serum-depleted medium. After incubation for up to 60 min at room temperature the tubes were centrifuged (5 min, 490 *g*), 450 μl of supernatant was removed and both supernatant and pellet were counted in a Wallac 1282 Compugamma Universal Gamma Counter. Pellet activity was corrected for the residual 50 μl of supernatant. Similar methods were used with higher activities (up to 40 MBq) and cell numbers (up to 5 x 10^7) and with [^{111}In]oxinate$_3$ for comparison. After these initial evaluations a standard labelling incubation period of 30 min was adopted for all subsequent biological evaluation.

Efflux of radioactivity from cells

Cells were labelled with [^{89}Zr]oxinate$_4$ or [^{111}In]oxinate$_3$ in glass tubes (10^6 cells and 0.05 MBq ^{89}Zr or 0.1 MBq ^{111}In per tube), washed three times with PBS, resuspended in culture medium (500 μl) and incubated at 37 °C. Samples taken at intervals up to 24 h were centrifuged and pellets and supernatants counted.

Cell viability

To assess the effect of [^{89}Zr]oxinate$_4$ on viability of eGFP-5T33 cells, samples of 1.2–1.4×10^6 cells (initially 93 % viable based on trypan blue exclusion) were radiolabelled as described above, washed and incubated in 20 ml of RPMI-1640 (supplemented with 10 % FBS, 200 U/l penicillin, 0.1 g/l streptomycin and 2 mM L-glutamate) in T75 tissue culture flasks at 37 °C (5 % CO_2). After 24 h, viability of these cells

and of controls (treated similarly except for omission of [^{89}Zr]oxinate$_4$) was determined by trypan blue exclusion.

Labelling eGFP-5T33 cells for in vivo cell tracking

Cells were labelled with [^{111}In]oxinate$_3$ or [^{89}Zr]oxinate$_4$ as described above [4×10^6 and 5×10^7 eGFP-5T33 cells/tube; ca. 0.5 MBq per tube for ex vivo organ counting and up to 40 MBq per tube for PET/single photon emission computed tomography (SPECT) imaging], washed three times with PBS and resuspended in 0.2–1 ml of sterile PBS ready for inoculation. Cell viabilities were determined by trypan blue exclusion. To obtain radiolabelled cell lysates, labelled eGFP-5T33 cells were subjected to three cycles of flash-freezing in liquid nitrogen and rapid heating to 90 °C before resuspending in 200–500 μl PBS and repeatedly passing through 27- and 29-gauge needles until visibly homogeneous.

Ex vivo cell tracking of eGFP-5T33 murine multiple myeloma

Animal experiments complied with the Animals (Scientific Procedures) Act (UK 1986) and Home Office (UK) guidelines. Male C57Bl/KaLwRij mice, 6–7 weeks old (Harlan, UK) were acclimatised for >7 days with ad libitum access to water and diet. To assess early tissue distribution ten mice were inoculated via the tail vein with 2×10^6 cells labelled with 0.6–0.8 MBq [^{89}Zr]oxinate$_4$ in 100 μl sterile PBS and culled by cervical dislocation at 9 (n=3), 24 (n=4) and 48 h (n=3) post-injection for ex vivo tissue counting. The longer-term biodistribution of [^{89}Zr]oxinate$_4$- and [^{111}In]oxinate$_3$-labelled cells was compared in three mice injected with 0.9 MBq [^{89}Zr]oxinate$_4$ in 6×10^6 cells and three with 1.7 MBq [^{111}In]oxinate$_3$ in 5×10^6 cells), culled by cervical dislocation after 7 days. Major thoraco-abdominal organs, the left femur and thigh muscle were excised, weighed and gamma-counted.

Ex vivo fluorescence-activated cell sorting (FACS)

Mice were culled by CO_2 asphyxiation 2 (n=3) and 7 days (n=3) after inoculation with 10^7 eGFP-5T33 cells labelled with 1.5 MBq [^{89}Zr]oxinate$_4$. Livers, spleens and femora were harvested. Livers and spleens were homogenised. Homogenates were filtered through a 40-μm cell strainer (BD, USA), diluted to 10^7 cells/ml in ice-cold FACS buffer [1 v/v% FBS, 2 μM ethylenediaminetetraacetate (EDTA) in PBS] and kept on ice. Marrow was flushed from the femora with 5–6 ml of ice-cold FACS buffer, filtered through a 40-μm cell strainer and kept on ice. Samples were analysed on a BD FACSAria III cell sorter (BD, USA) collecting 10,000 each of eGFP-positive and eGFP-negative cells (day 2) and 20,000 each of eGFP-positive and eGFP-negative cells (day 7) for gamma counting.

PET imaging

Preclinical PET/CT images were acquired in a nanoScan® PET/CT (Mediso, Budapest, Hungary) scanner with mice under isoflurane (2 % in oxygen) anaesthesia, starting 60 s before inoculation with 10^7 eGFP-5T33 cells labelled with 5 MBq [^{89}Zr]oxinate$_4$ in a 200-μl bolus via the right lateral tail vein. Scanning was continued for 2 h and repeated 1, 2, 5, 7 and 14 days after inoculation, acquiring a CT scan after each PET scan. Control mice were inoculated with [^{89}Zr]oxinate$_4$ (4 MBq in 100 μl saline) but no cells, and lysate from 1.1×10^6 cells labelled with 0.9 MBq [^{89}Zr]oxinate$_4$, and scanned between 5 and 50 min post-injection and at 24 h post-injection.

SPECT imaging

SPECT scans were acquired for 4 h immediately after inoculation of 10^7 eGFP-5T33 cells labelled with 10 MBq [^{111}In]oxinate$_3$ in a 200-μl bolus, using a nanoSPECT/CT (silver upgrade, Mediso, Budapest, Hungary) with four high-resolution multi-pinhole collimators. Further SPECT scans were acquired 1, 2, 3, 5 and 7 days post-injection, each followed by a CT scan. As a control, cell lysate from ca. 1.1×10^6 cells labelled with 1.1 MBq [^{111}In]oxinate$_3$ was injected intravenously followed by SPECT/CT scanning at 60 and 105 min post-injection.

Statistics

Statistical significance was tested using a two-tailed Student's t test with significance defined as a confidence level of 95 % or above.

Results

Synthesis and quality control of [^{89}Zr]oxinate$_4$

A biphasic system, with the radiolabel in aqueous solution and oxine in chloroform, was used to synthesise [^{89}Zr]oxinate$_4$. Yields of radioactivity in the chloroform phase were ca. 60 %. Repeated extraction with further aliquots of oxine solution in chloroform led to increased yields (see ESM). Both chloroform extraction and instant thin-layer chromatography (ITLC, R_f=0.9, cf. zero for [^{89}Zr]oxalate) before and after dilution of the DMSO solution in saline/serum-depleted RPMI-1640 reproducibly showed radiochemical purity above 99 %.

Cell labelling

Initial labelling experiments in all cell lines and leukocytes showed rapid accumulation of [^{89}Zr]oxinate$_4$, approaching

plateau levels by 30 min (Fig. S1). In all subsequent labelling experiments a standard labelling incubation time of 30 min was adopted, leading to labelling efficiencies in the range of 40–61 % for up to 9×10^7 cells, as shown in Table 1. By contrast, uptake of neutralised [^{89}Zr]oxalate, although increasing with time, was much lower and never exceeded 5 % (Fig. S1).

Efflux from cells

Efflux of ^{89}Zr from all three labelled cell lines in vitro was significantly slower than efflux of ^{111}In; at 24 h, >90 % of ^{89}Zr was retained by J774 macrophages (cf. 51.9 % for ^{111}In), >83 % by MDA-MB-231 cells (cf. 43.7 % for ^{111}In) and >71 % by eGFP-5T33 cells (Fig. S2). Retention of ^{89}Zr in leukocytes after 24 h was 85.1 and 86.9 % (n=2).

Cell viability

[^{89}Zr]Oxinate$_4$ labelling reduced viability of eGFP-5T33 cells from 93 % before labelling to 76.3±3.2 % immediately post-labelling [cf. 89.7±1.2 % (p=0.01) for ^{89}Zr-free controls], but there was no further significant loss in viability 24 h after labelling (87.3±4.0 %, cf. 89.3±3.0 % for ^{89}Zr-free controls, n=3).

In vivo cell tracking

PET imaging after inoculation of [^{89}Zr]oxinate$_4$-labelled eGFP-5T33 myeloma cells demonstrated accumulation of cells in lungs at 30 min followed by migration to liver, spleen and bone marrow by 24 h. Ex vivo tissue sampling (Table 2 and Fig. S3) confirmed location of radioactivity predominantly in liver, spleen and bone marrow between 9 and 48 h.

The in vivo biodistribution of ^{89}Zr-labelled eGFP-5T33 myeloma cells was compared alongside that of cells from the same culture labelled with ^{111}In longitudinally over 7 days using PET and SPECT imaging and ex vivo tissue sampling up to 7 days (Fig. 1, Table 3). Cell viabilities were 85–95 % with both radiolabels before inoculation. PET and SPECT images between 30 min and 7 days are shown in Fig. 2. A PET image acquired on day 14 is shown in Fig. S4 and ex vivo tissue uptake data for both radionuclides at 7 days are listed in Table 3. ^{111}In SPECT and ^{89}Zr PET showed qualitatively similar migration patterns in the first few hours after inoculation. However, there was significantly higher %ID/g of ^{89}Zr than ^{111}In in the main target organs (liver, spleen, bone) at 7 days (by factors of 1.5, 1.8 and 1.8, p=0.03, p=0.02 and p=0.03, respectively) (Table 3). The %ID/g of ^{111}In in kidneys increased with time, reaching 3.75-fold higher (p<0.0001) than that of ^{89}Zr by 7 days.

When radiolabelled cell lysates were injected i.v., uptake in the liver, spleen and skeleton was observed but there was also a much more marked accumulation in the kidneys, both for ^{111}In and ^{89}Zr (Fig. 3). Intravenously injected [^{89}Zr]oxinate$_4$ gave a qualitatively similar biodistribution to labelled cell lysates but there was also significant uptake in the heart and lungs after 24 h.

FACS sorting (based on eGFP fluorescence) of organ homogenates from animals culled 2 and 7 days after inoculation with cells labelled with [^{89}Zr]oxinate$_4$ showed that the eGFP-positive cells contained more activity per cell (by a factor of >23 at 2 days and a factor of >12 at 7 days) than eGFP-negative cells (p<0.02) (Fig. 4). Example FACS data are reported in Fig. S5.

Discussion

A general-purpose radiolabel that allows the advantages of PET to be implemented for tracking cells in vivo over several days should satisfy several criteria: the radioisotope must have a suitably long half-life and appropriate positron energy and abundance, convenient and economic availability, a simple and efficient labelling procedure, no major selectivity for different cell types, minimal effects on cell survival and function in vivo and minimal efflux from cells. These criteria should be met at least as well as [^{111}In]oxinate$_3$ meets them and better than positron-emitting alternatives reported to date. We have synthesised a lipophilic, metastable complex, [^{89}Zr]oxinate$_4$, evaluated it biologically in a range of cell lines in vitro and selected one cell line (eGFP-5T33 myeloma cells) for evaluation in vivo. The results indicate that [^{89}Zr]oxinate$_4$

Table 1 Cell labelling efficiencies with [^{89}Zr]oxinate$_4$ and [^{111}In]oxinate$_3$ in different cell types

	Cell number (concentration)	Labelling efficiency ^{89}Zr	Labelling efficiency ^{111}In	Medium
J774 mouse macrophages	10^6 (2×10^6/ml)	23.1±1.8 (n=3) (not optimised)	–	Cell culture medium (DMEM)
MDA-MB-231 breast cancer	10^6 (2×10^6/ml)	20.2±3.7 (n=3) (not optimised)	–	Cell culture medium (DMEM)
eGFP-5T33 mouse myeloma	$<5\times10^7$ ($<1.3\times10^7$/ml)	43.2±6.4 (n=3)	96, 82 (n=2)	Cell culture medium (RPMI 1640)
Human leukocytes	9×10^7 (4.5×10^7/ml)	54.3±11.9 (n=3)	46.8±12.3 (n=3)	Saline
	2×10^7 (10^7/ml)	47.0±10.5 (n=3)	–	Saline

Table 2 Tissue distribution of ^{89}Zr after i.v. inoculation of [^{89}Zr]oxinate$_4$-labelled eGFP-5T33 cells in C57Bl/KaLwRij mice

Organ	^{89}Zr-oxine 9 h (n=3) %ID/g	^{89}Zr-oxine 9 h (n=3) %ID	^{89}Zr-oxine 24 h (n=4) %ID/g	^{89}Zr-oxine 24 h (n=4) %ID	^{89}Zr-oxine 48 h (n=3) %ID/g	^{89}Zr-oxine 48 h (n=3) %ID
Heart	0.85±0.09	0.18±0.02	0.50±0.13	0.09±0.01	0.32±0.07	0.08±0.02
Lungs	2.28±0.41	0.60±0.11	1.35±0.07	0.41±0.04	0.68±0.06	0.21±0.04
Liver	44.6±10.6	73.9±6.3	42.2±9.1	69.2±7.5	30.9±4.2	57.6±5.3
Spleen	75.0±13.1	5.8±0.80	99.5±11.0	6.6±0.38	54.9±1.2	4.7±0.52
Stomach	0.29±0.08	0.14±0.01	0.45±0.17	0.16±0.08	0.28±0.07	0.12±0.01
Small int.	0.35±0.01	0.34±0.05	0.34±0.02	0.28±0.02	0.27±0.07	0.32±0.04
Large int.	0.34±0.04	0.36±0.04	0.27±0.02	0.29±0.14	0.21±0.04	0.26±0.10
Kidneys	3.9±0.45	1.8±0.15	4.0±0.44	1.65±0.26	3.0±0.43	1.42±0.21
Muscle	0.19±0.03	–	0.21±0.05	–	0.13±0.03	–
Femur	7.1±1.4	0.63±0.08	8.4±0.47	0.76±0.02	5.3±0.85	0.52±0.04
Salivary gl.	0.54±0.06	0.12±0.004	0.52±0.14	0.10±0.02	0.44±0.04	0.10±0.03
Blood	1.8±0.18	–	1.0±0.18	–	0.53±0.18	–
Liver:spleen	0.60±0.18	12.7±2.1	0.42±0.10	10.5±1.3	0.56±0.08	12.1±1.7
Liver:femur	6.28±1.94	116.8±17.2	5.02±1.12	91.1±10.2	5.83±1.23	110.8±13.5
Spleen:femur	10.6±2.78	9.2±1.7	11.9±1.47	8.7±0.56	10.4±1.68	9.1±1.22
Liver:kidneys	11.4±3.0	40.9±4.8	10.6±2.6	42.0±8.1	10.3±2.0	40.5±7.1
Spleen:kidneys	19.2±4.0	3.2±0.52	24.9±3.9	4.0±0.67	18.3±2.7	3.3±0.61
Femur:kidneys	1.8±0.42	0.35±0.05	2.1±0.26	0.46±0.07	1.8±0.38	0.37±0.06

%ID and %ID/g were calculated after ex vivo tissue counting; mean ± SD

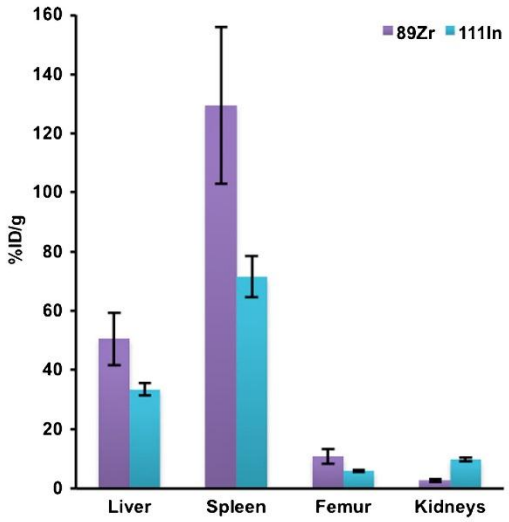

Fig. 1 Radioactivity distribution 7 days after inoculation of mice with [^{89}Zr]oxinate$_4$- and [^{111}In]oxinate$_3$-labelled eGFP-5T33 cells. %ID and %ID/g were calculated after ex vivo tissue counting and are given as mean ± SD (n=3 per group). Data are selected from Table 3 to show accumulation of ^{89}Zr and ^{111}In in haemopoietic tissues and kidneys (the main locations of radioactivity)

meets these criteria. The half-life of ^{89}Zr is 3.3 days (longer than that of ^{111}In and potential positron-emitting competitors ^{64}Cu, ^{18}F and ^{68}Ga); only ^{124}I (4.2 days) is comparable in this respect but cell labelling with ^{124}I has not been reported. The positron abundance and energies and gamma emissions of ^{89}Zr, although not ideal compared to ^{18}F, ^{64}Cu and ^{68}Ga, proved adequate to give better-resolved images than SPECT with ^{99m}Tc in a direct comparison (human sentinel node imaging) [41]. ^{89}Zr is now commercially and economically available as a GMP product. The cell labelling procedure described here is simple, indeed identical to that used with [^{111}In]oxinate$_3$; good labelling efficiencies are achieved within a few minutes. The labelling method is effective for several different cell lines and human leukocytes. The survival of labelled eGFP-5T33 cells in vitro is comparable to or better than that of [^{111}In]oxinate$_3$-labelled cells and not significantly different to that of control cells treated identically except for omission of radioactivity. While leukocytes are efficiently labelled and show good retention of radioactivity at 24 h, the effects of labelling on survival and function have not been determined, and further investigation of these aspects in the different leukocyte types are required. The in vivo biodistribution and FACS sorting data suggest that labelled eGFP-5T33 cells remain viable for at least 7 days, since the ^{89}Zr-labelled cells continue to express eGFP after this period in vivo. Retention of ^{89}Zr by cells studied here in vitro over 24 h compares well with published cell radiolabels; it is significantly better than that of ^{111}In and markedly

Table 3 Radioactivity distribution 7 days after i.v. inoculation of C57Bl/KaLwRij mice with [^{89}Zr]oxinate$_4$- and [^{111}In]oxinate$_3$-labelled eGFP-5T33 cells

Organ	^{89}Zr-oxine 7 days (n=3) %ID/g	^{89}Zr-oxine 7 days (n=3) %ID	^{111}In-oxine 7 days (n=3) %ID/g	^{111}In-oxine 7 days (n=3) %ID
Heart	0.24±0.04	0.03±0.005	0.71±0.12	0.12±0.02
Lungs	0.35±0.04	0.09±0.009	0.66±0.05	0.20±0.009
Liver	50.6±8.9	58.2±5.5	33.4±2.1	43.8±3.1
Spleen	129.5±26.5	7.9±0.76	71.6±6.9	4.59±0.34
Stomach	0.43±0.12	0.12±0.06	0.66±0.14	0.19±0.03
Small int.	0.17±0.07	0.16±0.06	0.43±0.11	0.44±0.12
Large int.	0.17±0.08	0.18±0.09	0.45±0.07	0.58±0.16
Kidneys	2.64±0.39	0.96±0.06	9.9±0.64	4.2±0.39
Muscle	0.16±0.02	–	0.43±0.05	–
Femur	10.8±2.5	0.88±0.12	6.0±0.5	0.56±0.04
Salivary gl.	0.40±0.03	0.06±0.01	1.96±0.24	0.35±0.08
Blood	0.23±0.1	–	0.22±0.06	–
Liver:spleen	0.39±0.11	7.3±1.0	0.47±0.05	9.5±1.0
Liver:femur	4.69±1.36	66.0±11.2	5.57±0.58	78.7±8.4
Spleen:femur	12.0±3.71	9.0±1.5	11.9±1.52	8.3±0.9
Liver:kidneys	19.2±4.4	60.6±6.7	3.4±0.4	10.5±1.25
Spleen:kidneys	49.1±12.4	8.3±0.92	7.23±0.8	1.1±0.13
Femur:kidneys	4.1±1.1	0.92±0.14	0.61±0.06	0.13±0.02

%ID and %ID/g were calculated after ex vivo tissue counting and are given as mean ± SD (n=3 per group)

superior to that of cells labelled with ^{64}Cu complexes of PTSM [11, 20–22] and GTSM [23] or with ^{18}F-FDG. The superior retention of ^{89}Zr compared to ^{111}In by eGFP-5T33 cells in vivo is inferred from the much slower transfer of ^{89}Zr than ^{111}In from liver, spleen and bone marrow to kidneys and suggests that replacing ^{111}In SPECT with ^{89}Zr PET can extend the period over which cells can be reliably tracked in vivo; indeed, we have been able to acquire good PET images up to 2 weeks post-inoculation. The 14-day image showed a similar biodistribution of radioactivity to that seen at 7 days in the same mouse suggesting that the radiolabel continued to be retained by 5T33 cells in vivo (Fig. S4).

The overall biodistribution observed with both ^{111}In- and ^{89}Zr-labelled cells (initial uptake in lung followed by migration to liver, spleen and bone marrow) is consistent with earlier studies of the migration of related murine myeloma cells, by histology and by radiolabelling with ^{51}Cr [35]. Organ to organ uptake ratios among the main target organs (liver, spleen, bone marrow) did not vary significantly throughout the study, either for ^{89}Zr or ^{111}In, suggesting that labelled cells, or radioactivity, did not migrate from one haematopoietic tissue to another and that the radiolabel used did not change the tissue preference of eGFP-5T33 cells. To test the implicit assumption that migration of radioactivity from liver, spleen and bone marrow to kidney and bladder is an indicator of gradual efflux of radioactivity from living or dead labelled cells, we examined the distribution of activity after injection of [^{89}Zr]oxinate$_4$ and that of cells that had been killed/lysed after radiolabelling with ^{89}Zr and ^{111}In. The resulting biodistribution qualitatively resembled that seen with labelled healthy cells, but both ^{89}Zr- and ^{111}In-labelled cell lysate showed greatly increased uptake in kidney and also liver and reduced uptake in spleen, even at early time points (30 min, 24 h, Fig. 3), compared to labelled healthy cells. This contrast in behaviour of ^{89}Zr injected in the form of living labelled cells and dead/lysed labelled cells is consistent with the hypothesis that migration of radioactivity from initially targeted organs to kidney and bladder is a non-invasive marker for efflux of radioactivity from living or dying labelled cells in vivo.

^{89}Zr injected in the form of neutralised [^{89}Zr]-oxalate also shows marked differences from the behaviour of labelled cells, consistent with the assumption that the images obtained after injection of ^{89}Zr-labelled cells reflect the location of the cells. With [^{89}Zr]oxinate$_4$ significant uptake in heart was observed that was not seen with labelled cells, while [^{89}Zr]oxalate shows gradual skeletal accumulation: radioactivity can be imaged in the joints as early as 15 min post-injection [42, 43].

The novel experimental approach of ex vivo FACS sorting of eGFP-positive and eGFP-negative populations from organ homogenates, followed by radiation counting of these fractions, showed that the radioactivity in the target tissues

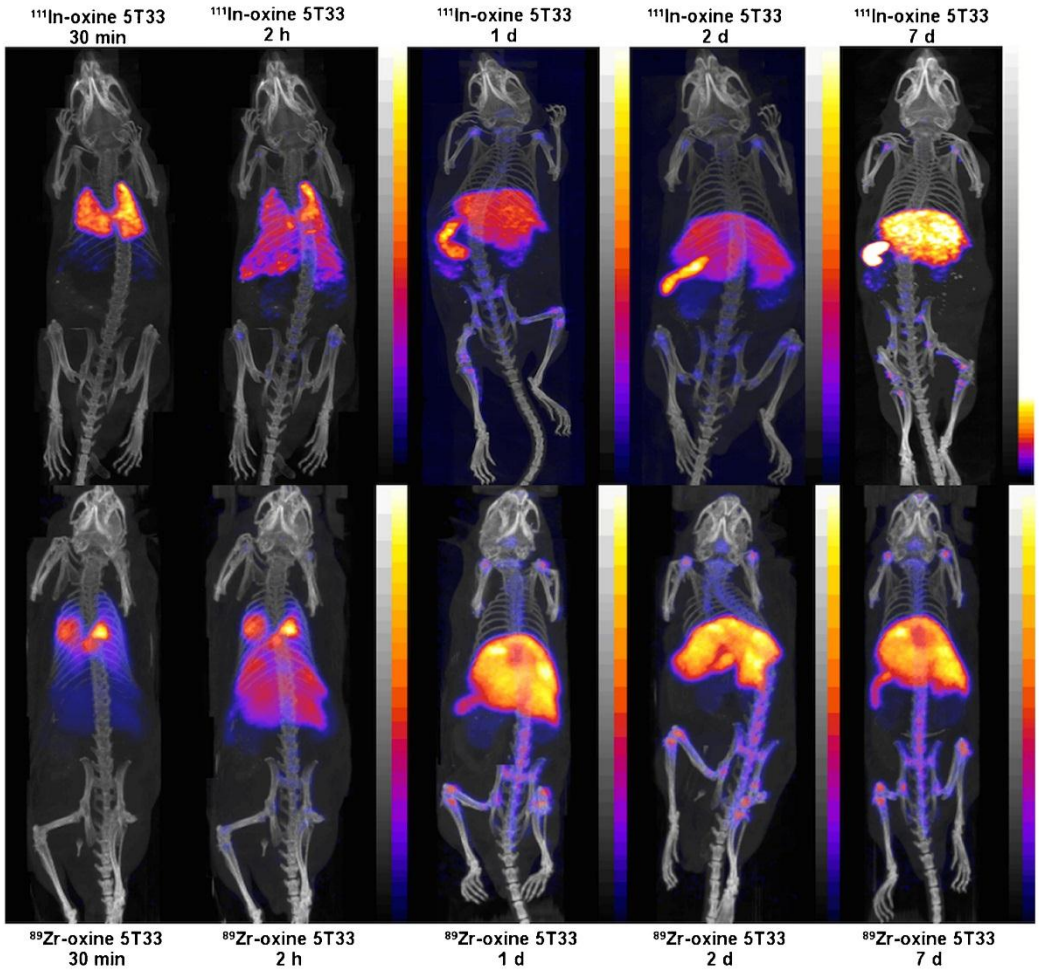

Fig. 2 PET/CT and SPECT/CT images of C57Bl/KaLwRij mice inoculated with [^{89}Zr]oxinate$_4$- or [^{111}In]oxinate$_3$-labelled eGFP-5T33 cells. Scans of ^{111}In (*top*) and ^{89}Zr (*bottom*) are reported from 30 min to 7 days after i.v. inoculation of C57Bl/KaLwRij mice with 10^7 eGFP-5T33 cells labelled with 5 MBq [^{89}Zr]oxinate$_4$ or 10 MBq [^{111}In]oxinate$_3$. Image scales were adjusted to the maximum activity concentration within each image except for the 2-h images where the activity scale was adjusted to the maximum activity per voxel used in the 30-min image in order to quantitatively visualise the rapid change in the early homing pattern of eGFP-5T33 cells after i.v. inoculation

remains associated with the originally labelled eGFP-expressing cells (Fig. 4), and hence that these labelled cells remain alive during the 7 days in vivo; 96 % of liver radioactivity, 99 % of spleen radioactivity and >99 % of bone marrow radioactivity remains associated with eGFP-positive cells at 2 days, falling to 95, 92 and 98 %, respectively, by 7 days. Although we observed excellent in vivo survival of labelled eGFP-5T33 cells in this study, a more thorough understanding of the possible cytotoxic effects of the wider use of both ^{89}Zr and ^{111}In labelling of cells is required for a proper interpretation of cell tracking data generally. This ex vivo FACS-based method provides a potential experimental approach to this challenging problem.

These highly promising results warrant further development including refinement of the radiosynthesis and labelling process to improve radiochemical and cell labelling yields, select the most suitable medium for cell labelling and eliminate undesirable use of chloroform, and determine the functional and survival effects of labelling in a variety of cell types, prior to evaluation of the method for cell tracking in humans.

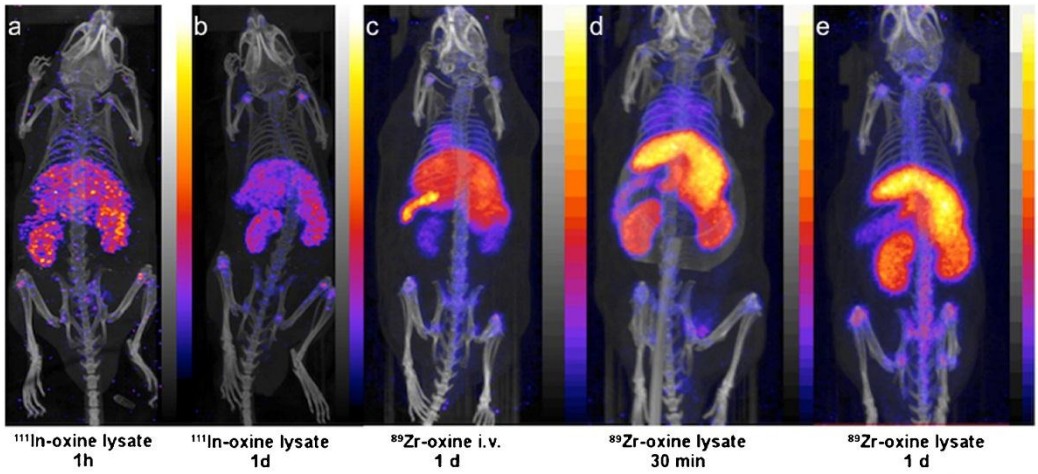

Fig. 3 SPECT/CT and PET/CT images of mice injected with radiolabelled eGFP-5T33 cell lysates or [^{89}Zr]oxinate$_4$. **a**, **b** SPECT/CT images of mice injected with lysates of 1.1×10^6 eGFP-5T33 cells labelled with 1.1 MBq [^{111}In]oxinate$_3$ at 1 and 24 h post-injection, respectively. **c** PET/CT image of mouse 24 h after injection with 4 MBq [^{89}Zr]oxinate$_4$. **d**, **e** PET/CT images of mice injected with lysates of 1.1×10^6 eGFP-5T33 cells labelled with 0.9 MBq [^{89}Zr]oxinate$_4$ at 1 and 24 h post-injection, respectively

While estimates of likely dosimetry in humans have not yet been performed, it will also be important to assess the potential advantages of cell tracking by PET with ^{89}Zr against the likely increased radiation burden per megabecquerel associated with ^{89}Zr, balancing the increased dose per decay, the low positron yield of ^{89}Zr and the increased detection efficiency of PET compared to SPECT.

Conclusion

The new lipophilic, metastable complex of ^{89}Zr can radiolabel a range of cells, independently of specific phenotypes, providing a long-sought solution to the unmet need for a long half-life positron-emitting radiolabel to replace ^{111}In for cell migration imaging. In addition to the expected advantages (enhanced sensitivity, resolution and quantification) of cell tracking with PET rather than scintigraphy or SPECT, ^{89}Zr shows less efflux from eGFP-5T33 cells in vitro and in vivo than ^{111}In during at least 7 days after labelling. The excellent in vivo survival and retention of radioactivity by the cells at 7 days, coupled with the demonstrated ability to acquire useful PET images up to 14 days, significantly extend the typical period over which cells can be tracked by radionuclide imaging with directly labelled cells. This method offers a potential solution to the emerging need for a long half-life PET tracer for cell tracking in vivo and deserves further evaluation of its effects on survival and behaviour of different cell types, and the dosimetric and radiobiological implications of application in humans.

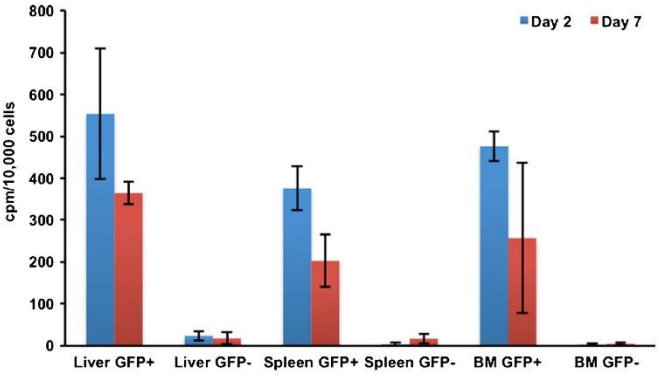

Fig. 4 ^{89}Zr activities in eGFP-positive and eGFP-negative cell populations sorted from organ samples. Liver, spleen and femoral marrow (*BM*) organ homogenates were harvested from mice 2 and 7 days after i.v. inoculation with [^{89}Zr]oxinate$_4$-labelled eGFP-5T33 cells (n=3/group, decay corrected)

Acknowledgments This research was supported by a Leukaemia and Lymphoma Research, the Centre of Excellence in Medical Engineering Centre funded by the Wellcome Trust and EPSRC (WT088641/Z/09/Z), the King's College London and UCL Comprehensive Cancer Imaging Centre funded by the CRUK and EPSRC in association with the MRC and DoH (England), and by the NIHR Biomedical Research Centre at Guy's and St Thomas' NHS Foundation Trust and King's College London. PC was supported by a scholarship from Ramathibodi Hospital, Mahidol University, Thailand. The views expressed are those of the author(s) and not necessarily those of the NHS, the NIHR or the DoH. PET and SPECT scanning equipment was funded by an equipment grant from the Wellcome Trust.

Conflicts of interest None.

References

1. Segal AW, Arnot RN, Thakur ML, Lavender JP. Indium-111-labelled leucocytes for localisation of abscesses. Lancet 1976;2:1056–8.
2. Peters AM. A brief history of cell labelling. Q J Nucl Med Mol Imaging 2005;49:304–7.
3. Basu S, Zhuang HM, Torigian DA, Rosenbaum J, Chen WG, Alavi A. Functional imaging of inflammatory diseases using nuclear medicine techniques. Semin Nucl Med 2009;39:124–45.
4. Intenzo CM, Desai AG, Thakur ML, Park CH. Comparison of leukocytes labeled with indium-111-2-mercaptopyridine-N-oxide and indium-111 oxine for abscess detection. J Nucl Med 1987;28:438–41.
5. Kotzé HF, Heyns AD, Lötter MG, Pieters H, Roodt JP, Sweetlove MA, et al. Comparison of oxine and tropolone methods for labeling human platelets with indium-111. J Nucl Med 1991;32:62–6.
6. Ellis BL, Sampson CB, Abeysinghe RD, Porter JB, Hider RC. 6-Alkoxymethyl-3-hydroxy-4H-pyranones: potential ligands for cell-labelling with indium. Eur J Nucl Med 1999;26:1400–6.
7. Peters AM. The utility of [^{99m}Tc]HMPAO-leukocytes for imaging infection. Semin Nucl Med 1994;24:110–27.
8. Puncher MRB, Blower PJ. Autoradiography and density gradient separation of technetium-99m-exametazime (HMPAO) labelled leucocytes reveals selectivity for eosinophils. Eur J Nucl Med 1994;21:1175–82.
9. Lukawska JJ, Livieratos L, Sawyer BM, Lee T, O'Doherty M, Blower PJ, et al. Real-time differential tracking of human neutrophil and eosinophil migration in vivo. J Allergy Clin Immunol 2014;133:233–9.
10. Sharif-Paghaleh E, Sunassee K, Tavaré R, Ratnasothy K, Koers A, Ali N, et al. In vivo SPECT reporter gene imaging of regulatory T cells. PLoS One 2011;6:e25857. doi:10.1371/journal.pone.0025857.
11. Griessinger CM, Kehlbach R, Bukala D, Wiehr S, Bantleon R, Cay F, et al. In vivo tracking of Th1 cells by PET reveals quantitative and temporal distribution and specific homing in lymphatic tissue. J Nucl Med 2014;55:301–7.
12. Ruparelia P, Szczepura KR, Summers C, Solanki CK, Balan K, Newbold P, et al. Quantification of neutrophil migration into the lungs of patients with chronic obstructive pulmonary disease. Eur J Nucl Med Mol Imaging 2011;38:911–9.
13. Tavaré R, Sagoo P, Varama G, Tanriver Y, Warely A, Diebold SS, et al. Monitoring of in vivo function of superparamagnetic iron oxide labelled murine dendritic cells during anti-tumour vaccination. PLoS One 2011;6:e19662. doi:10.1371/journal.pone.0019662.
14. Leech JM, Sharif-Paghaleh E, Maher J, Livieratos L, Lechler RI, Mullen GE, et al. Whole-body imaging of adoptively transferred T cells using magnetic resonance imaging, single photon emission computed tomography and positron emission tomography techniques, with a focus on regulatory T cells. Clin Exp Immunol 2013;172:169–77.
15. Zanzonico P, Koehne G, Gallardo HF, Doubrovin M, Doubrovina E, Finn R, et al. [^{131}I]FIAU labeling of genetically transduced, tumor-reactive lymphocytes: cell-level dosimetry and dose-dependent toxicity. Eur J Nucl Med Mol Imaging 2006;33:988–97.
16. Elhami E, Goertzen AL, Xiang B, Deng JX, Stillwell C, Mzengeza S, et al. Viability and proliferation potential of adipose-derived stem cells following labeling with a positron-emitting radiotracer. Eur J Nucl Med Mol Imaging 2011;38:1323–34.
17. Forstrom LA, Mullan BP, Hung JC, Lowe VJ, Thorson LM. ^{18}F-FDG labelling of human leukocytes. Nucl Med Commun 2000;21:691–4.
18. Stojanov K, de Vries EFJ, Hoekstra D, van Waarde A, Dierckx R, Zuhorn IS. [^{18}F]FDG labeling of neural stem cells for in vivo cell tracking with positron emission tomography: inhibition of tracer release by phloretin. Mol Imaging 2012;11:1–12.
19. Welch MJ, Thakur ML, Coleman RE, Patel M, Siegel BA, Terpogossian MM. Gallium-68 labeled red cells and platelets: new agents for positron tomography. J Nucl Med 1977;18:558–62.
20. Huang J, Lee CCI, Sutcliffe JL, Cherry SR, Tarantal AF. Radiolabeling rhesus monkey CD34(+) hematopoietic and mesenchymal stem cells with ^{64}Cu-pyruvaldehyde-bis(N4-methylthiosemicarbazone) for microPET imaging. Mol Imaging 2008;7:1–11.
21. Park JJ, Lee TS, Son JJ, Chun KS, Song IH, Park YS, et al. Comparison of cell-labeling methods with ^{124}I-FIAU and ^{64}Cu-PTSM for cell tracking using chronic myelogenous leukemia cells expressing HSV1-tk and firefly luciferase. Cancer Biother Radiopharm 2012;27:719–28.
22. Adonai N, Nguyen KN, Walsh J, Iyer M, Toyokuni T, Phelps ME, et al. Ex vivo cell labeling with ^{64}Cu-pyruvaldehyde-bis(N-4-methylthiosemicarbazone) for imaging cell trafficking in mice with positron-emission tomography. Proc Natl Acad Sci U S A 2002;99:3030–5.
23. Charoenphun P, Paul R, Weeks A, Berry D, Shaw K, Mullen G, et al. PET tracers for cell labelling with the complexes of copper 64 with lipophilic ligands. Eur J Nucl Med Mol Imaging 2011;38:S294.
24. Li ZB, Chen K, Wu ZH, Wang H, Niu G, Chen XY. ^{64}Cu-labeled PEGylated polyethylenimine for cell trafficking and tumor imaging. Mol Imaging Biol 2009;11:415–23.
25. Bhargava KK, Gupta RK, Nichols KJ, Palestro CJ. In vitro human leukocyte labeling with ^{64}Cu: an intraindividual comparison with ^{111}In-oxine and ^{18}F-FDG. Nucl Med Biol 2009;36:545–9.
26. Meszaros LK, Charoenphun P, Chuamsaamarkkee K, Ballinger JR, Mullen G, Ferris TJ, et al. ^{89}Zr-Oxine complex: a long-lived radiolabel for cell tracking using PET. 2013 World Molecular Imaging Congress. http://www.wmis.org/abstracts/2013/data/index.htm. Accessed 15 June 2014.
27. Ferris T, Charoenphun P, Went M, Blower P. Medical imaging utilising zirconium complexes (abstract). Nucl Med Commun 2013;34:362–411.
28. Kathirgamanathan P, Surendrakumar S, Antipan-Lara J, Ravichandran S, Reddy VR, Ganeshamurugan S, et al. Discovery of two new phases of zirconium tetrakis(8-hydroxyquinolinolate): synthesis, crystal structure and their electron transporting characteristics in organic light emitting diodes (OLEDs). J Mater Chem 2011;21:1762–71.
29. Muetterties EL, Algeranti CW. Chelate chemistry. VI. Solution behavior of tropolonates. J Am Chem Soc 1969;91:4420–5.
30. Guérard F, Lee YS, Tripier R, Szajek LP, Deschamps JR, Brechbiel MW. Investigation of Zr(IV) and 89Zr(IV) complexation with hydroxamates: progress towards designing a better chelator than

desferrioxamine B for immuno-PET imaging. Chem Commun 2013;49:1002–4.
31. Nepveu F, Jasanada F, Walz L. Structural characterization of two lipophilic tris(tropolonato) gallium(III) and indium(III) complexes of radiopharmaceutical interest. Inorg Chim Acta 1993;211: 141–7.
32. Abrahams I, Choi N, Henrick K, Joyce H, Matthews RW, McPartlin M, et al. The crystal and molecular-structures of the blood-cell labeling agents tris(2-hydroxy-2,4,6-cycloheptatrien-1-onato-O,O ')indium(III) and trans-(tris(4-iso-propyl-2-hydroxy-2,4,6-cycloheptatrien-1-onato-O,O') indium(III)). Polyhedron 1994;13: 513–6.
33. Radl J, Croese JW, Zurcher C, Van den Enden-Vieveen MHM, de Leeuw AM. Animal model of human disease. Multiple myeloma. Am J Pathol 1988;132:593–7.
34. Vanderkerken K, Asosingh K, Croucher P, Van Camp B. Multiple myeloma biology: lessons from the 5TMM models. Immunol Rev 2003;194:196–206.
35. Vanderkerken K, De Greef C, Asosingh K, Arteta B, De Veerman M, Vande Broek I, et al. Selective initial in vivo homing pattern of 5T2 multiple myeloma cells in the C57BL/KalwRij mouse. Br J Cancer 2000;82:953–9.
36. Vanderkerken K, De Raeve H, Goes E, Van Meirvenne S, Radl J, Van Riet I, et al. Organ involvement and phenotypic adhesion profile of 5T2 and 5T33 myeloma cells in the C57BL/KaLwRij mouse. Br J Cancer 1997;76:451–60.
37. Garrett IR, Dallas S, Radl J, Mundy GR. A murine model of human myeloma bone disease. Bone 1997;20:515–20.
38. Snyderman R, Pike MC, Fischer DG, Koren HS. Biologic and biochemical activities of continuous macrophage cell lines P388D1 and J774.1. J Immunol 1977;119:2060–6.
39. Cailleau R, Olivé M, Cruciger QV. Long-term human breast carcinoma cell lines of metastatic origin: preliminary characterization. In Vitro 1978;14:911–5.
40. Alici E, Konstantinidis KV, Aints A, Dilber MS, Abedi-Valugerdi M. Visualization of 5T33 myeloma cells in the C57BL/KaLwRij mouse: establishment of a new syngeneic murine model of multiple myeloma. Exp Hematol 2004;32:1064–72.
41. Heuveling DA, van Schie A, Vugts DJ, Hendrikse NH, Yaqub M, Hoekstra OS, et al. Pilot study on the feasibility of PET/CT lymphoscintigraphy with ^{89}Zr-nanocolloidal albumin for sentinel node identification in oral cancer patients. J Nucl Med 2013;54: 585–9.
42. Abou DS, Ku T, Smith-Jones PM. In vivo biodistribution and accumulation of ^{89}Zr in mice. Nucl Med Biol 2011;38:675–81.
43. Ma MT, Meszaros L, Berry DJ, Cooper M, Clark SJ, Ballinger JR, et al. A tripodal tris(hydroxypyridinone) ligand for immunoconjugate PET imaging with zirconium-89. J Biol Inorg Chem 2014;19:S649.

[^{89}Zr]-Zr(oxinate)$_4$ for long term *in vivo* cell tracking by positron emission tomography

(Submitted to the European Journal of Nuclear Medicine and Molecular Imaging)

Putthiporn Charoenphun[†1], Levente K Meszaros[†1], Krisanat Chuamsaamarkkee[1], Ehsan Sharif-Paghaleh[1], James R Ballinger[1], Trevor J Ferris[2], Michael J Went[2], Gregory ED Mullen[1], Philip J Blower*[1,3]

[1]King's College London, Division of Imaging Sciences and Biomedical Engineering, 4th Floor Lambeth Wing, St Thomas' Hospital, London SE1 7EH, UK.

[2]University of Kent, School of Physical Sciences, Canterbury CT2 7NH, UK

[3]King's College London, Division of Chemistry, Britannia House, 7 Trinity St, London SE11DB, UK

[†]PC and LKM contributed equally to this work and are joint first authors.

*Author for correspondence: Prof Phil Blower, King's College London, Division of Imaging Sciences and Biomedical Engineering, 4th Floor Lambeth Wing, St Thomas' Hospital, London SE1 7EH, UK. Tel: +44-207-188-9513; fax: +44-207-188-5442; email: Philip.Blower@kcl.ac.uk

Synthesis of [^{89}Zr]-Zr(oxinate)$_4$

^{89}Zr was supplied as Zr^{4+} in a 0.1M oxalic acid (Perkin-Elmer, Seer Green, UK), brought to pH 7 with 1M Na_2CO_3 and diluted to 500 µl with distilled water. This "neutralised [^{89}Zr]-Zr-oxalate" was used both as a control in cell labelling experiments *in vitro*, and to prepare [^{89}Zr]-Zr(oxinate)$_4$ as follows: 8-hydroxyquinoline (oxine) (Sigma, Gillingham, UK) in chloroform (500 µl, 1 mg/ml) was added to a glass reaction vessel containing 500 µl (20-90 MBq, measured with a Capintec CRC-25 dose calibrator) of neutralised [^{89}Zr]-Zr-oxalate The vessel was shaken (vortexed, 1000 RPM) for 15 minutes to facilitate phase transfer. The two phases were then allowed to separate and the aqueous phase was transferred into a separate vessel. The chloroform extract was evaporated at 60 °C and the residue containing [^{89}Zr]-Zr(oxinate)$_4$ was dissolved in 10-20 µl of DMSO and diluted to 1-3 ml with PBS or cell culture medium. In some experiments the used aqueous phase was extracted again with further aliquots of oxine solution in chloroform to increase the yield. Quality control was performed with instant thin layer chromatography (ITLC) and solvent extraction as described below.

Quality control of [^{89}Zr]-Zr(oxinate)$_4$

ITLC: Samples were analysed on silica gel coated ITLC strips (ITLC-SG; Agilent, UK) with ethyl acetate mobile phase. 8-9 cm long strips were developed in 50 ml centrifuge tubes. Chromatograms were evaluated on a LabLogic MINI-SCAN radio TLC linear scanner connected to a LabLogic B-FC-3200 NaI detector for gamma photon detection.

Solvent extraction: A biphasic solvent system of phosphate buffered saline (PBS) and chloroform (1:1) was prepared 24 hours before the study to allow equilibration (PBS saturated in chloroform and *vice versa*). Five hundred µl of both phases were transferred into a 1.5 ml microcentrifuge tube. To this mixture 0.5 µl of [^{89}Zr]-Zr(oxinate)$_4$ in DMSO or 0.5 µl of neutralised ^{89}Zr in water were added. The mixtures were vortexed at a high speed for 1

minute. Upon separation of the two phases 100 µl of each phase were transferred into a scintillation vial and activities associated with the organic and aqueous phase were determined in the gamma counter.

Cell culture

The J774 cell line was kindly provided by Dr. Helen Collins, Department of Infectious Diseases, King's College London. Cells were cultured in Dulbecco's Modified Eagle's Medium (DMEM, 4.5 g/l glucose) supplemented with 10% foetal bovine serum (FBS), 2mM L-glutamine, penicillin (100 U/ml), streptomycin (0.1 mg/ml), 1 mM sodium pyruvate and 10 mM HEPES. MDA-MB-231 cells were cultured in DMEM (4.5 g/l glucose) supplemented with 10% foetal bovine serum, 2mM L-glutamine, penicillin (100 U/ml) and streptomycin (0.1 mg/ml). Cell lines were cultured in a tissue culture incubator with humidified 95% air 5% CO_2 atmosphere at a constant temperature of 37°C. Both cell lines were grown in adherent cultures in T75 or T175 cell culture flasks and split twice a week (typically when full confluence was reached). Cells were harvested from culture as follows. Supernatant was discarded and cells were washed twice with PBS. To obtain J774 cells culture medium (complete medium for culture maintenance and FBS depleted for labelling) was added and cells were removed from the plastic surface by gentle scraping. MDA-MB-231 cells were trypsinised as follows. 1-2 ml of trypsin-EDTA (containing 0.5 g/l porcine trypsin and 0.2 g/l EDTA in Hank's Balanced Salt Solution) were added to the cell culture flask and dispersed on the plastic surface. The flask was then incubated in a tissue culture incubator for 5 min. Cells were obtained by adding at least 20 ml of medium to the flask then diluted to the required concentration.

The eGFP-5T33 murine multiple myeloma cell line was provided by Dr Yolanda Calle (University of Roehampton). This cell line was used for *in vivo* cell tracking. Cells were grown in suspension culture in RPMI 1640 supplemented with 10% FBS, 2 mM L-glutamine,

penicillin (100 U/ml) and streptomycin (0.1 mg/ml). This cell line was maintained in suspension culture.

When cells were prepared for labelling with one of the radiotracers they were repeatedly washed by resuspending in PBS and centrifuging (5 min, 490 g; three times in total) to remove residues of serum and other culture medium constituents.

White blood cell separation and radiolabelling

These studies were approved by an independent United Kingdom national research ethics committee. This procedure (approximating a standard method used clinically for ^{111}In-labelling - not identical to that provided in EANM guidelines[1]), was carried out on three different occasions. Fifty ml blood was withdrawn from a peripheral blood of a healthy volunteer as follows: 500 U heparin (0.5 ml) were withdrawn into a 50 ml syringe. The syringe was then fitted with a 20 gauge scalp vein set and 50 ml blood was slowly withdrawn from a peripheral vein of the volunteer. Upon completion the scalp vein set was replaced with a luer lock syringe cap to seal the syringe. The syringe was gently turned around several times to mix its contents. The syringe was then transferred into a class 2 tissue culture cabinet where WBC separation was performed aseptically as follows. Two ml of Methocel 2% and 40 ml of whole blood were added to a 50 ml centrifuge tube. The tube was sealed then contents were mixed gently. The remaining 10 ml of whole blood were transferred to a 15 ml centrifuge tube. Both tubes were placed in a plastic rack in upright position. To separate white blood cells for subsequent radiolabelling the 50 ml centrifuge tube was centrifuged at 4.9 g for 15 min. After centrifugation, the supernatant containing white blood cells, platelets and leukocyte rich plasma (LRP) was transferred into a new centrifuge tube and centrifuged at 91 g for 5 min. After centrifugation, white blood cells formed a pellet at the bottom of the tube, the supernatant contained platelet-rich plasma (PRP). The supernatant was discarded and the pellet was re-suspended in 10 ml of isotonic saline. The tube was centrifuged at 91 g

for 5 min then the supernatant was discarded. The pellet was re-suspended in 1 ml of saline then transferred into a glass test tube. [^{89}Zr]-Zr(oxinate)$_4$ in 15 µl DMSO was diluted in 1 ml normal saline then added to the above cell suspension and mixed very gently. Cells were incubated with the tracer at room temperature for 15 min. The experiment was repeated three times with different levels of activity (3.05, 11.10, and 16.10 MBq). In the meantime platelet poor plasma (PPP) was prepared from 10 ml whole blood by centrifuging the sample at 490 g for 5 min. Supernatant layer containing platelet-poor plasma was collected in a fresh centrifuge tube. PPP was later used to dilute and re-suspend WBCs after radiolabelling. After incubating WBCs with the radiotracer the labelled WBC suspension was transferred into a 50 ml centrifuge tube. Three ml of PPP were added to the WBC suspension which was then diluted to 10 ml in saline. The resulting suspension was centrifuged at 91 g for 5 min. The supernatant containing unbound [^{89}Zr]-Zr(oxinate)$_4$ was transferred into a fresh tube. The radiolabelled WBC pellet was gently re-suspended in 3 ml of PPP. Activity of the labelled cells and supernatant (unreacted tracer) were measured in the dose calibrator. The labelled cell suspension in PPP was transferred into a glass test tube and incubated in a tissue culture incubator for 24 h when retention of the radiotracer was assessed after centrifugation and separation of the supernatant and labelled WBC pellet.

References

1. Roca M, de Vries EFJ, Jamar F, Israel O, Signore A. Guidelines for the labelling of leucocytes with 111In-oxine. *Eur J Nucl Med Mol Imaging*. 2010; 37: 835–841.

Figures

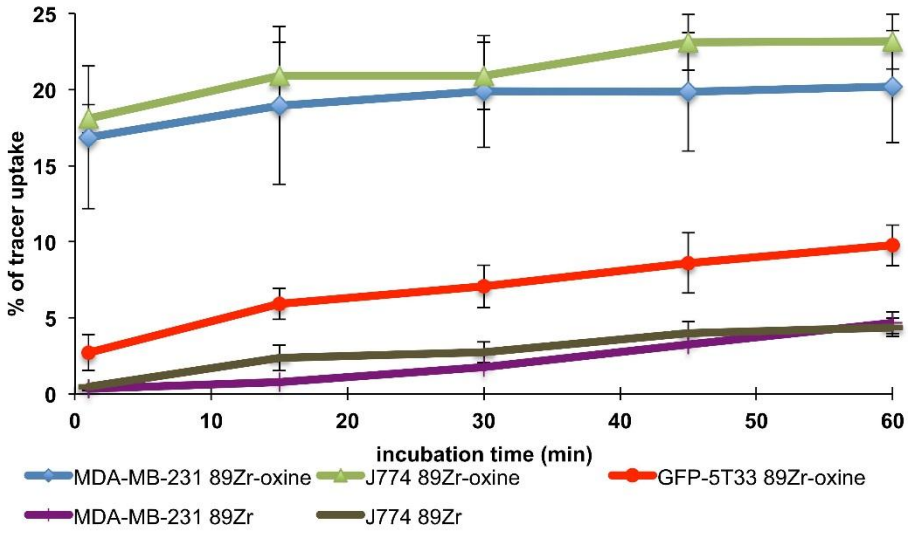

Fig. S1 Results of preliminary labelling experiments to investigate time course of uptake in cells. Cellular uptake in three cell lines of [^{89}Zr]-Zr(oxinate)$_4$ ("^{89}Zr-oxine") and neutralised [^{89}Zr]-Zr-oxalate ("^{89}Zr") (10^6 cells were incubated with 0.05 MBq of each tracer, in triplicate; mean ± SD)

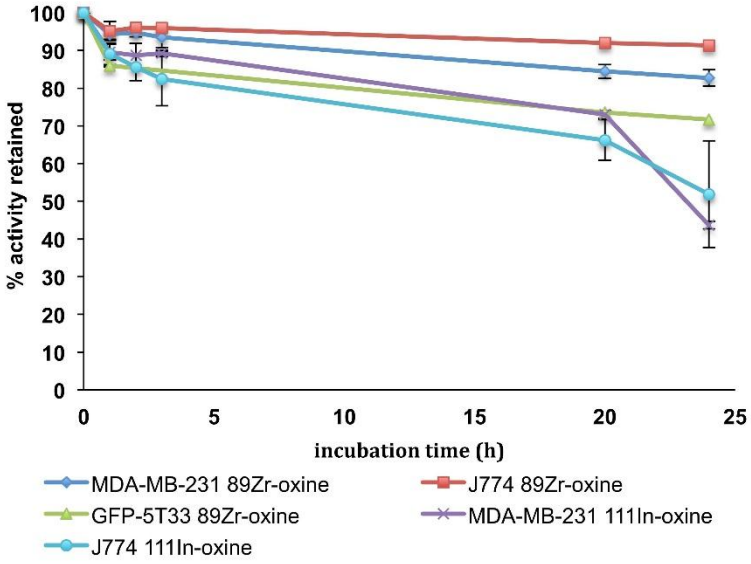

Fig. S2 Cellular retention *in vitro* of [^{89}Zr]-Zr(oxinate)$_4$ ("^{89}Zr-oxine") and [^{111}In]-In(oxinate)$_3$ ("^{111}In-oxine") (n=3/time point, mean ± SD, 100% refers to activity in washed cells at the end of the labelling process)

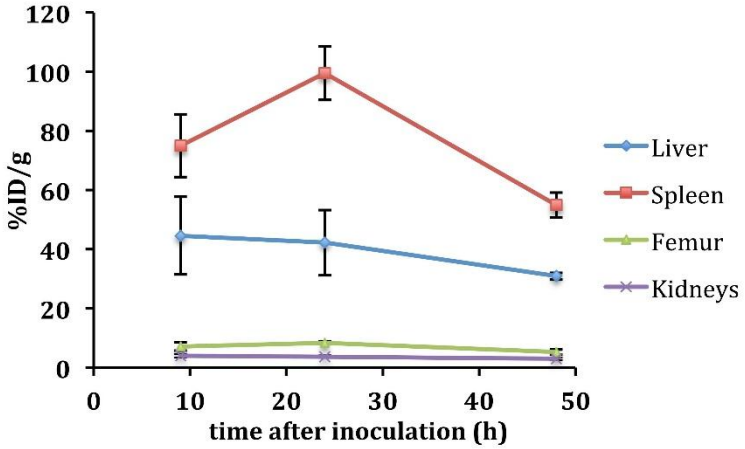

Fig. S3 Accumulation of [^{89}Zr]-Zr(oxinate)$_4$ labelled eGFP-5T33 cells in major sites of uptake in C57Bl/KaLwRij mice after i.v. inoculation (mean ± SD)

8

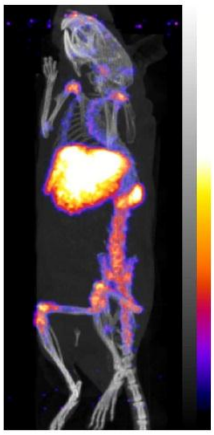

Fig. S4 PET/CT scan of ^{89}Zr 14 days after i.v. inoculation of a C57Bl/KaLwRij mouse with 10^7 eGFP-5T33 cells labelled with 5 MBq [^{89}Zr]-Zr(oxinate)$_4$

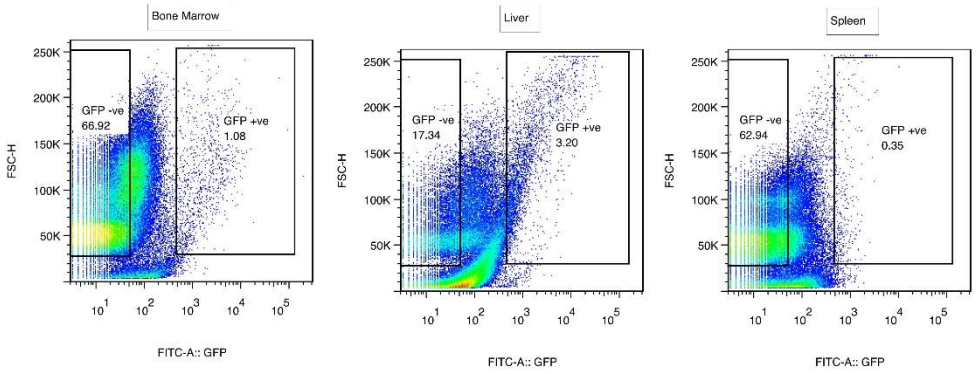

Fig. S5 Representative FACS plots (Forward scatter (FSC) *vs.* GFP signal) of bone marrow, liver and spleen homogenates obtained from a mouse inoculated with [^{89}Zr]-Zr(oxinate)$_4$ labelled eGFP-5T33 cells. eGFP-positive ("GFP +ve") and eGFP-negative ("GFP –ve") populations are marked; the same gate settings were used to process every sample. Note that eGFP-positive and eGFP-negative populations are very well separated to prevent cross-contamination during FACS sorting

References

1. Thakur ML, Lavender JP, Arnot RN, Silvester DJ, Segal AW. Indium-111-labeled autologous leukocytes in man. J Nucl Med. 1977 Oct;18(10):1014-21. PubMed PMID: 409745. Epub 1977/10/01.
2. Lukawska JJ, Livieratos L, Sawyer BM, Lee T, O'Doherty M, Blower PJ, et al. Real-time differential tracking of human neutrophil and eosinophil migration in vivo. J Allergy Clin Immunol. 2014 Jan;133(1):233-9 e1. PubMed PMID: 23953710. Epub 2013/08/21.
3. Frangioni JV, Hajjar RJ. In vivo tracking of stem cells for clinical trials in cardiovascular disease. Circulation. 2004 Nov 23;110(21):3378-83. PubMed PMID: 15557385. Epub 2004/11/24.
4. Sharif-Paghaleh E, Sunassee K, Tavare R, Ratnasothy K, Koers A, Ali N, et al. In vivo SPECT reporter gene imaging of regulatory T cells. PLoS One. 2011;6(10):e25857. PubMed PMID: 22043296. Pubmed Central PMCID: 3197183. Epub 2011/11/02.
5. Segal AW, Arnot RN, Thakur ML, Lavender JP. Indium-111-labelled leucocytes for localisation of abscesses. Lancet. 1976 Nov 13;2(7994):1056-8. PubMed PMID: 62903. Epub 1976/11/13. eng.
6. Intenzo CM, Desai AG, Thakur ML, Park CH. Comparison of leukocytes labeled with indium-111-2-mercaptopyridine-N-oxide and indium-111 oxine for abscess detection. J Nucl Med. 1987 Apr;28(4):438-41. PubMed PMID: 3106593. Epub 1987/04/01.
7. Puncher MR, Blower PJ. Frozen section microautoradiography in the study of radionuclide targeting: application to indium-111-oxine-labeled leukocytes. J Nucl Med. 1995 Mar;36(3):499-505. PubMed PMID: 7884517. Epub 1995/03/01.
8. Yoon JK, Park BN, Shim WY, Shin JY, Lee G, Ahn YH. In vivo tracking of 111In-labeled bone marrow mesenchymal stem cells in acute brain trauma model. Nucl Med Biol. 2010 Apr;37(3):381-8. PubMed PMID: 20346878. Epub 2010/03/30.
9. Kotze HF, Heyns AD, Lotter MG, Pieters H, Roodt JP, Sweetlove MA, et al. Comparison of oxine and tropolone methods for labeling human platelets with indium-111. J Nucl Med. 1991 Jan;32(1):62-6. PubMed PMID: 1899112. Epub 1991/01/01.
10. Thakur ML, McKenney SM. Indium 111-mercaptopyridine N-oxide-labeled human leukocytes and platelets: mechanism of labeling and intracellular location of 111In and mercaptopyridine N-oxide. J Lab Clin Med. 1986 Feb;107(2):141-7. PubMed PMID: 3944495. Epub 1986/02/01.
11. Thakur ML, McKenney SL, Park CH. Simplified and efficient labeling of human platelets in plasma using indium-111-2-mercaptopyridine-N-oxide: preparation and evaluation. J Nucl Med. 1985 May;26(5):510-7. PubMed PMID: 3989607. Epub 1985/05/01.
12. Ellis BL, Sampson CB, Abeysinghe RD, Porter JB, Hider RC. 6-Alkoxymethyl-3-hydroxy-4H-pyranones: potential ligands for cell-labelling with indium. Eur J Nucl Med. 1999 Nov;26(11):1400-6. PubMed PMID: 10552080. Epub 1999/11/07.
13. Ruparelia P, Szczepura KR, Summers C, Solanki CK, Balan K, Newbold P, et al. Quantification of neutrophil migration into the lungs of patients with chronic obstructive pulmonary disease. Eur J Nucl Med Mol Imaging. 2011 May;38(5):911-9. PubMed PMID: 21308374. Epub 2011/02/11.
14. Peters AM. The utility of [99mTc]HMPAO-leukocytes for imaging infection. Semin Nucl Med. 1994 Apr;24(2):110-27. PubMed PMID: 8023168. Epub 1994/04/01.
15. Acton PD, Kung HF. Small animal imaging with high resolution single photon emission tomography. Nucl Med Biol. 2003 Nov;30(8):889-95. PubMed PMID: 14698793. Epub 2003/12/31. eng.
16. Chatziioannou AF. Molecular imaging of small animals with dedicated PET tomographs. Eur J Nucl Med Mol Imaging. 2002 Jan;29(1):98-114. PubMed PMID: 11807613. Epub 2002/01/25. eng.

17. Lucignani G, Ottobrini L, Martelli C, Rescigno M, Clerici M. Molecular imaging of cell-mediated cancer immunotherapy. Trends Biotechnol. 2006 Sep;24(9):410-8. PubMed PMID: 16870284. Epub 2006/07/28. eng.
18. Bindslev L, Haack-Sorensen M, Bisgaard K, Kragh L, Mortensen S, Hesse B, et al. Labelling of human mesenchymal stem cells with indium-111 for SPECT imaging: effect on cell proliferation and differentiation. Eur J Nucl Med Mol Imaging. 2006 Oct;33(10):1171-7. PubMed PMID: 16763813. Epub 2006/06/10. eng.
19. Carter NJ, Eustance CN, Barrington SF, O'Doherty MJ, Coakley AJ. Imaging of abdominal infection using 99m Tc stannous fluoride colloid labelled leukocytes. Nucl Med Commun. 2002 Feb;23(2):153-60. PubMed PMID: 11891469. Epub 2002/03/14. eng.
20. Thakur ML, Segal AW, Louis L, Welch MJ, Hopkins J, Peters TJ. Indium-111-labeled cellular blood components: mechanism of labeling and intracellular location in human neutrophils. J Nucl Med. 1977 Oct;18(10):1022-6. PubMed PMID: 409746. Epub 1977/10/01. eng.
21. Ponto JA, Seabold JE. Time course of indium-111 oxine labelling of human leukocytes. Nucl Med Commun. 1984 Dec;5(12):769-73. PubMed PMID: 6442764. Epub 1984/12/01. eng.
22. McAfee JG. What is the best method for imaging focal infections? J Nucl Med. 1990 Apr;31(4):413-6. PubMed PMID: 2324818. Epub 1990/04/01. eng.
23. Ballinger JR, Gnanasegaran G. Radiolabelled leukocytes for imaging inflammation: how radiochemistry affects clinical use. Q J Nucl Med Mol Imaging. 2005 Dec;49(4):308-18. PubMed PMID: 16407814. Epub 2006/01/13. eng.
24. Aicher A, Brenner W, Zuhayra M, Badorff C, Massoudi S, Assmus B, et al. Assessment of the tissue distribution of transplanted human endothelial progenitor cells by radioactive labeling. Circulation. 2003 Apr 29;107(16):2134-9. PubMed PMID: 12695305. Epub 2003/04/16. eng.
25. Fisher B, Packard BS, Read EJ, Carrasquillo JA, Carter CS, Topalian SL, et al. Tumor localization of adoptively transferred indium-111 labeled tumor infiltrating lymphocytes in patients with metastatic melanoma. J Clin Oncol. 1989 Feb;7(2):250-61. PubMed PMID: 2644399. Epub 1989/02/01. eng.
26. Brenner W, Aicher A, Eckey T, Massoudi S, Zuhayra M, Koehl U, et al. 111In-labeled CD34+ hematopoietic progenitor cells in a rat myocardial infarction model. J Nucl Med. 2004 Mar;45(3):512-8. PubMed PMID: 15001696. Epub 2004/03/06. eng.
27. Danpure HJ, Osman S. Optimum conditions for radiolabelling human granulocytes and mixed leucocytes with 111In-tropolonate. Eur J Nucl Med. 1988;13(10):537-42. PubMed PMID: 3371376. Epub 1988/01/01. eng.
28. Thakur ML, McKenney SL, Park CH. Evaluation of Indium-111-2-Mercaptopyridine-N-Oxide for Labeling Leukocytes in Plasma: A Kit Preparation. Journal of Nuclear Medicine. 1985 May 1, 1985;26(5):518-23.
29. Becker W, Schomann E, Fischbach W, Borner W, Gruner KR. Comparison of 99Tcm-HMPAO and 111In-oxine labelled granulocytes in man: first clinical results. Nucl Med Commun. 1988 Jun;9(6):435-47. PubMed PMID: 3137513. Epub 1988/06/01. eng.
30. Hammersley PA, Nkohkwo AT. Studies on white blood cell labelling: (99)Tc(m)-HMPAO preferentially labels granulocytes. Nucl Med Commun. 2001 Sep;22(9):981-6. PubMed PMID: 11505207. Epub 2001/08/16. eng.
31. Chianelli M, Mather SJ, Martin-Comin J, Signore A. Radiopharmaceuticals for the study of inflammatory processes: a review. Nucl Med Commun. 1997 May;18(5):437-55. PubMed PMID: 9194086. Epub 1997/05/01.
32. Botti C, Negri DR, Seregni E, Ramakrishna V, Arienti F, Maffioli L, et al. Comparison of three different methods for radiolabelling human activated T lymphocytes. Eur J Nucl Med. 1997 May;24(5):497-504. PubMed PMID: 9142729. Epub 1997/05/01. eng.
33. Ridolfi R, Riccobon A, Galassi R, Giorgetti G, Petrini M, Fiammenghi L, et al. Evaluation of in vivo labelled dendritic cell migration in cancer patients. J Transl Med. 2004 Jul

30;2(1):27. PubMed PMID: 15285807. Pubmed Central PMCID: 509425. Epub 2004/08/03. Eng.
34. Tsopelas C. The radiopharmaceutical chemistry of 99mTc-tin fluoride colloid-labeled-leukocytes. Q J Nucl Med Mol Imaging. 2005 Dec;49(4):319-24. PubMed PMID: 16407815. Epub 2006/01/13. eng.
35. Puncher MR, Blower PJ. Labelling of leucocytes with colloidal technetium-99m-SnF2: an investigation of the labelling process by autoradiography. Eur J Nucl Med. 1995 Feb;22(2):101-7. PubMed PMID: 7758495. Epub 1995/02/01. eng.
36. Tsopelas C, Smith E, Drew PA, Bartholomeusz FDL. Preparation and biological evaluation of Tc-99m-stannous fluoride colloid-labelled-leucocytes in rats Tc-99m-stannous fluoride-labelled-leucocytes in rats. Journal of Labelled Compounds & Radiopharmaceuticals. 2003 Jul;46(8):751-63. PubMed PMID: ISI:000184229300006. English.
37. Lin Y, Weissleder R, Tung CH. Novel near-infrared cyanine fluorochromes: synthesis, properties, and bioconjugation. Bioconjug Chem. 2002 May-Jun;13(3):605-10. PubMed PMID: 12009952. Epub 2002/05/16. eng.
38. Berry DJ, Torres Martin de Rosales R, Charoenphun P, Blower PJ. Dithiocarbamate complexes as radiopharmaceuticals for medical imaging. Mini Rev Med Chem. 2012 Oct;12(12):1174-83. PubMed PMID: 22931590. Epub 2012/08/31. eng.
39. Sampson CB, Solanki C. Technetium-labelled leucocytes using diethyldithiocarbamate: preliminary report on in vitro studies. Nucl Med Commun. 1988 Feb;9(2):123-7. PubMed PMID: 2838773. Epub 1988/02/01. eng.
40. Demaimay F, Dazord L, Roucoux A, Noiret N, Patin H, Moisan A. Rhenium-188 and technetium-99m nitridobis(N-ethoxy-N-ethyldithiocarbamate) leucocyte labelling radiopharmaceuticals: [188ReN(NOET)2] and [99mTcN(NOET)2], NOET = Et(EtO)NCS2: their in vitro localization and chemical behaviour. Nucl Med Biol. 1997 Nov;24(8):701-5. PubMed PMID: 9428593. Epub 1998/01/15. eng.
41. Demaimay F, Noiret N, Roucoux A, Patin H, Bellande E, Pasqualini R, et al. New bis(dithiocarboxylato) nitridotechnetium-99m radiopharmaceuticals for leucocyte labelling: in vitro and in vivo studies. Nucl Med Biol. 1997 Jul;24(5):439-45. PubMed PMID: 9290080. Epub 1997/07/01. eng.
42. Taylor A, Wilson KM, Murray P, Fernig DG, Levy R. Long-term tracking of cells using inorganic nanoparticles as contrast agents: are we there yet? Chem Soc Rev. 2012 Apr 7;41(7):2707-17. PubMed PMID: 22362426. Epub 2012/03/01.
43. Berman SC, Galpoththawela C, Gilad AA, Bulte JW, Walczak P. Long-term MR cell tracking of neural stem cells grafted in immunocompetent versus immunodeficient mice reveals distinct differences in contrast between live and dead cells. Magn Reson Med. 2011 Feb;65(2):564-74. PubMed PMID: 20928883. Pubmed Central PMCID: 3031985. Epub 2010/10/12.
44. Fenchel M, Kramer U, Nael K, Miller S. Cardiac magnetic resonance imaging at 3.0 T. Top Magn Reson Imaging. 2007 Apr;18(2):95-104. PubMed PMID: 17621223. Epub 2007/07/11. eng.
45. Beckmann N, Cannet C, Fringeli-Tanner M, Baumann D, Pally C, Bruns C, et al. Macrophage labeling by SPIO as an early marker of allograft chronic rejection in a rat model of kidney transplantation. Magn Reson Med. 2003 Mar;49(3):459-67. PubMed PMID: 12594748. Epub 2003/02/21. eng.
46. Callera F, de Melo CM. Magnetic resonance tracking of magnetically labeled autologous bone marrow CD34+ cells transplanted into the spinal cord via lumbar puncture technique in patients with chronic spinal cord injury: CD34+ cells' migration into the injured site. Stem Cells Dev. 2007 Jun;16(3):461-6. PubMed PMID: 17610376. Epub 2007/07/06. eng.
47. Huang H, Shen L, Ford J, Gao L, Pearlman J. Early lung cancer detection based on registered perfusion MRI. Oncol Rep. 2006;15 Spec no.:1081-4. PubMed PMID: 16525705. Epub 2006/03/10. eng.

48. Jacobs RE, Fraser SE. Magnetic-Resonance Microscopy of Embryonic-Cell Lineages and Movements. Science. 1994 Feb 4;263(5147):681-4. PubMed PMID: ISI:A1994MU96400049. English.
49. Terreno E, Geninatti Crich S, Belfiore S, Biancone L, Cabella C, Esposito G, et al. Effect of the intracellular localization of a Gd-based imaging probe on the relaxation enhancement of water protons. Magn Reson Med. 2006 Mar;55(3):491-7. PubMed PMID: 16450336. Epub 2006/02/02. eng.
50. Crich SG, Biancone L, Cantaluppi V, Duo D, Esposito G, Russo S, et al. Improved route for the visualization of stem cells labeled with a Gd-/Eu-chelate as dual (MRI and fluorescence) agent. Magn Reson Med. 2004 May;51(5):938-44. PubMed PMID: 15122675. Epub 2004/05/04. eng.
51. Suzuki Y, Zhang S, Kundu P, Yeung AC, Robbins RC, Yang PC. In vitro comparison of the biological effects of three transfection methods for magnetically labeling mouse embryonic stem cells with ferumoxides. Magn Reson Med. 2007 Jun;57(6):1173-9. PubMed PMID: 17534917. Epub 2007/05/31. eng.
52. Anderson SA, Lee KK, Frank JA. Gadolinium-fullerenol as a paramagnetic contrast agent for cellular imaging. Invest Radiol. 2006 Mar;41(3):332-8. PubMed PMID: 16481917. Epub 2006/02/17. eng.
53. Thorek DLJ, Chen A, Czupryna J, Tsourkas A. Superparamagnetic iron oxide nanoparticle probes for molecular imaging. Annals of Biomedical Engineering. 2006 Jan;34(1):23-38. PubMed PMID: ISI:000236354800004. English.
54. Wilhelm C, Gazeau F. Universal cell labelling with anionic magnetic nanoparticles. Biomaterials. 2008 Aug;29(22):3161-74. PubMed PMID: ISI:000257012700001. English.
55. Fleige G, Seeberger F, Laux D, Kresse M, Taupitz M, Pilgrimm H, et al. In vitro characterization of two different ultrasmall iron oxide particles for magnetic resonance cell tracking. Invest Radiol. 2002 Sep;37(9):482-8. PubMed PMID: 12218443. Epub 2002/09/10. eng.
56. Ho C, Hitchens TK. A non-invasive approach to detecting organ rejection by MRI: monitoring the accumulation of immune cells at the transplanted organ. Curr Pharm Biotechnol. 2004 Dec;5(6):551-66. PubMed PMID: 15579044. Epub 2004/12/08. eng.
57. Sipe JC, Filippi M, Martino G, Furlan R, Rocca MA, Rovaris M, et al. Method for intracellular magnetic labeling of human mononuclear cells using approved iron contrast agents. Magn Reson Imaging. 1999 Dec;17(10):1521-3. PubMed PMID: 10610001. Epub 1999/12/28. eng.
58. Billotey C, Wilhelm C, Devaud M, Bacri JC, Bittoun J, Gazeau F. Cell internalization of anionic maghemite nanoparticles: quantitative effect on magnetic resonance imaging. Magn Reson Med. 2003 Apr;49(4):646-54. PubMed PMID: 12652535. Epub 2003/03/26. eng.
59. Weissleder R, Cheng HC, Bogdanova A, Bogdanov A. Magnetically labeled cells can be detected by MR imaging. Jmri-Journal of Magnetic Resonance Imaging. 1997 Jan-Feb;7(1):258-63. PubMed PMID: ISI:A1997WG33100039. English.
60. Jendelova P, Herynek V, Urdzikova L, Glogarova K, Kroupova J, Andersson B, et al. Magnetic resonance tracking of transplanted bone marrow and embryonic stem cells labeled by iron oxide nanoparticles in rat brain and spinal cord. J Neurosci Res. 2004 Apr 15;76(2):232-43. PubMed PMID: 15048921. Epub 2004/03/30. eng.
61. Berger C, Rausch M, Schmidt P, Rudin M. Feasibility and limits of magnetically labeling primary cultured rat T cells with ferumoxides coupled with commonly used transfection agents. Mol Imaging. 2006 Apr-Jun;5(2):93-104. PubMed PMID: 16954023. Epub 2006/09/07. eng.
62. Walczak P, Kedziorek DA, Gilad AA, Lin S, Bulte JW. Instant MR labeling of stem cells using magnetoelectroporation. Magn Reson Med. 2005 Oct;54(4):769-74. PubMed PMID: 16161115. Epub 2005/09/15. eng.

63. Weissleder R, Lee AS, Fischman AJ, Reimer P, Shen T, Wilkinson R, et al. Polyclonal Human Immunoglobulin-G Labeled with Polymeric Iron-Oxide - Antibody Mr Imaging. Radiology. 1991 Oct;181(1):245-9. PubMed PMID: ISI:A1991GF73600048. English.
64. Weissleder R, Lee AS, Khaw BA, Shen T, Brady TJ. Antimyosin-Labeled Monocrystalline Iron-Oxide Allows Detection of Myocardial Infarct - Mr Antibody Imaging. Radiology. 1992 Feb;182(2):381-5. PubMed PMID: ISI:A1992HA58600018. English.
65. Genove G, DeMarco U, Xu H, Goins WF, Ahrens ET. A new transgene reporter for in vivo magnetic resonance imaging. Nat Med. 2005 Apr;11(4):450-4. PubMed PMID: 15778721. Epub 2005/03/22. eng.
66. Cohen B, Ziv K, Plaks V, Israely T, Kalchenko V, Harmelin A, et al. MRI detection of transcriptional regulation of gene expression in transgenic mice. Nat Med. 2007 Apr;13(4):498-503. PubMed PMID: 17351627. Epub 2007/03/14. eng.
67. Zurkiya O, Chan AW, Hu X. MagA is sufficient for producing magnetic nanoparticles in mammalian cells, making it an MRI reporter. Magn Reson Med. 2008 Jun;59(6):1225-31. PubMed PMID: 18506784. Epub 2008/05/29. eng.
68. Islam T, Harisinghani MG. Overview of nanoparticle use in cancer imaging. Cancer Biomarkers. 2009;5(2):61-7. PubMed PMID: ISI:000265829400002. English.
69. Bulte JW, Ben-Hur T, Miller BR, Mizrachi-Kol R, Einstein O, Reinhartz E, et al. MR microscopy of magnetically labeled neurospheres transplanted into the Lewis EAE rat brain. Magn Reson Med. 2003 Jul;50(1):201-5. PubMed PMID: 12815696. Epub 2003/06/20. eng.
70. Spibey CA, Jackson P, Herick K. A unique charge-coupled device/xenon arc lamp based imaging system for the accurate detection and quantitation of multicolour fluorescence. Electrophoresis. 2001 Mar;22(5):829-36. PubMed PMID: 11332749. Epub 2001/05/03. eng.
71. Wang X, Rosol M, Ge S, Peterson D, McNamara G, Pollack H, et al. Dynamic tracking of human hematopoietic stem cell engraftment using in vivo bioluminescence imaging. Blood. 2003 Nov 15;102(10):3478-82. PubMed PMID: 12946998. Epub 2003/08/30. eng.
72. Bhaumik S, Gambhir SS. Optical imaging of Renilla luciferase reporter gene expression in living mice. Proc Natl Acad Sci U S A. 2002 Jan 8;99(1):377-82. PubMed PMID: 11752410. Pubmed Central PMCID: 117568. Epub 2001/12/26. eng.
73. Tang Y, Shah K, Messerli SM, Snyder E, Breakefield X, Weissleder R. In vivo tracking of neural progenitor cell migration to glioblastomas. Hum Gene Ther. 2003 Sep 1;14(13):1247-54. PubMed PMID: 12952596. Epub 2003/09/04. eng.
74. Licha K, Olbrich C. Optical imaging in drug discovery and diagnostic applications. Adv Drug Deliv Rev. 2005 Jun 15;57(8):1087-108. PubMed PMID: 15908041. Epub 2005/05/24. eng.
75. Xiong T, Zhang Z, Liu BF, Zeng S, Chen Y, Chu J, et al. In vivo optical imaging of human adenoid cystic carcinoma cell metastasis. Oral Oncol. 2005 Aug;41(7):709-15. PubMed PMID: 15935724. Epub 2005/06/07. eng.
76. Sutton EJ, Henning TD, Pichler BJ, Bremer C, Daldrup-Link HE. Cell tracking with optical imaging. Eur Radiol. 2008 Oct;18(10):2021-32. PubMed PMID: 18506449. Epub 2008/05/29.
77. Ahrens ET, Flores R, Xu H, Morel PA. In vivo imaging platform for tracking immunotherapeutic cells. Nat Biotechnol. 2005 Aug;23(8):983-7. PubMed PMID: 16041364. Epub 2005/07/26. eng.
78. Serganova I, Moroz E, Moroz M, Pillarsetty N, Blasberg R. Non-invasive molecular imaging and reporter genes. Central European Journal of Biology. 2006 Mar;1(1):88-123. PubMed PMID: ISI:000246919400008. English.
79. Weissleder R, Ntziachristos V. Shedding light onto live molecular targets. Nature Medicine. 2003 Jan;9(1):123-8. PubMed PMID: ISI:000208640400007. English.
80. Jaiswal JK, Mattoussi H, Mauro JM, Simon SM. Long-term multiple color imaging of live cells using quantum dot bioconjugates. Nat Biotechnol. 2003 Jan;21(1):47-51. PubMed PMID: 12459736. Epub 2002/12/03. eng.

81. Ottobrini L, Martelli C, Trabattoni DL, Clerici M, Lucignani G. In vivo imaging of immune cell trafficking in cancer. Eur J Nucl Med Mol Imaging. 2011 May;38(5):949-68. PubMed PMID: 21170525. Epub 2010/12/21.
82. Puncher MR, Blower PJ. Autoradiography and density gradient separation of technetium-99m-exametazime (HMPAO) labelled leucocytes reveals selectivity for eosinophils. Eur J Nucl Med. 1994 Nov;21(11):1175-82. PubMed PMID: 7859768. Epub 1994/11/01.
83. Tavare R, Sagoo P, Varama G, Tanriver Y, Warely A, Diebold SS, et al. Monitoring of in vivo function of superparamagnetic iron oxide labelled murine dendritic cells during anti-tumour vaccination. PLoS One. 2011;6(5):e19662. PubMed PMID: 21637760. Pubmed Central PMCID: 3103517. Epub 2011/06/04.
84. Leech JM, Sharif-Paghaleh E, Maher J, Livieratos L, Lechler RI, Mullen GE, et al. Whole-body imaging of adoptively transferred T cells using magnetic resonance imaging, single photon emission computed tomography and positron emission tomography techniques, with a focus on regulatory T cells. Clin Exp Immunol. 2013 May;172(2):169-77. PubMed PMID: 23574314. Pubmed Central PMCID: 3628320. Epub 2013/04/12.
85. Zanzonico P, Koehne G, Gallardo HF, Doubrovin M, Doubrovina E, Finn R, et al. [131I]FIAU labeling of genetically transduced, tumor-reactive lymphocytes: cell-level dosimetry and dose-dependent toxicity. Eur J Nucl Med Mol Imaging. 2006 Sep;33(9):988-97. PubMed PMID: 16607546. Epub 2006/04/12.
86. Ak I, Stokkel MP, Pauwels EK. Positron emission tomography with 2-[18F]fluoro-2-deoxy-D-glucose in oncology. Part II. The clinical value in detecting and staging primary tumours. J Cancer Res Clin Oncol. 2000 Oct;126(10):560-74. PubMed PMID: 11043393. Epub 2000/10/24. eng.
87. Rudd JH, Warburton EA, Fryer TD, Jones HA, Clark JC, Antoun N, et al. Imaging atherosclerotic plaque inflammation with [18F]-fluorodeoxyglucose positron emission tomography. Circulation. 2002 Jun 11;105(23):2708-11. PubMed PMID: 12057982. Epub 2002/06/12. eng.
88. Osman S, Danpure HJ. The use of 2-[18F]fluoro-2-deoxy-D-glucose as a potential in vitro agent for labelling human granulocytes for clinical studies by positron emission tomography. Int J Rad Appl Instrum B. 1992 Feb;19(2):183-90. PubMed PMID: 1601671. Epub 1992/02/01. eng.
89. Forstrom LA, Mullan BP, Hung JC, Lowe VJ, Thorson LM. 18F-FDG labelling of human leukocytes. Nucl Med Commun. 2000 Jul;21(7):691-4. PubMed PMID: 10994674. Epub 2000/09/20.
90. Rini JN, Bhargava KK, Tronco GG, Singer C, Caprioli R, Marwin SE, et al. PET with FDG-labeled leukocytes versus scintigraphy with 111In-oxine-labeled leukocytes for detection of infection. Radiology. 2006 Mar;238(3):978-87. PubMed PMID: 16505395. Epub 2006/03/01. eng.
91. Dumarey N, Egrise D, Blocklet D, Stallenberg B, Remmelink M, del Marmol V, et al. Imaging infection with 18F-FDG-labeled leukocyte PET/CT: initial experience in 21 patients. J Nucl Med. 2006 Apr;47(4):625-32. PubMed PMID: 16595496. Epub 2006/04/06. eng.
92. Bhargava KK, Gupta RK, Nichols KJ, Palestro CJ. In vitro human leukocyte labeling with (64)Cu: an intraindividual comparison with (111)In-oxine and (18)F-FDG. Nucl Med Biol. 2009 Jul;36(5):545-9. PubMed PMID: 19520295. Pubmed Central PMCID: 2695937. Epub 2009/06/13.
93. Prince HM, Wall DM, Ritchie D, Honemann D, Harrrison S, Quach H, et al. In Vivo Tracking of Dendritic Cells in Patients With Multiple Myeloma. Journal of Immunotherapy. 2008;31(2):166-79 10.1097/CJI.0b013e31815c5153.
94. Hofmann M, Wollert KC, Meyer GP, Menke A, Arseniev L, Hertenstein B, et al. Monitoring of bone marrow cell homing into the infarcted human myocardium. Circulation. 2005 May 3;111(17):2198-202. PubMed PMID: 15851598. Epub 2005/04/27. eng.

95. Doyle B, Kemp BJ, Chareonthaitawee P, Reed C, Schmeckpeper J, Sorajja P, et al. Dynamic tracking during intracoronary injection of 18F-FDG-labeled progenitor cell therapy for acute myocardial infarction. J Nucl Med. 2007 Oct;48(10):1708-14. PubMed PMID: 17909258. Epub 2007/10/03. eng.
96. Stojanov K, de Vries EF, Hoekstra D, van Waarde A, Dierckx RA, Zuhorn IS. [18F]FDG labeling of neural stem cells for in vivo cell tracking with positron emission tomography: inhibition of tracer release by phloretin. Mol Imaging. 2012 Feb;11(1):1-12. PubMed PMID: 22418021. Epub 2012/03/16.
97. Welch MJ, Thakur ML, Coleman RE, Patel M, Siegel BA, Ter-Pogossian M. Gallium-68 labeled red cells and platelets: new agents for positron tomography. J Nucl Med. 1977 Jun;18(6):558-62. PubMed PMID: 404404. Epub 1977/06/01.
98. Yano Y, Budinger TF, Ebbe SN, Mathis CA, Singh M, Brennan KM, et al. Gallium-68 Lipophilic Complexes for Labeling Platelets. Journal of Nuclear Medicine. 1985 December 1, 1985;26(12):1429-37.
99. Goodwin DA, Lang EV, Atwood JE, Dalman RL, Ransone CM, Diamanti CI, et al. Viability and biodistribution of 68Ga MPO-labelled human platelets. Nuclear medicine communications. 1993;14(11):1023-9.
100. Anderson CJ, Pajeau TS, Edwards WB, Sherman EL, Rogers BE, Welch MJ. In vitro and in vivo evaluation of copper-64-octreotide conjugates. J Nucl Med. 1995 Dec;36(12):2315-25. PubMed PMID: 8523125. Epub 1995/12/01. eng.
101. Adonai N, Nguyen KN, Walsh J, Iyer M, Toyokuni T, Phelps ME, et al. Ex vivo cell labeling with 64Cu-pyruvaldehyde-bis(N4-methylthiosemicarbazone) for imaging cell trafficking in mice with positron-emission tomography. Proc Natl Acad Sci U S A. 2002 Mar 5;99(5):3030-5. PubMed PMID: 11867752. Pubmed Central PMCID: 122467. Epub 2002/02/28.
102. Huang J, Lee CC, Sutcliffe JL, Cherry SR, Tarantal AF. Radiolabeling rhesus monkey CD34+ hematopoietic and mesenchymal stem cells with 64Cu-pyruvaldehyde-bis(N4-methylthiosemicarbazone) for microPET imaging. Mol Imaging. 2008 Jan-Feb;7(1):1-11. PubMed PMID: 18384718. Epub 2008/04/04.
103. Park JJ, Lee TS, Son JJ, Chun KS, Song IH, Park YS, et al. Comparison of cell-labeling methods with (1)(2)(4)I-FIAU and (6)(4)Cu-PTSM for cell tracking using chronic myelogenous leukemia cells expressing HSV1-tk and firefly luciferase. Cancer Biother Radiopharm. 2012 Dec;27(10):719-28. PubMed PMID: 23009582. Pubmed Central PMCID: 3516418. Epub 2012/09/27.
104. Li ZB, Chen K, Wu Z, Wang H, Niu G, Chen X. 64Cu-labeled PEGylated polyethylenimine for cell trafficking and tumor imaging. Mol Imaging Biol. 2009 Nov-Dec;11(6):415-23. PubMed PMID: 19430846. Epub 2009/05/12.
105. Blower PJ, Lewis JS, Zweit J. Copper radionuclides and radiopharmaceuticals in nuclear medicine. Nucl Med Biol. 1996 Nov;23(8):957-80. PubMed PMID: 9004284. Epub 1996/11/01. eng.
106. Griessinger CM, Kehlbach R, Bukala D, Wiehr S, Bantleon R, Cay F, et al. In Vivo Tracking of Th1 Cells by PET Reveals Quantitative and Temporal Distribution and Specific Homing in Lymphatic Tissue. Journal of Nuclear Medicine. 2014 February 1, 2014;55(2):301-7.
107. Dearling J, Lewis J, Mullen G, Welch M, Blower P. Copper bis(thiosemicarbazone) complexes as hypoxia imaging agents: structure-activity relationships. JBIC Journal of Biological Inorganic Chemistry. 2002 2002/03/01;7(3):249-59. English.
108. Mcpherson DW, Umbricht G, Knapp FF. Radiolabeling of Proteins with Radioisotopes of Copper Using Para-Carboxyalkylphenylglyoxal Bis-(N-4-Methylthiosemicarbazone) (Tsc) Bifunctional Chelates. Journal of Labelled Compounds & Radiopharmaceuticals. 1990 Aug;28(8):877-99. PubMed PMID: ISI:A1990DT03900002. English.
109. Dearling JL, Lewis JS, Mullen GE, Rae MT, Zweit J, Blower PJ. Design of hypoxia-targeting radiopharmaceuticals: selective uptake of copper-64 complexes in hypoxic cells in vitro. Eur J Nucl Med. 1998 Jul;25(7):788-92. PubMed PMID: 9662602. Epub 1998/07/15. eng.

110. Lewis JS, McCarthy DW, McCarthy TJ, Fujibayashi Y, Welch MJ. Evaluation of 64Cu-ATSM in vitro and in vivo in a hypoxic tumor model. J Nucl Med. 1999 Jan;40(1):177-83. PubMed PMID: 9935074. Epub 1999/02/06. eng.
111. Lewis J, Laforest R, Buettner T, Song S, Fujibayashi Y, Connett J, et al. Copper-64-diacetyl-bis(N4-methylthiosemicarbazone): An agent for radiotherapy. Proc Natl Acad Sci U S A. 2001 Jan 30;98(3):1206-11. PubMed PMID: 11158618. Pubmed Central PMCID: 14733. Epub 2001/02/07. eng.
112. Dehdashti F, Grigsby PW, Lewis JS, Laforest R, Siegel BA, Welch MJ. Assessing tumor hypoxia in cervical cancer by PET with 60Cu-labeled diacetyl-bis(N4-methylthiosemicarbazone). J Nucl Med. 2008 Feb;49(2):201-5. PubMed PMID: 18199612. Epub 2008/01/18. eng.
113. Acton PD, Zhou R. Imaging reporter genes for cell tracking with PET and SPECT. Q J Nucl Med Mol Imaging. 2005 Dec;49(4):349-60. PubMed PMID: 16407818. Epub 2006/01/13. eng.
114. Ogawa O, Umegaki H, Ishiwata K, Asai Y, Ikari H, Oda K, et al. In vivo imaging of adenovirus-mediated over-expression of dopamine D2 receptors in rat striatum by positron emission tomography. Neuroreport. 2000 Mar 20;11(4):743-8. PubMed PMID: 10757512. Epub 2000/04/11. eng.
115. Liang Q, Satyamurthy N, Barrio JR, Toyokuni T, Phelps MP, Gambhir SS, et al. Noninvasive, quantitative imaging in living animals of a mutant dopamine D2 receptor reporter gene in which ligand binding is uncoupled from signal transduction. Gene Ther. 2001 Oct;8(19):1490-8. PubMed PMID: 11593362. Epub 2001/10/11. eng.
116. Rogers BE, McLean SF, Kirkman RL, Della Manna D, Bright SJ, Olsen CC, et al. In vivo localization of [(111)In]-DTPA-D-Phe1-octreotide to human ovarian tumor xenografts induced to express the somatostatin receptor subtype 2 using an adenoviral vector. Clin Cancer Res. 1999 Feb;5(2):383-93. PubMed PMID: 10037188. Epub 1999/02/26. eng.
117. Koehne G, Doubrovin M, Doubrovina E, Zanzonico P, Gallardo HF, Ivanova A, et al. Serial in vivo imaging of the targeted migration of human HSV-TK-transduced antigen-specific lymphocytes. Nat Biotechnol. 2003 Apr;21(4):405-13. PubMed PMID: 12652311. Epub 2003/03/26. eng.
118. Yaghoubi SS, Jensen MC, Satyamurthy N, Budhiraja S, Paik D, Czernin J, et al. Noninvasive detection of therapeutic cytolytic T cells with 18F-FHBG PET in a patient with glioma. Nat Clin Pract Oncol. 2009 Jan;6(1):53-8. PubMed PMID: 19015650. Pubmed Central PMCID: 3526373. Epub 2008/11/19. eng.
119. Su H, Forbes A, Gambhir SS, Braun J. Quantitation of cell number by a positron emission tomography reporter gene strategy. Mol Imaging Biol. 2004 May-Jun;6(3):139-48. PubMed PMID: 15193248. Epub 2004/06/15. eng.
120. Dingli D, Russell SJ, Morris JC, 3rd. In vivo imaging and tumor therapy with the sodium iodide symporter. J Cell Biochem. 2003 Dec 15;90(6):1079-86. PubMed PMID: 14635183. Epub 2003/11/25. eng.
121. Van Sande J, Massart C, Beauwens R, Schoutens A, Costagliola S, Dumont JE, et al. Anion selectivity by the sodium iodide symporter. Endocrinology. 2003 Jan;144(1):247-52. PubMed PMID: 12488351. Epub 2002/12/19. eng.
122. Dingli D, Kemp BJ, O'Connor MK, Morris JC, Russell SJ, Lowe VJ. Combined I-124 positron emission tomography/computed tomography imaging of NIS gene expression in animal models of stably transfected and intravenously transfected tumor. Mol Imaging Biol. 2006 Jan-Feb;8(1):16-23. PubMed PMID: 16328647. Epub 2005/12/06. eng.
123. Terrovitis J, Kwok KF, Lautamaki R, Engles JM, Barth AS, Kizana E, et al. Ectopic expression of the sodium-iodide symporter enables imaging of transplanted cardiac stem cells in vivo by single-photon emission computed tomography or positron emission tomography. J Am Coll Cardiol. 2008 Nov 11;52(20):1652-60. PubMed PMID: 18992656. Epub 2008/11/11. eng.

124. Eskandari S, Loo DD, Dai G, Levy O, Wright EM, Carrasco N. Thyroid Na+/I- symporter. Mechanism, stoichiometry, and specificity. J Biol Chem. 1997 Oct 24;272(43):27230-8. PubMed PMID: 9341168. Epub 1997/10/27. eng.
125. Jauregui-Osoro M, Sunassee K, Weeks AJ, Berry DJ, Paul RL, Cleij M, et al. Synthesis and biological evaluation of [(18)F]tetrafluoroborate: a PET imaging agent for thyroid disease and reporter gene imaging of the sodium/iodide symporter. European Journal of Nuclear Medicine and Molecular Imaging. 2010 Nov;37(11):2108-16. PubMed PMID: 20577737. Pubmed Central PMCID: 2948172. Epub 2010/06/26. eng.
126. Cao F, Lin S, Xie X, Ray P, Patel M, Zhang X, et al. In vivo visualization of embryonic stem cell survival, proliferation, and migration after cardiac delivery. Circulation. 2006 Feb 21;113(7):1005-14. PubMed PMID: 16476845. Epub 2006/02/16. eng.
127. McArdle HJ. The transport of iron and copper across the cell membrane: different mechanisms for different metals? Proc Nutr Soc. 1992 Aug;51(2):199-209. PubMed PMID: 1438328. Epub 1992/08/01. eng.
128. McCarthy DW, Shefer RE, Klinkowstein RE, Bass LA, Margeneau WH, Cutler CS, et al. Efficient production of high specific activity 64Cu using a biomedical cyclotron. Nucl Med Biol. 1997 Jan;24(1):35-43. PubMed PMID: 9080473. Epub 1997/01/01. eng.
129. Wadas TJ, Wong EH, Weisman GR, Anderson CJ. Copper chelation chemistry and its role in copper radiopharmaceuticals. Curr Pharm Des. 2007;13(1):3-16. PubMed PMID: 17266585. Epub 2007/02/03. eng.
130. Moi MK, Meares CF, Mccall MJ, Cole WC, Denardo SJ. Copper-Chelates as Probes of Biological-Systems - Stable Copper-Complexes with a Macrocyclic Bifunctional Chelating Agent. Analytical Biochemistry. 1985;148(1):249-53. PubMed PMID: ISI:A1985ALX8200034. English.
131. Anderson CJ, Dehdashti F, Cutler PD, Schwarz SW, Laforest R, Bass LA, et al. 64Cu-TETA-octreotide as a PET imaging agent for patients with neuroendocrine tumors. J Nucl Med. 2001 Feb;42(2):213-21. PubMed PMID: 11216519. Epub 2001/02/24. eng.
132. Paul RL, Halsted P, Ballinger J, Marsden PK, O'Doherty MJ, Blower PJ, et al. Production of 64Cu on the CTI RDS 112 11 MeV cyclotron and synthesis and biological evaluation of 64CuATSM second generation analogues. European Journal of Nuclear Medicine and Molecular Imaging. 2006 2006/09/01;33(2):S174. English.
133. Gingras BA, Suprunchuk T, Bayley CH. THE PREPARATION OF SOME THIOSEMICARBAZONES AND THEIR COPPER COMPLEXES: PART III. Canadian Journal of Chemistry. 1962 1962/06/01;40(6):1053-9.
134. Verel I, Visser GWM, Boellaard R, Stigter-van Walsum M, Snow GB, van Dongen GAMS. 89Zr Immuno-PET: Comprehensive Procedures for the Production of 89Zr-Labeled Monoclonal Antibodies. Journal of Nuclear Medicine. 2003 August 1, 2003;44(8):1271-81.
135. Dijkers ECF, Kosterink JGW, Rademaker AP, Perk LR, van Dongen GAMS, Bart J, et al. Development and Characterization of Clinical-Grade 89Zr-Trastuzumab for HER2/neu ImmunoPET Imaging. Journal of Nuclear Medicine. 2009 June 1, 2009;50(6):974-81.
136. Nayak TK, Garmestani K, Milenic DE, Brechbiel MW. PET and MRI of Metastatic Peritoneal and Pulmonary Colorectal Cancer in Mice with Human Epidermal Growth Factor Receptor 1–Targeted 89Zr-Labeled Panitumumab. Journal of Nuclear Medicine. 2012 January 1, 2012;53(1):113-20.
137. Holland JP, Divilov V, Bander NH, Smith-Jones PM, Larson SM, Lewis JS. 89Zr-DFO-J591 for immunoPET of prostate-specific membrane antigen expression in vivo. J Nucl Med. 2010 Aug;51(8):1293-300. PubMed PMID: 20660376. Pubmed Central PMCID: 2998794. Epub 2010/07/28.
138. Saha GB, Porile NT, Yaffe L. (p, xn) and (p, pxn) Reactions of Yttrium-89 with 5-85-MeV Protons. Physical Review. 1966 04/22/;144(3):962-71.
139. Zweit J, Downey S, Sharma HL. Production of no-carrier-added zirconium-89 for positron emission tomography. International Journal of Radiation Applications and Instrumentation Part A Applied Radiation and Isotopes. 1991 //;42(2):199-201.

140. Meijs WE, Herscheid JDM, Haisma HJ, Wijbrandts R, van Langevelde F, Van Leuffen PJ, et al. Production of highly pure no-carrier added 89Zr for the labelling of antibodies with a positron emitter. Applied Radiation and Isotopes. 1994 12//;45(12):1143-7.
141. Kathirgamanathan P, Surendrakumar S, Antipan-Lara J, Ravichandran S, Reddy VR, Ganeshamurugan S, et al. Discovery of two new phases of zirconium tetrakis(8-hydroxyquinolinolate): synthesis, crystal structure and their electron transporting characteristics in organic light emitting diodes (OLEDs). Journal of Materials Chemistry. 2011;21(6):1762-71.
142. Muetterties EL, Wright CM. Chelate Chemistry. III. Chelates of High Coordination Number. Journal of the American Chemical Society. 1965 1965/11/01;87(21):4706-17.
143. Guerard F, Lee YS, Tripier R, Szajek LP, Deschamps JR, Brechbiel MW. Investigation of Zr(IV) and 89Zr(IV) complexation with hydroxamates: progress towards designing a better chelator than desferrioxamine B for immuno-PET imaging. Chem Commun (Camb). 2013 Feb 1;49(10):1002-4. PubMed PMID: 23250287. Pubmed Central PMCID: 3538910. Epub 2012/12/20.
144. Lee WS, Kim HJ, Lee EM, Kim JH, Suh SK, Kwon KJ, et al. Genetic toxicity test of 8-hydroxyquinoline by Ames Micronucleus comet assays and microarray analysis. Mol Cell Toxicol2007. p. 8.
145. Ellis BL, Sharma HL. Co, Fe and Ga chelates for cell labelling: a potential use in PET imaging? Nucl Med Commun. 1999 Nov;20(11):1017-21. PubMed PMID: 10572911. Epub 1999/11/26. eng.
146. Thakur ML, Edward Coleman R, Glen Mayhall C, Welch MJ. Preparation and Evaluation of 111In-Labeled Leukocytes as an Abscess Imaging Agent in Dogs. Radiology. 1976;119(3):731-2. PubMed PMID: 935418.
147. Ballinger JR, Boxen I. Gallium-67-labelled red blood cells as a blood-pool marker for dual-isotope imaging. Int J Rad Appl Instrum B. 1992 Jan;19(1):79-81. PubMed PMID: 1577616. Epub 1992/01/01. eng.
148. Yu J, Häfeli UO, Sands M, Dong Y. 90Y-oxine-ethiodol, a potential radiopharmaceutical for the treatment of liver cancer. Applied Radiation and Isotopes. 2003 5//;58(5):567-73.
149. Heuveling DA, Visser GWM, Baclayon M, Roos WH, Wuite GJL, Hoekstra OS, et al. 89Zr-Nanocolloidal Albumin–Based PET/CT Lymphoscintigraphy for Sentinel Node Detection in Head and Neck Cancer: Preclinical Results. Journal of Nuclear Medicine. 2011 October 1, 2011;52(10):1580-4.
150. Keliher EJ, Yoo J, Nahrendorf M, Lewis JS, Marinelli B, Newton A, et al. 89Zr-Labeled Dextran Nanoparticles Allow in Vivo Macrophage Imaging. Bioconjugate Chemistry. 2011 2011/12/21;22(12):2383-9.
151. Heuveling DA, van Schie A, Vugts DJ, Hendrikse NH, Yaqub M, Hoekstra OS, et al. Pilot Study on the Feasibility of PET/CT Lymphoscintigraphy with 89Zr-Nanocolloidal Albumin for Sentinel Node Identification in Oral Cancer Patients. Journal of Nuclear Medicine. 2013 April 1, 2013;54(4):585-9.
152. Radl J, Croese JW, Zurcher C, Van den Enden-Vieveen MH, de Leeuw AM. Animal model of human disease. Multiple myeloma. Am J Pathol. 1988 Sep;132(3):593-7. PubMed PMID: 3414786. Pubmed Central PMCID: 1880745. Epub 1988/09/01.
153. Vanderkerken K, De Greef C, Asosingh K, Arteta B, De Veerman M, Vande Broek I, et al. Selective initial in vivo homing pattern of 5T2 multiple myeloma cells in the C57BL/KalwRij mouse. Br J Cancer. 2000 Feb;82(4):953-9. PubMed PMID: 10732771. Pubmed Central PMCID: 2374415. Epub 2000/03/25.
154. Alici E, Konstantinidis KV, Aints A, Dilber MS, Abedi-Valugerdi M. Visualization of 5T33 myeloma cells in the C57BL/KaLwRij mouse: establishment of a new syngeneic murine model of multiple myeloma. Experimental hematology. 2004;32(11):1064-72.
155. Varma NR, Shankar A, Iskander A, Janic B, Borin T, Ali M, et al. Differential biodistribution of intravenously administered endothelial progenitor and cytotoxic T-cells in

rat bearing orthotopic human glioma. BMC Medical Imaging. 2013;13(1):17. PubMed PMID: doi:10.1186/1471-2342-13-17.
156. Abou DS, Ku T, Smith-Jones PM. In vivo biodistribution and accumulation of 89Zr in mice. Nuclear medicine and biology. 2011;38(5):675-81.